# STRUCTURAL RESPONSE TO LONG-DURATION EARTHQUAKES

WA-RD 340.2

Final Technical Report
January 1994

**Washington State Department of Transportation**

Washington State Transportation Commission
Transit, Research, and Intermodal Planning (TRIP) Division
in cooperation with the U.S. Department of Transportation
Federal Highway Administration

# TECHNICAL REPORT STANDARD TITLE PAGE

| 1. REPORT NO. | 2. GOVERNMENT ACCESSION NO. | 3. RECIPIENT'S CATALOG NO. |
|---|---|---|
| WA-RD 340.2 | | |

| 4. TITLE AND SUBTITLE | 5. REPORT DATE |
|---|---|
| Structural Response to Long-Duration Earthquakes | January 1994 |
| | 6. PERFORMING ORGANIZATION CODE |

| 7. AUTHOR(S) | 8. PERFORMING ORGANIZATION REPORT NO. |
|---|---|
| M. Lee Marsh and Christopher M. Gianotti | |

| 9. PERFORMING ORGANIZATION NAME AND ADDRESS | 10. WORK UNIT NO. |
|---|---|
| Washington State Transportation Center (TRAC)<br>Civil and Environmental Engineering; Sloan Hall, Room 101<br>Washington State University<br>Pullman, Washington 99164 | 11. CONTRACT OR GRANT NO.<br>T9234, Task 9 |

| 12. SPONSORING AGENCY NAME AND ADDRESS | 13. TYPE OF REPORT AND PERIOD COVERED |
|---|---|
| Washington State Department of Transportation<br>Transportation Building, MS 7370<br>Olympia, Washington 98504-7370 | Technical Report, 1/92-12/93 |
| | 14. SPONSORING AGENCY CODE |

15. SUPPLEMENTARY NOTES

This study was conducted in cooperation with the U.S. Department of Transportation, Federal Highway Administration.

16. ABSTRACT

The effects of postulated Cascadia subduction zone earthquakes on inelastic structural response have been quantified. The earthquakes studied ranged in size from those previously recorded to the largest plausible event, a magnitude 9.5, 240 second duration earthquake. Artificial acceleration records attenuated to epicentral distances corresponding to coastal range sites and Puget Sound sites were generated. These records were used as input for inelastic response history analyses of single-degree-of-freedom systems with either bilinear or degrading stiffness hysteretic relationships. The results indicate that the maximum displacements are not significantly greater than those produced by previously recorded events or by records that are compatible with current design code response spectra. However, the inelastic energy dissipated and the numbers of displacement cycles are somewhat greater for the largest events, although the energy demands and cyclic demands are similar to those from previous events for magnitudes up to 8.5. Since, the maximum credible event is not well established at this time no changes to the current design procedures are recommended.

| 17. KEY WORDS | 18. DISTRIBUTION STATEMENT |
|---|---|
| Key words: Earthquakes, subduction zone, duration effects, inelastic response, damage demands, response spectra, inelastic energy, cyclic loading. | No restrictions. This document is available to the public through the National Technical Information Service, Springfield, VA 22616 |

| 19. SECURITY CLASSIF. (of this report) | 20. SECURITY CLASSIF. (of this page) | 21. NO. OF PAGES | 22. PRICE |
|---|---|---|---|
| None | None | 192 | |

**Technical Report**
for
Research Project T9234-09
"Structural Response to Long-Duration Earthquakes"

# STRUCTURAL RESPONSE TO LONG-DURATION EARTHQUAKES

by

M. Lee Marsh and Christopher M. Gianotti
**Washington State Transportation Center (TRAC)**
Washington State University
Sloan Hall
Pullman, Washington 99164-2910

Technical Monitor: Ed Henley
Bridge Technology Development Engineer
Washington State Department of Transportation

Prepared for

**Washington State Transportation Commission**
Department of Transportation
and in cooperation with
**U.S. Department of Transportation**
Federal Highway Administration

January 1994

## DISCLAIMER

The contents of this report reflect the views of the authors, who are responsible for the facts and accuracy of the data presented herein. The contents do not necessarily reflect the official views or policies of the Washington State Transportation Commission, Department of Transportation, or the Federal Highway Administration. This report does not constitute a standard, specification, or regulation.

## TABLE OF CONTENTS

## LIST OF TABLES

## LIST OF FIGURES

# CHAPTER 1

## SUMMARY

Recently discovered evidence suggests that large Pacific Northwest subduction earthquakes have occurred and may occur again. These earthquakes would be caused by slippage along the interface between the Juan de Fuca and North American crustal plates in the Cascadia subduction zone (CSZ). Such events could be of larger magnitude and longer duration than any of the Pacific Northwest earthquakes experienced in modern times. The shaking from such events could produce demands on structures that would exceed those accounted for by the current design criteria.

The objective of this study was to estimate and assess structural demands that such large-magnitude, long-duration earthquakes might produce. The demands were determined using inelastic response-history analyses of single-degree-of-freedom models with load-displacement relations for steel (bi-linear) and for concrete (degrading stiffness). In the analyses, the models were subjected to ground acceleration histories for the postulated earthquakes, for previously recorded earthquakes, and for earthquakes with elastic spectra similar to those of the current design criteria. The response was quantified by maximum displacement, dissipated inelastic energy, and displacement cycle counts. Analyses were performed for structure vibration periods between 0.1 and 4 seconds and for structure lateral yield strengths between 12.5 and 50 percent of the structure weight.

Since no recorded acceleration histories of such earthquakes are available, artificial histories were generated. These were based upon elastic response spectra that have been proposed for Pacific Northwest subduction earthquakes. The magnitudes of the artificial events ranged from those of previously recorded earthquakes to the largest plausible event, a magnitude 9.5. Earthquake duration increases as the magnitude increases; thus durations to 240 seconds were used. Artificial records that produced elastic response

spectra approximately equal to the current design spectra were used for comparison as were records from the 1949 Olympia and 1940 El Centro earthquakes. Additionally, acceleration records that reflect the amplification expected for certain Washington State soil types were used. Attenuation of motion due to epicentral distance was accounted for in the generation of the records.

The results show that the maximum inelastic displacements increase when earthquake magnitude is increased, structure yield strength is decreased, or the epicentral distance is reduced. However, the displacement is not strongly affected by duration. Energy demand, which is a measure of expected damage, is increased slightly by an increase in earthquake magnitude or a decrease in epicentral distance. Energy demand is greatly increased by lengthening earthquake duration or by decreasing structural yield strength. Of the two structural hysteretic models used in this research, the degrading stiffness models had greater damage demands placed on them than did the bi-linear models. Damage demand may also be measured by inelastic cycle counts. Inelastic cycle counts are affected in the same manner by the same parameters as inelastic dissipated energy.

Response for long-period structures of both structural models was elastic. The shortest period, for which the response was entirely elastic, depended on the structural strength and the intensity of the acceleration record. That long period structures remained elastic is important since the ground motion estimates are have the greatest uncertainty in the long period range.

The CSZ earthquakes with magnitudes smaller that 8.5 and durations less than 180 seconds that were attenuated for Puget Sound sites produced demands lower than those produced by the 1940 El Centro acceleration record and demands similar to the code compatible records and the 1949 Olympia record. Larger magnitude and longer

duration records produced larger displacement and damage demands. Also, sites located closer to the epicenter experienced larger displacement and damage demands.

Displacement demands from the larger events for sites in Puget Sound are probably tolerable for well-constructed structures. However, the energy and cycle count demands produced by the larger events may not be tolerable. Much of the demand is caused by many inelastic cycles with displacements between one and three times the yield displacement. It should be noted that typical laboratory testing schemes do not evaluate response to such low ductility demands.

Displacements are amplified when certain soil conditions are considered. Additionally, both the inelastic energy dissipation demands and the inelastic cycle counts show greater increases than displacement for the two soil types investigated, a shallow and a deep cohesionless soil. These increases were most evident in the 0.1 to 1 second period range and were also functions of the structure yield force to weight ratio.

The maximum displacements, inelastic energy dissipated, and the inelastic cycle counts can all be reduced by increasing the structural strength. This could be achieved by reducing the structural quality factor used for design. The amount of reduction depends upon the size of the design earthquake, structural period, and the level of response desired.

Displacement, inelastic energy, and cycle count demands are all affected by the elastic spectrum used as a basis for artificial acceleration generation. Currently, a maximum credible event for the Pacific Northwest subduction zone has not been agreed upon. Therefore the recommendation from this study is to retain the current design procedures until more is known about the subduction zone and its ability to produce great earthquakes. This is based upon the comparisons made in the study, which indicate that the demands expected from all but the largest events are not significantly greater than those produced by previously recorded and design spectra compatible events.

# CHAPTER 2

# INTRODUCTION AND RESEARCH APPROACH

## 2.1 INTRODUCTION AND PROBLEM IDENTIFICATION

The subduction of the Juan de Fuca Plate beneath the North American plate is thought to be the cause of the earthquakes experienced in the Pacific Northwest in modern times. Two types of focal mechanisms have been attributed to these earthquakes. One type is the fracturing of the Juan de Fuca plate as it reaches great depths (about 50 kilometers). This has been postulated as the mechanism causing the magnitude 7.1, 1949 Olympia earthquake, the largest recorded Pacific Northwest earthquake. The fracturing of the over-riding North American plate, as it shifts and adjusts to the subduction action, is thought to be the other type of mechanism causing Pacific Northwest earthquakes in modern times.

However, recent evidence produced by geophysicists, seismologists, and geologists indicates large subduction earthquakes could occur in the Pacific Northwest. Such earthquakes would be caused by the rupture of the locked interface between the Juan de Fuca and North American tectonic plates. The Juan de Fuca-North American plate interface surface has not ruptured in modern times. Earthquakes from such a rupture could be of as large a magnitude and of as long a duration as the 1960 Chile and 1964 Alaska subduction earthquakes. If such an earthquake occurs, the magnitude, duration, and area shaking that is felt could be much larger than that considered in the current design criteria.

Current Pacific Northwest seismic design criteria are partially based on the historic seismicity of the region. Such criteria use ground motion predictions based on the magnitude, durations, and attenuation of historic events. Overall design criteria concerning structural quality, detailing, dynamic amplification, and site soil effects are

based on worldwide experiences, as well as analytical and experimental data accumulated since 1900. Much of the knowledge has arisen from California, where there is high recurrence of earthquakes along the San Andreas fault system, extensive instrumentation and high population density.

Re-evaluation of the Pacific Northwest design criteria includes estimating responses to potential subduction earthquake ground motions for the Pacific Northwest and comparing them to the response to ground motions that are the basis for current design criteria. The parameters defining earthquake strong ground motion are typically peak ground motion, duration of shaking, and frequency content (1). Different source mechanisms will alter the value of these parameters. Possible Pacific Northwest subduction earthquake magnitudes, durations, frequency content, and attenuation relationships have been estimated by the joint efforts of seismologists, geologists, geophysicists, and historians.

This report is not a seismic hazard study of the Pacific Northwest. As will be shown, several seismic sources exist in the area. This paper only reports research on the hypothetical large earthquakes resulting from the slip between the Juan de Fuca and North American plates in the Cascadia subduction zone. The epicenters of such earthquakes are postulated to be between the coast and the toe of the continental slope.

One difference in strong ground motion in subduction earthquakes, as compared to historical Western United States earthquakes, is the duration of strong motion shaking Total perceptible shaking in previous Western Washington and California earthquakes has typically lasted less than 30 seconds. Subduction type earthquakes, which have been hypothesized for the Pacific Northwest, would have longer durations. The maximum credible event in Western Washington may produce shaking lasting as long as four minutes (2). Long duration ground motion and structural response have been recorded for only a

few recent earthquakes. Very little research has been conducted on the effects of long-duration ground motion.

Another postulated difference is the magnitude of earthquakes. Subduction zones in other parts of the world have produced earthquakes with moment magnitudes greater than 9.0. Current design criteria for the Pacific Northwest does not consider the possibility of such a large energy release.

Determining structural response to ground motion requires a response-history analysis using an acceleration record of the ground motion. Since no subduction earthquakes have occurred in the Pacific Northwest in historic times, no acceleration records of Cascadia subduction earthquakes exist. Also there are no near source acceleration records for the largest subduction earthquakes in recent times: the 1960 Chile and 1964 Alaska earthquakes. Artificial ground motion records may serve as a substitute for actual acceleration records provided the artificial records are compatible with the postulated ground motion.

Evaluation of postulated Pacific Northwest subduction earthquake response and comparison of that response to design code predicted response should reflect the differences between ground motion produced by different source mechanisms. The primary differences between Pacific Northwest subduction and Pacific Northwest crustal, intraplate earthquakes, and California strike-slip earthquakes may be duration and magnitude. Parameters such as peak ground acceleration, response spectra, and effective peak acceleration may not effectively relate the effects of duration. Accumulated damage, as measured by dissipated hysteretic energy and the number of inelastic hysteretic cycles, may better reflect the influence of duration.

It has been established that site soil conditions alter the ground motion. Tsiatas, et al (3) have characterized the acceleration amplification of soil conditions in Washington State with relations that are more representative than standard curves found in the

*Uniform Building Code* (4) and the *Guide Specifications for Seismic Design of Highway Bridges* published by the American Association of State Highway and Transportation Officials (Hereafter referred as ASSHTO, (5)). Artificial acceleration records can be developed for a site with specific Washington State soil conditions using Tsiatas, et al's acceleration amplification factors. Structural response to such records will reflect the influence of those soil conditions.

The method for re-evaluating the current design criteria is as follows. Using the ground motion parameters established by engineering seismologists and geotechnical engineers, artificial earthquakes were created. Response-history analyses were performed on single-degree-of-freedom structural models using the artificial earthquakes. The hysteretic models included both bi-linear and degrading stiffness models. The models' response to the artificial earthquakes was quantified by inelastic spectra, hysteretic energy dissipated, and the number of inelastic half-cycle reversals. The response to hypothetical Pacific Northwest earthquakes was compared to the displacement, hysteretic energy dissipated, and inelastic cycle counts produced by recorded earthquakes which played a key role in establishing current design criteria (e.g. El Centro, 1940 and Olympia, 1949) and for artificial acceleration records based on the AASHTO design spectra.

## 2.2 BACKGROUND

### 2.2.1 Seismicity of Western Washington

#### 2.2.1.1 Plate Tectonics

The tectonic feature thought to be capable of producing large subduction earthquakes in the Pacific Northwest is the subduction of the Juan de Fuca Plate under the North American Plate. The intersection of these plates occurs off the Pacific coast of Northern California, Oregon, Washington, and British Columbia in the CSZ. Unlike other subduction zones in the world, the Cascadia subduction zone does not contain a deep ocean trench. Noson, et al, (6) state that the evidence of a subduction process lies in: 1) the zone of deep earthquakes near the probable boundary of the North American and Juan de Fuca plates, 2) the presence of active or recently active volcanoes in the nearby Cascade range, 3) the presence of young terranes of oceanic origin accreted to the North American plate on the Olympic Peninsula, and 4) the folding and faulting of the ocean rocks and sediments near the plate boundary. McCrumb, et al (7) state that the presence of younger upper layers of sediments pierced by older layers of underlying rock points to a folding of the Juan de Fuca plate. That folding is explained by a subduction action.

The eastern boundary of the Pacific Plate and the western boundary of the Juan de Fuca Plate includes the Gorda ridge spreading zone, the Blanco Fracture Zone (a transform boundary) and the Juan de Fuca ridge spreading zone. North and south of the Juan de Fuca Plate are two smaller plates, the Explorer and the Gorda plates, both of which are separated from the Juan de Fuca plate by transform boundaries. See Figure 1

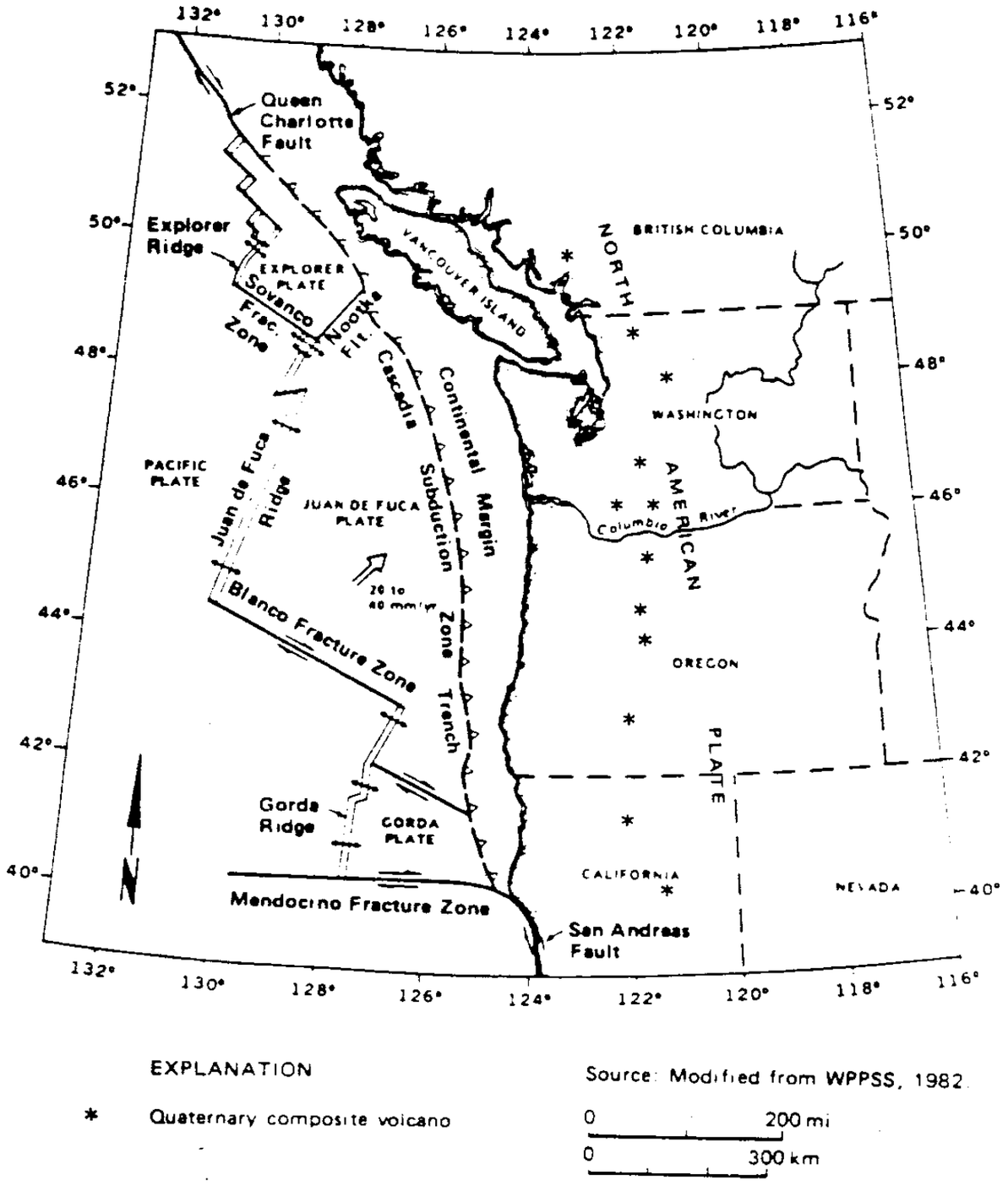


Figure 1 Plate Tectonic Structure in the Pacific Northwest (From (7))

McCrumb, et al (7) observe that: the Juan de Fuca Plate is moving in a northeasterly direction at a rate of 3.5 to 4.5 cm. per year relative to the North American Plate; the boundary between the Juan de Fuca plate and the North American Plate is approximately 1000 kilometers long; and that the Juan de Fuca plate extends 250 to 380 kilometers from the toe of the continental slope to the region of the volcanic rock beneath the Cascades. The dip of the Juan de Fuca plate is between 10 to 20 degrees in the Puget sound region, between 15 to 20 degrees beneath southwestern Washington, and between 30 to 50 degrees under the volcanic arc of the Cascades (7). The depth of the underlying plate ranges from 20 kilometers along the coastline to 100 to 200 kilometers under the Cascades (7). See Figure 2.

According to McCrumb, et al (7) the subduction process has produced accretion of terranes to the North American continent, volcanic action in the Cascade Range, and deformation of the North American plate. The continental slope and shelf, Olympic Mountains, Willipa Hills, and Puget Sound Basin all contain oceanic materials which were accreted to the North American plate from Paleocene time to the present. The subduction process has raised earlier rock deposits to form the Cascades and has caused magma upwellings which produce the volcanoes of the Cascades. Evidence of uplift and subsidence in the accreted terranes has been found by Atwater (8), Savage and Lisowski (9), as well as others listed by McCrumb, et al.(7).

The Cascadia subduction zone is similar in many respects to other subduction zones in the world that have experienced large earthquakes (10 and 11). The rate of convergence between the Juan de Fuca and North American plates is approximately equal to that of southwestern Japan, just less than 4 centimeters per year (10). The age of the subducting lithosphere is estimated to be between 10 to 15 million years (7). This age is close to that of the subducting plates in Columbia, southwestern Japan and southern

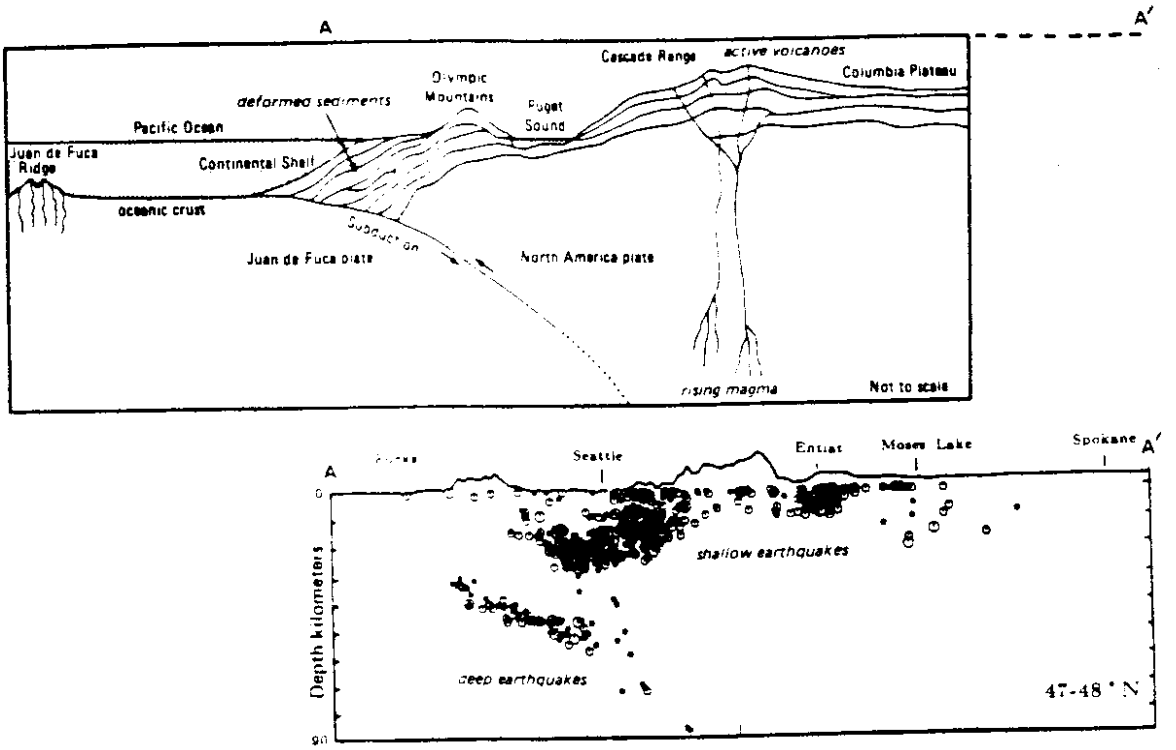


Figure 2. "Cross-sections of Washington showing plate tectonic convergence (top figure) and earthquake hypocenter locations. Some major topographic features and underlying geologic structures of Washington are shown diagrammatically in the upper figure. In the lower figure, selected hypocenters of earthquakes that occurred in 1982 through 1986 between latitudes 47° and 48° N are projected on a vertical plane that generally corresponds to the diagram in the upper figure. Because of the great number of shallow earthquakes that occurred between 1982 and 1986, only the hypocenters of those having magnitudes greater than 1.8 are shown in the lower figure. Below 30 km., hypocenters of all earthquakes having magnitude 1.0 or greater that occurred during this period are shown. The distributions of deep earthquakes indicates the slope of the zone of subduction. In the lower figure there is a vertical exaggeration of 2 to 1 below sea level; this creates the illusion that the Juan de Fuca plate dips more steeply than it actually does. Topography indicated on the lower figure has an exaggeration of 12 to 1." (From (9))

Chile, all of which are about 20 million years old (10). See Figure 3. The depth of recorded seismic action is shallow, less than 90 kilometers. This is similar to the subduction areas in Chile and Alaska which also have shallow active zones (10). The initial dip of subduction is relatively small, between 10 and 15 degrees (10). This is a common characteristic of subduction zones with strong coupling (10). Strong coupling exists when there is no slipping across a plate interface and there is relative movement between the two plates. The plates are then said to be locked and are accumulating strain energy. If the plates are not locked (coupled) there is sliding at the plate interface and a condition of aseismic creep exists. When compared to characteristics of subduction zones that experience aseismic creep, such as the Marianas Trench, all of the above mentioned characteristics of the Cascadia subduction zone are dissimilar (10 and 12).

A plot of earthquake foci on a cross-section of Western Washington reveals that earthquakes are centered at two distinct depths. See Figure 2. The shallower events primarily are centered in the Puget Sound Basin and have focal depths within the North American plate. Taber and Smith (13) report these earthquakes may be due to body forces within the plate related to the direction change in the boundary between the subducting plate and the North American plate. The deeper events, often referred to as intra-plate earthquakes, occur in the top of the subducting Juan de Fuca plate and are attributed to bending of the subducting plate caused by phase changes which produce negative buoyancy (13). McCrumb, et al (7), concur that earthquakes with deeper foci are not centered in the plate interface but in the subducting plate. The 1965 Puget Sound earthquake and the 1949 Olympia earthquake both had hypocenters within the deeper zone.

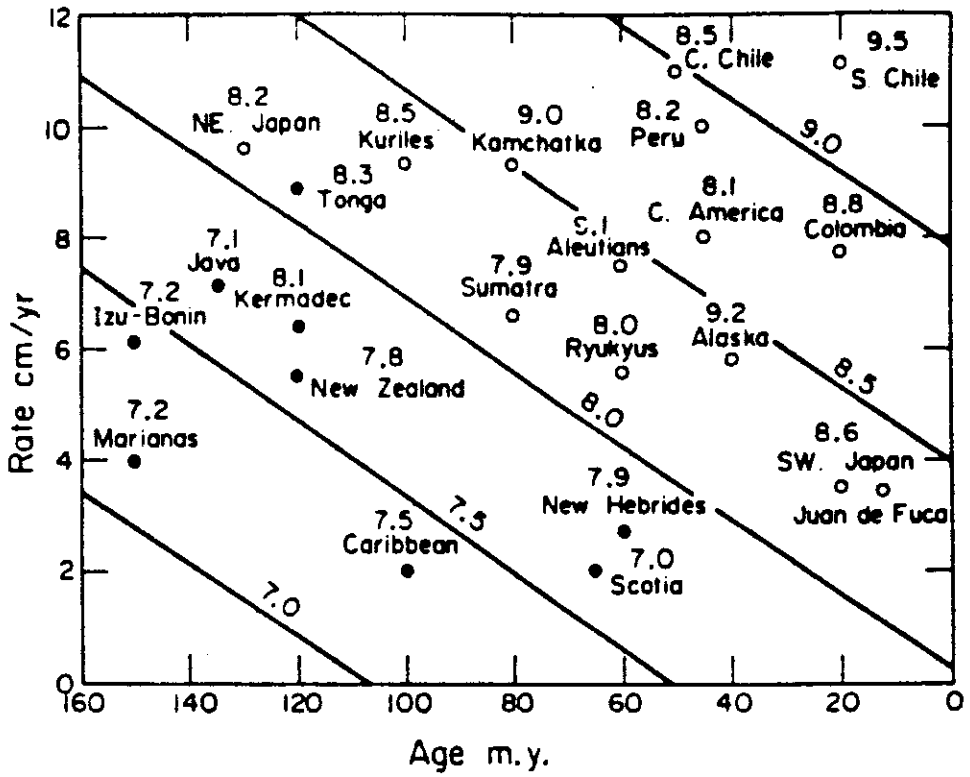


Figure 3 Moment magnitude, convergence rate and lithosphere age. "Relation of maximum energy magnitude, Mw, to the convergence rate and age of subducted lithosphere for major subduction zones. The contours of Mw are predicted maximum earthquake magnitudes resulting from linear regression of observed maximum earthquake magnitude against the other two variables Dots and circles are subduction zones with and without active back-arc basins, respectively." (From (10))

The lack of giant subduction earthquakes under the continental slope and shelf, in historic time, has raised some concern regarding the subduction process in the Cascadia Zone; is it aseismic and weakly coupled or locked and strongly coupled? If the plates are locked then strain energy is accumulating in the plates. When the accumulated strain energy in the locked plates exceeds the locking energy, the plate interface will rupture. The rocks along the fault will rebound and seismic waves will be emitted through the earth's crust. If the plates are not locked, the plates slide across each other aseismically. With aseismic sliding, little energy is accumulated, no significant ruptures occur, and thus no seismic waves are emitted.

Research postulating that the plates are locked has been presented by Weaver and Smith (14) and Savage and Lisowski (9). Weaver and Smith (14) studied small earthquake focal mechanisms in southwest Washington. They inferred from these mechanisms that the rock in the North American Plate is being compressed in a northeasterly direction and they concluded that such compression is evidence of locking between the plates beneath an area between the Coast Ranges and the Cascades. Savage and Lisowski (9) elastically modeled the Juan de Fuca plate and the North American plate as locked under the continental slope and outer continental shelf. Their model allowed slippage to occur elsewhere on the plate's interface. This model produced east-northeast tending compressive strains and uplift of the Olympic Mountains. The strains and uplift rates in their model agreed with measured strains and uplift. They used tidal gage measurements and geodetic surveys to measure both the actual compressive strains and uplifts.

The partial locking of plates postulated by Savage and Lisowski and Weaver and Smith is supported by others. Heaton and Hartzell (11) hypothesize that certain portions of the subduction zone are locked and are accruing strain energy while other areas are undergoing aseismic slip. Heaton and Kanamori (10) note similar behavior has occurred along the San Andreas fault. Taber and Smith (13) state that others have estimated that

the amount of calculated seismic moment is one tenth of that implied by the net slip of the plates along the boundary. The seismic moment quantifies the amount of energy released in an earthquake. It is determined according to the following equation:

$$M_O = \mu A D \qquad \text{(Equation 1)}$$

where:

| | |
|---|---|
| Mo | is the seismic moment |
| $\mu$ | is the rigidity modulus of the rock |
| A | is the area of the surface rupture |
| D | is the average slip across the rupture |

Taber and Smith cite that Abe (15) observed similar behavior in the Japanese trench, where the recurrence interval of great earthquakes is about 800 years. In Japan this has been attributed to long intervals of aseismic slip followed by short intervals of coupling (13).

Taber and Smith (13), Heaton and Snavely (16), Heaton and Hartzell (11 and 12), Savage and Lisowski (9), and McCrumb, et al (7) all mention the possibility that the Juan de Fuca plate is not coupled as it subducts under the North American plate. Ando and Balazs (17) report that the uplift rates, at locations 50 kilometers east of the plate intersection, as measured by leveling surveys conducted between 1906 and 1974, indicate the Juan de Fuca plate is not locked or coupled. Taber and Smith (13) report that earthquakes centered within the subducting Juan de Fuca plate are due to in-plate bending as it is pulled down by gravity. They say shallower crustal earthquakes are due to the body forces of the North American plate. They say the entire shallow dipping zone of the Juan de Fuca plate is undergoing aseismic creep.

The discussion concerning the condition of the plate interface continues. No conclusive evidence has been presented which proves that the CSZ is locked or unlocked.

If the subduction zone is locked over its entire 1000 kilometer length, earthquakes may be as large as the 1960 Chile or the 1964 Alaska earthquake (11). If only a portion of the zone is locked, smaller moment magnitude earthquakes are more probable. The ground motion postulated for such earthquakes is discussed later in this chapter. If there is no locking and the plates are sliding aseismically, then no large subduction earthquakes are expected to occur. Even with no locking, earthquakes the size of the 1949 Olympia and 1965 Puget Sound earthquakes can be expected.

### 2.2.1.2 Historic Seismicity

The Pacific Northwest is a seismically active region. In the past several hundred years twenty-two damaging earthquakes have been recorded. Figure 4 shows the epicenters of these major events. Potential evidence of giant earthquakes occurring near the coast in the past has been found. Indian legends exist which possibly describe tsunamis in the region. In this section each of these topics will be discussed to help establish the size and recurrence intervals of large earthquakes in the region.

#### 2.2.1.2.1 Historic Records

The following is a brief overview of the major earthquakes in the Pacific Northwest. This information is a summary provided by Noson, et al (6) and McCrumb, et al (7).

An earthquake which occurred in 1872 in the North Cascades was Washington's most widely felt earthquake The magnitude has been estimated as 7.4 and was felt over

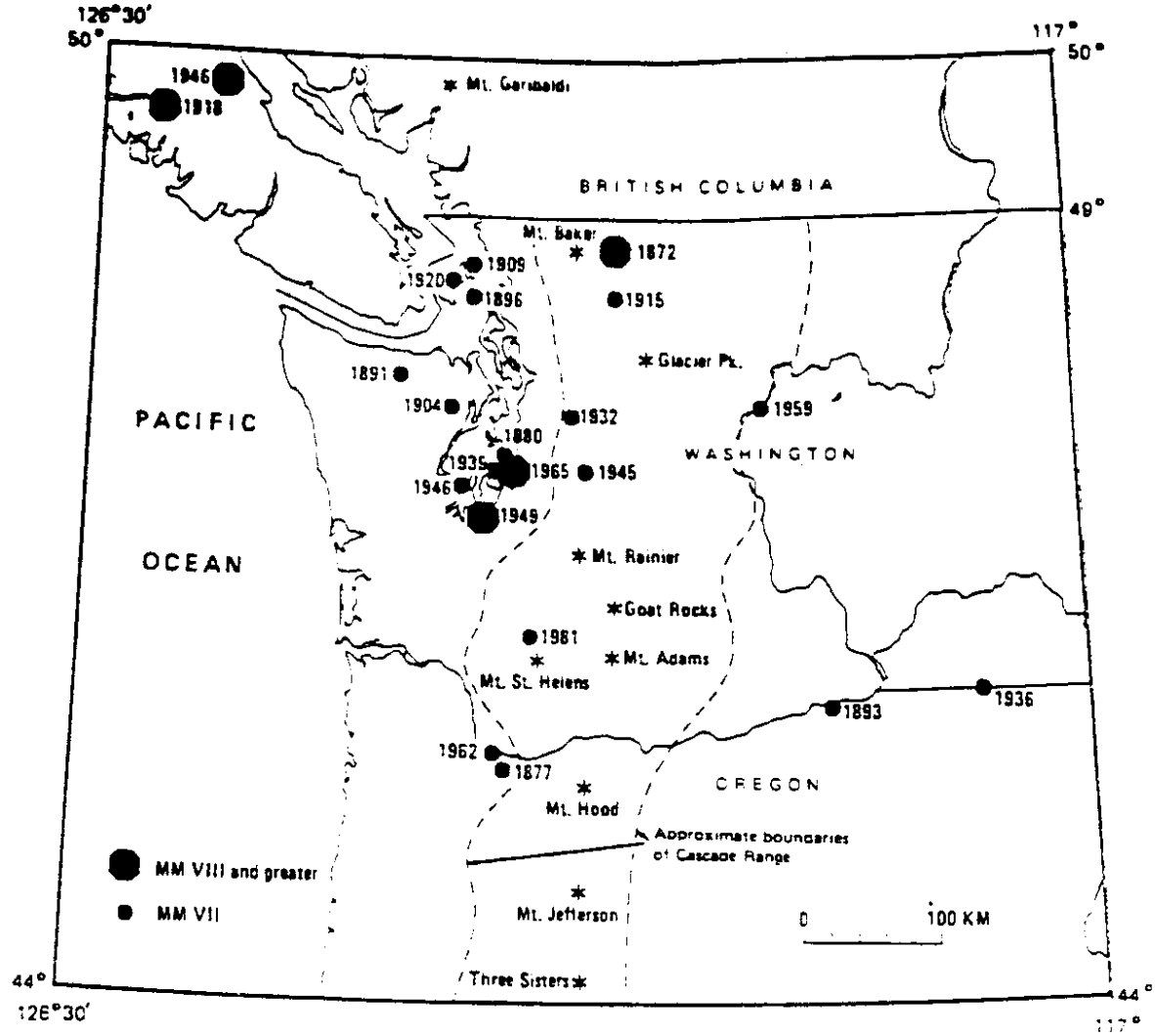


Figure 4 "Epicenters of the largest Pacific Northwest earthquakes that occurred between 1872 and 1987. The large symbols are epicenters of earthquakes whose maximum intensities were reported as VIII or greater on the Modified Mercalli Intensity Scale (MM); smaller symbols are MM intensities of VII. The locations of principal volcanoes in the region are also shown." (From (6))

1,000,000 square kilometers. The maximum intensity is estimated between VII and IX on the Modified Mercalli Index (MMI). The exact epicenter location has been approximated using estimated intensity contours for the main shock and aftershock sequence. The focal depth was believed to be less than 25 kilometers, which is similar to that of subsequent earthquakes in the area.

On July 15, 1936 an earthquake with a maximum intensity of VII MMI occurred near Milton-Freewater, Oregon (6). According to McCrumb, et al (7) the magnitude of this event is estimated to be between 5.7 and 5.8. It is believed to have had a shallow focal depth because of the numerous aftershocks.

Minor damage, mostly to masonry buildings and chimneys, was reported near the epicenter in the 1939 Olympia and the 1945 North Bend earthquakes.

In 1946, a magnitude 7.2 to 7.3 earthquake occurred on the east side of Vancouver Island, British Columbia (7). Noson, et al (6), report that there was as much damage caused by this earthquake as by the 1965 Puget Sound earthquake. It is thought to have been a strike-slip earthquake generated in the transition zone between the Juan de Fuca and Explorer Plates (7).

The 1949 earthquake centered near Olympia, Washington had a Richter magnitude 7.1 and had a focal depth of 54 kilometers and had a strike-slip focal mechanism. This is the largest Pacific Northwest earthquake recorded. Noson, et al (6), report that there was considerable damage to masonry buildings in Centralia, Chehalis, Castle Rock, Olympia, Tacoma, and Seattle. Damage costs have been estimated at $150 million, in 1984 dollars. Thirty schools were damaged, ten of which were permanently closed. Water lines were damaged, power outages occurred, gas lines were ruptured, and lift bridges were damaged so they could not operate. Much of the damage in Seattle occurred in fill areas near the waterfront.

In 1962 a magnitude 5.1 earthquake occurred near Portland, Oregon (7). Minor damage in Portland was reported in this event (7).

In 1965 there was substantial damage caused by an earthquake centered between Seattle and Tacoma (6). McCrumb, et al (7), report that it had a maximum intensity of VII and a focal depth of 60 kilometers. It had a Richter magnitude of 6.5 (6).

2.2.1.2.2 Geologic Evidence of Large Subduction Earthquakes

Atwater (8) has found geologic evidence of past giant earthquakes occurring in the Cascadia zone. Stratification of vegetative and alluvial deposits suggests sudden subsidence and deposits of sand left by tsunamis. The 1960 Chile and 1964 Alaskan earthquakes produced similar elevation changes (18 and 19) and tsunami deposits. Atwater (8) has found thick peaty layers with conifer stumps buried beneath muddy inter tidal deposits. The conifer stumps may be remnants of trees killed due to a sudden land subsidence followed by sea water flooding. During the 1964 Alaska earthquake many trees were killed near the town of Portage because the land subsided to below sea level and was flooded. The mud deposits Atwater analyzed contained rhizomes found in salt water. Such conditions suggest a sudden subsidence of the area. Thin sand deposits have been found at Willipa Bay on the Washington Coast and are similar to the sand deposits in Chile left by tsunamis generated from the great 1960 Chile earthquake. Atwater also found long term rates of continental uplift in Western Washington do not correlate with the present uplift rates. Current uplift rates are much higher than those inferred from Pleistocene marine terrace rates. Subsidence caused by subduction earthquakes provides one explanation for the difference. Based on the number and thickness of mud deposit

layers, Atwater (8) estimates that giant earthquakes occurred as often 6 times in the last 7000 years.

Similarly Heaton and Hartzell (11) state that the current evidence indicates a return period of 400 to 500 years, although a range from 100 to over 1000 years is plausible. The evidence they cite is sedimentary deposits found in the Cascadia channel, the dating of mud slide and landslide debris, uplift rates of marine terraces, and geodetic strains. Sixteen types of turbidites, deposited in the Cascadia channel after the deposition of Mazama ash there 6600 years ago, have been found. It is thought that each turbidite deposit was caused by subsidence occurring during a large subduction earthquake. From this, an average return period of 410 years is inferred. Several different landslides and mud slides have debris with carbon 14 dating ages of 350 and 800 years before present. It is hypothesized that the landslides were caused by large earthquakes. Near Cape Mendecino there are nine terraces. Maximum uplift is about 16.8 meters. Carbon 14 dating of terrace materials estimates a maximum uplift rate of about 3.6 centimeters per year. This results in a return period of about 500 years. Measured geodetic strains in Puget Sound and the Straight of Juan de Fuca are 0.05 and 0.22 μstrain per year. By comparison, the strains in Chile and Alaska prior to the 1960 and 1964 respective earthquakes were between 15 and 50 μstrain. At current rates it would take between several hundred and one thousand years to accumulate a comparable amount of strain in the CSZ.

2.2.1.2.3 Indian Legend Accounts of Tsunamis

Indian legends contain references to potential earthquakes and tsunamis (16) These references are found in the 1868 publication by a judge, James Swan, who lived on the Olympic Peninsula and recorded some traditions of the Makah tribe that lives near

Cape Flattery Washington. One legend includes an account of a great flood in the recent past. Swan (20) describes the telling of the tradition as follows:

> "A long time ago," said by informant, "but not a very remote period, the water of the Pacific flowed through what is now a swamp and prairie between Waatch village and Neah Bay, making an island of Cape Flattery. The water suddenly receded leaving Neah Bay perfectly dry. It was four days reaching its lowest ebb, and then rose again without any waves or breakers, till it submerged the Cape, and in fact the whole country, excepting the tops of the mountains at Clyoquot. The water on its rise became very warm, and as it came up to the houses, those who had canoes put their effects into them, and floated off with the current, which set very strongly to the north. Some drifted one way, some another; and when the waters assumed their accustomed level, a portion of the tribe found themselves beyond Nootka, where their descendants now reside, and are known as the Makahs in Classett, or Kwenaitchechat. Many canoes came down in the trees and were destroyed, and numerous lives were lost. The water was four days regaining its accustomed level."

Swan noted that the legend is plausible. There is a lowland area separating the cape from the nearby hills. There is sand beneath the topsoil in the lowland area. The validity of the legend is questionable since the flood apparently lasted four days and the water covered all of Cape Flattery. Heaton and Snavely (16) note that tsunamis have lasted from tens of minutes to hours but not days. Also, the legend contains no mention of earthquakes or ground shaking. Heaton and Snavely question the validity of the legend but note that there may be some truth in it, with the incongruities being exaggeration.

They also note there are legends from the Yurak Indians in Northern California that include an earthquake god (16). However, they dismiss these as mostly anecdotal myths.

### 2.2.2. Characteristics of Subduction Earthquakes Relative to Historical Western U.S. Earthquakes

#### 2.2.2.1 Peak Ground Motion

Measurements of near source, large subduction earthquakes are few. Heaton and Hartzell (12) report that the largest recorded motion is for the 1968 Tokachi Oki earthquake which had a moment magnitude of 8.2. However, data from smaller earthquakes and investigations of large unrecorded earthquakes may provide some insight into peak ground motion. For instance, Housner and Jennings (21) estimated the peak horizontal acceleration felt in Anchorage in the 1964 Alaskan earthquake to be about 14 percent of gravity. The peak ground acceleration (PGA) recorded in the 1985 Michoacan earthquake (Ms= 8.1, Mw = 8.0) was 15 percent of gravity near the epicenter (22), 4 percent of gravity on firm soil in Mexico City and 17 percent of gravity on soft soils in the old lake bed region of Mexico City (23). Mexico City is approximately 400 kilometers from the epicenter. In contrast the PGA in the 1985 Chilean Earthquake (Ms = 7.8, Mw = 7.5) was approximately 70 percent of gravity in the epicentral region. A nearly equal PGA was recorded at a site 100 kilometers away. However, in some areas the PGA had attenuated to approximately 10 percent of gravity at 300 kilometers from the epicenter (22). The 1964 Alaska, the 1985 Mexico City and 1985 Chile earthquakes were all subduction earthquakes. The wide range in PGA points to a large variability in peak ground accelerations for large subduction earthquakes.

Other non-subduction earthquakes have produced a large variation in PGA. The maximum ground acceleration was 33 percent of gravity in the El Centro 1940 earthquake, and 122 percent of gravity at Pacoima Dam in the 1971 San Fernando Earthquake. The 1985 Nahanni, Northwest Territories earthquake vertical component had a PGA of over 200 percent of gravity. The 1966 Parkfield earthquake had a PGA of near 50 percent of gravity.

PGA has been argued to be a poor estimate of earthquake ground motion, especially in terms of engineering significance. Newmark maintained that the effective peak acceleration (EPA) is a more meaningful indicator than PGA (24). EPA is proportional to the elastic spectral response ordinates for periods between 0.1 and 0.5 seconds. NEHRP (25) defines the EPA as the average 5% damped spectral acceleration for periods between 0.1 and 0.5 seconds, divided by 2.5. This is approximately the acceleration amplification factor applied to the peak ground motion to obtain the acceleration of an elastic system in the period range from 0.1 to 0.5 seconds. Thus EPA represents a value for the peak ground motion as measured by the structural response to that ground motion, averaged over periods from 0.1 to 0.5 seconds.

Heaton and Hartzell (11) compared the response spectra of 56 strong ground motion recordings from shallow subduction earthquakes having moment magnitude greater than 7.0 and less than 8.25. There was much scatter in the data. However, they found cases of accelerations greater than 5 percent of gravity at distances over 150 kilometers. This lack of attenuation is not found in Western United States data (12). In Figure 5, peak acceleration and spectral velocity attenuation curves for Japanese subduction zone earthquakes, compiled by Kawashima, are compared to Western United States earthquakes (Joyner and Boore). This figure suggests that the ground motion is higher at greater distances in subduction earthquakes than in western United States

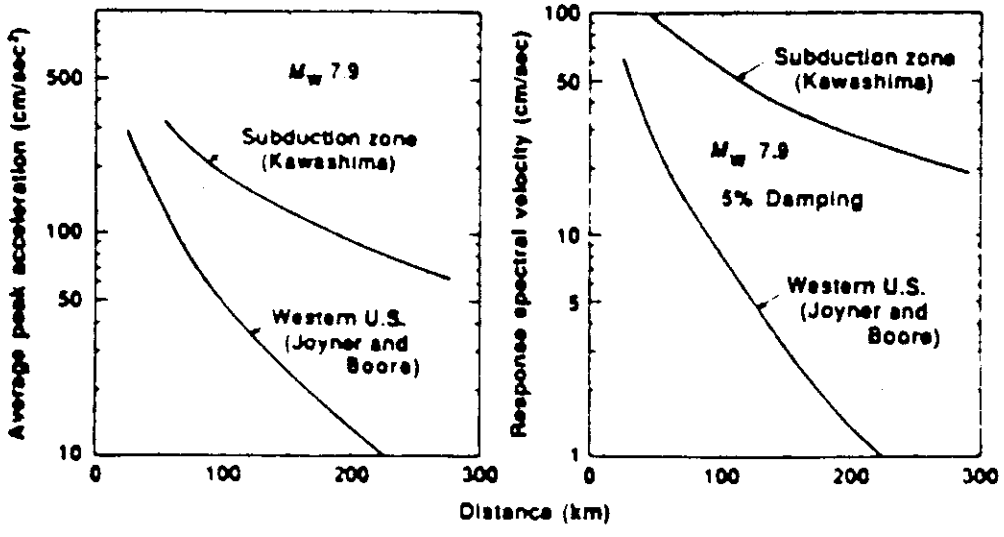


Figure 5 Ground Motion Attenuation Curves "Comparison of predictions of average peak ground motions obtained by regression analysis of data from the Southwestern United States and from Japan. Soil sites and 5% damping are assumed for the response spectra." (From 12)

earthquakes. Kawashima found acceleration greater than 10 percent of gravity at distances over 150 kilometers.

Magnitudes and energy released from large subduction earthquakes are also potentially higher than that of the earthquakes experienced in California. The 1906 San Francisco earthquake is estimated to have had a surface wave magnitude of 8.25, but a moment magnitude of only 7.9 (26). However, the May 22, 1960 Chilean Earthquake had a surface wave magnitude of 8.3 and moment magnitude of 9.5; the 1964 Alaskan Earthquake had a surface wave magnitude of 8.4 and a moment magnitude of 9.2 (26). Moment magnitudes are directly related to the energy released since they are determined from the seismic moment. On the other hand, surface wave magnitudes are a measure of the acceleration amplitude of surface waves with a period of 20 seconds. (26). While surface wave magnitudes were the same for the 1960 Chile and 1906 San Francisco earthquakes, the 1960 Chile earthquake released 250 times the energy of the 1906 San Francisco Earthquake.

#### 2.2.2.2 Duration of Strong Ground Motion

Current Pacific Northwest design criteria is based on historical Western United States earthquakes. Such earthquakes have had shorter durations than large-magnitude long-duration subduction earthquakes. Durations of Western United States earthquakes were studied by Trifunac and Brady (27). Large subduction earthquake durations can be determined from documented observations.

In a study on the correlation between duration and the parameters of magnitude, Modified Mercalli Intensity, site geology and epicentral distance, Trifunac and Brady (27) used 188 Western United States earthquake acceleration records. They defined the

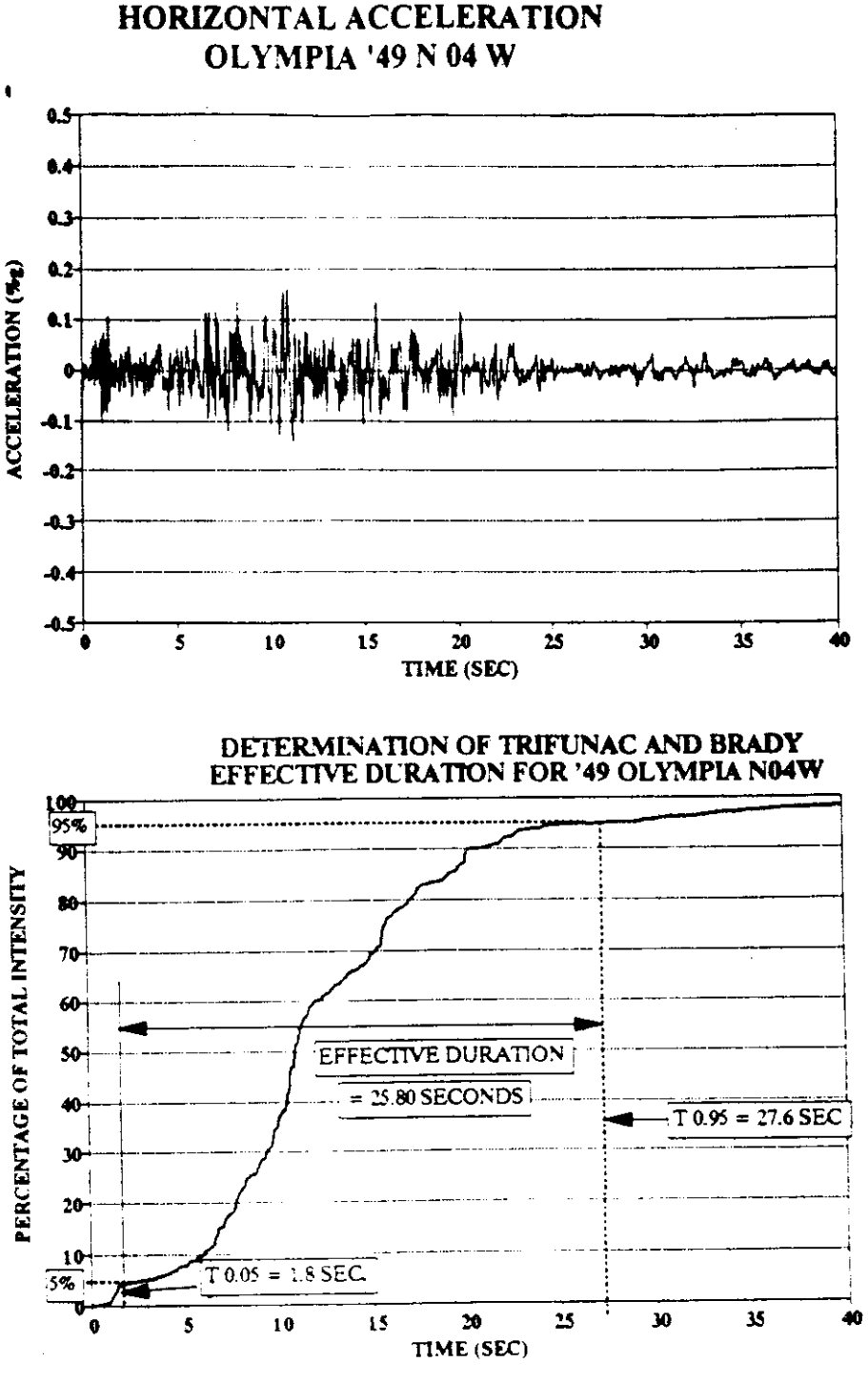


Figure 6 Definition of Trifunac and Brady duration

effective duration as the time in which 90 percent of the Arias intensity (accelogram intensity) is accumulated. The intensity is determined according to:

$$I_A = (\pi/2g) \int a^2 \, dt \qquad \text{(Equation 2)}$$

where:

$I_A$ is the Arias intensity

a is the acceleration as a function of time

t is time

g is the acceleration due to gravity

Times are determined corresponding to when the accumulation is 5 and 95 percent of the total. The difference between these two respective times is the effective Trifunac and Brady duration. The accumulation process can be represented as in Figure 6. The average effective duration plus one standard deviation, of all of the events studied by Trifunac and Brady, was less than one minute, for horizontal components. The 1949 Western Washington earthquake, northwest component as recorded in Olympia, was among those used in Trifunac and Brady's study. It has one of the largest overall durations, 89 seconds, and it has an effective Trifunac and Brady duration of 25.8 seconds (1).

Even though few acceleration records of recent large subduction earthquakes exist, most have had their durations estimated by observers. The strong shaking in the 1964 Alaskan earthquake was estimated to be 2 minutes and the overall duration 4 minutes (21). St. Amand (28) states that the duration of the largest of the earthquakes that occurred in Southern Chile in 1960 was three and a half minutes. The shaking felt in Mexico City in the 1985 Michoacan earthquake lasted five minutes (22). In 1835, Charles

Darwin writing in his diary of an earthquake that he experienced in Chile, noted that the shaking lasted 2 minutes (29). The 1964 Alaska, the 1985 Michoacan and the 1960 and 1985 Chile earthquakes were subduction earthquakes. Because of the large rupture areas, such large subduction earthquakes may have significantly longer durations than earthquakes involving smaller rupture areas such as those in California. Crouse (30) notes that the long duration of shaking of large subduction earthquakes may need to be considered in seismic design. Additionally, he emphasizes the need to consider duration if the structure is subject to degradation when loaded cyclically.

#### 2.2.2.3 Frequency Content

There are conflicting reports concerning the frequency content of subduction type earthquakes compared to California earthquakes. The large subduction earthquakes used by Heaton and Hartzell (12) had a large part of their seismic energy in the very long period range. Although they do not define "very long period" they comment that this energy of very long period is outside that of engineering interest. Consistent with their comment, St Amand (28) documented observations of ground motion in the largest earthquake occurring in May 1960 in Chile. It was described as similar to being in a small boat in very heavy sea swells. Ground motion apparently had components with periods in the range of 10 to 20 seconds or higher. In the 1985 Michoacan earthquake ground motion, shaking of the ancient lake bed in Mexico City, produced motion with a dominant period of approximately 2 seconds (22). Anderson, et al (22) also note that more near field records of subduction events are needed to determine if such frequency content is usual. However, Crouse (30) notes that short-period (high frequency) ground motions in subduction zones are greater than those in California and that long-period motions in subduction zones are less than those in California.

### 2.2.3 Hypothetical Strong Ground Motion in the Pacific Northwest.

#### 2.2.3.1 Maximum Credible Event.

There are different approximations of the maximum credible earthquake hypothesized for the Cascadia subduction zone. Heaton and Hartzell (11) have predicted that if the entire 1000 kilometer length of the CSZ ruptures then an event similar to the 1960 Chilean earthquake (Mw = 9.5) may result. Crouse (30) argues that a moment magnitude 8.5 earthquake is a more reasonable estimate of the maximum credible event. He bases this estimate on the 1984 work of Heaton and Kanamori and the 1988 study by Washington Public Power Supply System (WPPSS) (31). Heaton and Kanamori (10) estimate that a moment magnitude of 8.3 ± 0.5 is possible. This estimate is based on a regression equation relating the age of the subducting plate and the rate of convergence to moment magnitude:

$$M_W = -0.00889\ T + 0.134\ V + 7.96 \qquad \text{(Equation 3)}$$

where:

$M_W$ is the moment magnitude

T is the age of the subducting plate, in millions of years

V is the convergence rate in centimeters per year

The regression equation is based on the tabulation of age of crustal rocks, rate of convergence, and recorded earthquake magnitude for subduction zones throughout the world. See Figure 3.

McCrumb, et al (7) and Noson, et al (6), summarize the estimates of magnitudes of possible intraplate and crustal earthquakes in Western Washington. Both of these mechanisms are distinct from the postulated subduction mechanism. In the Puget Sound region, a magnitude 6.5 event is thought to be the upper bound for shallow focus earthquakes, and a magnitude 7.5 is thought to be the upper bound for deep focus (50 kilometers) earthquakes. A return period of 10 years is given for magnitude 6 earthquakes of either type in the Puget Sound region (6). Return periods for Puget Sound region magnitude 6.5 and 7.0 earthquakes are estimated to be 35 and 100 years respectively. There is the potential for a magnitude 7, shallow focus earthquake in the North Cascades area and in the St. Helens seismic zone in southern Washington (6). However, McCrumb, et al (7) estimates a maximum credible event of magnitude 7.3 in the North Cascades and 6.5 in the Cascades in Southern Washington.

### 2.2.3.2 Heaton and Hartzell's Hypothetical Strong Ground Motion

Heaton and Hartzell (2) used kinematic modeling (an influence or Green's function technique) to build accelograms for large Cascadia subduction zone earthquakes. Reiter (24) explains this method as follows: the earthquake mechanism is modeled as a surface rupture, the total rupture area is divided into small areas, faultlets, that will each produce a small rupture, the influence of seismic waves from the many small rupture areas are superimposed at the site in question to produce the estimated total ground motion. The superposition method considers the effects of stagger in time of slip and the location of the small areas. Heaton and Hartzell (2) estimated the entire rupture area for the CSZ to be 1000 kilometers long and 200 kilometers wide. They used the 1978 Mw 7.5 Miyagi-Oki subduction earthquake as the acceleration record of the small area rupture. To determine the number of equivalent Miyagi-Oki earthquakes that could occur over the entire CSZ

rupture area, the CSZ rupture area was first divided by the rupture area of the Miyagi-Oki earthquake. However, this approach produced too large of a predicted event since it is unlikely that the entire rupture CSZ area is locked. Due to asperities in the interface, they believe only a portion of the interface is locked.

To constrain the total number of equivalent Miyagi-Oki earthquakes possible on the CSZ rupture area, Heaton and Hartzell (2) used kinematic modeling to create teleseismic records of actual earthquakes (e.g. 1960 Chile and 1964 Alaska) using Miyagi-Oki earthquakes. Teleseismic records are ground motion histories recorded at very large epicentral distances. Heaton and Hartzell varied the total number of Miyagi-Oki earthquakes until the created teleseismic record resembled the actual teleseismic record recorded in Pasadena, California. A teleseismic record using 120 Miyagi-Oki records was determined to best matched the actual teleseismic record of the 1960 Chile earthquake.

The maximum credible earthquake in the CSZ is considered to be an earthquake of the size of the 1960 Chilean earthquake and would be centered off the Washington or Oregon coast. This maximum credible event, the 120 Miyagi-Oki record, would be the acceleration record for the maximum credible earthquake on the CSZ. Figure 7 shows the acceleration history for this artificial earthquake at a coastal range site. This particular acceleration record has a total duration of approximately 240 seconds. Heaton and Hartzell (2) have attenuated this acceleration record to coast, coast range, and Puget Sound locations, using attenuation relations by Crouse and Kawashima. After attenuation, the motion on the Pacific coast has a peak ground acceleration of 89 percent of gravity. Attenuating the same motion to Puget Sound produces a peak ground acceleration of 49 percent of gravity. Heaton and Hartzell (2) generated smoothed elastic response spectra for this maximum ground motion at the coast, coast ranges and at Puget Sound. These spectra are shown in Figure 8

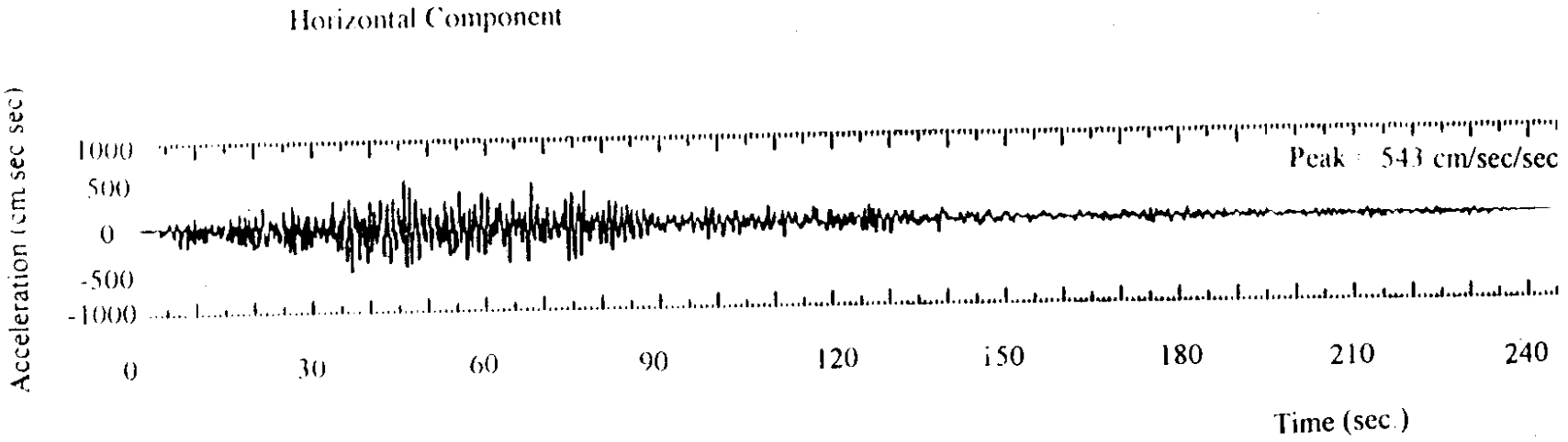


Figure 7 Artificial acceleration, horizontal component for maximum credible event on the CSZ as generated by Heaton and Hartzell (2)

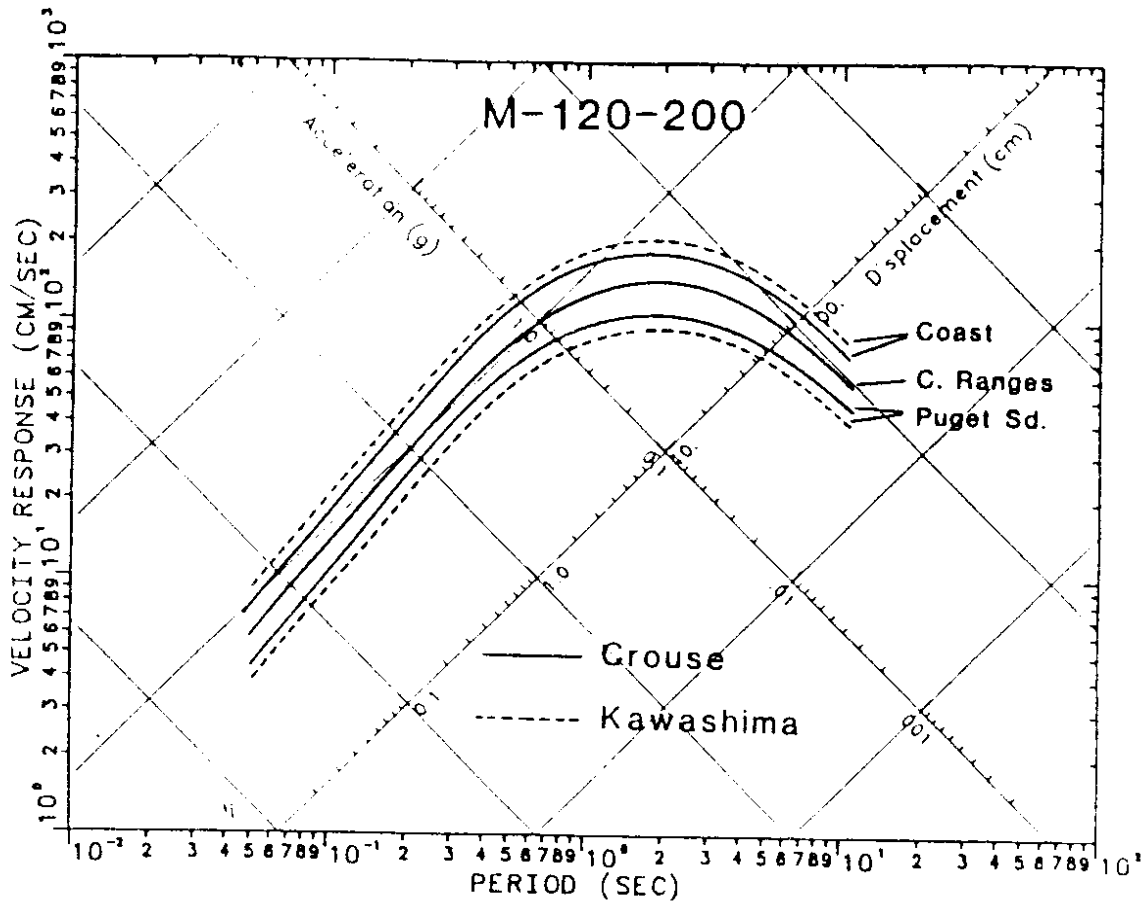


Figure 8 Smoothed Elastic Response spectra for maximum credible event on the CSZ attenuated to Coast, Coast Ranges and Puget Sound sites. (From [2])

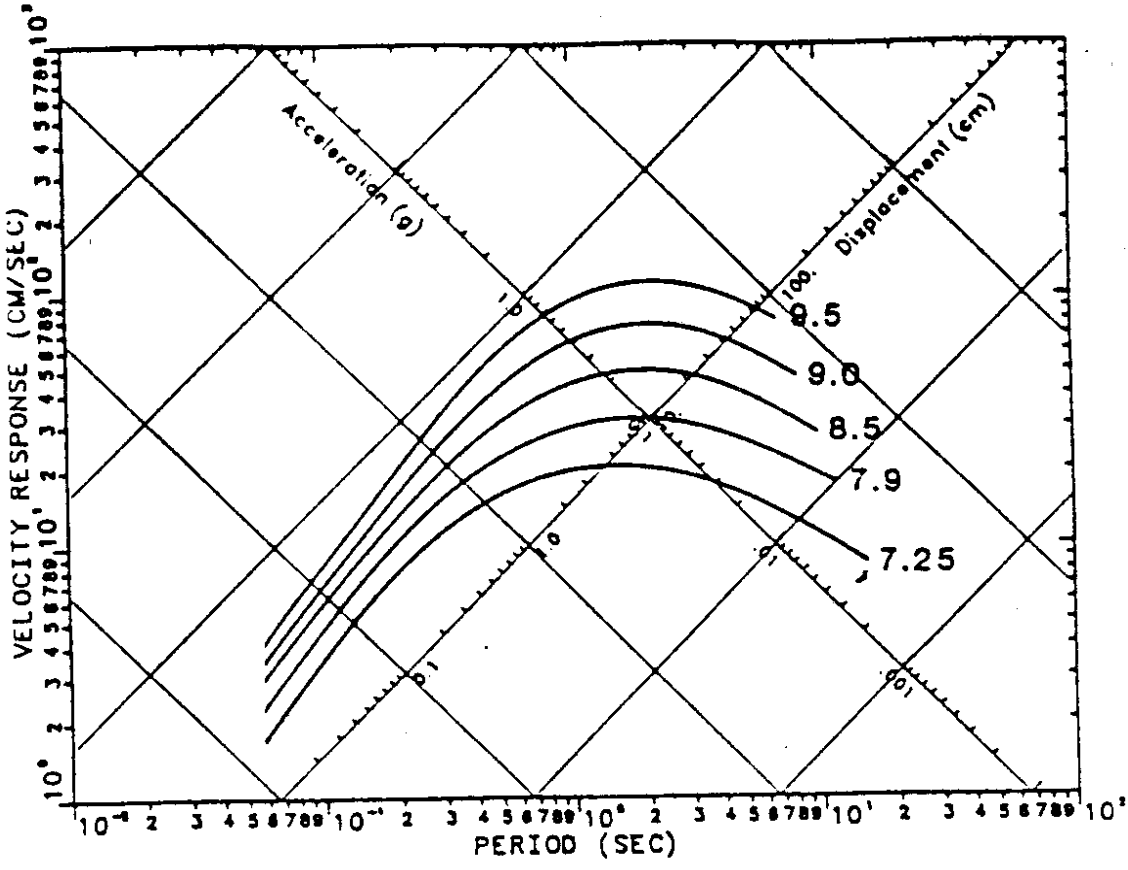


Figure 9 Smoothed elastic response spectra for average postulated earthquakes with motion attenuated to Coast Ranges site. (From (2))

Heaton and Hartzell (2) also determined the elastic response spectra for 56 recordings of strong ground motion from 25 shallow subduction earthquakes, which had moment magnitudes between 7.0 and 8.25. The response spectra were smoothed and averaged, then grouped in terms of magnitude and epicentral distance. The results are average elastic response spectra for moment magnitude 7.25 and 7.9 earthquake ground motions attenuated to a coast range site. These are shown in Figure 9. Also in the figure are average response spectra for moment magnitude 8.5, 9.0 and 9.5 earthquakes, attenuated to the same site. The magnitude 9.5 response spectra was determined by averaging and smoothing the largest and smallest synthetic earthquakes which they believed to be compatible with the 1960 Chile teleseismic record. They then interpolated response spectra for average magnitude 8.5 and 9.0 earthquakes.

#### 2.2.3.3 Crouse's Attenuation Relationships

Crouse (30) developed attenuation relations for median subduction earthquakes in the Pacific Northwest. 697 records were used as a data base for regressions of peak ground acceleration and 237 records for regressions of spectral velocity response spectra The largest of these accelograms had a moment magnitude of 8.2. The peak ground acceleration (PGA) equation for a median earthquake of a given magnitude is:

$$\ln(PGA) = 6.36 + 1.76M - 2.73 \ln(R + 1.58\exp(0.608M)) + 0.00916h, \quad \sigma = 0.773$$

(Equation 4)

where:

| | |
|---|---|
| M | is the moment magnitude |
| PGA | is the peak ground acceleration in gals |
| R | is the center of energy release distance in kilometers |

h is the focal depth in kilometers

$\sigma$ is the standard error of the formula.

Although there is a significant reduction in peak ground motions from attenuation for Puget Sound sites, such earthquakes would be strong events and the Puget Sound region would experience considerable ground motion. For a magnitude 8.5 event peak ground motion is estimated to be 28 percent of the acceleration of gravity, based on an epicentral distance of 75 kilometers and a focal depth of 32.5 kilometers. Such distances would be representative of the Tacoma-Seattle-Everett area. A magnitude 9.5 event would have a peak ground motion of 40 percent of gravity using the same distances.

Crouse (30) also developed regression equations for smoothed elastic response spectra for median Pacific Northwest subduction earthquakes. The equation is in the form:

$$\ln(PSV) = p_1 + p_2M + p_3M^2 + p_4\ln(R+p_5\exp(p_6M)) + p_7h \qquad \text{(Equation 5)}$$

where:

PSV is the pseudo velocity in centimeters per second

The constants $p_1$ to $p_7$ are listed in Table 1

Median response spectra produced by this equation, the constants in Table 1, epicentral distance and focal depth both equal to 30 kilometers, and magnitudes 7.25 to 9.5, are shown in Figure 10. These distances reflect distances for the coastal ranges. Heaton and Hartzell's response spectra for average Cascadia zone earthquakes are superimposed on Figure 10 for comparison. Figure 11 shows median response spectra for epicentral distances typical of Puget Sound sites (R=75, h=32.5).

Table 1 **PSV Regression Constants. (From (30))**

| Period | $p_1$ | $p_2$ | $p_3$ | $p_4$ | $p_5$ | $p_6$ | $p_7$ | $\sigma^2$ |
|---|---|---|---|---|---|---|---|---|
| 0.1 sec | 3.26 | 1.12 | 0 | -1.93 | 1.58 | 0.608 | 0.00566 | 0.544 |
| 0.2 | 4.44 | 1.09 | 0 | -1.92 | 1.58 | 0.608 | 0.00531 | 0.455 |
| 0.4 | 3.03 | 1.18 | 0 | -1.69 | 1.58 | 0.608 | 0.00357 | 0.406 |
| 0.6 | 2.86 | 1.41 | 0 | -1.93 | 1.58 | 0.608 | 0.00257 | 0.477 |
| 0.8 | 1.82 | 1.50 | 0 | -1.83 | 1.58 | 0.608 | 0.00215 | 0.497 |
| 1.0 | 1.43 | 1.56 | 0 | -1.83 | 1.58 | 0.608 | 0.00114 | 0.560 |
| 1.5 | -0.433 | 1.50 | 0 | -1.45 | 1.58 | 0.608 | -0.000843 | 0.542 |
| 2.0 | -0.987 | 1.50 | 0 | -1.38 | 1.58 | 0.608 | -0.00220 | 0.517 |
| 3.0 | -1.67 | 1.59 | 0 | -1.41 | 1.58 | 0.608 | -0.00367 | 0.647 |
| 4.0 | -2.20 | 1.67 | 0 | -1.46 | 1.58 | 0.608 | -0.00439 | 0.656 |
| PGA-gals | 11.5 | 0.657 | 0 | -2.09 | 63.7 | 0.128 | -0.00397 | 0.398 |

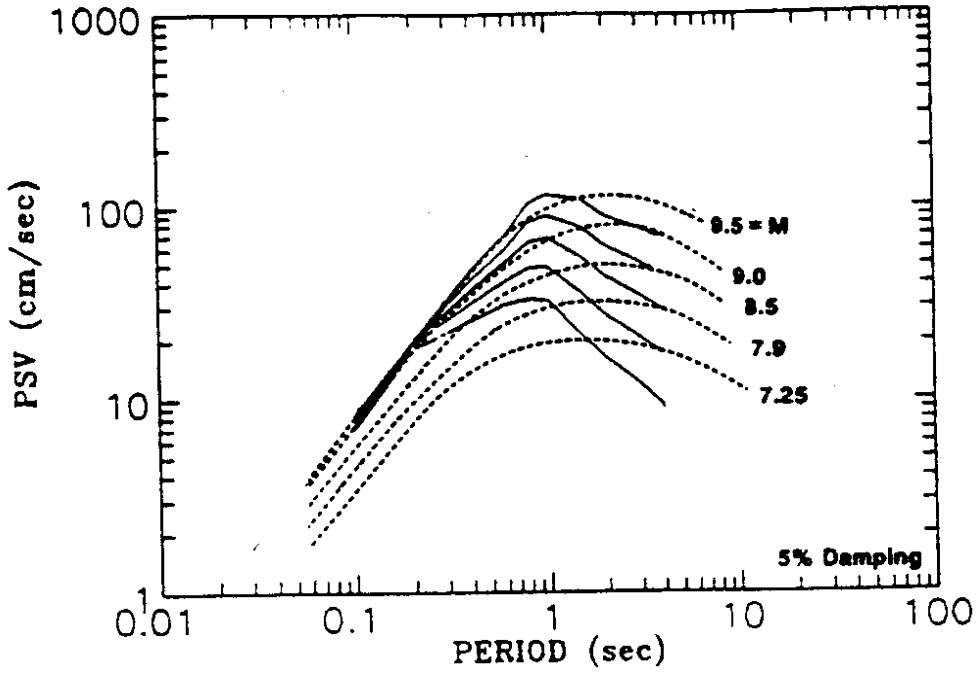


Figure 10 Average and median CSZ response spectra, coast ranges sites.

"Comparison of [Crouse's] median PSV spectra (solid lines) estimated for Washington Coastal Ranges site and PSV spectra (dashed lines) based on simulations of Heaton and Hartzell (2)" (From (30))

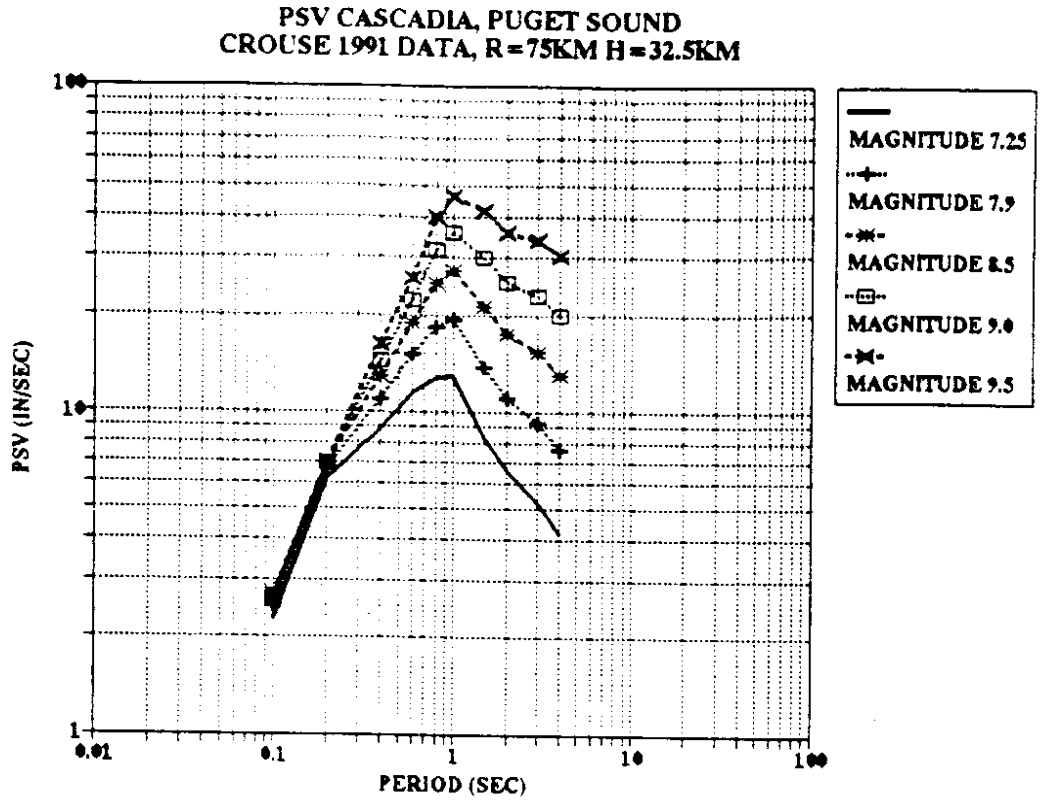


Figure 11 Median PSV spectra estimated for Puget Sound Sites (After (30))

### 2.2.3.4 Postulated Duration of Cascadia Subduction Earthquakes

There is little definitive information describing the duration of a hypothetical large subduction earthquake in the Cascadia Subduction zone. Heaton and Hartzell (11) estimate 4 minutes total shaking, as noted above, to be an upper bound. Chang and Krinitzsky (32) provide estimates of upper bounds for durations of earthquakes at soil and rock sites. These are shown in Table 2. The duration they used was bracketed duration, defined as the time between the acceleration's first and last exceedence of 5 percent of gravity. Krinitzsky, et al (33) performed regression analyses for duration versus magnitude and epicentral distance. They performed separate analyses on shallow focus and subduction earthquakes. For the subduction zones, data from Japanese earthquakes with focal depths greater than 20 kilometers duration was used. Results from this study are shown in Figures 12 and 13. These figures show that duration increases with increasing epicentral distance. Donovan (34) performed similar regression analyses using a worldwide data base of all types of earthquakes. See Figure 14. Data in both Krinitzsky, et al (33) and Donovan's (34) studies does not exceed Richter magnitude 8.3. Historical accounts of large subduction earthquakes, such as the 1960 Chile and 1964 Alaska earthquakes, may provide a better estimation of the upper bound of the expected duration in a large subduction earthquake in the Cascadia subduction zone.

According to kinematic modeling, earthquake duration is proportional to the rupture area. Each faultlet has a slip function that defines when it begins relative to that of other mini-earthquakes. The entire rupture is assumed to initiate at one location (the hypocenter) and spread over the entire interface. The furthest mini-rupture area from the source of the earthquake will begin last. The greater the faultlet's hypocentral distance the greater its slip function will be and the later its mini rupture will begin. The effect of larger slip functions is a longer duration.

Table 2 Durations for Different Earthquake Magnitudes (after (32))

| | Duration (sec)* | |
|---|---|---|
| Magnitude | Rock | Soil |
| 5.0 | 4 | 8 |
| 5.5 | 6 | 12 |
| 6.0 | 8 | 16 |
| 6.5 | 11 | 23 |
| 7.0 | 16 | 32 |
| 7.5 | 22 | 45 |
| 8.0 | 31 | 62 |
| 8.5 | 43 | 86 |

* using bracketed duration

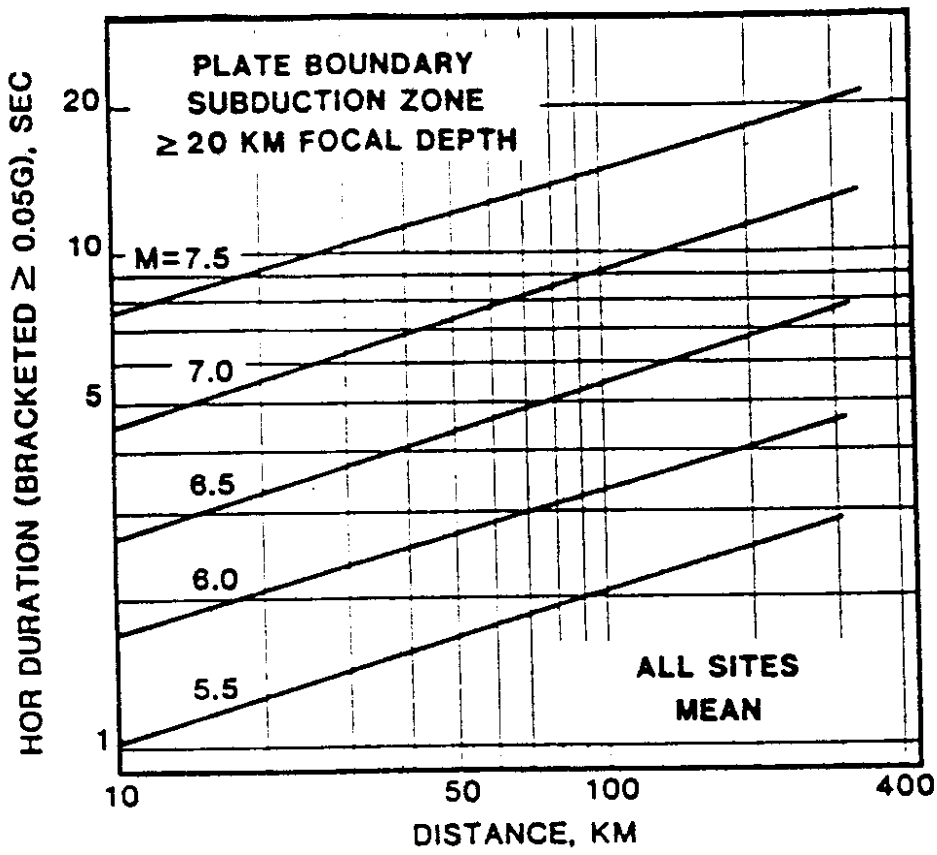


Figure 12 Mean duration for subduction zones (From (33))

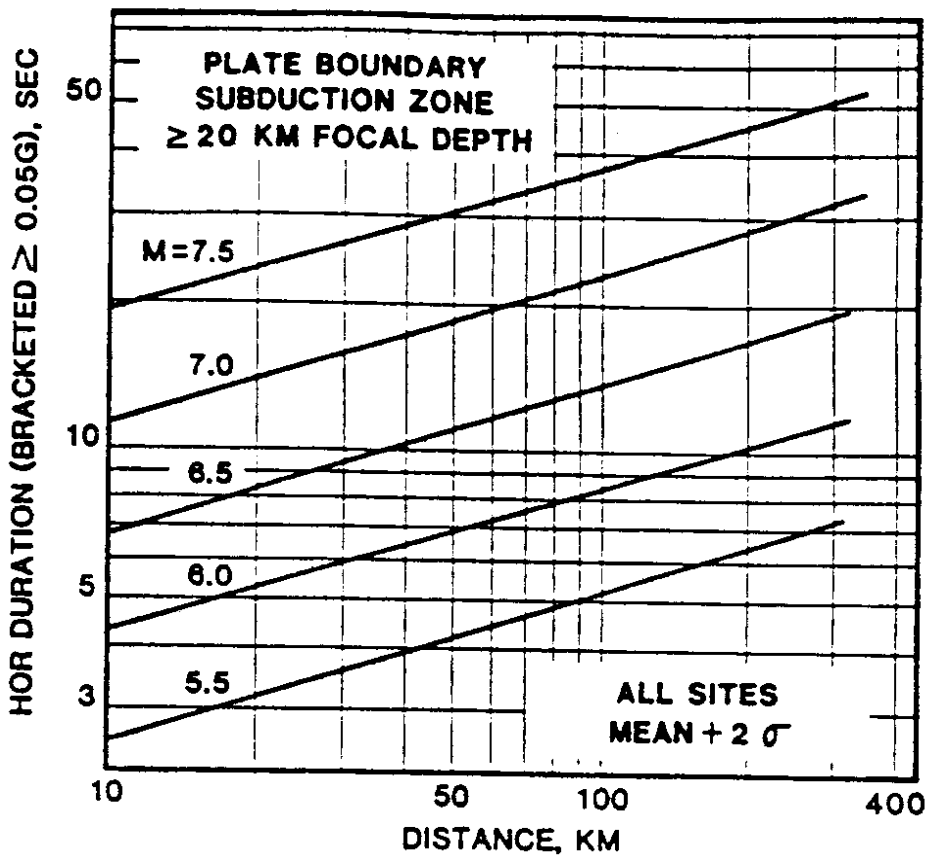


Figure 13 Subduction zone duration, 98th percentile. (From (33))

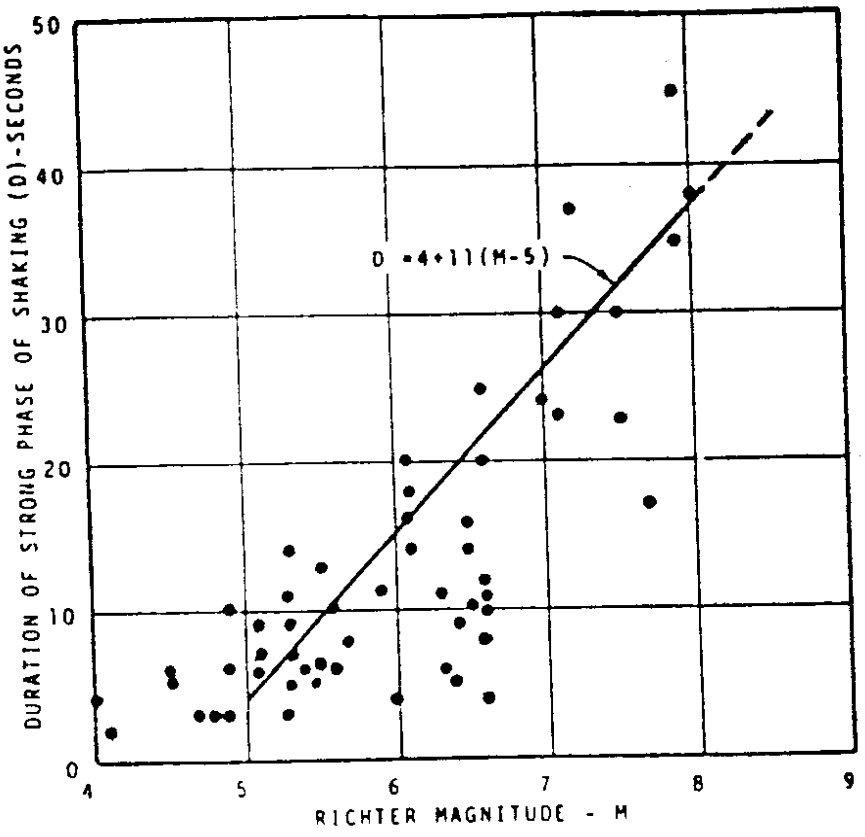


Figure 14 Relationship between magnitude and duration of strong phase of shaking (after (34) from (1))

Because moment magnitude is directly related to fault rupture area, moment magnitude should have a direct relationship with earthquake duration. This is reflected in the work by Donavan and Krinitzsky, et al. Chang and Krinitzsky's (32) upper bound of duration at a given magnitude was used to define the upper bound of the durations of artificial acceleration records used in this research. See Section 2.3.1 of this report.

### 2.2.4 Quantifying the Effects of Duration

It is necessary to identify parameters that reflect the effects of earthquake duration. Various quantities have been used to relate the effects of strong ground motion on structural response: peak ground acceleration, response spectra, effective peak acceleration and cumulative damage. Peak ground acceleration does not reflect structural response, only ground motion. Elastic response spectra reports the maximum structural acceleration and structural displacement occurring during an earthquake. Inelastic response spectra reports the structural yield force (or acceleration), the structural yield displacement, and the total structural displacement occurring during an earthquake. Response spectra do not relate the time at which the peak displacement occurs. Since peak displacement is not a cumulative quantity it will not be strongly affected by duration. With longer durations there is conceivably a higher probability that larger structural displacements may occur, however the relationship is not a strong one. As noted previously in this chapter, effective peak acceleration is defined in terms of the response spectra (25), therefore it also does not strongly reflect duration.

Measuring the hysteretic energy dissipated has been used to quantify cumulative damage on the structure ((35), (36),(37)). Studies show that energy dissipation is related to ground motion duration ((37),(38)). Powell and Allahabadi (35) state that hysteretic

cycle counts may also be used to quantify damage. This section of the report reviews work in quantifying the effects of ground motion duration, specifically in terms of damage.

### 2.2.4.1 Damage Parameters

Care must be exercised when evaluating damage parameters. As noted herein, damage is a parameter that, with all other factors being the same, reflects earthquake duration. According to Powell and Allahabadi (35) damage can be measured by two types on indices. One compares damage demand to capacity. This can be expressed as follows:

$$DI_s = ((\delta_c - \delta t) / (\delta u - \delta t))^m \qquad \text{(Equation 6)}$$

where:

- $DI_s$ is the structural damage index
- $\delta_c$ is the calculated damage parameter
- $\delta_u$ is the damage parameter corresponding to ultimate failure
- $\delta_t$ is the threshold damage parameter
- m is an exponent describing the rise of the damage index (see Figure 15 )

For $DI_s$ less than 1.0 the structure will be damaged but not to the point of failure. Once $DI_s$ reaches unity the structure is theoretically at the failure condition. The damage parameter $\delta$ could express the energy dissipated by a structure. In that case $\delta_t$ would be the strain energy stored at yield, $\delta_u$ the hysteretic energy dissipation capacity plus the strain energy at yield, and $\delta_c$ the strain and hysteretic energy demanded of a structure.

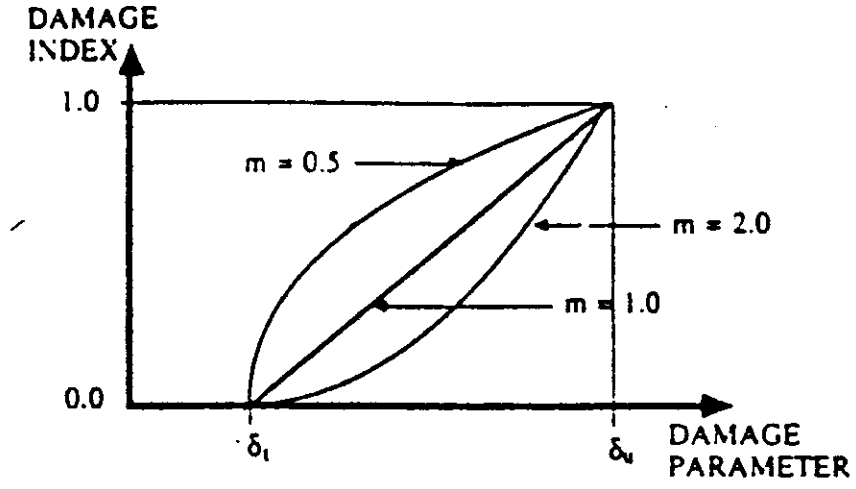


Figure 15 Damage parameter and index relationships (from (35))

A demand versus capacity damage index can be based on the maximum values, maximum ranges, or cumulative values of strength, displacement deformation, or energy dissipation. Powell and Allahabadi (35) state that a maximum value approach is most appropriate with strength and total energy demand based indices. A cumulative value approach is appropriate for inelastic deformation based indices. They also note that although it is relatively easy to determine demand, capacity estimates are more difficult. Structure capacity ($\delta_u - \delta_t$) may not be constant, rather it may be a function of the inelastic displacement sequence. For example, structure capacity might be one value for one single displacement excursion to failure and it might be another value for sustained cycling at a lower ductility level. Powell and Allahabadi (35) also note that the ground motion is the largest source of uncertainty in any earthquake damage index computation.

The second type of damage index is evaluating damage in terms of degradation of a parameter. Degradation indices are based on comparing a structural property in an undamaged state to that in a damaged state. They may be expressed as in the case of the demand versus capacity damage indices, however the damage parameter, $\delta$, may be defined as follows:

$$\delta = 1 - P_D / P_O \qquad \text{(Equation 7)}$$

where:

$\delta$ is the damage parameter

$P_D$ is a property of a structure in an damaged state

$P_O$ is a property of a structure in an undamaged state.

Stiffness, strength, and potential energy (strain energy at yield plus hysteretic energy capacity) are possible choices for damage parameters (35). This type on index does not

predict failure, it only compares a damaged property value to an undamaged property value. Because a degrading index does not predict failure, it was not used in this research.

Damage indices can be calculated at the entire structure level or on an element or substructure level. Powell and Allahabadi (35) note that measuring damage at the structure level will yield overall response quantities but will lack precision. More information is obtained from a substructure or member level approach.

In their discussion on energy dissipation, Powell and Allahabadi (35) state "it can be postulated that a structure has a limited capacity to dissipate energy and that damage occurs as this capacity is exhausted. Hence, a possible choice for a damage parameter is the amount of energy dissipated." Energy dissipation can be calculated at the member, substructure or structure level. As total energy dissipated is a maximum value calculated on a cumulative basis, it combines the maximum value and cumulative value approaches of measuring damage.

Since capacities of structures are difficult to determine, this research did not determine damage indices based on demands and capacities. Rather, only demands were determined. Demands from CSZ records were compared with demands of actual acceleration records and code compatible records. See the Section 2.3 and Chapters 3 and 4 of this report.

Duration of strong ground motion is often listed as one of the major factors in determining response and is therefore an important parameter (1). The longer the duration the more energy is imparted to the structure. When the structure yields, the structure dissipates energy. Most structures are designed to behave inelastically during larger earthquakes. When a structure behaves inelastically, it is dissipating hysteretic energy and, thus, it is being damaged. Damage, as measured by hysteretic energy dissipated, is therefore directly related to the duration of strong shaking, provided that the ground motion is strong enough to cause inelastic behavior. A dynamic response-history analysis

is performed to measure the energy dissipation demands and so the inferred damage. A history of damage parameter values is obtained (36). The history of values can be monitored to determine when a demand to capacity damage index exceeds unity, thus implying failure.

Another parameter used to measure the cumulative damage is the number of hysteretic cycles a structure or member experiences. Powell and Allahabadi (35) note that in an earthquake the deformation history is unlikely to consist of full regular cycles, and thus it is more appropriate to count half-cycles rather than full cycles.

According to Dowling (39) there are a number of methods to count half cycles: rain flow counting, range pair counting, peak counting, level crossing counting, range counting, and mean crossing peak counting. He states that only two methods, rain flow and range pair counting, account for all the effects of varying cycle amplitude, varying cycle frequency, and random sequencing of peaks from cycle to cycle. All these characteristics are found in structural response to earthquake ground motion.

Since rain flow counting was used in this research, it is briefly described conceptually. The displacement history is plotted with the time axis vertical and the lines connecting cycle peaks are imagined to be pagoda roofs, half cycles are defined by the flow of rain off the "roofs". A half cycle that starts as a relative maximum will continue until a subsequent displacement, in the direction opposite to the initial direction, has a greater absolute displacement. A half cycle that starts as a relative minimum will continue until a subsequent displacement, in the direction opposite to the initial direction, has a lesser absolute displacement. A half cycle amplitude will continue to increase if displacement in the initial direction continues to increase. See Figure 17.

In rain flow counting methods, cycles and half cycles can be categorized in ranges of displacement or, in the case of bi-linear inelastic elements, ductility demand. This counting method can then be used to compare predicted earthquake cyclic demands to

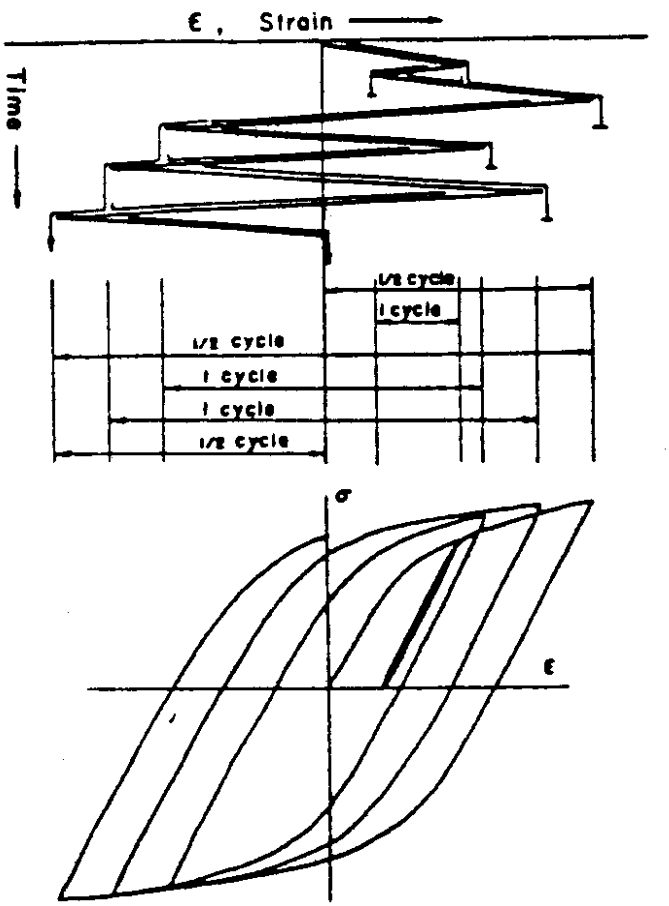


Figure 17 Example of rainflow counting (from (39))

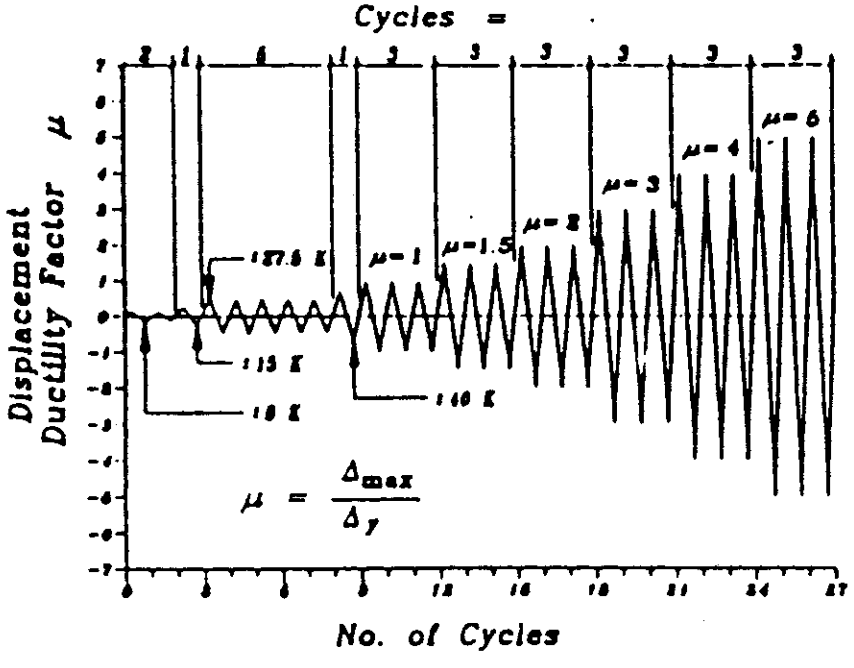


Figure 18 Example of displacement history used in laboratory testing (from (40))

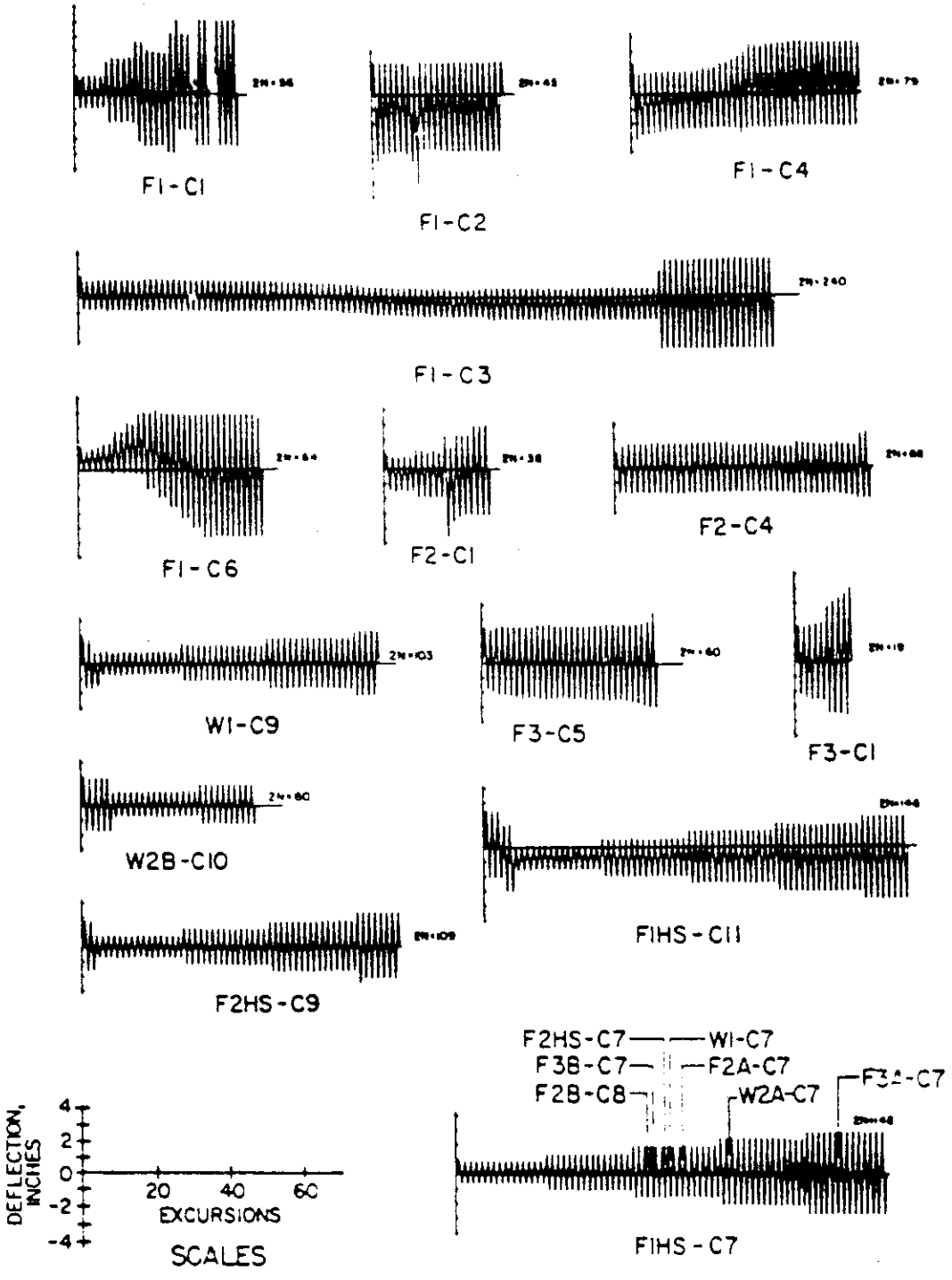


Figure 19 Examples of displacement histories used in laboratory testing (from (41))

those imposed during typical laboratory testing. Some examples of laboratory cyclic loading are shown in Figures 18 and 19. In Figure 18 the structure is loaded elastically first for many cycles, then to the yield displacement for three cycles, then to one and a half times the yield displacement (ductility equal to 1.5) for three cycles, then to twice the yield displacement (ductility equal to two) for three cycles, and so on, increasing the ductility after every three cycles. This pattern is continued until failure occurs. Such a pattern is similar but not necessarily identical to most testing sequences. Although laboratory cyclic testing sequences are regular in sequence and the amplitudes increase uniformly, unlike seismic behavior, a comparison between such tests and actual seismic behavior may assist in the assessment of demand on a structure relative to capacity of the structure.

Another method of determining the earthquake demand on a structure or substructure is to determine the total hysteretic energy demand in terms of equivalent hysteretic cycles at a specified ductility level. This calculation is simply the total hysteretic energy demand, determined from a response-history analysis, divided by the hysteretic energy dissipated in one cycle at the specified ductility. This demand may be compared to the capacity exhibited by laboratory testing of a structure displaced in hysteretic cycles to the same specified ductility level. Although this method ignores the random amplitude and sequencing of cycles occurring during an earthquake, it does provide a direct comparison between a structure's tested capacity to the demands made on similar elements during an earthquake.

#### 2.2.4.2 Studies Relating Damage and Earthquake Duration

For actual earthquakes, Trifunac and Brady (27) correlated duration with damage by comparing duration to the Modified Mercalli Intensity. They defined duration as the time it takes to accumulate 90 percent of the accelogram intensity (the integral of the

acceleration squared with respect to time). See Equation 2 and Figure 6. They observed that an increase in duration was accompanied by an increase in damage as measured by the Modified Mercalli rating. They also estimated duration based on the magnitude of the earthquake. Their data base was composed of mostly California data: thus their regression equations and constants should not be extrapolated to subduction zone events.

Krinitzsky and Chang (42) also used this approach, but they used a worldwide data base. Subduction earthquakes were separated from other earthquakes when comparing magnitude to duration but not when comparing intensity to duration. They used a bracketed duration, defined as the time between the first and last exceedence of 0.05 g. Typically the Trifunac and Brady duration is slightly shorter than the bracketed duration. They compared earthquake magnitude with duration. However the upper limit of their data, in terms of magnitude, is about Richter magnitude 8 and in terms of Modified Mercalli Intensity is about VIII. Extrapolating to larger magnitude levels may be inaccurate since there are few strong motion records of events greater than magnitude 7.5.

As noted above, most structures are designed to behave inelastically during a large earthquake. If a structure is properly designed to maintain its strength and stiffness while experiencing such inelastic action, damage caused by yielding should be minimal. However, damage will occur despite proper detailing when the energy demand of the earthquake exceeds the capacity of the structure to dissipate energy. The energy demand of an earthquake depends on the time history, the intensity of the event and the sequence of acceleration pulses, and the response of the structure. It is important to note that there is currently no widely accepted method for assessing the energy dissipation capacity of a structure.

Currently, the use of response spectra is one method to represent the response of a system to earthquake motion. With inelastic response spectra, the displacement ductility

demand can be used to quantify maximum inelastic deformation. Displacement ductility demand is defined by the maximum inelastic displacement divided by the yield displacement. Zahrah and Hall (36) note that displacement ductility does not account for cumulative damage, since it is a single point-in-time maximum. Displacement ductility demand, likewise does not reflect the number of reversal cycles incurred, only the maximum response at one or more inelastic excursions. They quantified cumulative damage from an earthquake ground motion by measuring the energy imparted to the structure, the energy dissipated by damping and hysteresis, and the number of yield excursions and reversals experienced. They observe that, with longer duration, there is more inelastic action, the number of yield excursions increases as the maximum displacement ductility demand increases, increasing damping reduces the number of yield excursions, and inelastic (or secondary) stiffness has little effect on the number of yield excursions. They also defined an index to measure the amount of damage demand. The index is the measure of the equivalent number of hysteretic cycles at the maximum ductility level, experienced during an earthquake. It is calculated by dividing the total hysteretic energy dissipated by the area under the resistance-displacement curve for the structure when loaded monotonically to the maximum ductility level. This may be written as:

$$N = E_h / \omega^2 U_y^2(\mu-1) \qquad \text{(Equation 8)}$$

where:

- $N$ is the damage index
- $E_h$ is the total hysteretic energy dissipated
- $\omega$ is the natural circular frequency of the structure
- $U_y$ is the structure's yield displacement

$\mu$ is the maximum ductility demand

Jeong and Iwan (38) performed an analytical study of duration effects on damage of structures. They used the linear cumulative damage rule proposed by Palmgren and Miner to quantify damage. With this rule, damage at a given ductility level is calculated as the number of cycles experienced at that ductility level divided by the total number of cycles at that level to produce failure. Failure was determined according to:

$$N\mu^s = C \qquad \text{(Equation 9)}$$

where:

| | |
|---|---|
| N | is the number of cycles to failure at a constant ductility |
| $\mu$ | is the ductility |
| C and s | are empirical constants |

Cycle counting was determined by the level crossing method. Total damage is the sum of the damage caused at all ductility levels. They used maximum deformation and absorbed hysteretic energy to measure damage. They used artificial earthquakes generated as a random white noise process. The overall longest artificial earthquake duration was 30 seconds. With this analysis Jeong and Iwan (38) found a direct relation between damage (hysteretic energy dissipated) and both response ductility demand and duration of excitation.

Uang and Bertero (37) found a strong, nearly linear relation between Trifunac and Brady duration and an amplification factor. The amplification factor relates absolute structural spectral velocity to maximum ground acceleration. For given ductility levels, system damping value and ground motion intensities (maximum velocity and duration),

they determined the maximum structure velocity and absolute energy supplied to the structure. To avoid failure, the energy capacity of the structure should be greater than the energy demanded of the structure. Energy capacity consists of the sum of kinetic energy capacity, strain energy storage capacity, damping dissipating capacity and hysteretic dissipating capacity. The correlation between duration and energy demand reveals a positive relation between earthquake duration and structural damage.

Common conclusions from the above mentioned research are: 1) damage demand is reflected by the hysteretic energy demand and the number of inelastic cycle counts but not by response spectra (either elastic or inelastic) or by ductility demand; 2) duration is directly related to damage, as reported quantitatively in the form of hysteretic energy dissipated or inelastic cycle counts, or as reported qualitatively in the form of Modified Mercalli Intensities.

How damage demand can be compared to damage capacity is difficult, as it is difficult to determine a structure's capacity. Cycle counts for and hysteretic energy dissipated by lab specimens provide one method of determining a substructure capacity. Damage demands can be compared to such capacities, as will be discussed in Chapter 4.

Another method to evaluate damage demand of postulated subduction earthquake ground motion is to compare it with the damage demands of actual ground motions and design code compatible ground motions. Capacities of structures designed to current codes should be greater than the demands of code compatible ground motions. If postulated ground motion damage demand is greater than code compatible motion damage demand, then capacities based on current design codes may or may not be adequate. Code designed structures may still have capacities greater than postulated demands, however the factor of safety against failure may be reduced. The comparison of postulated damage demands with code compatible damage demands provides an initial

evaluation to see if further investigation is warranted. The comparison will not provide a conclusion that failure is likely.

## 2.3 RESEARCH APPROACH

To determine the inelastic structural response to earthquakes, a response-history analysis is required. Response-history analysis requires an acceleration record of the ground motion under investigation. In order to estimate structural response to postulated Pacific Northwest long-duration, large-magnitude earthquakes, acceleration records reflecting the postulated ground motion are required. As was pointed out in Section 2.2, there are no acceleration records with long-durations and large-magnitudes available. The largest acceleration records of earthquakes in the region are from the 1949 Olympia and the 1965 Puget Sound earthquakes. Both of these are of magnitude and duration much smaller than that postulated for a large subduction earthquake. Therefore, artificial acceleration records are used as a substitute for actual acceleration records.

This portion of the report explains how artificial earthquakes were generated and how response-history analyses were performed for this research. Programs, program input, magnitude and duration combinations, and structural models used are discussed in this section.

### 2.3.1 Artificial Acceleration Generation

According to Housner and Jennings (43) artificial acceleration records were first modeled as a random process by Housner in 1947. However the process cannot be totally random, that is, with an end product of accelograms with the characteristics of white noise. An artificial acceleration record that resembles white noise produces an undamped

velocity spectrum which is constant. Such is not the case for actual earthquake records. An artificial acceleration record should produce velocity spectra that match the spectra that actual earthquake records produce.

This research used the program SIMQKE (44) to generate artificial Pacific Northwest subduction earthquakes. SIMQKE produces artificial acceleration records that are compatible with a user supplied "target" elastic response spectra. A detailed description of the theories and methods incorporated into SIMQKE is found in *SIMQKE, A program for Artificial Motion Generation User's Manual and Documentation* (45). The reader is referred to that document for anything more than the brief overview in this section, which includes only general principles explaining the generation of Pacific Northwest ground motions.

SIMQKE generates an artificial earthquake record by randomly generating a series of sinusoidal waves and then superimposing them. This may be written as:

$$x(t) = \sum A_i \sin(\omega_i t + \phi_i) \qquad \text{(Equation 10)}$$

where:

$A_i$ is the amplitude of the ith contributing sinusoid

$\phi_i$ is the phase angle of the ith contributing sinusoid

$\omega_i$ is the natural frequency of the sinusoid

t is time

x is acceleration

To determine wave frequencies and amplitudes, SIMQKE determines the power spectral density of a user supplied target elastic response spectrum and attempts to match it. The amplitudes, $A_i$, are determined by the target spectrum. Then, SIMQKE uses a

random number generation algorithm to determine the phase angles of the sinusoids. A seed value is specified by the user for the random generation of phase angles. A change in the seed value will create a different acceleration record that is also compatible with the target spectrum.

SIMQKE also allows the user to specify the acceleration record envelope and the total duration. The envelope describes how the acceleration history varies in the time domain. The envelope function may be trapezoidal, exponential, compound, or level, as is shown in Figure 20.

The response spectra used in this research were those of: Crouse (30), Heaton and Hartzell (11), and AASHTO (5). Crouse's spectra is for median Cascadia subduction zone earthquakes. Both epicentral distance and focal depth of 30 kilometers were used in Crouse's regression formulae for coast range response spectra. The resulting response spectra may be seen in Figure 10. An epicentral distance of 75 kilometers and a focal depth of 32.5 kilometers were used for Puget Sound spectra. The response spectra for Puget Sound sites may be seen in Figure 11. Heaton and Hartzell's spectra were used for generation of magnitude 9.5 giant earthquakes. These spectra and the resulting acceleration records are considered to be the upper bound spectra and records of possible CSZ earthquakes. They are shown in Figure 8.

AASHTO spectra were used to generate acceleration records compatible with current design code criteria. These spectra are shown in Figure 21. Note that 0.2 was used for $A_a$, the effective peak acceleration coefficient. This may be lower than what local transportation officials use, but it is what is specified in the AASHTO Code (5). A value of 1.0 was used for the soil coefficient, S, for firm soil sites. Values for softer soil sites were also used to generate code compatible acceleration records reflecting softer soils.

To generate earthquakes that represent ground motion of Washington soil sites, Crouse's spectra for median earthquakes were amplified by Tsiatas, et al's (3) acceleration

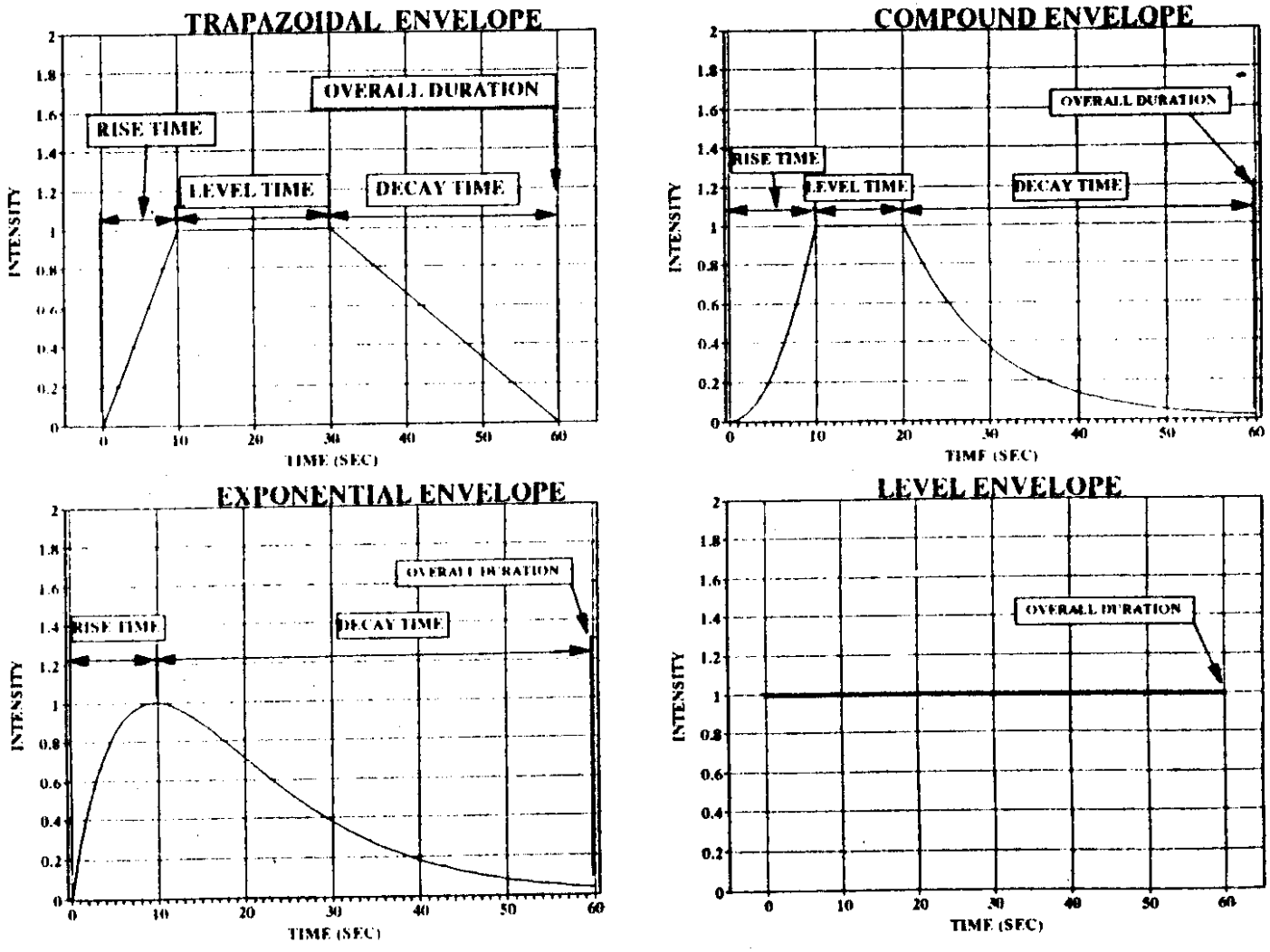


Figure 20 Intensity Envelopes used in SIMQKE

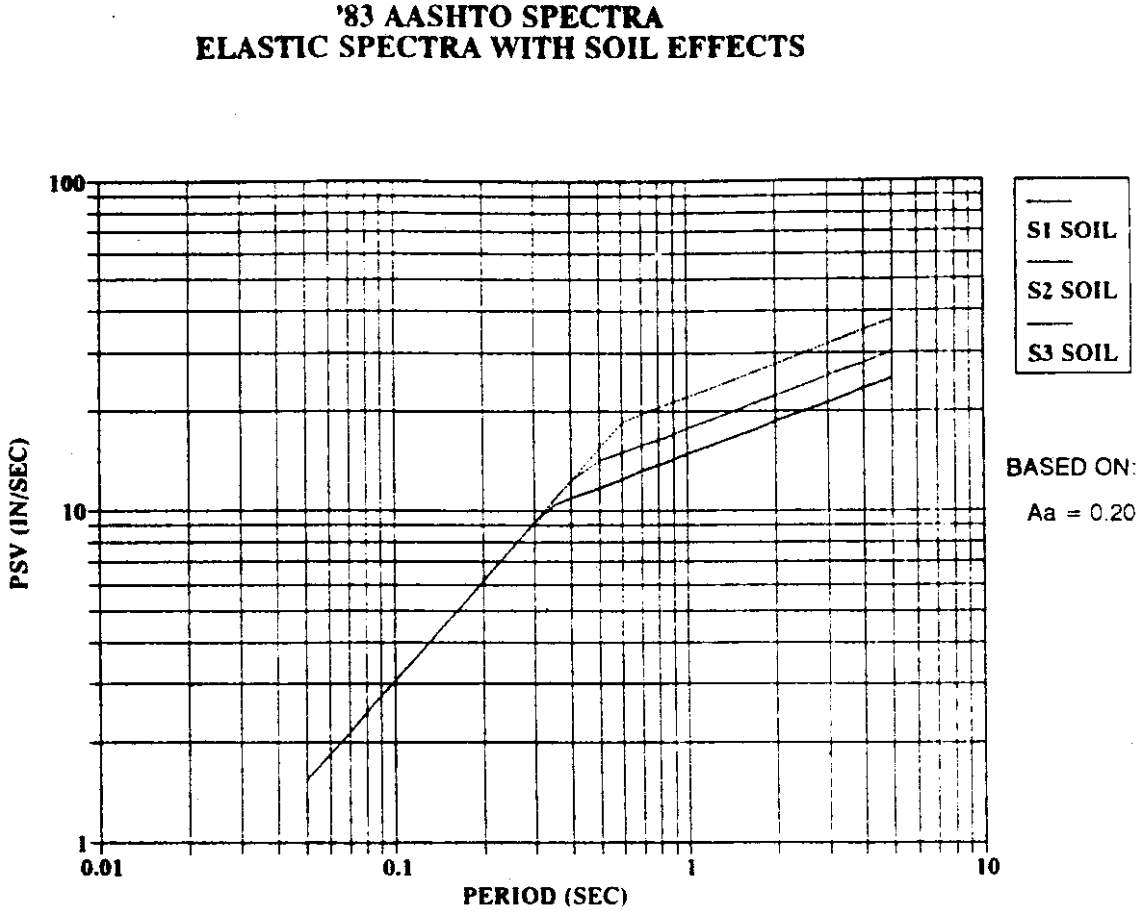


Figure 21 AASHTO Design Spectra

amplification factors. To use these amplification factors the effective peak acceleration (EPA) of the earthquake was needed. The EPA was determined for Crouse's (30) spectra for median CSZ earthquakes. The determined EPA values are listed in Table 3. The amplification factors were interpolated from the values provided by Tsiatas, et al (3). See Tables 4 and 5 for soil amplification factors and soil modified response spectra.

Only Soil Groups 1 and 5, as defined by Tsiatas, et al, were used in this study. Group 1 consists of medium to dense cohesionless soil less 20 to 50 feet thick with less than 5 feet of loose soil at the surface. Group 1 had the largest amplification factors, of all soil groups, in the period range less than 0.4 seconds. Group 5 soils consist of medium to dense cohesionless soils 50 to 100 feet thick. Group 5 has the largest amplification factors in the period range of 0.6 to 1.0 seconds.

A compound envelope, as shown in Figure 20, was used in SIMQKE. This envelope is similar to that used by Jeong and Iwan (38). It consists of a power curve rise section, a level section and an exponential decay section. The power curve rise portion was parabolic and the exponential decay was set to produce a final amplitude of 2 percent of the level portion.

Time lengths of the rise, level and decay portions of the envelope were proportional to those of Heaton and Hartzell's maximum acceleration history. See Figure 7. This is the record for their hypothesized giant earthquake as determined by using kinematic modeling. The overall duration was estimated to be 240 seconds, the rise portion to be 42 seconds, the level time 48 seconds and the decay period to be 150 seconds. The rise portion represents 17.5 percent of overall duration, the level potion 20 percent and the decay portion 62.5 percent. For other overall durations these percentages were multiplied by the desired overall duration to determine the rise, level, and decay times.

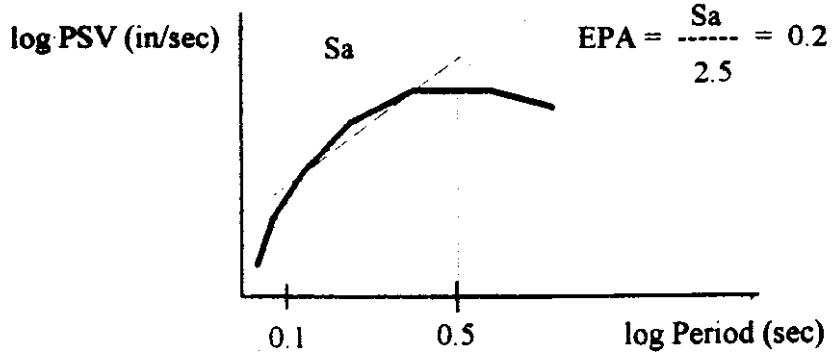


1) Determine EPA for site, magnitude and duration; eg: 0.2

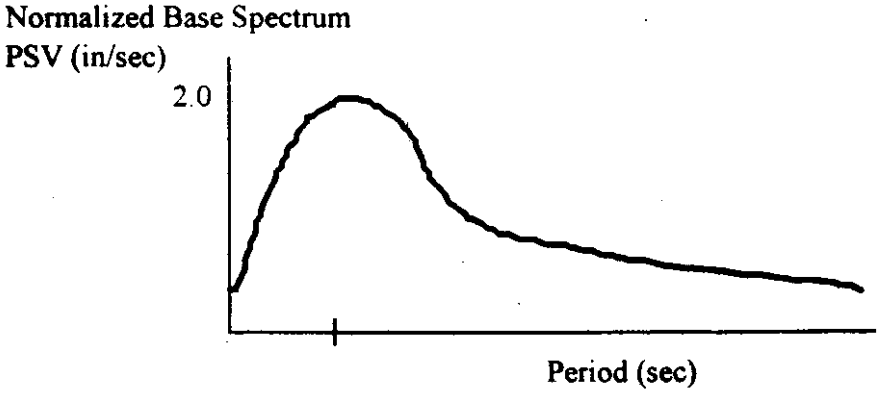


2) Determine Normalized Base Spectrum ordinate for period of interest; eg.: 2.0

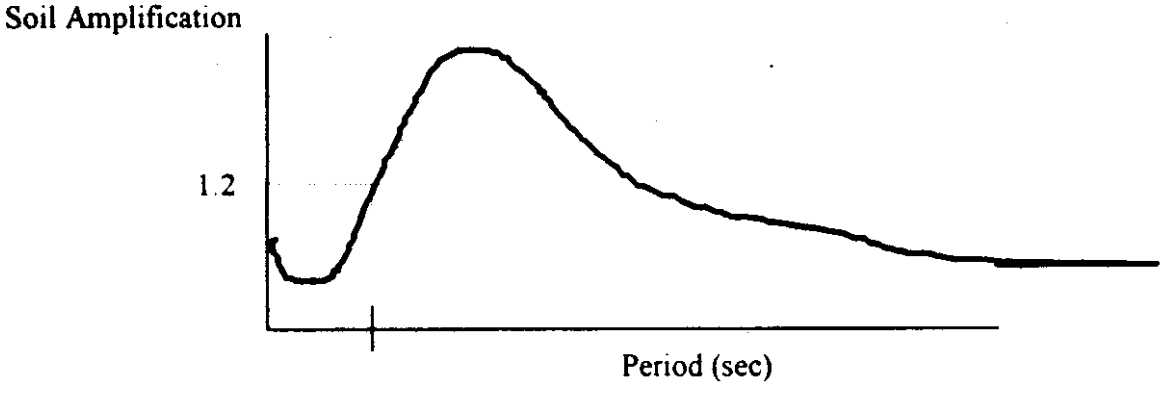


3) Determine Soil Amplification ordinate for period of interest eg.: 1.2

4) Then determine amplified spectrum ordinate at that period eg.: Cs = 0.2 x 2.0 x 1.2 = 0.48

Figure 22 Spectral Amplification for Washington Soils

**Table 3** EPA Values for Crouse's Spectra for Median CSZ Earthquakes

| Location | Puget Sound | Coast Range |
|---|---|---|
| Epicentral Distance, R | 75 | 30 |
| Focal Depth | 30 | 30 |
| EPA for Magnitude: | | |
| 7.25 | 0.103 | 0.161 |
| 7.9 | 0.134 | 0.185 |
| 8.5 | 0.162 | 0.206 |
| 9.0 | 0.185 | 0.222 |
| 9.5 | 0.207 | 0.237 |

Table 4 Soil Amplification Factors and Amplified Response Spectra for Soil Group 1

Puget Sound sites

Soil Group 1

| Period (sec) | Soil Amplification Factors EPA (gals) 0.10 | 0.20 | 0.30 | Amplified Response Spectra Values (in/sec) Magnitude (Mw) 7.25 | 7.9 | 8.5 | 9.0 | 9.5 |
|---|---|---|---|---|---|---|---|---|
| 0.10 | 1.309 | 1.244 | 1.169 | 1.88 | 2.28 | 2.59 | 2.87 | 2.92 |
| 0.20 | 1.326 | 1.327 | 1.296 | 5.19 | 6.31 | 7.15 | 7.69 | 8.04 |
| 0.40 | 1.168 | 1.241 | 1.280 | 6.91 | 9.64 | 12.51 | 15.08 | 17.74 |
| 0.60 | 1.082 | 1.134 | 1.185 | 7.72 | 11.68 | 16.21 | 20.60 | 25.53 |
| 0.80 | 1.043 | 1.072 | 1.100 | 8.48 | 13.88 | 20.79 | 28.20 | 37.36 |
| 1.00 | 1.016 | 1.032 | 1.047 | 8.35 | 14.17 | 21.94 | 30.59 | 41.65 |
| 1.50 | 0.999 | 1.006 | 1.015 | 5.84 | 10.52 | 17.40 | 25.81 | 37.57 |
| 2.00 | 1.006 | 1.011 | 1.016 | 4.69 | 8.61 | 14.51 | 21.88 | 32.42 |
| 3.00 | 1.003 | 1.006 | 1.010 | 3.69 | 7.12 | 12.54 | 19.63 | 30.18 |
| 4.00 | 0.980 | 0.983 | 0.985 | 2.84 | 5.69 | 10.37 | 16.69 | 26.35 |

Table 5 Soil Amplification Factors and Amplified Response Spectra for Soil Group 5

Puget Sound sites

Soil Group 5

| Period (sec) | Soil Amplification Factors EPA (gals) 0.10 | 0.20 | 0.30 | Amplified Response Spectra Values (in/sec) Magnitude (Mw) 7.25 | 7.9 | 8.5 | 9.0 | 9.5 |
|---|---|---|---|---|---|---|---|---|
| 0.10 | 1.008 | 0.743 | 0.643 | 1.43 | 1.63 | 1.72 | 1.74 | 1.73 |
| 0.20 | 1.019 | 0.786 | 0.633 | 3.96 | 4.48 | 4.72 | 4.76 | 4.71 |
| 0.40 | 1.538 | 1.202 | 1.021 | 9.02 | 11.52 | 13.70 | 15.35 | 16.96 |
| 0.60 | 1.770 | 1.620 | 1.493 | 12.57 | 18.26 | 24.39 | 30.05 | 36.16 |
| 0.80 | 1.612 | 1.714 | 1.666 | 13.11 | 21.71 | 32.83 | 44.88 | 59.51 |
| 1.00 | 1.502 | 1.544 | 1.552 | 12.35 | 21.04 | 32.66 | 45.66 | 62.23 |
| 1.50 | 1.372 | 1.420 | 1.390 | 8.03 | 14.60 | 24.33 | 36.30 | 52.95 |
| 2.00 | 1.129 | 1.236 | 1.251 | 5.28 | 9.96 | 17.19 | 26.42 | 39.66 |
| 3.00 | 1.070 | 1.124 | 1.145 | 3.94 | 7.71 | 13.77 | 21.79 | 33.75 |
| 4.00 | 1.046 | 1.072 | 1.086 | 3.03 | 6.11 | 11.22 | 18.15 | 28.77 |

The amplitude envelope described in the preceding paragraph may not be realistic in all cases but is a reasonable approximation. The amplitude envelope may vary as a function of site location and rupture sequence. The rise time may be less for a site closer to the rupture area. The decay time may also be less for a near site. If the rupture sequence is monotonic, that is it starts in one location and spreads across the rupture surface from that one source, then the envelope may resemble the compound envelope. However, if two hypocenters exist, as was the case in the 1964 Alaska earthquake, then the envelope will not resemble the compound envelope. It will be similar to two such envelopes, staggered and superimposed.

A matrix of magnitudes and overall durations was created to reflect realistic earthquakes. See Figure 23. The matrix also includes enough records to determine the sensitivity of response to duration. An upper bound of realistic durations for a given magnitude is given by Chang and Krinitzsky (32). The effective Trifunac and Brady duration of CSZ artificial earthquakes, generated by SIMQKE, was determined. Effective durations were compared with Chang and Krinitzsky's work. In general the bracketed duration used by Chang and Krinitzsky is about the same as the effective Trifunac and Brady duration (1). The differences were believed to be less than those from other significant sources of uncertainty. The magnitudes used by Chang and Krinitzsky were Richter magnitudes and not moment magnitudes as used by Crouse and Heaton and Hartzell. Because Chang and Krinitzsky's data was below magnitude 8 where moment magnitude and Richter magnitude are similar, the difference in magnitude scales was considered to be negligible.

AASHTO compatible earthquakes were created with an overall duration of 60 seconds. This overall duration, with the Heaton and Hartzell proportional envelope resulted in an acceleration record with an Arias intensity of the same order of magnitude as the 1940 El Centro record and the 1949 Olympia record.

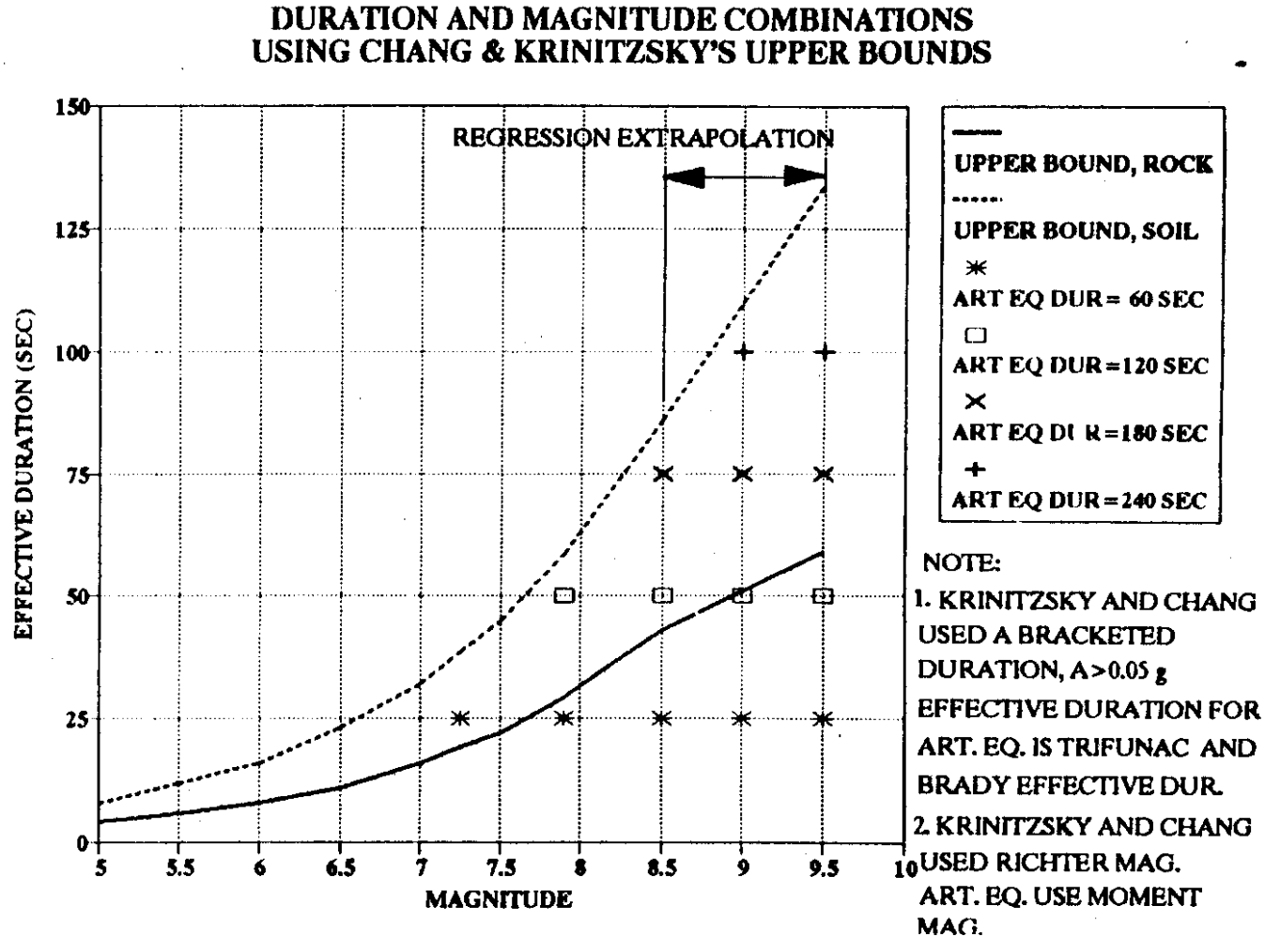


Figure 23 Magnitude-Duration Matrix

It should be noted that all of the magnitude and duration combinations were created for Puget Sound sites. Not all of the combinations were created for coast range sites. Only magnitude 7.9 and 8.5 earthquakes were created for coast range locations. Results from these coast range earthquakes were compared to Puget Sound earthquakes of the same magnitude and duration to determine sensitivity to attenuation of ground motion.

Two records were created using Heaton and Hartzell's spectra for giant earthquakes. These records had overall durations of 180 and 240 seconds to compare with the 240 second record of Heaton and Hartzell's artificial record. The three and four minute duration earthquakes also provide a comparison of artificial earthquakes based on Crouse's spectra with the same duration.

### 2.3.2 Response-History Analysis and Structural Models

Since this is one of the first research efforts in the area of long duration earthquake response, the results were intended to apply to a broad cross-section of structures. Thus, general structural models were chosen so that the number of affected variables would be limited, and single-degree-of-freedom (SDOF) models were used. Hysteretic behavior models were chosen to reflect realistic behavior. Therefore, two models were chosen to emulate actual behavior: a bi-linear model to emulate steel behavior, and a degrading stiffness model to emulate reinforced concrete behavior.

#### 2.3.2.1 Bi-linear Model Response Analysis

The response of the bi-linear model was determined using the program SPECTRUM (46). SPECTRUM performs a response-history analysis of an SDOF

structure following the structural model proposed by Menegotto and Pinto (47). Elastic and inelastic behavior, strain hardening and some non-linearity of the load-displacement curve near yielding are all incorporated into this model. See Figure 24.

SPECTRUM uses the Newmark Beta technique to perform response-history analysis. It allows the user to specify the acceleration interpolation method used in the program. Constant average acceleration was used in this research. Constant average acceleration was chosen because it is unconditionally stable in numerical integration. Other values used as SPECTRUM input were 5 percent original stiffness strain hardening, 5 percent of critical damping, and little curvature of the load displacement curve near yielding. To set the level of yielding, or the strength of the structure, SPECTRUM requires the user to specify the yield force to weight ratio of the structure. Yield force to weight ratios of 0.125, 0.25, and 0.50 were used to determine the sensitivity of the response to structural strength.

The yield force to weight ratio is defined as the lateral force that causes yielding in the structure divided by the structure weight. For a simple column structure, fixed at the base and supporting a relatively large weight at the top, the yield force is the lateral force that causes a plastic hinge to form at the base of the column. Shown on a lateral load-displacement plot, the yield force is the force at the point where the slope changes from the initial elastic stiffness to strain hardening stiffness. See Figure 25. However, for most structures there is potential for more than one plastic hinge forming and the determination of the yield force is more involved. A plastic collapse analysis is required to determine the load-displacement curve. An example of such a curve is shown in Figure 26. The yield force, in this case, is the load where extensions of the initial elastic stiffness path and strain hardening stiffness path intersect.

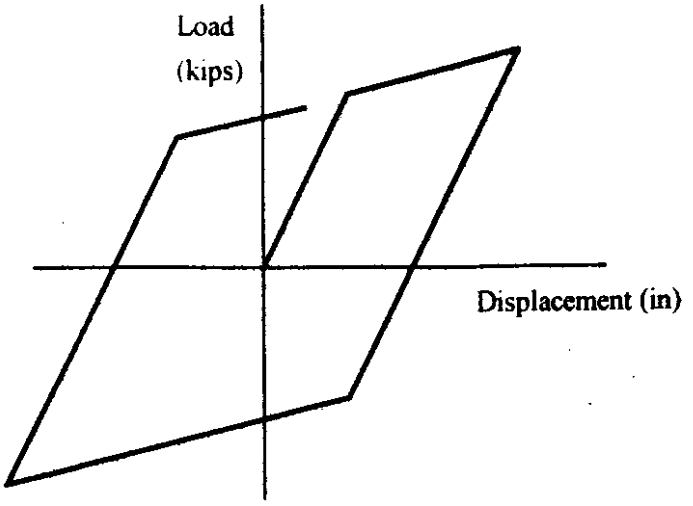


Figure 24 Bi-linear hysteretic model.

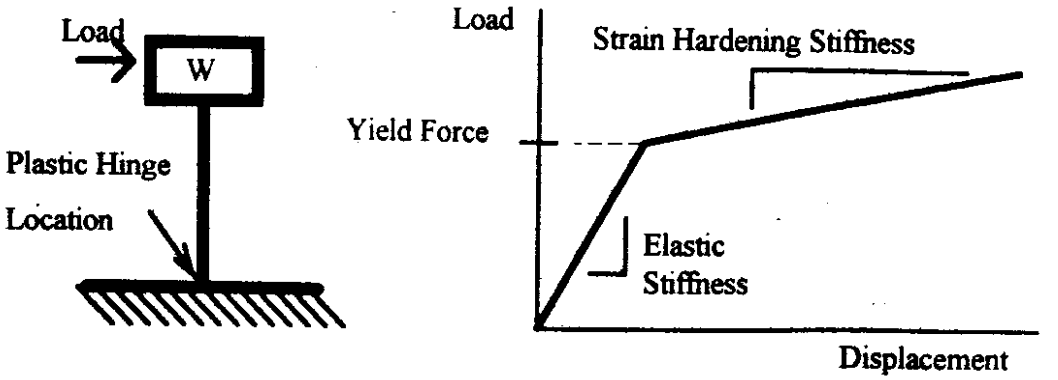


Figure 25 Determination of Yield Force for Simple Single-Column Structure

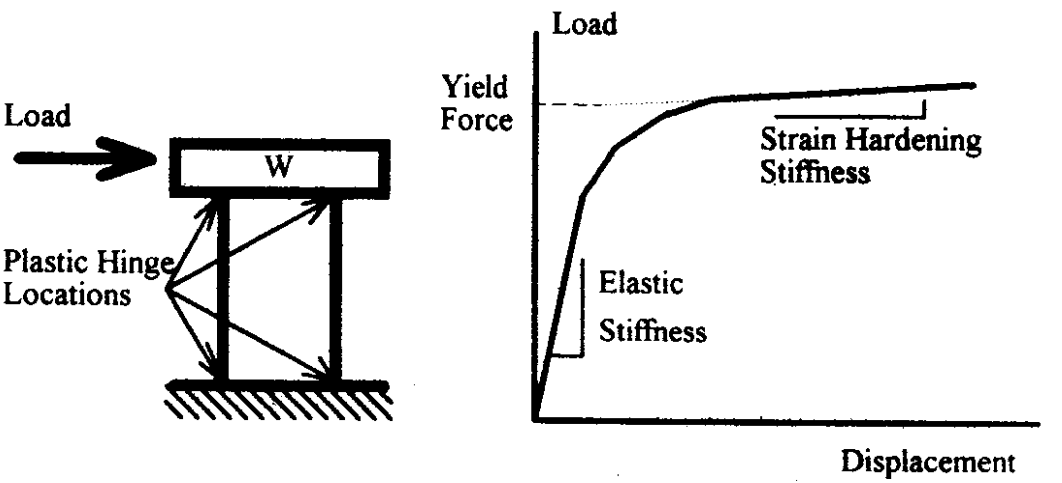


Figure 26 Determination of Yield Force for Multiple-Column Bent Structure

The yield force to weight ratios used in this research encompass the range of design yield force to weight ratios arising from the AASHTO Code provisions for the Pacific Northwest. For columns or piers that can be modeled with the inertial mass lumped at the top, the seismic base shear can be expressed as:

$$V = C_S W / R \qquad \text{(Equation 11)}$$

where:

| | |
|---|---|
| V | is the design base shear |
| W | is the weight of the structure |
| R | is the response modification factor |
| $C_S$ | is the seismic response coefficient, determined according to |

$$C_S = 1.2\ A\ S / T^{2/3} \quad < 2.5\ A \qquad \text{(Equation 12)}$$

where:

| | |
|---|---|
| A | is the acceleration coefficient (EPA) |
| S | is the dimensionless coefficient for the soil profile characteristics of the site |
| T | is the period of the bridge |

According to the AASHTO maps, A = 0.2 for the Puget Sound region. The site coefficient, S, varies from 1.0 to 1.5 and the response modification factor, R, varies from 2 to 5. For stiff structures, the maximum value for $C_S$ would be 0.50. For structures of higher periods, the value of $C_S$ would be lower. With an R value of 2, the maximum base shear to structure weight ratio would be 0.25. Higher values of R would result in lower base shear to weight ratios. For a simple single column structure with only one potential

plastic hinge location, the load-displacement behavior would be that shown in Figure 25. For such a case, with the load combination of lateral earthquake load plus dead load governing the design of the structure, the base shear would be the yield force.

However, most structures are more complex and the lateral earthquake load plus dead load combination rarely governs the design. Other load combinations typically control the determination of member cross-section properties. In such cases, the true yield force must be determined from a plastic collapse analysis. From the plastic collapse analysis, the load displacement curve of the structure can be determined. From that curve, the yield force can be determined as shown in Figure 26.

Standard output from SPECTRUM is an inelastic displacement response spectrum The user specifies the period range over which the response is to be calculated. Response was calculated for structures with periods of 27 different natural periods from 0.05 seconds to 5.0 seconds. This range of structural periods covers the majority of structures within engineering interest.

SPECTRUM was modified to calculate total hysteretic energy dissipated during time-history analysis and to count the number of inelastic half cycles. These two quantities provide estimates of the damage a structure experiences, as discussed in Section 2.2 of this report. Hysteretic energy was calculated by determining the cumulative area within the hysteretic loops. Inelastic half cycles were counted using the rain flow method.

#### 2.3.2.2 Degrading Stiffness Model Response

For degrading stiffness behavior, the program DRAIN2D (48) was used. DRAIN2D, like SPECTRUM, performs a response-history analysis of a structure subject to a specified acceleration record. Although the program is capable of analyzing a structure subject to both vertical and horizontal acceleration components simultaneously,

only horizontal components were used in this research. A SDOF system, composed of a vertical cantilever with a 100 kip weight on the top, was used. The cantilever was fixed in translation and rotation at the base while the top was allowed to translate and rotate. However, no rotational mass was assigned to the top of the column. This produced a structure that had only one yielding zone, at the base of the cantilever.

The column was modeled using the degrading stiffness element based on a Takeda model. The model allows no strength degradation, no pinching, but degrades in stiffness based on the maximum displacement attained. See Figure 27 for a description of the hysteretic load displacement cycle. For additional discussion see Kannan and Powell's report (48).

DRAIN2D provides several axial force-moment interaction relationships. In this research, a constant yielding surface, independent of axial load, was used. Although axial load changes shear and moment behavior, a simpler model was desirable. No geometric stiffness behavior was included in the model. Yield levels were set to reflect yield force to weight values of 0.125, 0.25 and 0.50.

DRAIN2D was modified to calculate hysteretic energy dissipated and the number of inelastic half cycles experienced. Hysteretic energy was determined by determining, in each time step, the product of plastic hinge rotation and the moment in the member. This was then added to the total energy of all the previous steps. Half cycle count was performed according to the rain flow method.

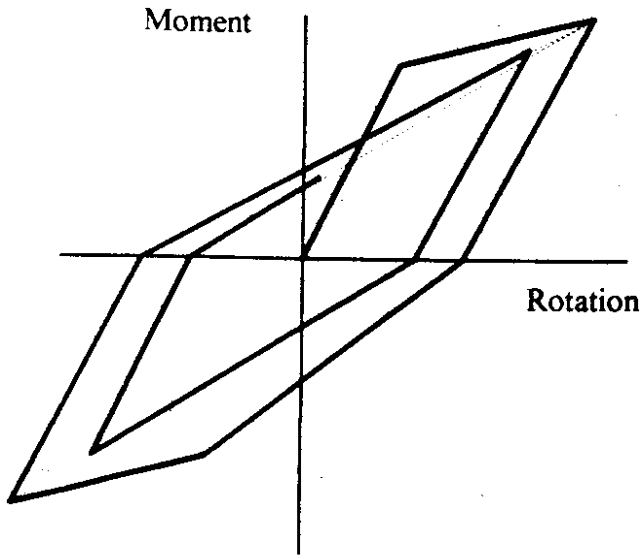


Figure 27 Degrading stiffness hysteretic model

# CHAPTER 3

# FINDINGS

This chapter reports the results of the response history analyses performed on SDOF models subjected to postulated CSZ artificial earthquakes. Results are reported in terms of maximum inelastic displacement, hysteretic energy dissipated, and inelastic cycle counts. This portion describes the sensitivity of response to earthquake magnitude and duration, structure strength as expressed as yield force to weight ratio, structural hysteretic model, site location, site soil condition, and the input spectra used in the artificial earthquake generation. Only results that illustrate the trends found in the research are provided in the figures in this portion of the paper. Additional figures are included in the appendices for a more detailed view of the findings.

## 3.1 Response Sensitivity to Magnitude-Duration

With all other variables held constant, inelastic total spectral displacement increases with an increase in earthquake magnitude. The same trend is apparent for damage as expressed as dissipated hysteretic energy and inelastic half-cycle counts. This direct relationship between magnitude and response holds for both the bi-linear and the degrading stiffness model.

Inelastic displacement was not affected significantly by variations in earthquake duration, while holding all other variables constant. This trend was not surprising, since the spectral displacement is a "point-in-time" maximum value and is not based on accumulated effects. A variation in duration, however, did effect damage. Both dissipated hysteretic energy and inelastic half-cycle counts increased with an increase in

earthquake duration. This trend was apparent for both bi-linear models and degrading stiffness models.

As moment magnitude is directly related to duration, response sensitivity to either duration or magnitude alone is misleading. Response to artificial records with the maximum reasonable duration for a given magnitude is shown in Figures 28, 29, 30, 31, and 32. These are responses to records based on Crouse's spectra for median CSZ earthquakes. Figures 28 and 29 show inelastic total displacement spectra for a bi-linear model to a ground motion attenuated to Puget Sound sites. Figure 28 shows the response of structures with yield force to weight ratios of 0.125 and Figure 29 shows the response of structures with yield force to weight ratios of 0.25. Figures 30 and 31 show hysteretic energy dissipated, normalized by strain energy stored in a structure at yield, for the same respective models subject to the same ground motion. The effect of increasing magnitude-duration on inelastic cycle counts is shown in Figure 32 for a bi-linear structure with a period of 0.6 seconds. In these figures, the increase in response due to simultaneous increase in both the magnitude and duration can be observed.

Inelastic cycle count results do not show as conclusively the direct relationship between response and magnitude-duration as the weakness may be due to the statistical nature of the results. If the response to multiple records of the same magnitude and duration was determined, a mean response for that magnitude and duration could be obtained. A standard deviation at each period and ductility level could also be obtained. If such results were found for all the magnitude-duration combinations and compared, the conclusiveness of trends and their uncertainties would be more evident.

Several significant characteristics of the response should be observed. One is that the displacement demands for structures with yield force to weight ratios of 0.25 are not large. Figure 29 shows that the displacement demands for the largest CSZ records, on

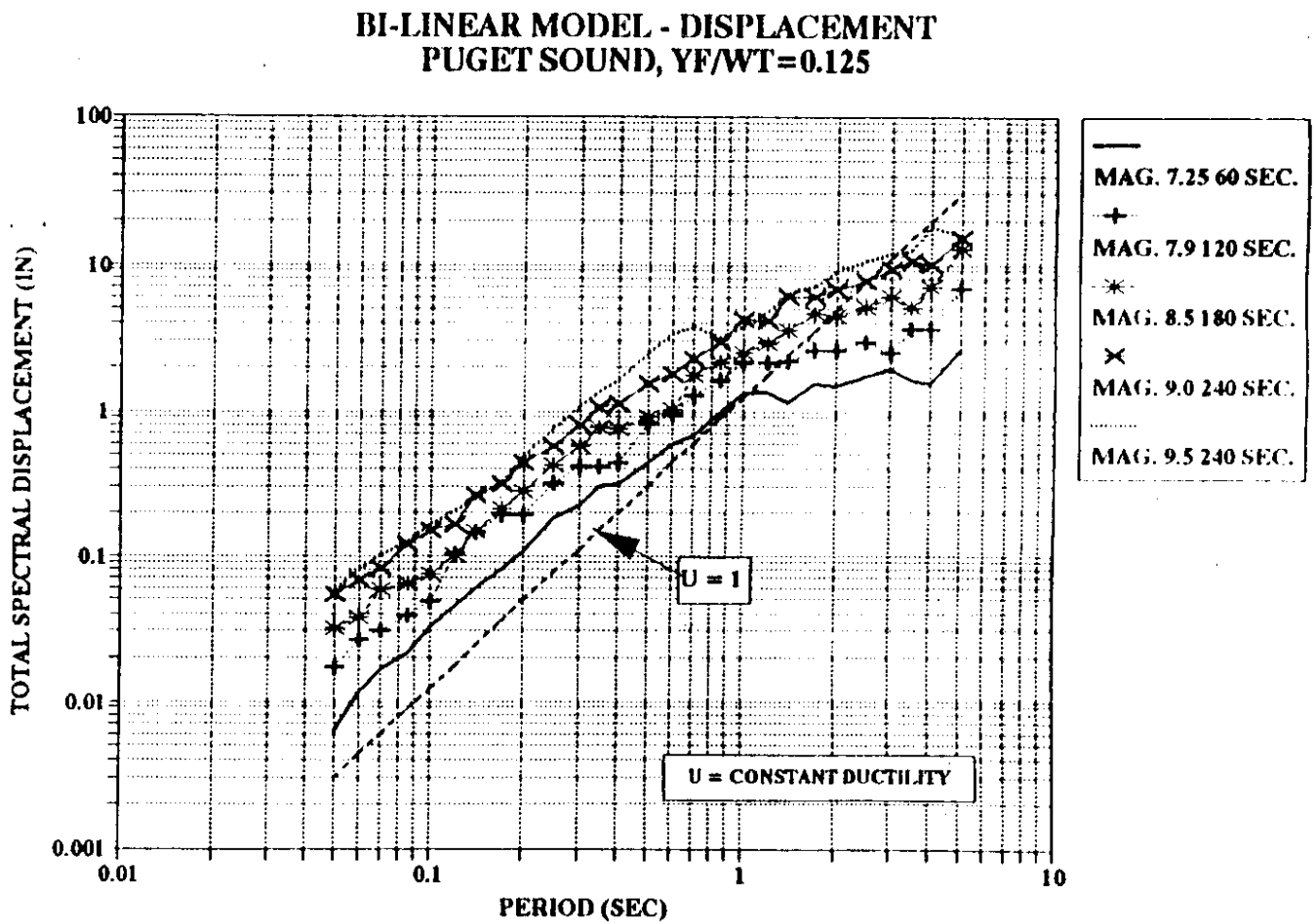


Figure 28 Sensitivity of inelastic displacement spectra to magnitude-duration: bi-linear models, yf/wt=0.125

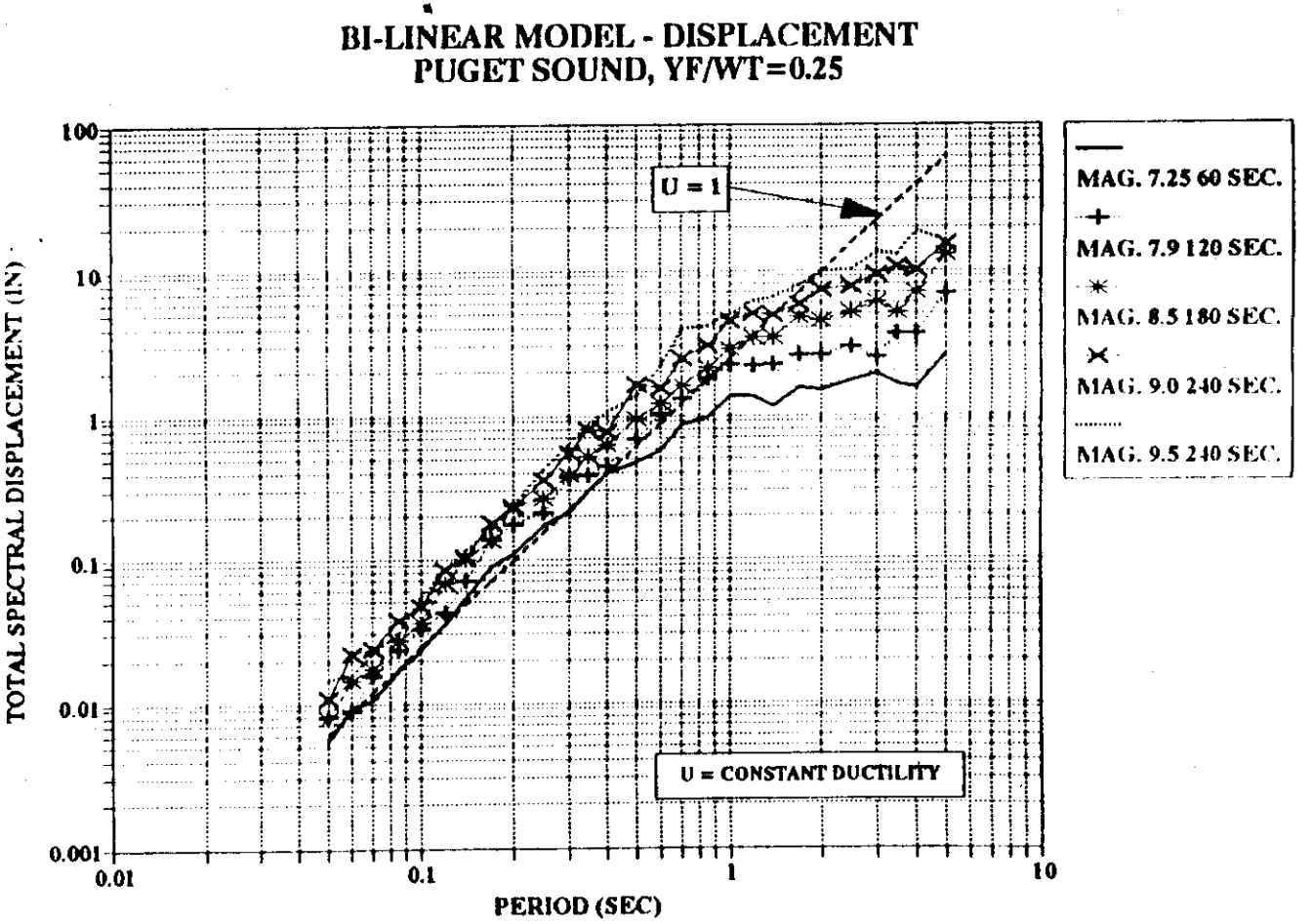


Figure 29 Sensitivity of inelastic displacement spectra to magnitude-duration: bi-linear models, yf/wt=0.25

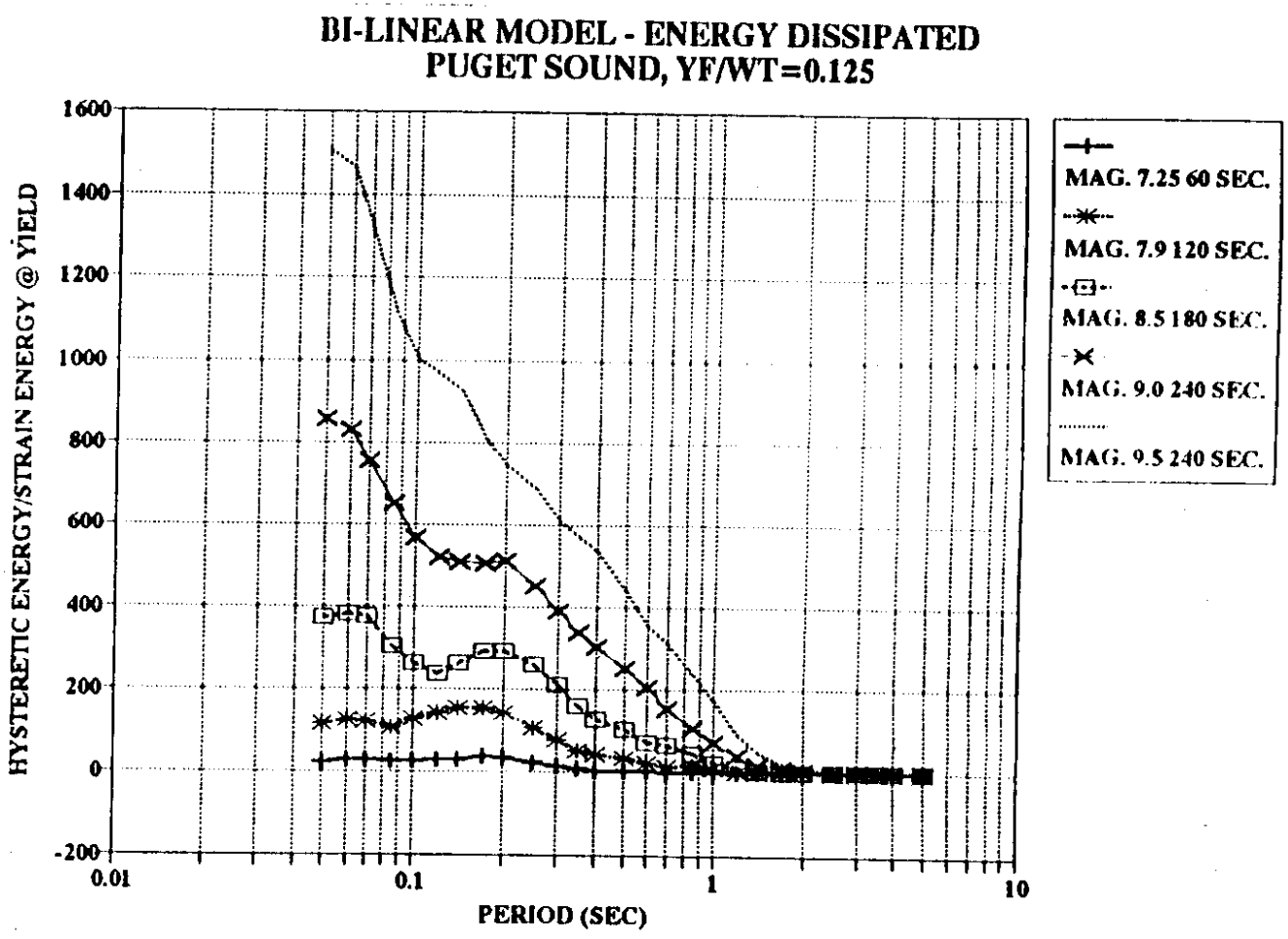


Figure 30 Sensitivity of hysteretic energy demand to magnitude-duration: bi-linear models, yf/wt=0.125

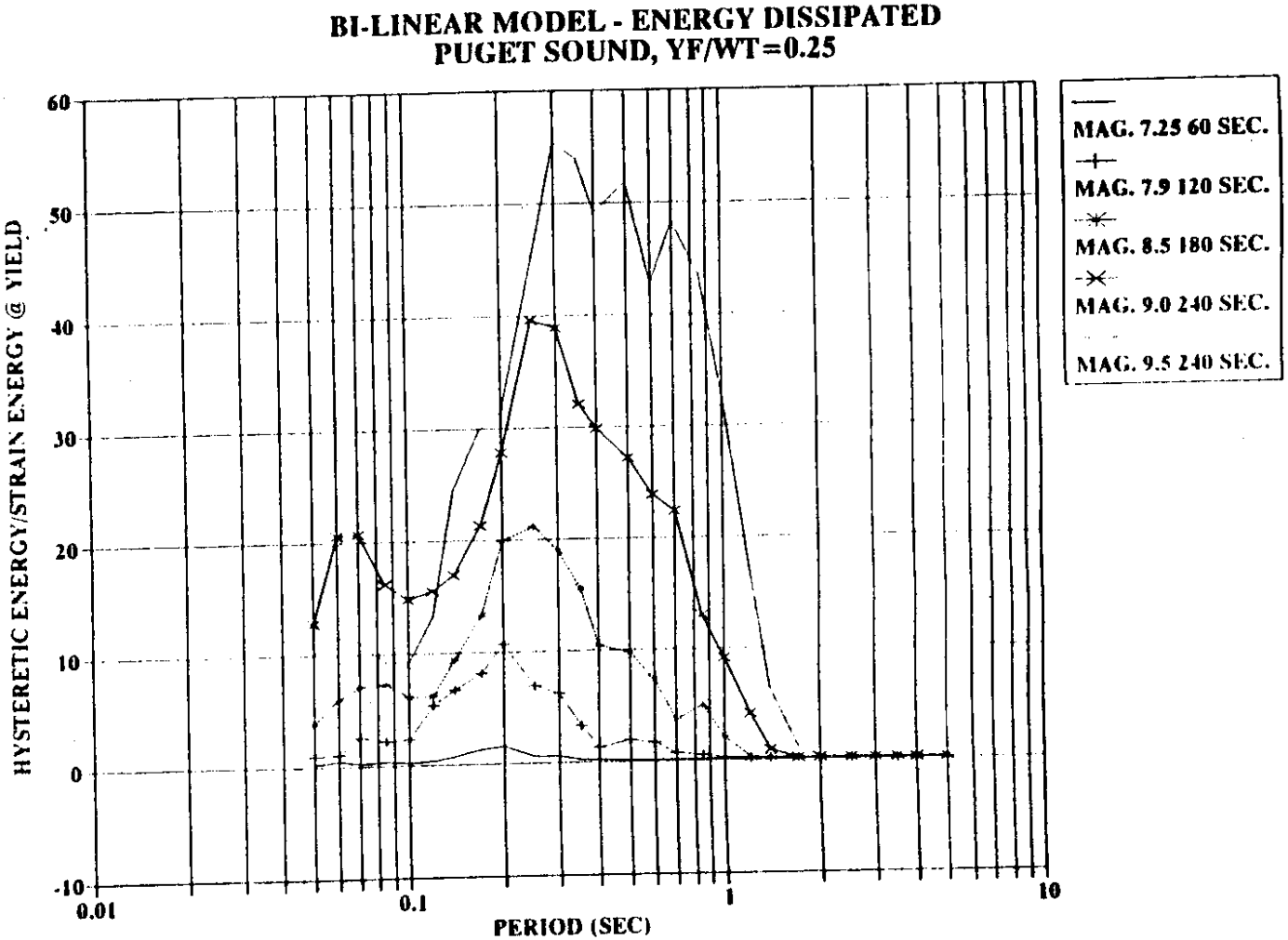


Figure 31 Sensitivity of hysteretic energy demand to magnitude-duration: bi-linear models, yf/wt=0.25

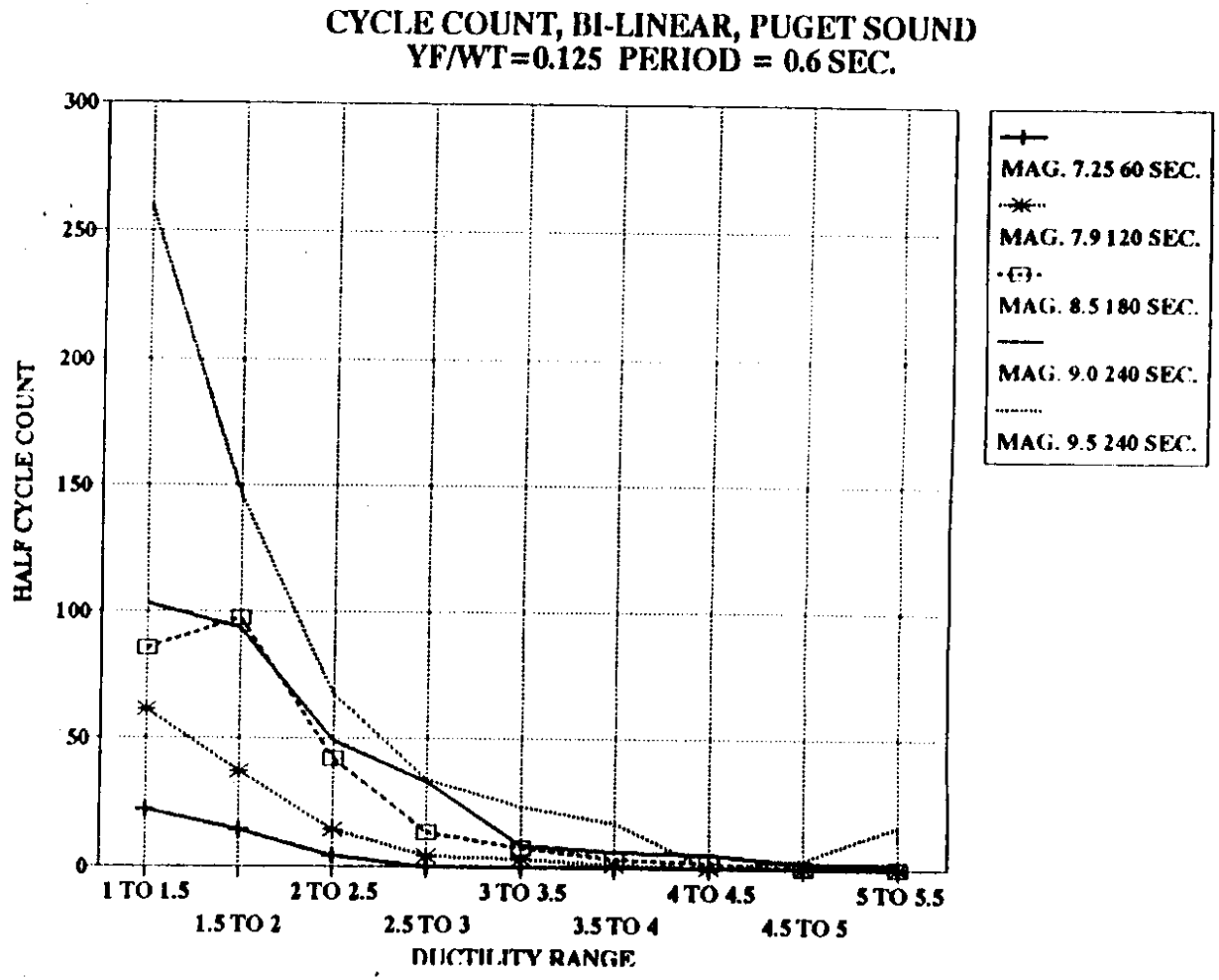


Figure 32 Sensitivity of inelastic half-cycle counts to magnitude-duration: bi-linear models

structures with periods below 1.0 second, have ductilities of approximately 2. However, as shown in Figure 28, structures with yield force to weight ratios of 0.125 have displacement demands with ductilities as high as 20. The highest ductility demands occur in stiff structures with periods of less than 0.1 seconds, and they are caused by the magnitude 9.5 record. Lesser magnitude records produce lower displacement demands on structures. Between periods of 0.1 and 0.6 seconds, ductility demands on structures with yield force to weight ratios of 0.125 are approximately 10, for the magnitude 9.5 record. These trends were found in response to both the bi-linear and the degrading stiffness models.

Another significant characteristic of the response is that it is elastic for structures above a certain period range. That period range varies with yield force to weight ratio and the magnitude-duration of the record. For structures with yield force to weight ratios of 0.125, response is elastic when structural period is greater than 1 to 3 seconds. For structures with yield force to weight ratios of 0.25, response is elastic when structural period is above 0.5 to 2.0 seconds. This is shown in Figure 28 and 29 when displacement demand is less than a constant ductility of one. Elastic response is also shown in Figures 30 and 31 where dissipated hysteretic energy is zero. Elastic response in this region is significant because ground motion predictions are more uncertain. See Figure 10.

## 3.2 Sensitivity of Response to Structure Strength

Structural response to earthquake ground motion is inversely related to the structure strength, as defined by a structure's yield force to weight ratio, provided all other parameters are held constant. Inelastic total displacement spectra, hysteretic energy dissipated, and inelastic half-cycle counts all decrease with an increase in the yield force to weight ratio. This is trend holds for both bi-linear and degrading stiffness models.

Figures 33 and 34 show the effect of varying the yield force to weight ratio, for a bi-linear model, on the inelastic spectral displacement and the hysteretic energy dissipated, respectively. Figure 35 shows the effect of varying the yield force to weight ratio on inelastic cycle counts.

By increasing the yield force to weight ratio from 0.125 to 0.25, for bi-linear models subject to the magnitude 8.5, 180 second duration CSZ record, displacement ductility demand is reduced from a maximum of approximately 10 to less than 2. For the same increase in structure strength, for the same model and acceleration record, the hysteretic energy demand is reduced by more than an order of magnitude. Correspondingly, inelastic half-cycle counts are reduced by as much as 75 percent, for structures with periods of 0.5 seconds.

Increasing the yield force to weight ratio from 0.25 to 0.5 does not cause as great a reduction in response as increasing the yield force to weight from 0.125 to 0.25. Response of bi-linear structures with a yield force to weight ratio of 0.5, to the 180 second magnitude 8.5 record, is nearly elastic. Displacement demands have ductilities at or less than 1.0 and hysteretic energy demands are near zero over all period ranges. The response to the same record for a bi-linear structure with a yield force to weight ratio of 0.25 has displacement demands near or less than 2.

## 3.3 Consistency of Response

Results shown thus far have shown the response to single artificial records of certain magnitude and duration No duplication of response was determined. It is desirable to have results that can be replicated, and if they can be replicated, to determine whether the replication is exact or whether there are uncertainties in the response to single

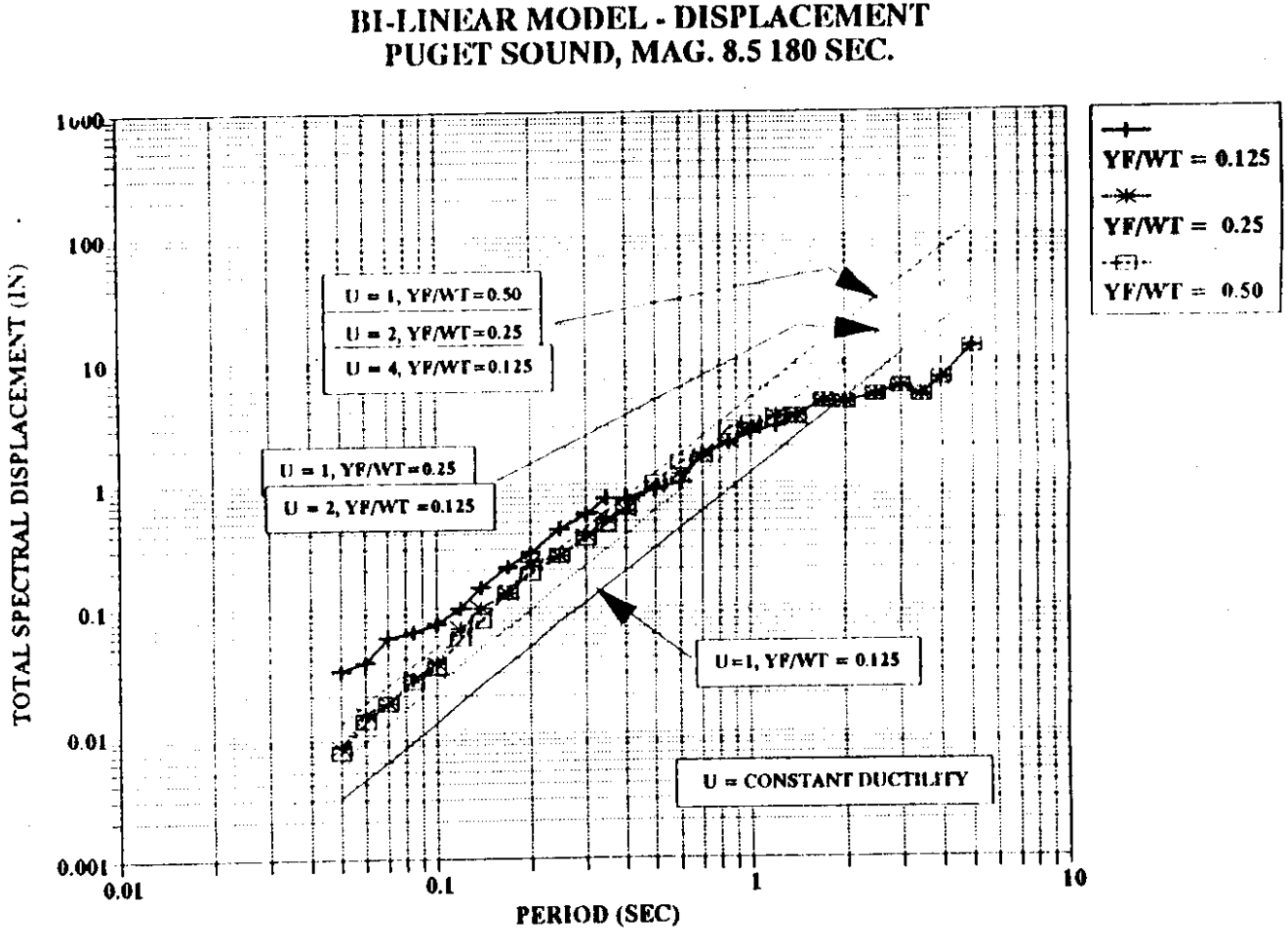


Figure 33 Sensitivity of displacement demand to yield force to weight ratio: bi-linear models

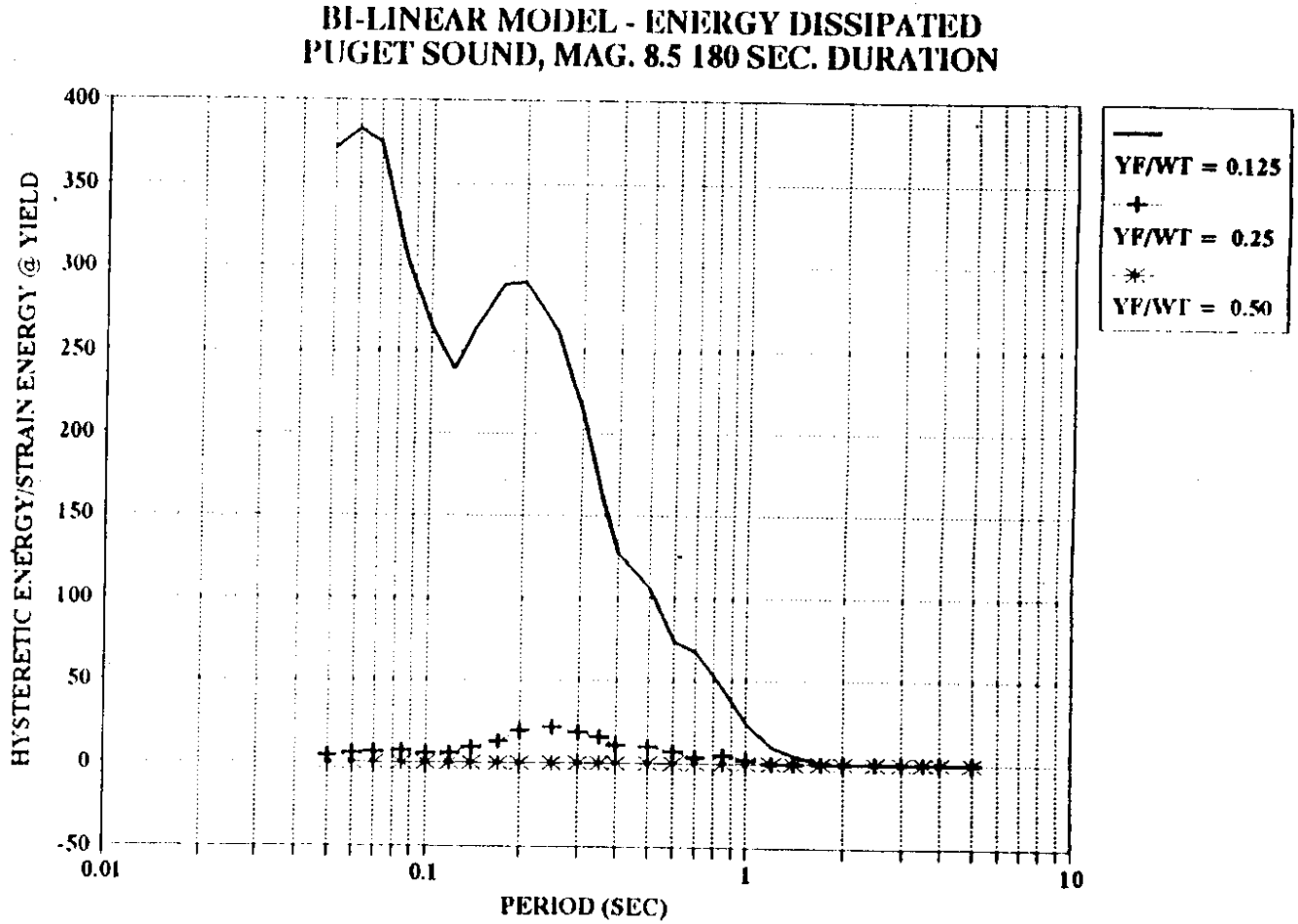


Figure 34 Sensitivity of hysteretic energy demand to yield force to weight ratio: bi-linear models

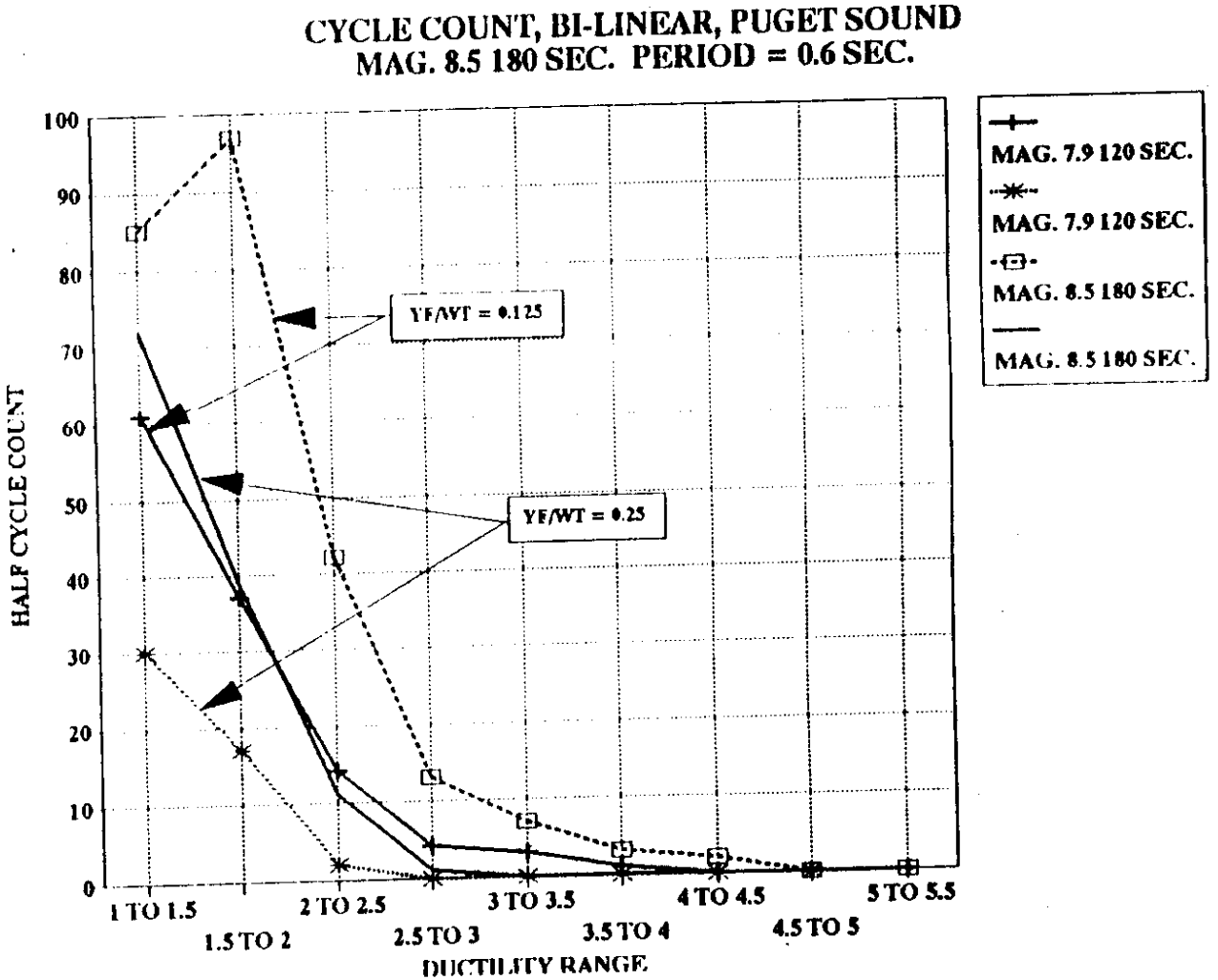


Figure 35 Sensitivity of inelastic half-cycle counts to yield force to weight ratio: bi-linear models

artificial records.

To verify that results could be replicated, the response to three records of several different magnitude-duration combinations were determined and compared. As an example, Figures 36 and 37, respectively, show the displacement demands and the hysteretic energy demands of three Puget Sound site, 180 second, magnitude 8.5 records. As can be seen in these figures, replication of response is not exact, and there is some uncertainty in the response. For bi-linear structures with yield force to weight ratios of 0.25, the difference between displacement demands of different 180 second magnitude 8.5 records can be as great as 50 percent. For hysteretic energy demand of the same strength and structural model, there is as much as 55 percent difference between the demands of different records. These differences are not surprising as there are many sources of uncertainty in the generation of artificial records. Sources of uncertainty are discussed in more detail in Chapter 6.

## 3.4 Sensitivity of Response to Site Location

Ground motion at a coastal range site is expected to be stronger than at a Puget Sound site because the coastal range site is closer to the center of energy release of a large CSZ earthquake. The structural response to the stronger coastal range ground motion is also expected to be greater than the response to ground motion at Puget Sound. Figure 38 and 39 show the differences in response between coast range ground motion and Puget Sound ground motion. In both figures, the artificial acceleration record is based on Crouse's (1991) median spectra. Figure 38 shows the differences between inelastic displacement spectra for a bi-linear model while Figure 39 shows the differences between normalized hysteretic energy dissipated by a bi-linear model.

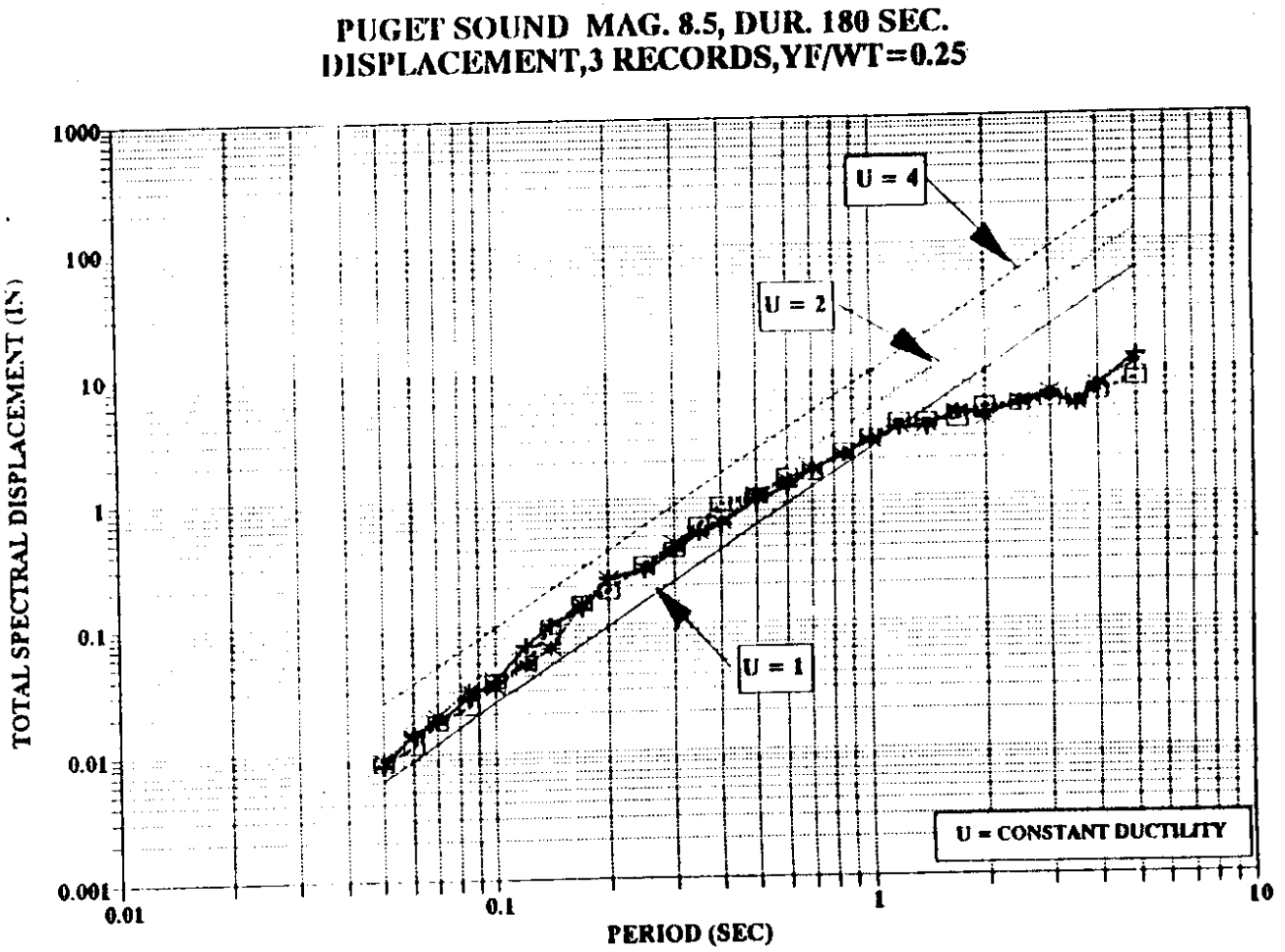


Figure 36 Displacement demand for three records of same magnitude and duration

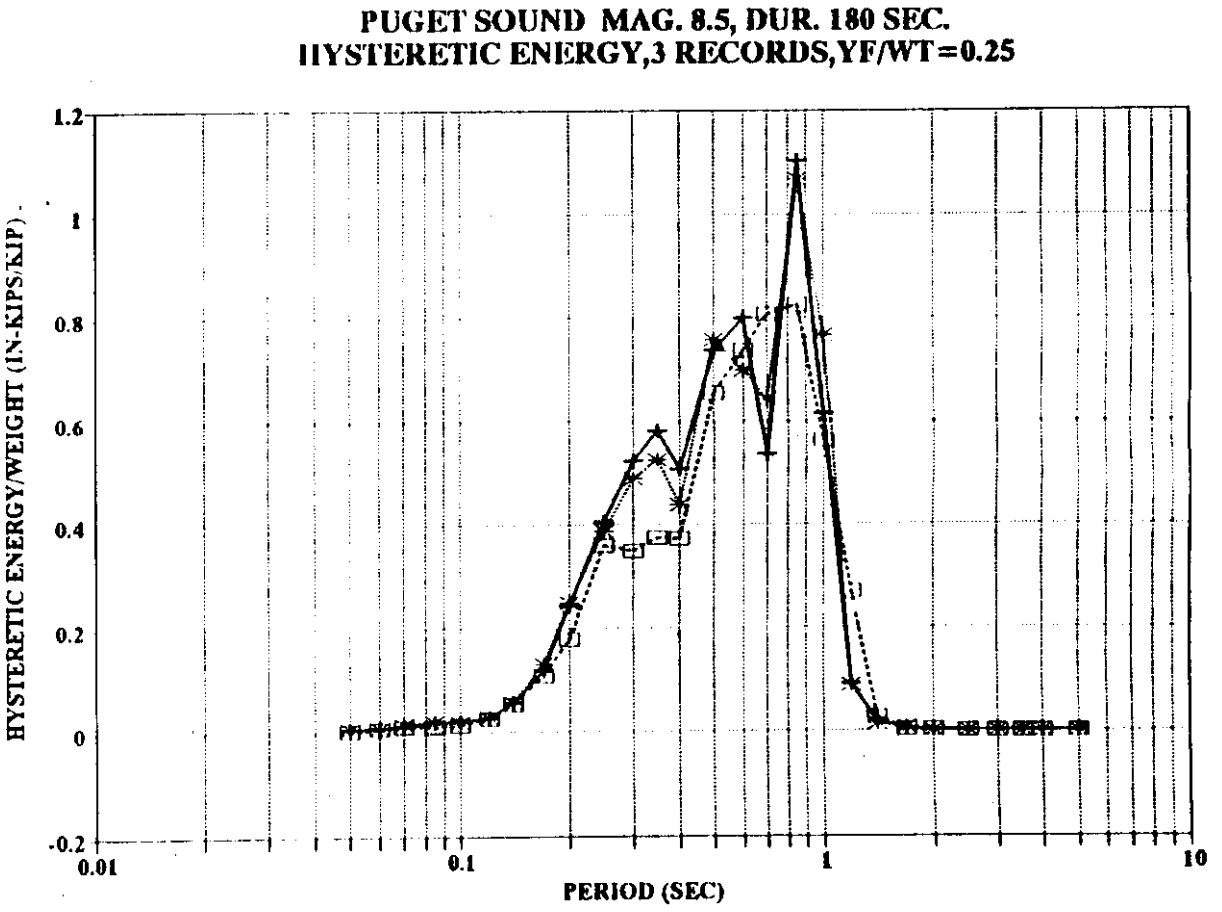


Figure 37 Hysteretic energy demand for three records of same magnitude and duration

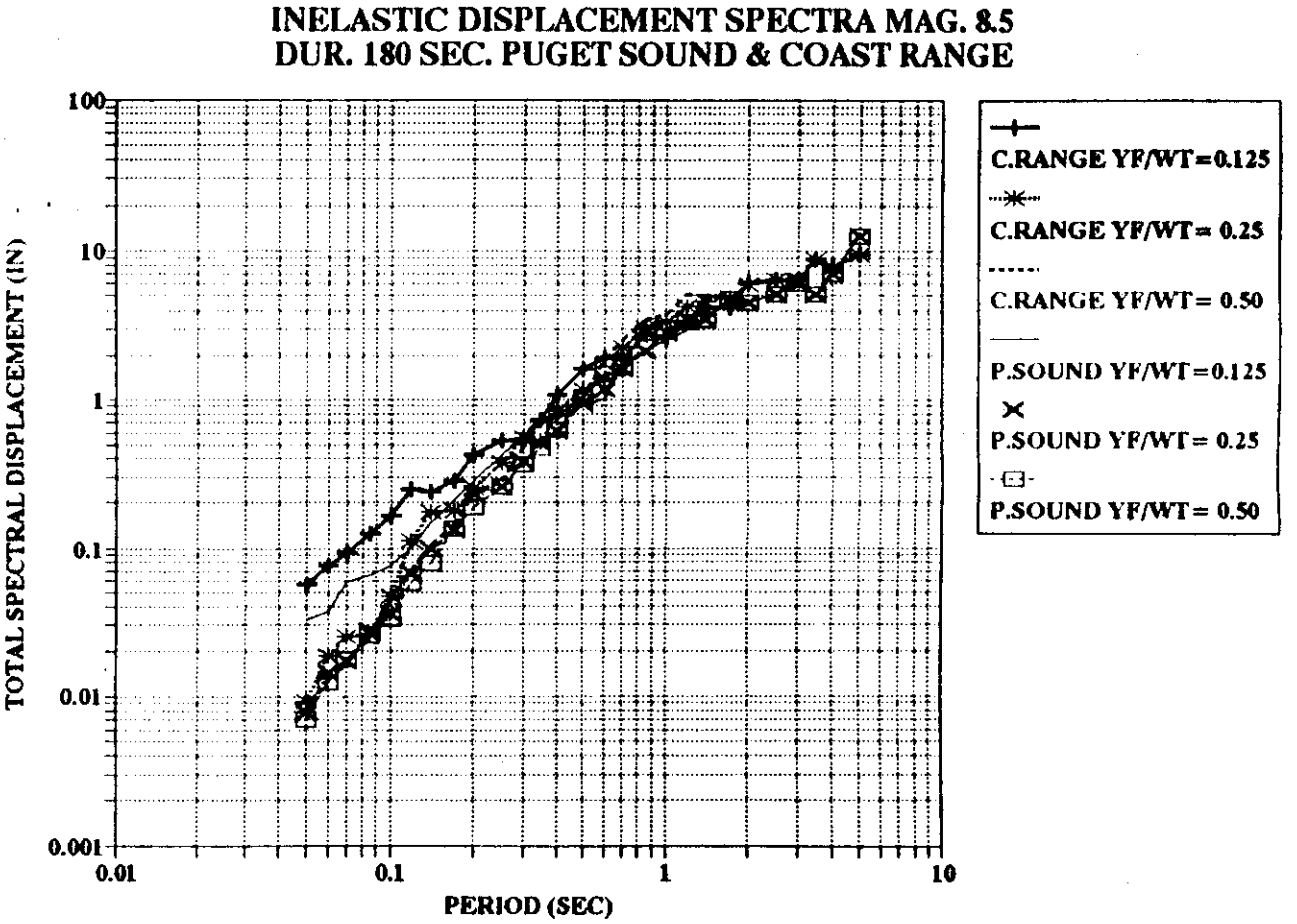


Figure 38 Sensitivity of inelastic spectral displacement to site location: bi-linear models.

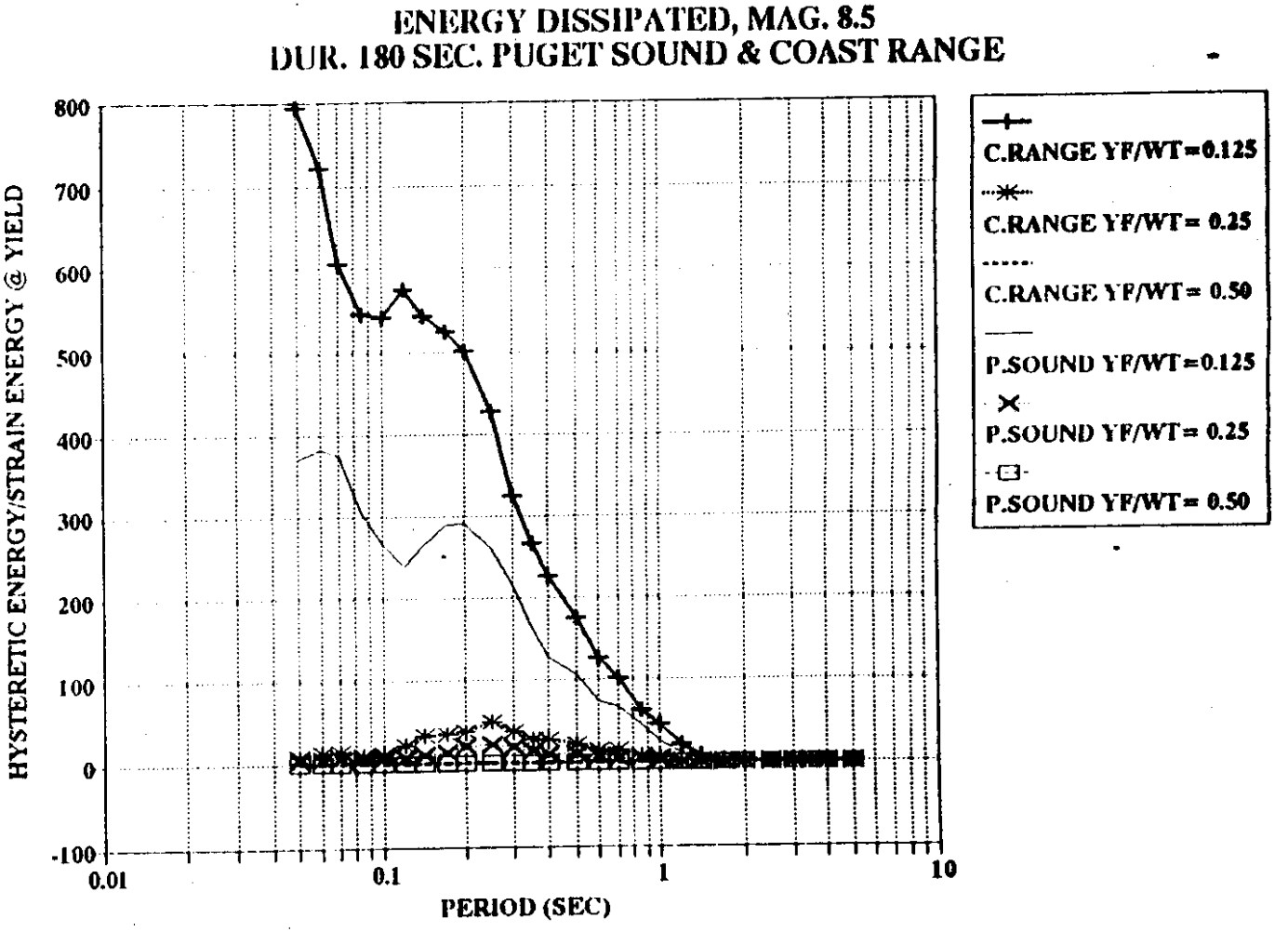


Figure 39 Sensitivity of hysteretic energy demand to site location: bi-linear models

Larger responses to coast range records as compared to Puget Sound records were apparent for structures with low yield force to weight ratios and in the lower to middle period ranges. For structures with periods below 0.1 seconds and with yield force to weight ratios of 0.125, the displacement demands from the coast range records are approximately twice the displacement demands of the Puget Sound records. For higher yield force to weight ratios and for more flexible structures this trend is not as dramatic. For structures with periods below 0.3 seconds the hysteretic energy demands from the coast range records are approximately twice the hysteretic energy demands of the Puget Sound records. Above 0.3 seconds the energy demands of the coast range and Puget Sound records converge from a difference of about two to zero. Above periods of 2 seconds response to records for both sites is nearly identical as response is elastic.

## 3.5 Sensitivity of Response to Input Spectra

The artificial acceleration records, which are based on Heaton and Hartzell's (1986) spectra for a giant (Mw=9.5) earthquake, are more intense than the artificial acceleration records based on Crouse's spectra for median earthquakes. The comparison of structural response to artificial records based on Heaton and Hartzell's giant earthquake spectra and Crouse's median spectra is expected to be correspondingly similar. Figure 40 shows a comparison of inelastic displacement spectra for acceleration records based on Heaton and Hartzell's giant spectra with the inelastic displacement spectra for acceleration records based on Crouse's median spectra. Figure 41 shows a comparison of normalized hysteretic energy for the same. Both figures are for bi-linear structural models, with yield force to weight ratios of 0.25

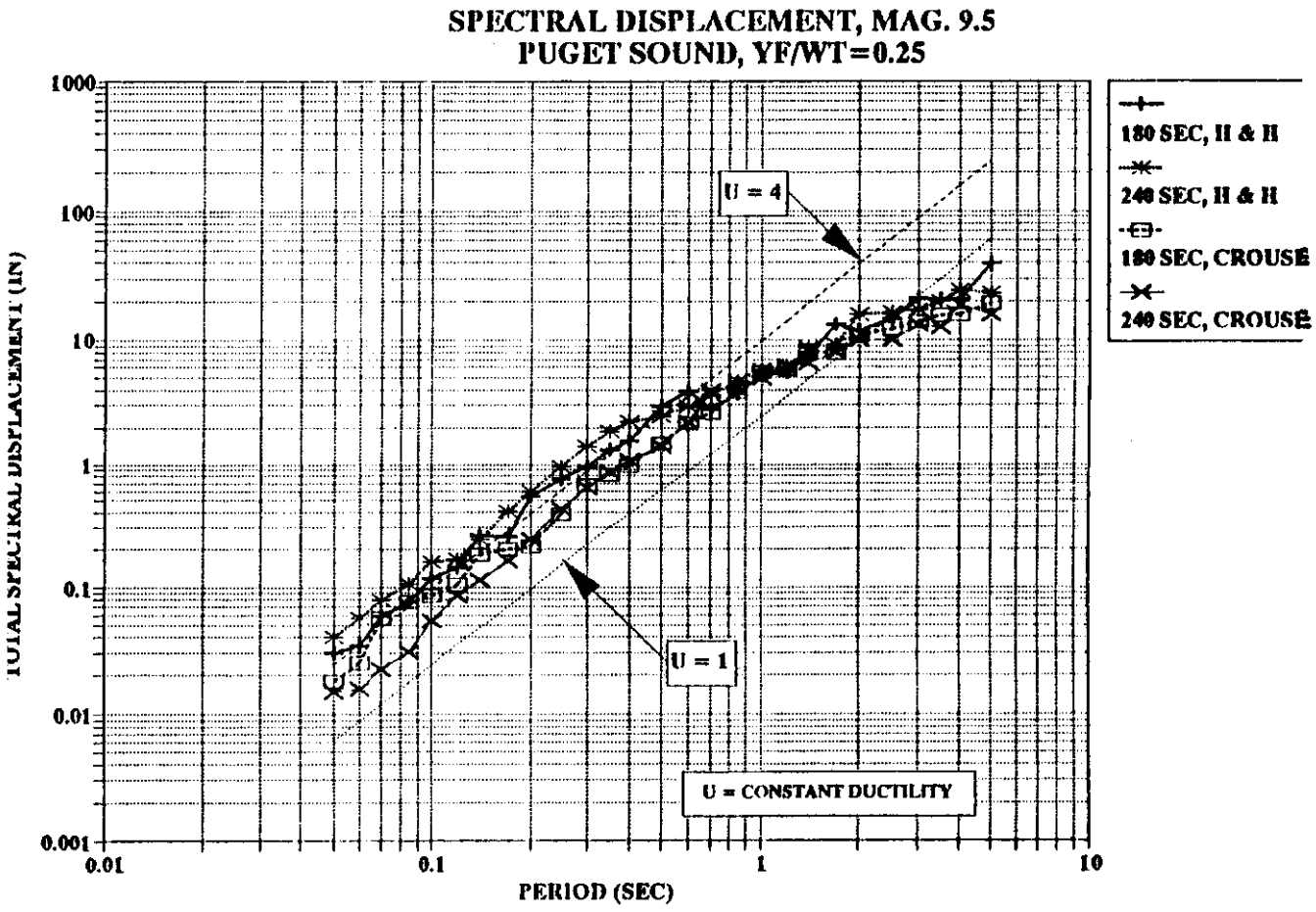


Figure 40 Sensitivity of inelastic spectral displacement to input spectra: bi-linear models

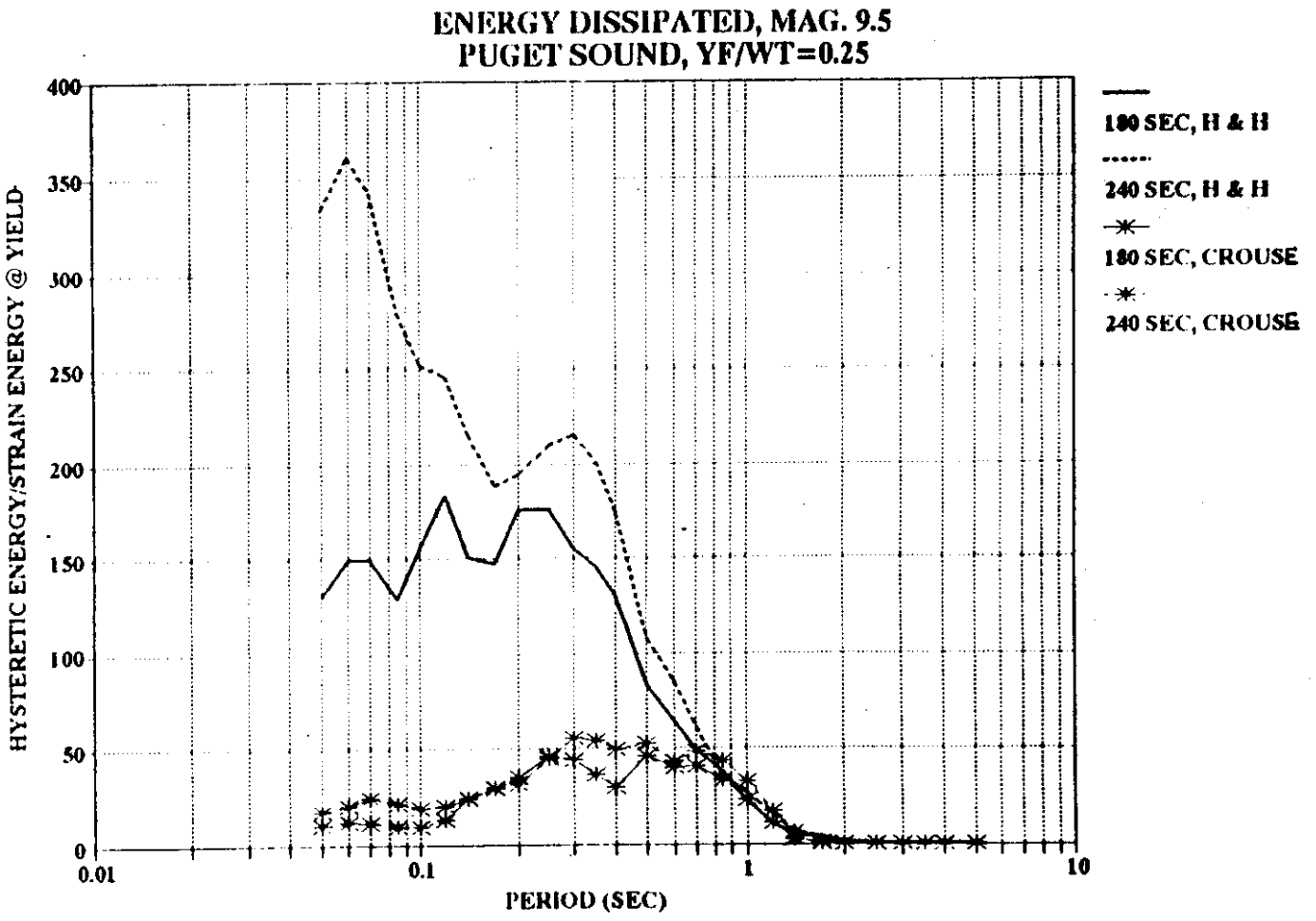


Figure 41 Sensitivity of hysteretic energy demand to input spectra: bi-linear models.

For Puget Sound sites, structures with yield force to weight ratios of 0.25 and with periods less than 0.5 seconds, displacement demands of records based on Heaton and Hartzell's giant spectra are approximately two times the displacement demands of records based on Crouse's median spectra. Above 0.5 seconds, the differences in displacement is not as conclusive. For the same site and structure strength, hysteretic energy demand for records based on Heaton and Hartzell's giant earthquake spectra are as much as 20 times the hysteretic energy demands for records based on Crouse's median spectra. The large difference in damage demands reflects the difference in the spectra on which the records are based.

## 3.6 Sensitivity of Response to Structural Model

The inelastic displacement spectra for the bi-linear and the degrading stiffness models are compared in Figure 42. There is little significant difference in the inelastic displacement response of these two models. For structures with yield force to weight ratios of 0.25, there is as much as 20 percent difference between the bi-linear and degrading stiffness response. This difference occurs for structures with periods less than 0.5 seconds, but the trend is not constant over all the periods in this range. Above periods of approximately 2 seconds, the response is elastic for both models and nearly identical.

Typically, a degrading stiffness structure will dissipate more hysteretic energy, during an earthquake, than will a bi-linear structure, due to the nature of their hysteretic behaviors. A degrading stiffness model will dissipate hysteretic energy even when displacements have ductilities less than 1.0. A bi-linear model will store and release strain energy when displacements have ductilities less than 1.0.

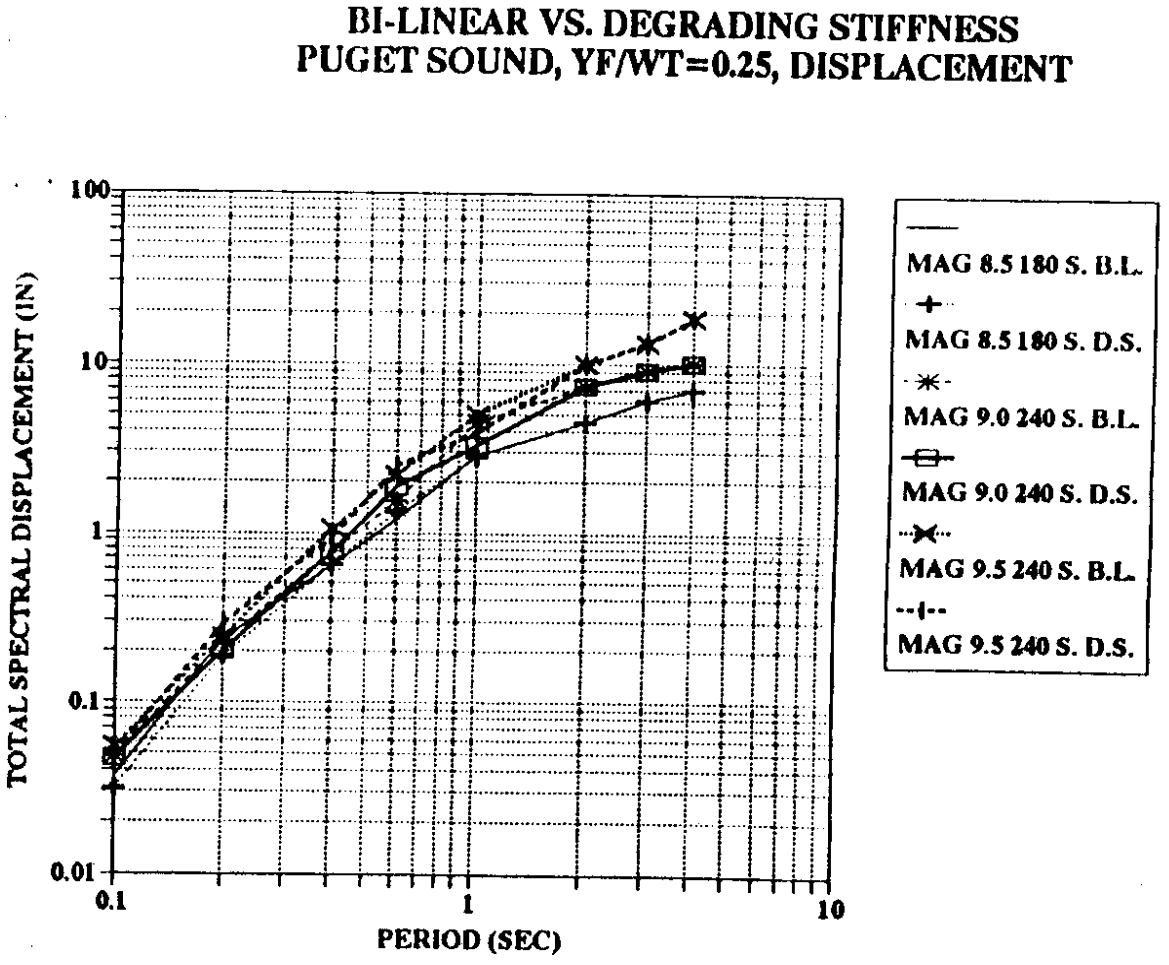


Figure 42 Sensitivity of inelastic spectral displacement to structural models.

The differences in energy demand for the two models are displayed in Figure 43. In this figure, the normalized hysteretic energy dissipated for bi-linear and degrading stiffness models is shown. All other variables are held constant. For a structure with a yield force to weight ratio of 0.25, the hysteretic energy demand of a degrading stiffness model, subject to a 3 minute magnitude 8.5 Puget Sound record, is as much as 3 times the hysteretic energy demand on a similar bi-linear model.

## 3.7 Response with Consideration of Washington State Soils

Two Washington State soil groups, in addition to the basic firm soil site spectra, were used in this research. Each of these soil groups amplify the ground motion in distinct period ranges. The soil groups each amplify earthquake ground motions according to their unique properties. The first, Soil Group 1, a shallow firm cohesionless soil, amplifies ground motion in the period range between 0.1 seconds and 1.0 seconds. Soil Group 5, a deep, firm, cohesionless soil, amplifies ground motions for periods between 0.5 seconds and 4.0 seconds. Structural response to soil amplified ground motions is expected to be greater than the un-amplified response in these same period ranges.

Figure 44 shows a comparison of inelastic displacement spectra resulting from Soil Group 1 amplified ground motion to the inelastic spectra for median earthquakes without soil amplification. Figure 45 shows the same for Soil Group 5 amplified ground motion. Both figures are for Puget Sound ground motion.

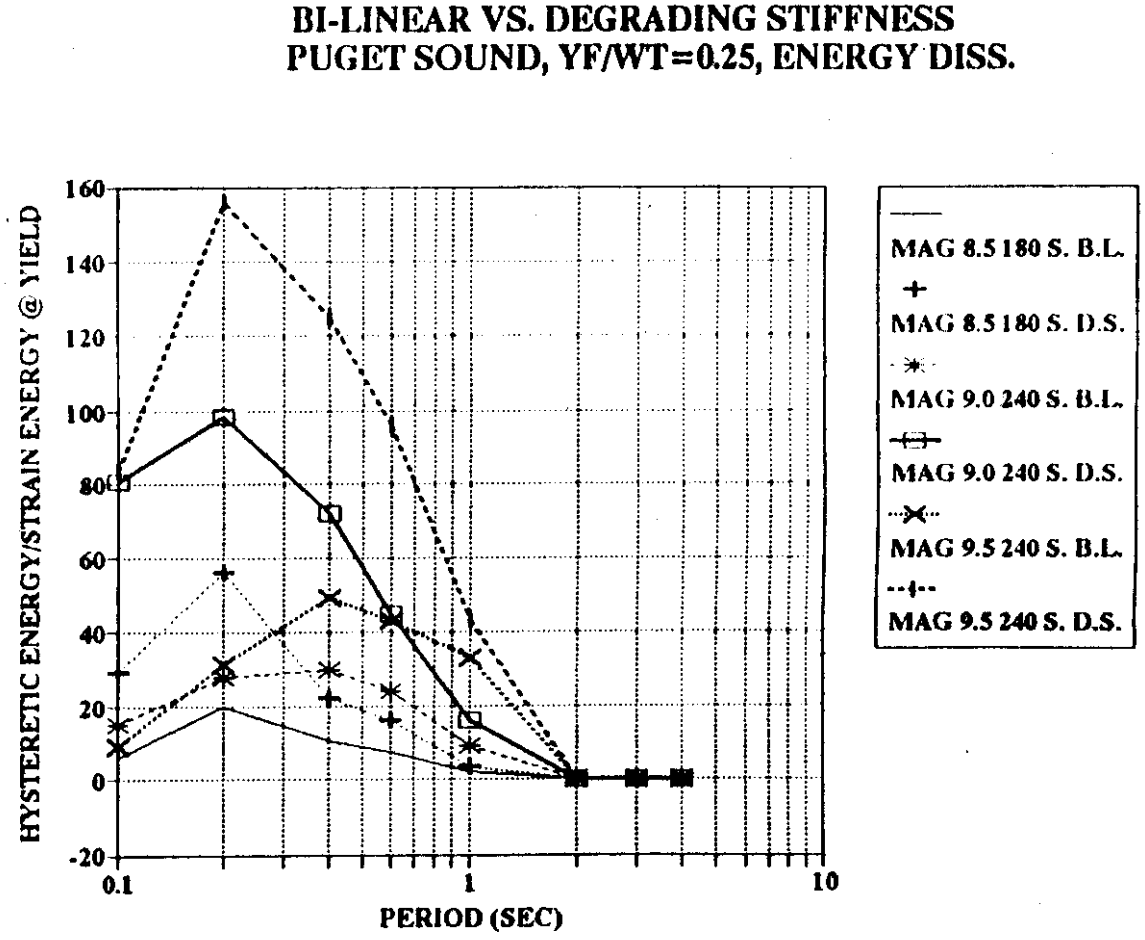


Figure 43 Sensitivity of hysteretic energy demand to structural model.

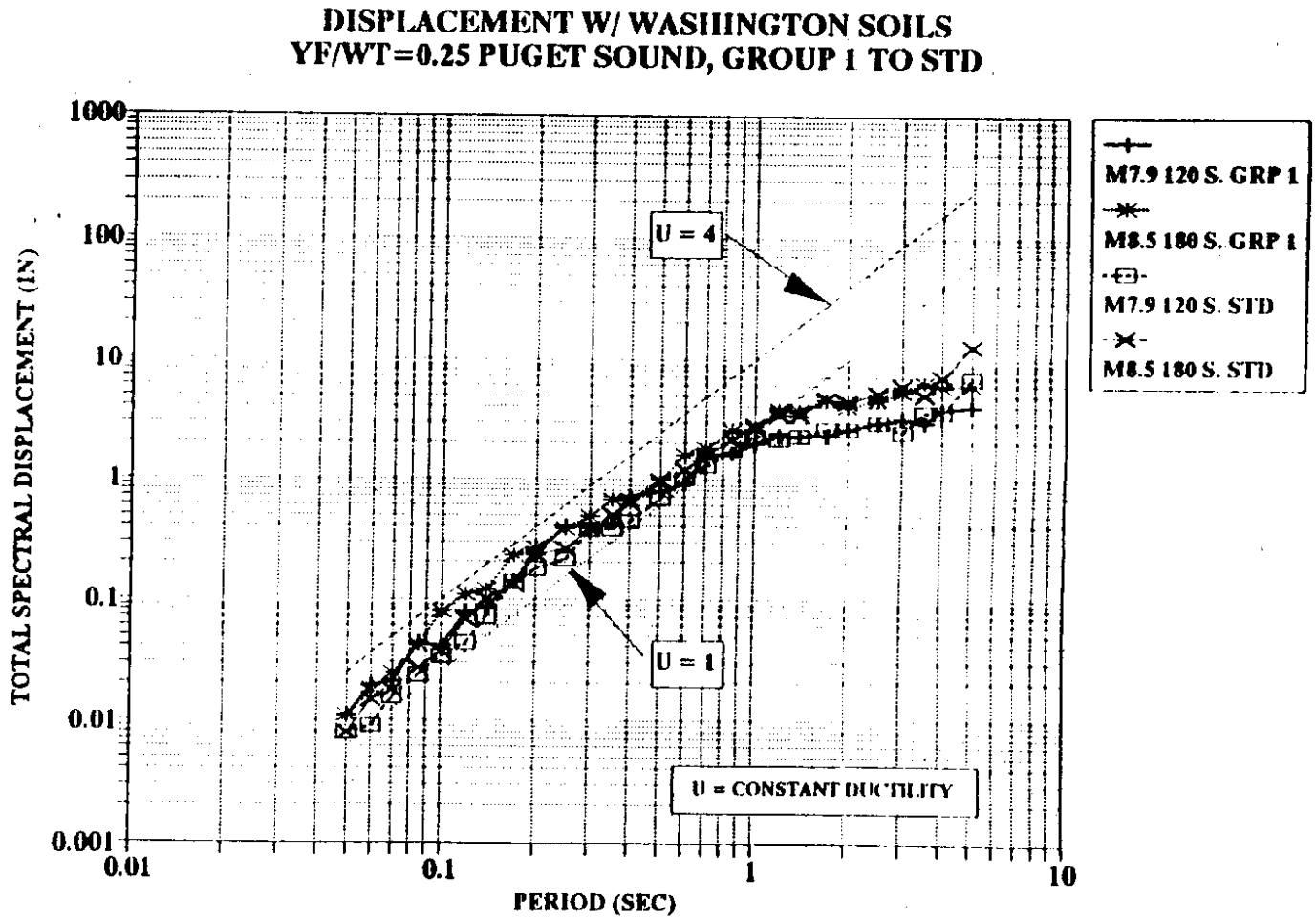


Figure 44 Sensitivity of inelastic spectral displacement to site soil conditions: bi-linear models, Soil Group 1, yf/wt = 0.25.

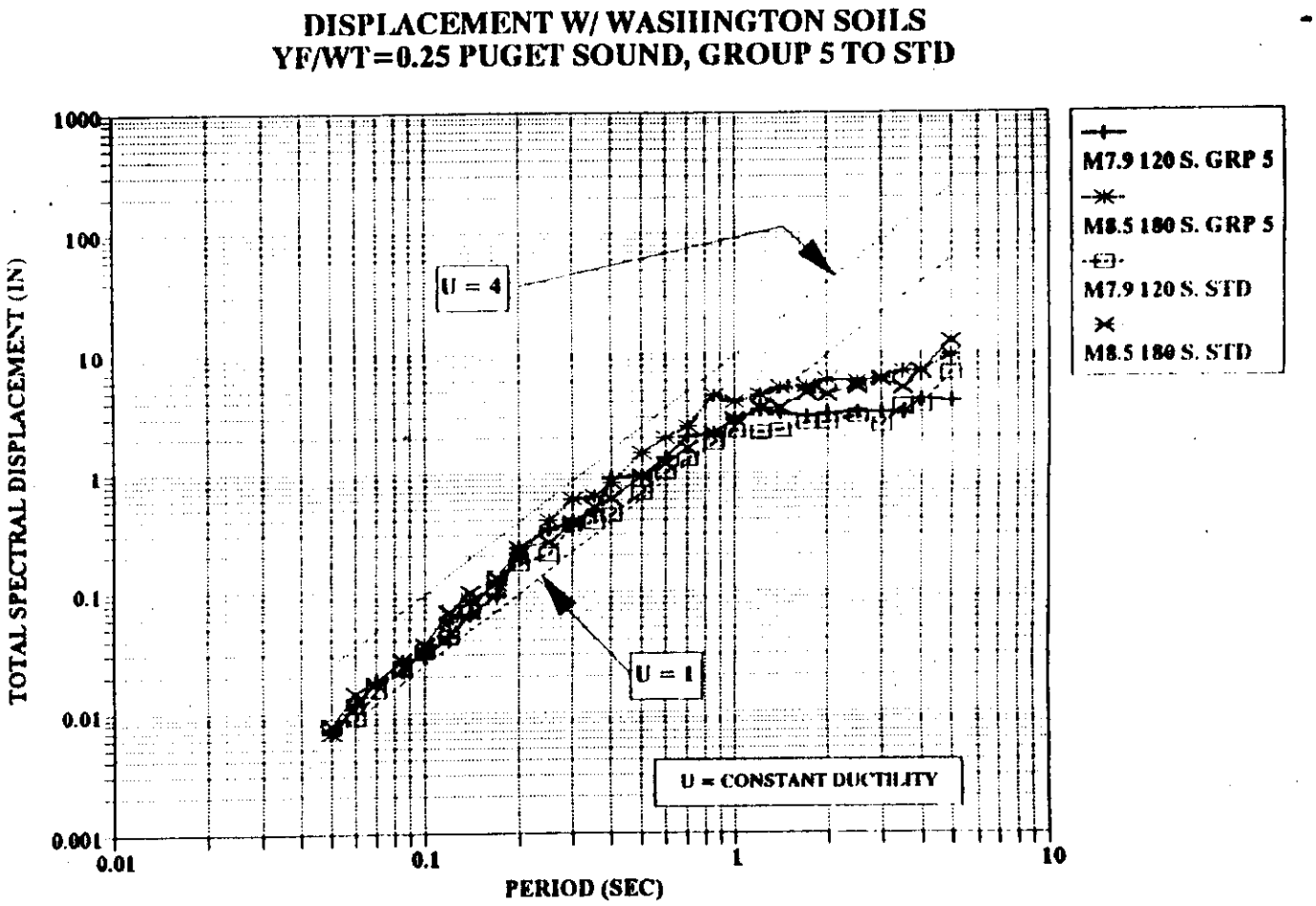


Figure 45 Sensitivity of inelastic spectral displacement to site soil conditions: bi-linear models, Soil Group 5, yf/wt = 0.25.

For bi-linear structures with a yield force to weight ratio of 0.25, at Puget Sound sites, the displacement demand for Soil Group 1 amplified records is as much as 2.5 times the displacement demand for un-amplified records. This difference occurs with periods below 0.2 seconds for a magnitude 7.9 record and 0.4 seconds for a magnitude 8.5 record. Above these periods, the amplification effects are not consistent. Differences become negligible as response becomes elastic. Elastic response occurs above periods of 1.5 seconds. For the same model, structure strength, and location, displacement demand for records amplified by Soil Group 5 are as much as 1.5 times the displacement demands of un-amplified records. This amplification in response occurs in the period range between 0.3 and 3.0 seconds. For periods below 0.3 seconds, the response for un-amplified records and records amplified for Soil Group 5 are very similar. For periods above 3.0 seconds, the response is elastic and nearly the same for amplified and un-amplified records.

Figures 46 and 47 compare the hysteretic energy dissipated for ground motion amplified by Soil Groups 1 and 5 to energy dissipated from ground motion defined by Crouse's (1991) spectra for median earthquakes. There is significant amplification of inferred damage when using an artificial record amplified for soil conditions in Washington State. For a structure with a yield force to weight ratio of 0.25 at a Puget Sound site, the hysteretic energy demand for records amplified by Soil Group 1 are as much as 3 to 4 times the demands for an un-amplified record. This amplification occurs at periods below 0.6 seconds. Hysteretic energy demands for records amplified by Soil Group 5 are as much as 4.5 times the demands for un-amplified records. This amplification occurs in the period range between 0.3 and 2 seconds.

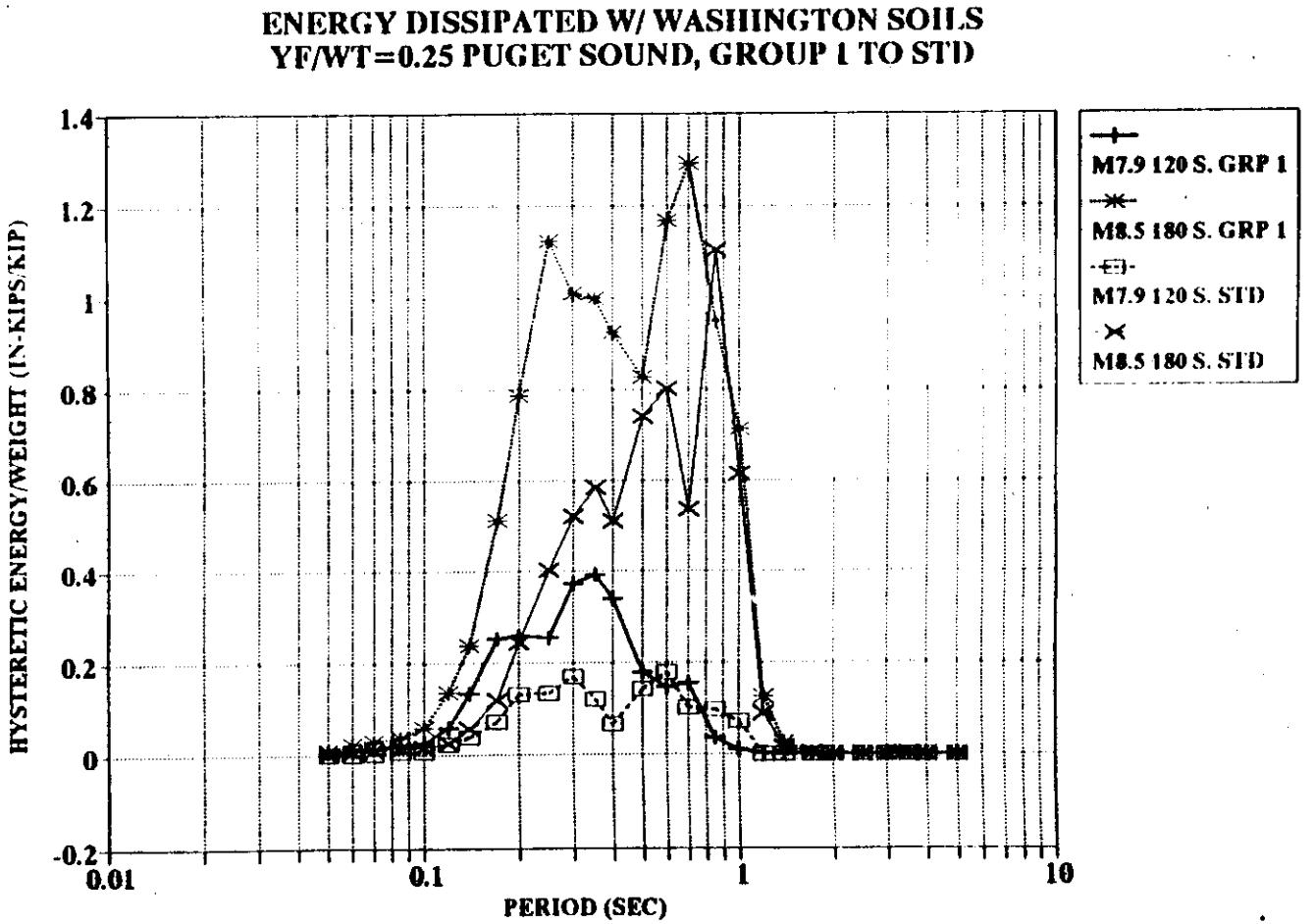


Figure 46 Sensitivity of hysteretic energy demand to site soil conditions: bi-linear models, Soil Group 1, yf/wt = 0.25.

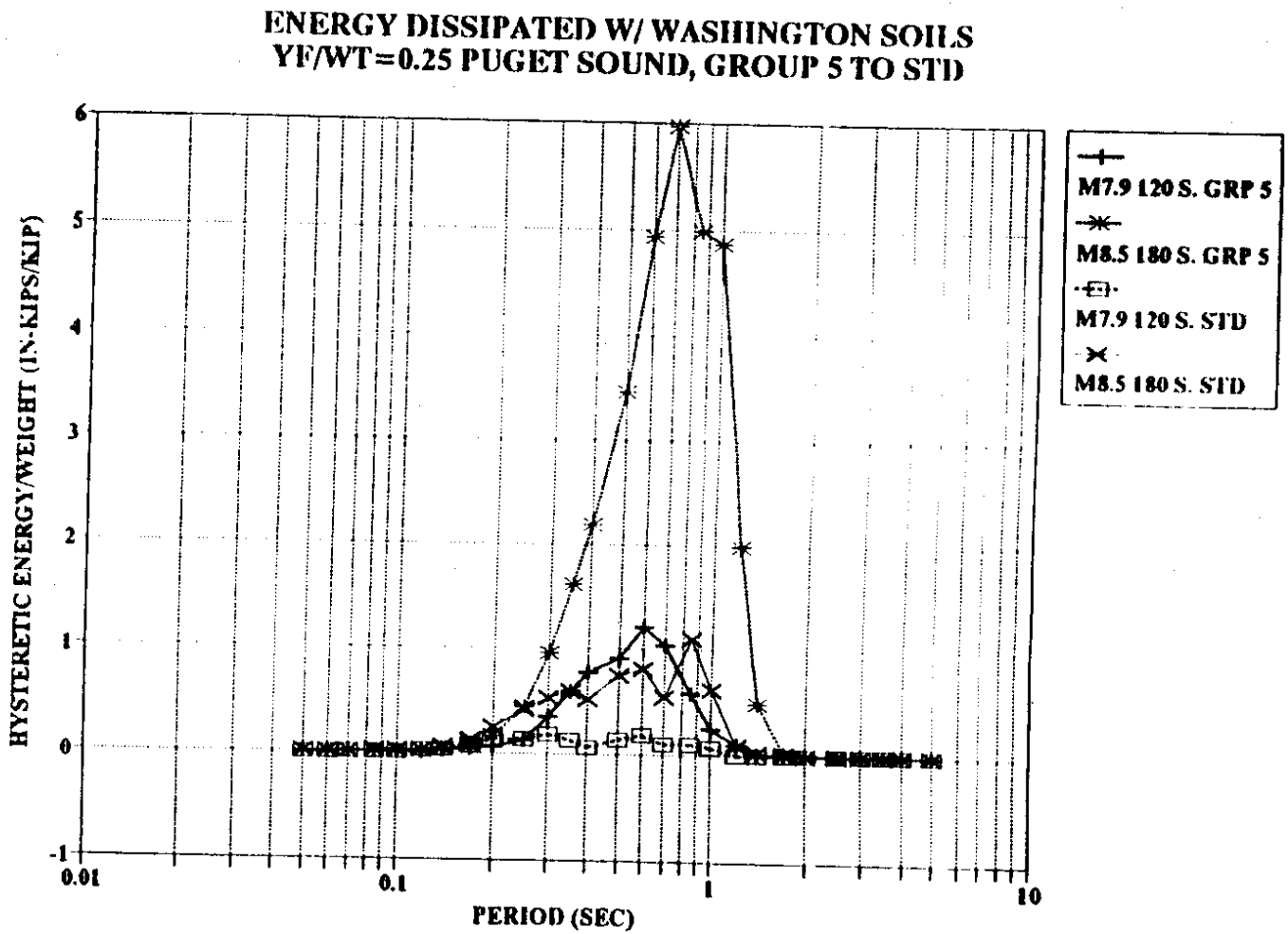


Figure 47 Sensitivity of hysteretic energy demand to site soil conditions: bi-linear models, Soil Group 5, yf/wt = 0.25.

For bi-linear structures, with yield force to weight ratios of 0.125, displacement demands for a magnitude 8.5 180 second record amplified by Soil Group 1 can be as great as twice the displacement demands for the Crouse's median spectra records of the same magnitude and duration. See Figure 48. This difference can be observed for structures with periods of less than 0.1 seconds. Differences between displacement demands of amplified and un-amplified records on structures with periods greater than 0.1 seconds are smaller. Above periods of 2 seconds, where response is elastic, displacement demands to both records is very similar.

For the same structural model and strength and magnitude 8.5 record, hysteretic energy demands for Soil Group 1 records are approximately twice the demands on Crouse's median spectra records, for periods less than 0.2 seconds. See Figure 49. For a magnitude 7.9 120 second record, the difference in the hysteretic energy demands is greater than 2 for periods below 0.1 seconds and approximately 2 between periods of 0.1 and 0.2 seconds. Above 0.2 seconds the demands of the soil amplified records converge with the demands for Crouse's median spectra records.

Records amplified by Soil Group 5 produce displacement demands 3.5 to 1.2 times the displacement demands of Crouse's median spectra records, with bi-linear models with yield force to weight ratios of 0.125 and 180 second magnitude 8.5 Puget Sound records. The largest difference occurs at a period of 0.05 seconds, the smallest difference occurs at a period of 2.0 seconds, where the response is nearly elastic. For 120 second magnitude 7.9 records, the difference between the hysteretic energy demand of Soil Group 5 amplified and un-amplified records is smaller. The trend of Soil Group 5 amplified record displacement demands being greater than Crouse's median spectra record demands holds for the entire period range below 2 seconds. See Figure 50.

Hysteretic energy demands, for the same model and strength, for Soil Group 5 amplified records, are as much as 3.5 times the demands of Crouse's median spectra

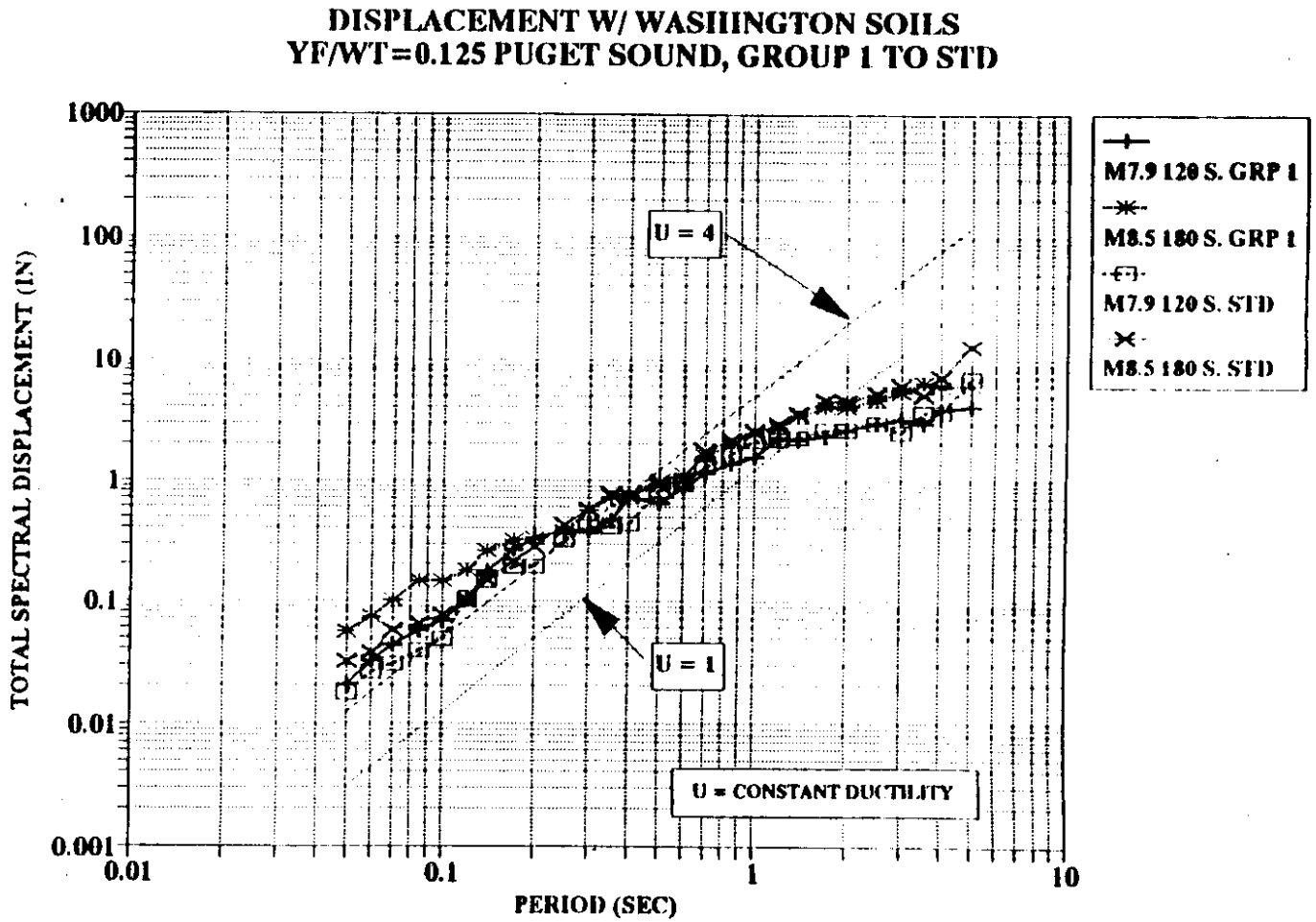


Figure 48 Sensitivity of inelastic spectral displacement to site soil conditions: bi-linear models, Soil Group 1, yf/wt = 0.125.

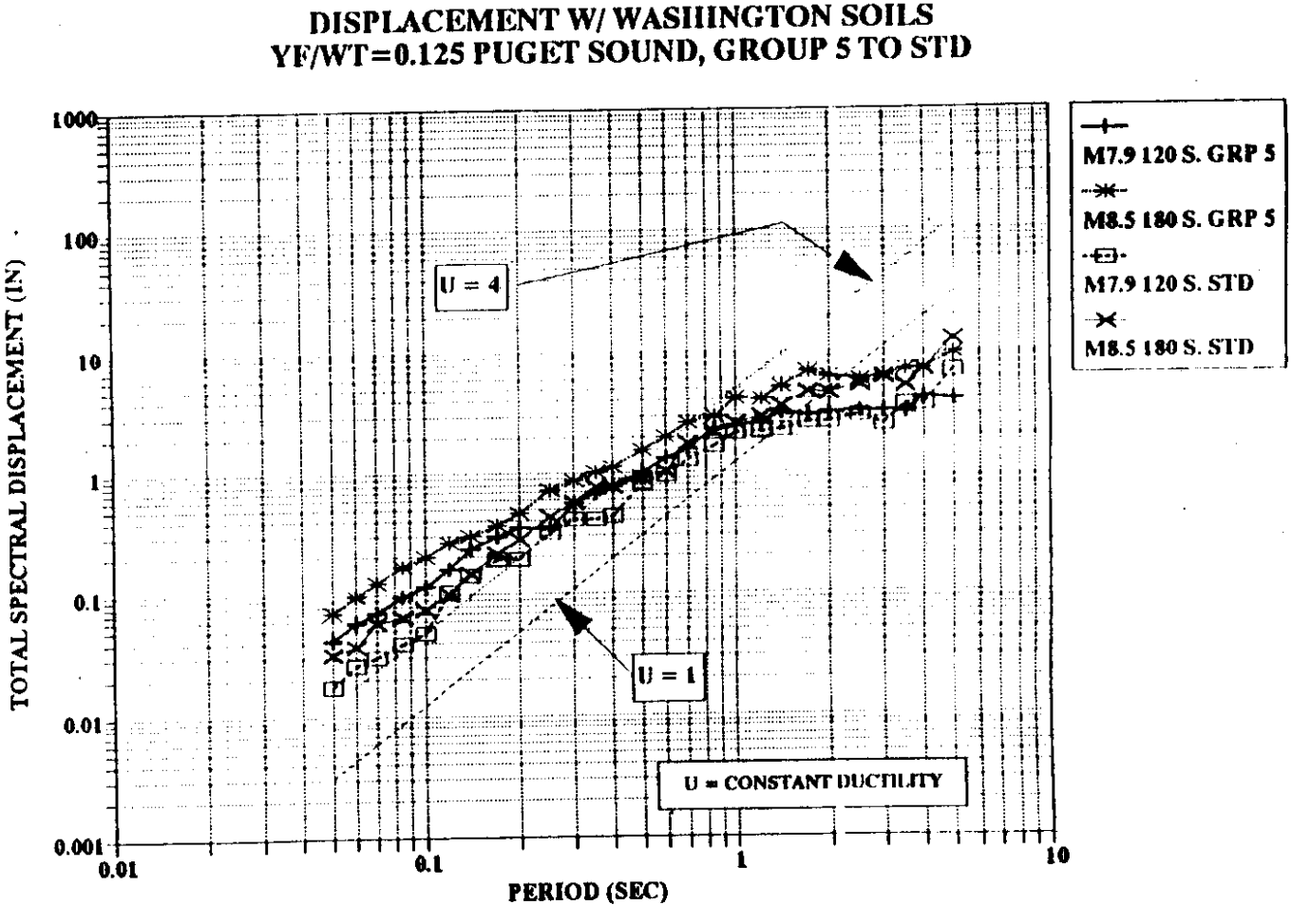


Figure 49 Sensitivity of inelastic spectral displacement to site soil conditions: bi-linear models, Soil Group 5, yf/wt = 0.125.

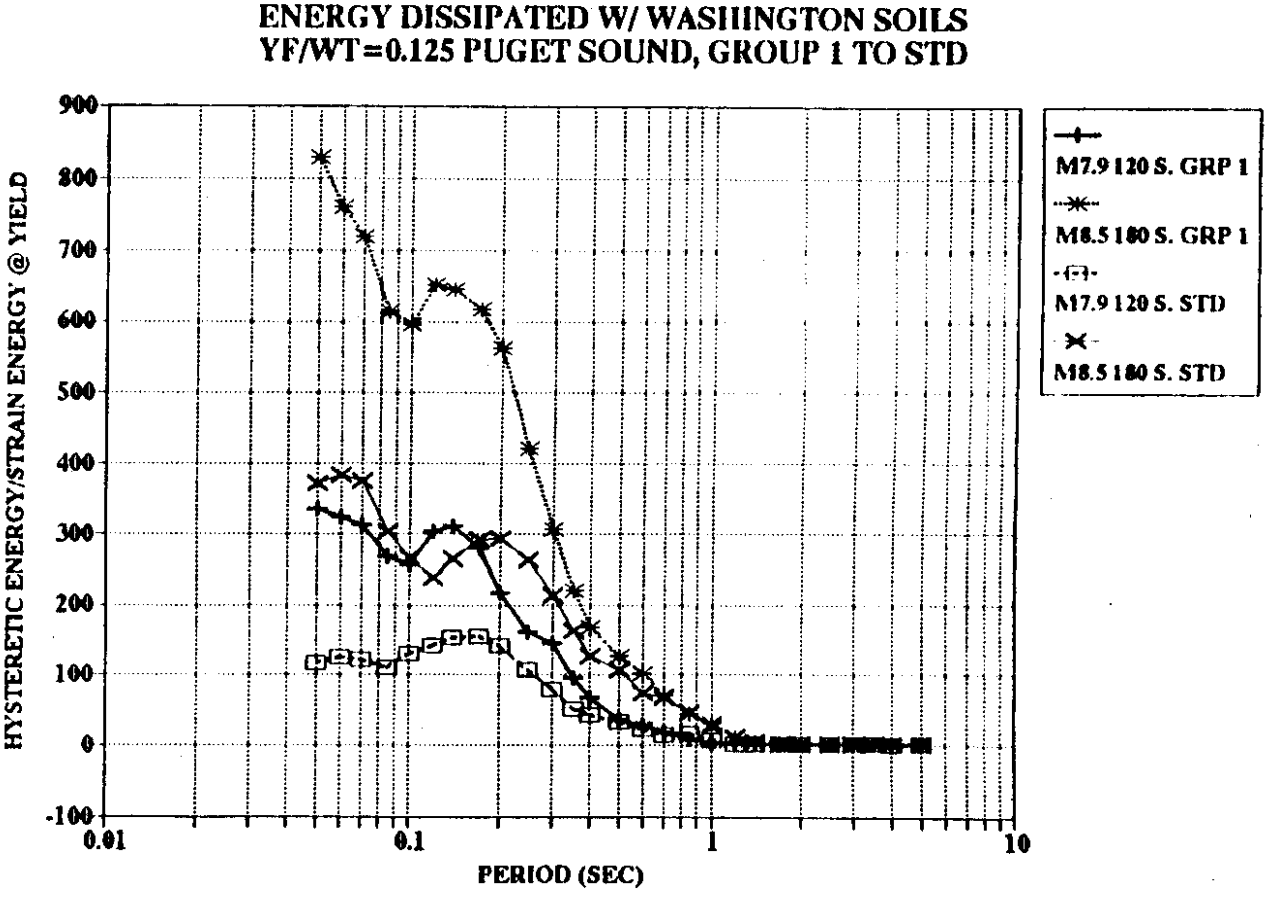


Figure 50 Sensitivity of hysteretic energy demand to site soil conditions: bi-linear models, Soil Group 1, yf/wt = 0.125.

records. This maximum difference occurs at a period of 0.5 seconds for a 180 second magnitude 8.5 Puget Sound record. The large amplification of demands, however, is consistent over the period range of inelastic response, for this magnitude and duration. See Figure 51. For a 120 second magnitude 7.9 record, the differences between hysteretic energy demands for a Soil Group 5 amplified record and Crouse's median spectra record is not as great. For such a magnitude and duration, amplified energy demands can be twice as large as un-amplified demands, but the trend is not consistent over the period range of inelastic response.

The amplification of response to soil amplified records is not proportional to the amplification of the elastic spectra. The amplified displacement demands are not alarming, however, for the acceleration records used. Ductility demands are probably tolerable, for well constructed structures. The amplification of damage, as expressed as dissipated hysteretic energy, is probably due to both the increase in displacements and the long durations.

## 3.8 Inelastic Cycle Counts

As was observed in Sections 4.2 and 4.4, inelastic cycle count demand is affected by both magnitude-duration and yield force to weight ratio. It is also influenced by the period of vibration of the structure. In Figures 52 and 53, the variation in cycle count demand with period is shown for response to a magnitude 8.5 180 second Puget Sound record, for the two different hysteretic models with a yield force to weight ratio of 0.125. In Figures 54 and 55, the same is shown for structures with a yield force to weight ratio of 0.25.

Some significant trends are: more cycle counts occur for degrading stiffness models than for bi-linear models, more cycle counts occur for structures with yield force

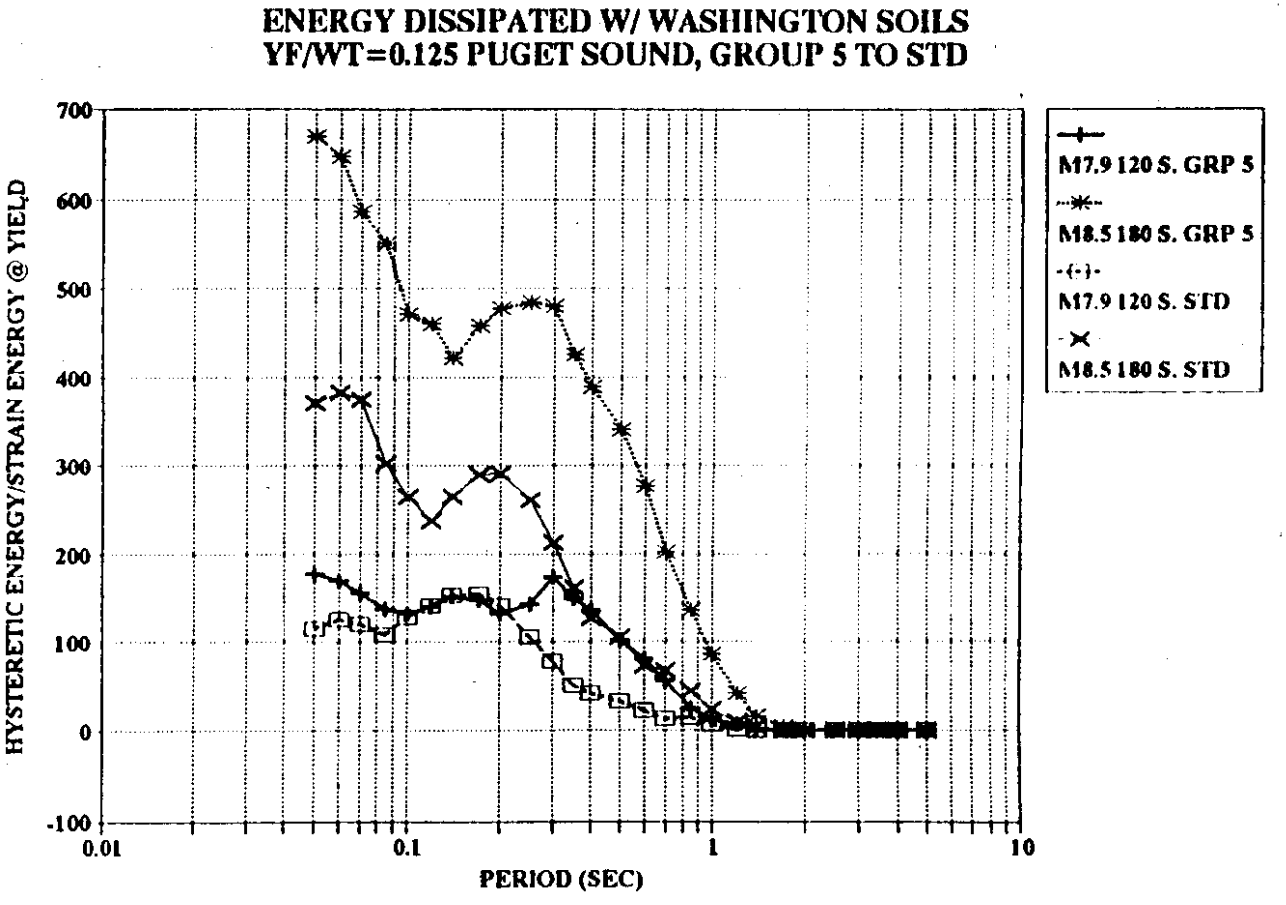


Figure 51 Sensitivity of hysteretic energy demand to site soil conditions: bi-linear models, Soil Group 5, yf/wt = 0.125.

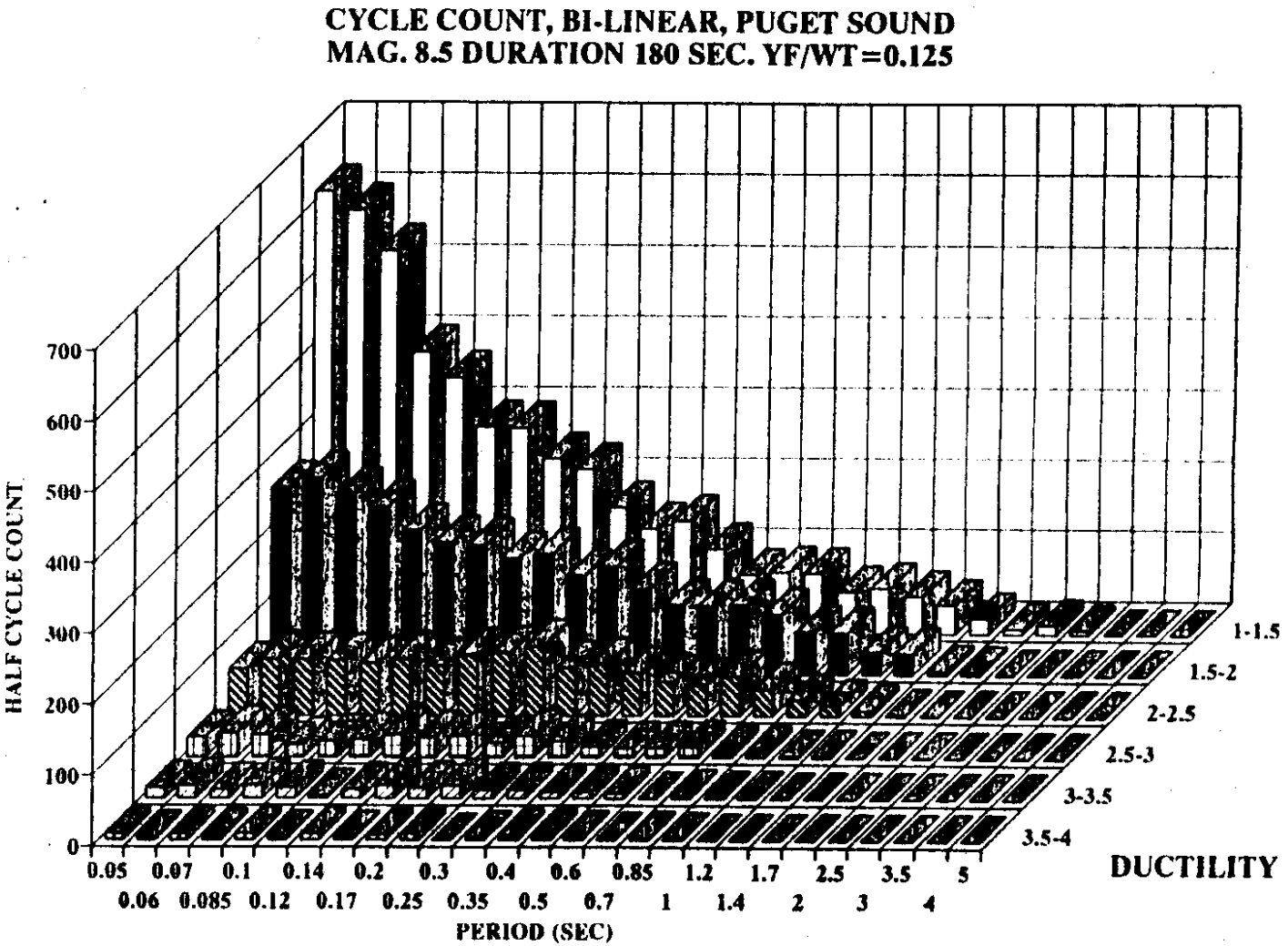


Figure 52 Inelastic cycle count, bi-linear model, yf/wt = 0.125.

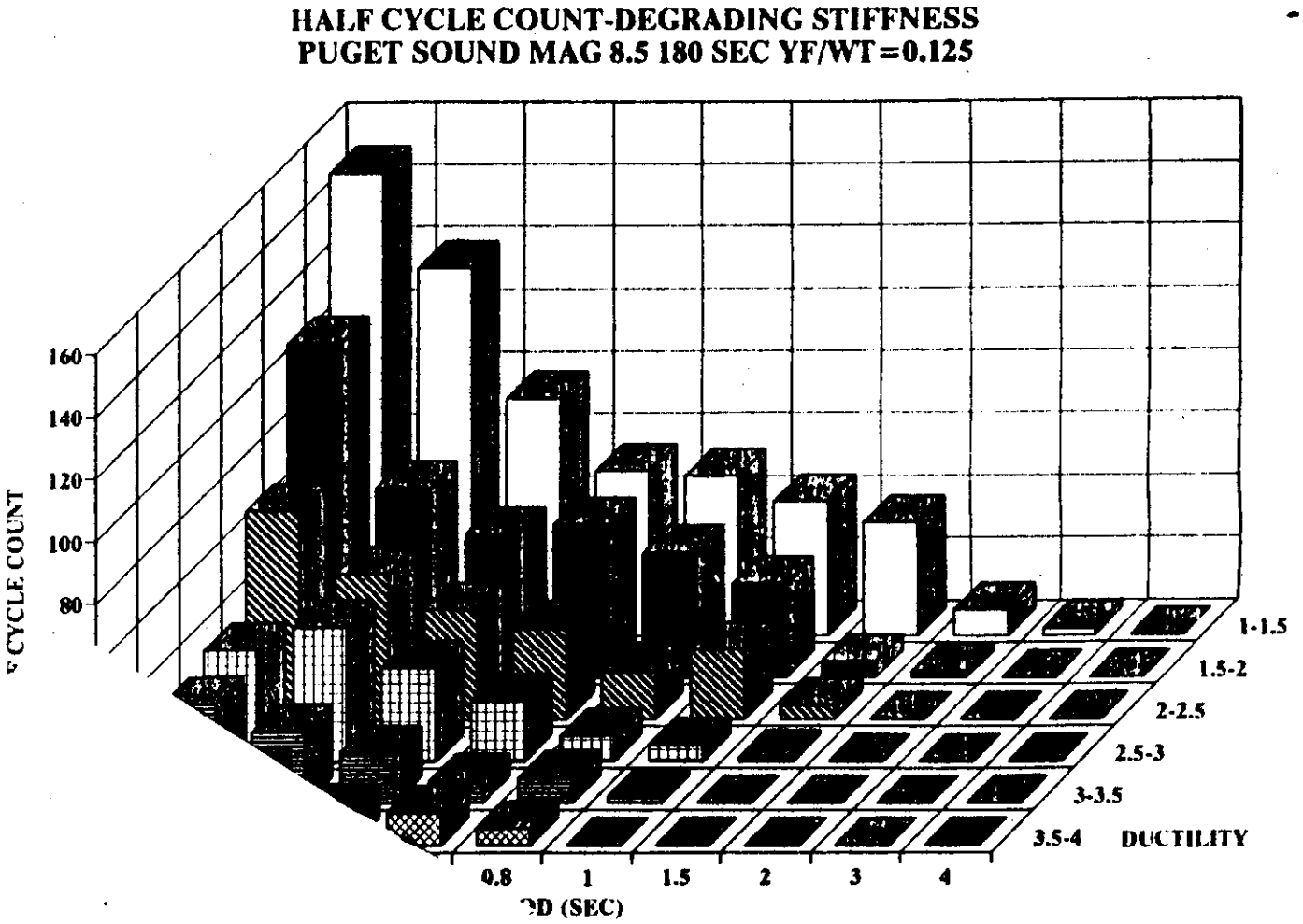


Figure 53 Inelastic cycle count, degrading stiffness model, yf/wt = 0.125.

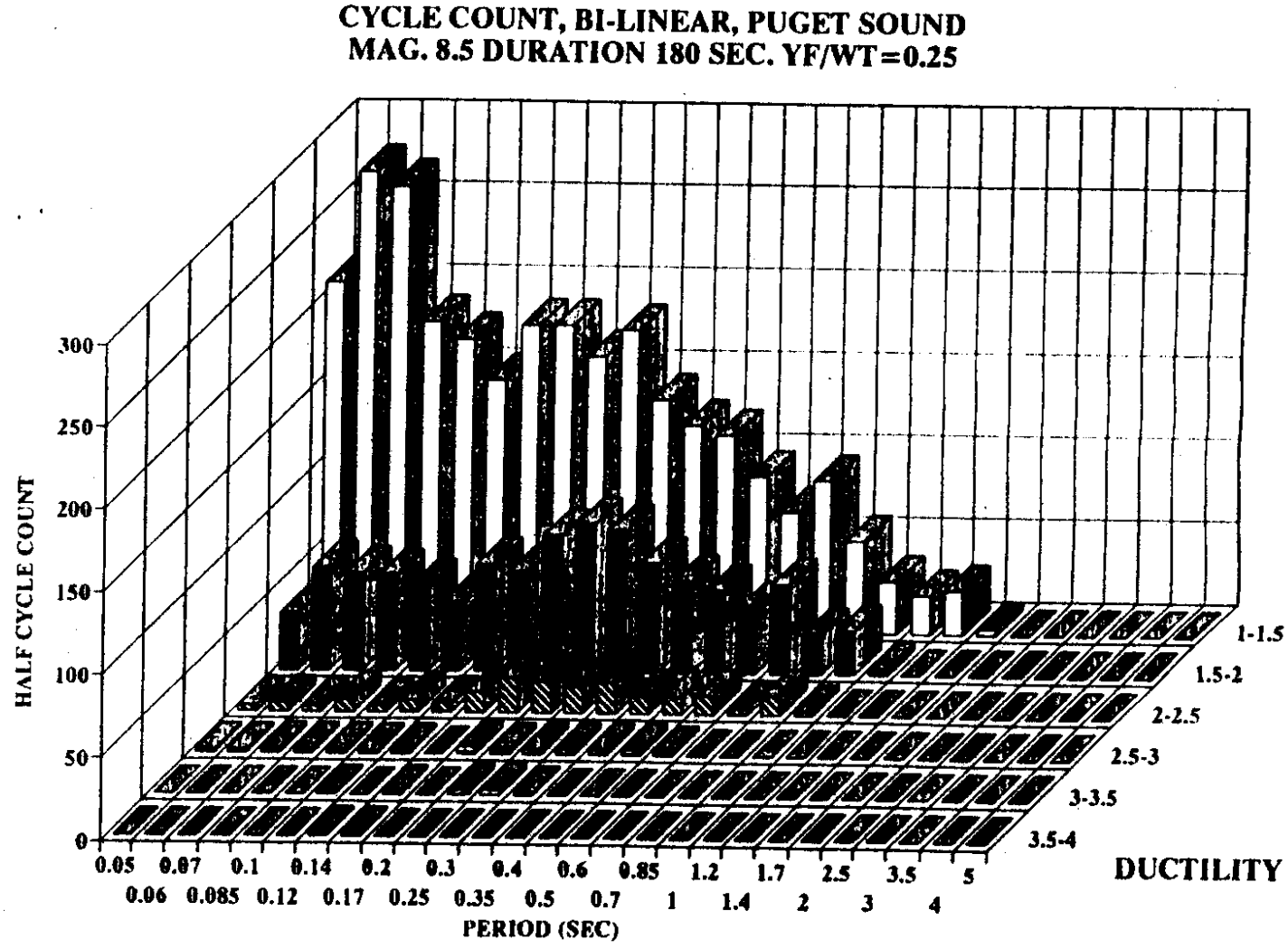


Figure 54 Inelastic cycle count, bi-linear model, yf/wt = 0.25.

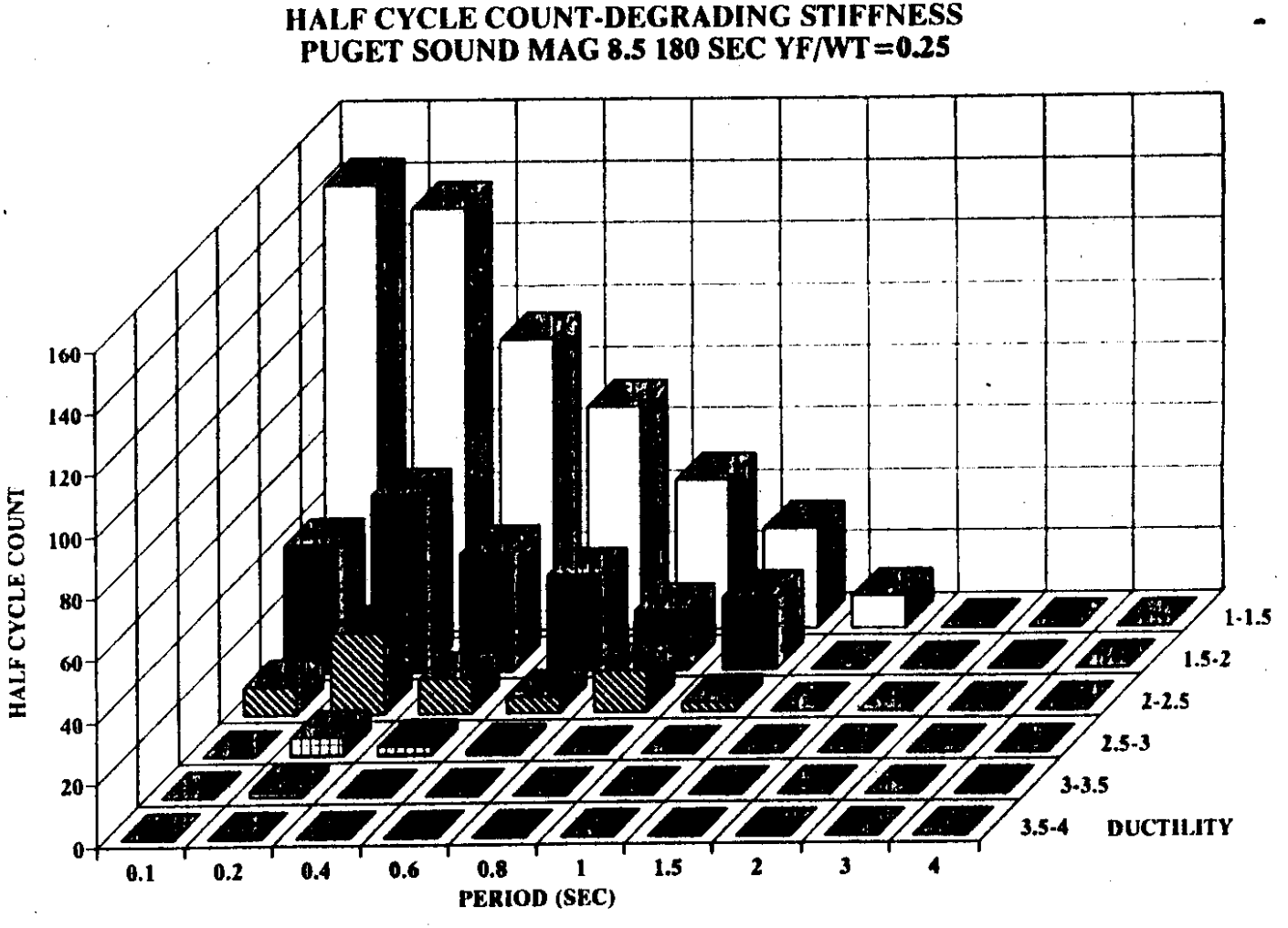


Figure 55 Inelastic cycle count, degrading stiffness model, yf/wt = 0.25.

to weight ratios of 0.125 than for those with 0.25, cycle counts peak in the mid-period ranges for structures with a yield force to weight ratio of 0.25 while cycle counts peak at the lowest period range for structures with a yield force to weight ratio of 0.125.

According to the method used in this research, for bi-linear models, cycles with ductility between 1 and 2 are counted as inelastic but they may, in fact, be elastic. If a reversal of structural displacement begins just prior to the onset of yielding in one direction and this half-cycle ends just prior to yield in the other direction, then the half-cycle is counted as having a ductility of nearly 2. Yet the cycle would, in fact, be elastic and so no hysteretic energy would be dissipated. On the other hand, if a reversal of structural displacement begins at the onset of yielding in one direction and the half-cycle ends at a reversal with displacement three times the yield displacement in the same direction, then the half-cycle is also counted as having a ductility of 2. In such a case hysteretic energy has been dissipated and the half-cycle is, in fact, inelastic. Therefore, the large number of half-cycles counted with ductilities between 1 and 2 may not represent damage. However, they were included because actual structures do not follow a truly bi-linear hysteretic cycle. For most structures, there is curvature of hysteresis loops near the yield point. In such actual structures, half-cycles with ductility between 1 and 2 would dissipate some hysteretic energy.

## 3.9 Hysteretic Energy Demands

Hysteretic energy demand has been shown in most of the preceding figures as the structure's dissipated hysteretic energy normalized by the strain energy stored in the structure at yield. However, it would be more useful to know, more directly, the dissipated hysteretic energy demands on the structure. For this reason, a set of hysteretic energy spectra are included in the appendices. An example is shown in Figure 56. To

determine the total hysteretic energy demand from such a spectrum, the ordinate of the hysteretic energy/weight spectrum is multiplied by the structure weight.

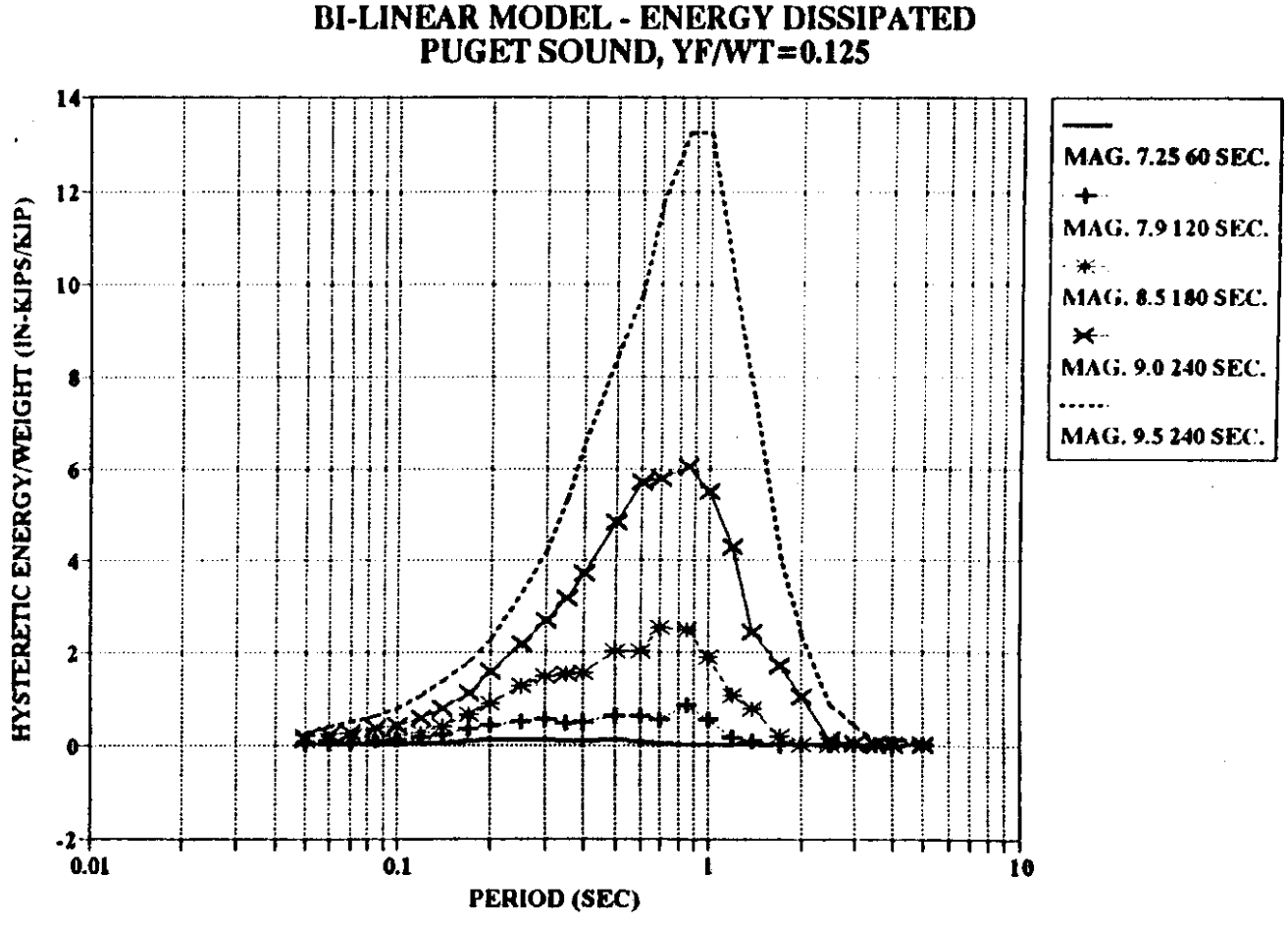


Figure 56 Hysteretic Energy per weight spectra

# CHAPTER 4

# INTERPRETATION, APPRAISAL AND APPLICATION

In this chapter the results that were presented in the Findings section are evaluated. First, the response of the single degree of freedom models to CSZ artificial records is compared with the response to two actual earthquake acceleration records. The south component of the 1940 Imperial Valley earthquake, recorded at El Centro, and the North 86° East component of the 1949 Western Washington earthquake, recorded at Olympia, are used for the comparisons. Next, the response to CSZ artificial records is compared with the response to artificial earthquakes whose spectra are compatible or similar to the AASHTO code design spectrum. Finally, the response to CSZ artificial records is compared with laboratory testing schemes.

## 4.1 Comparison to Actual Acceleration Record Response

Response history analyses were performed on structural models to the 1940 El Centro south acceleration record and the 1949 Olympia North 86° East record. These records have been important in the development of current seismic design criteria. Comparing CSZ response to the response to these records provides a comparison with actual Western U.S. strong ground motion response. In addition, the Olympia record provides a comparison between the artificial CSZ record responses and that of the strongest recorded earthquake in the Pacific Northwest.

Figure 57 shows inelastic displacement spectra for bi-linear models, with yield force to weight ratios of 0.25, for the maximum duration Puget Sound artificial records, and for the El Centro and Olympia records. The Puget Sound artificial records are based upon Crouse's median spectra. Note that for periods less than 0.2 seconds, the

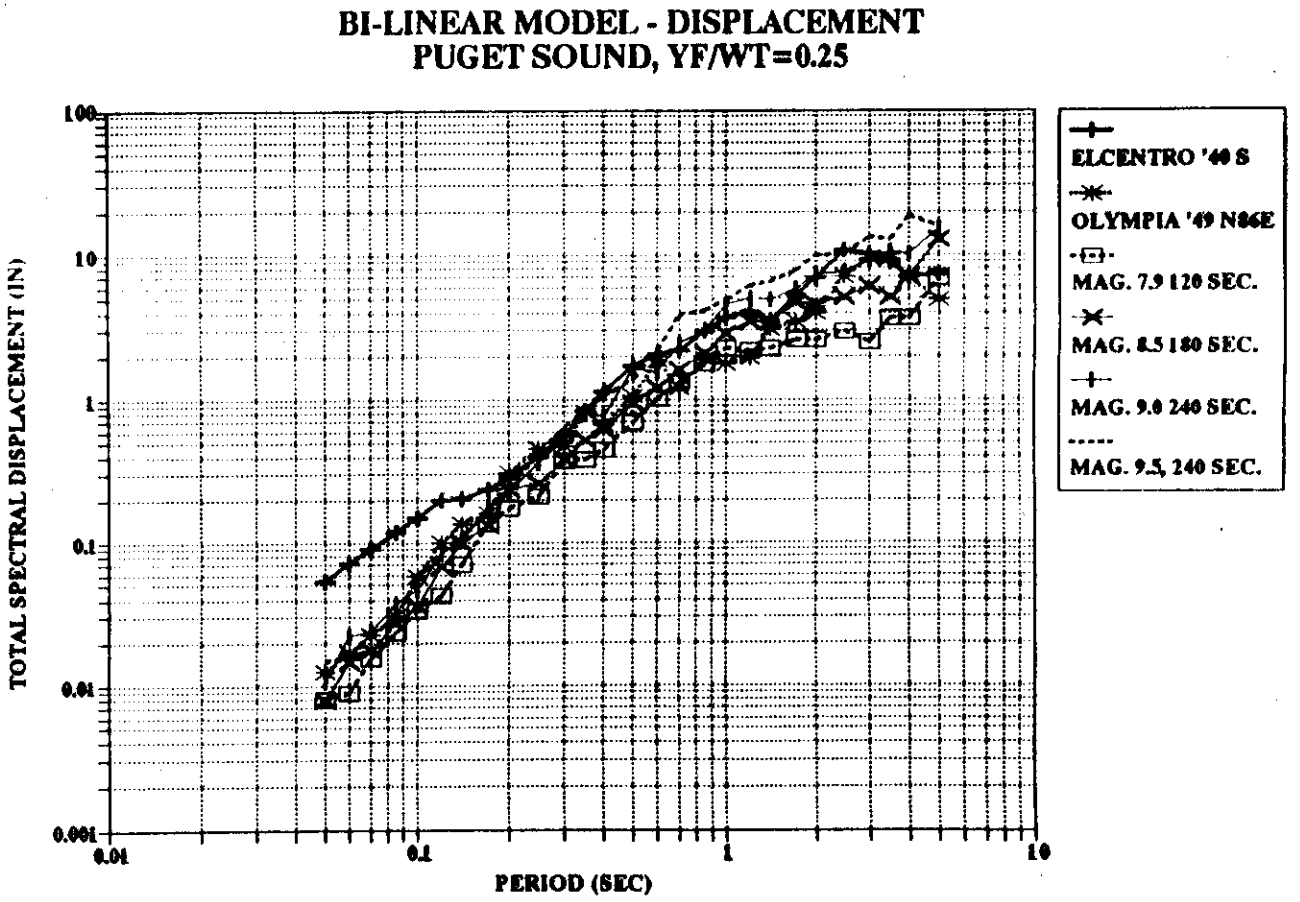


Figure 57 CSZ, El Centro, and Olympia displacement demands, bilinear models (yf/wt = 0.25).

displacement spectra for El Centro are higher than any of the displacement spectra for the Puget Sound artificial records. In the longer period region, the El Centro spectrum is close to those for the four minute duration, magnitude 9.0 and 9.5 artificial records. The Olympia spectrum is close to the spectra for the artificial records with 9.0 and 9.5 magnitudes for structures with periods below 0.3 seconds. In the range where periods are longer than 0.3 seconds, the Olympia spectrum is as low as the spectrum for the CSZ magnitude 7.9 record and as high as the spectrum for the CSZ magnitude 9.5 record.

Figure 58 shows the normalized hysteretic energy dissipated by a bi-linear structure with a yield force to weight ratio of 0.25. The normalization constant is the strain energy stored in the structure at yield. The results shown are for the El Centro and the Olympia records and those for the longest duration CSZ artificial records as felt in Puget Sound. In the low period region, less than 0.2 seconds, the hysteretic energy demand of the El Centro record is much greater than the demand of the Puget Sound artificial records. For periods longer than 0.2 seconds, the hysteretic energy demand of the El Centro record is less than the demands of the four minute magnitude 9 and 9.5 artificial records and greater than those of the three minute magnitude 8.5 artificial records. The hysteretic energy demand for the Olympia record is nearly equal to the demands of the magnitude 7.9 CSZ record for structures with periods either shorter than 0.1 seconds or longer than 0.4 seconds. For the intermediate period range, the Olympia hysteretic energy demand lies between the demands of the magnitude 7.9 and 9.5 CSZ records, although, at a period of 0.2 seconds the Olympia demand is slightly greater than the demand of the magnitude 9.5 CSZ record.

Figure 58 presents the energy demands as multiples of the energy stored in the system at first yield. Another meaningful way to consider the energy demands is to compare them to those of one complete inelastic displacement cycle at a given ductility demand, for instance a ductility demand of four. The energy dissipated in one complete

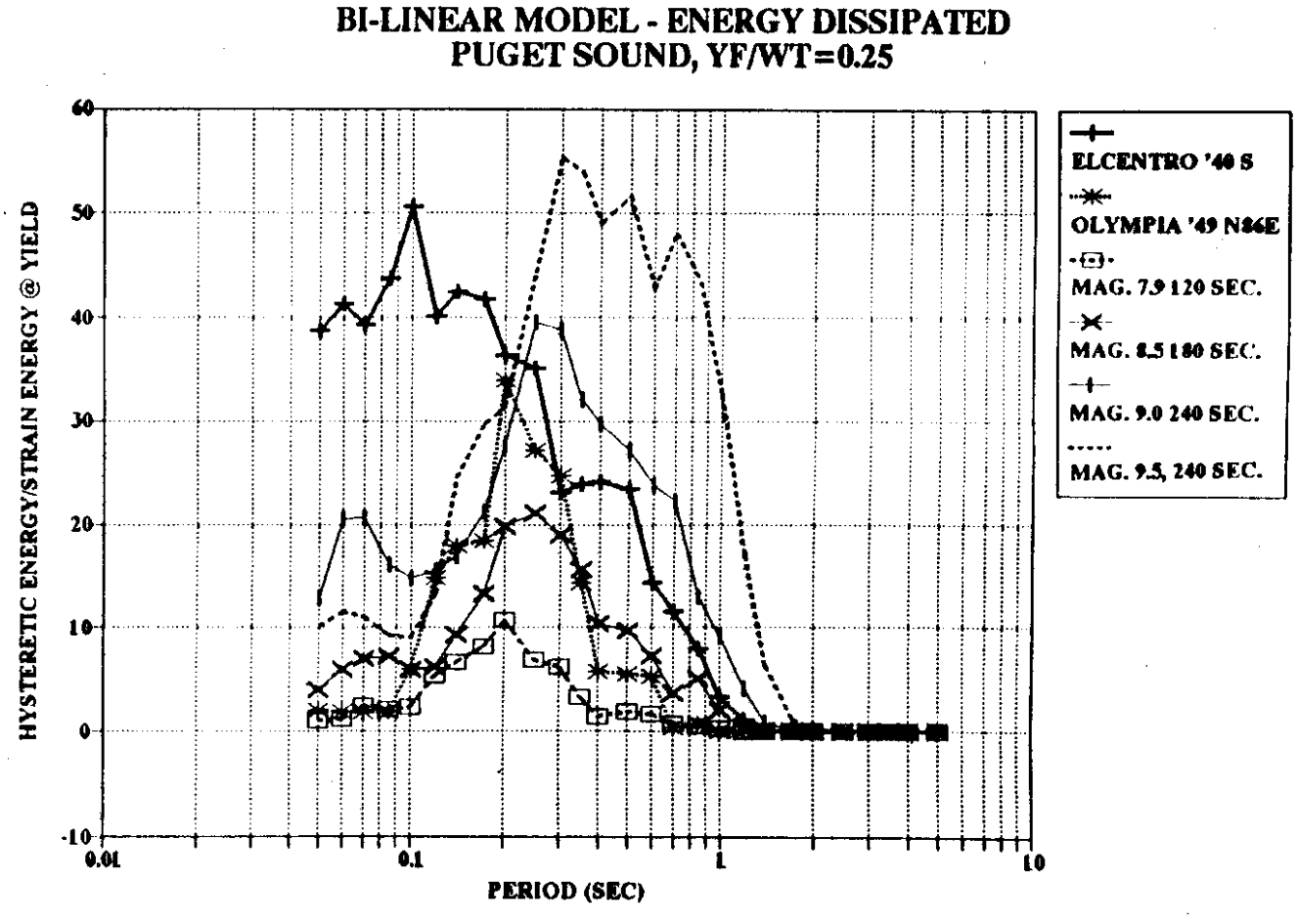


Figure 58 CSZ, El Centro, and Olympia hysteretic energy demands, bilinear models (yf/wt = 0.25).

displacement cycle between a ductility demand of positive four and negative four is 22.8 times the energy stored in the bilinear system at yield. This multiple is independent of period and of yield force to weight ratio. It depends only on the shape of the load-displacement relation and the hardening ratio, which was 5 percent in this study. Table 6 presents the constants for the models used in this study for ductility demands of 2, 3, and 4. Using these values and Figure 58, the maximum number of cycles at a ductility demand of 4 that the magnitude 9.5 event produced was 2.4. This is calculated by dividing the maximum normalized energy demand, 55, which occurs at a period of 0.3 seconds, by the constant 22.8. This demand is not severe for well-detailed structures. Note that the number of cycles calculated using this method considers that all the inelasticity occurs in cycles at the prescribed ductility level. Actually, cycles at various ductility levels occur as shown by the cycle count plots. The method of equating the energy demand to a number of cycles at a constant demand is simply a tool to assess the severity of the demands. The demands for the CSZ records related as equivalent cycles a ductility of 4 are also shown later in this chapter in Figure 78.

The degrading stiffness model maximum displacement and energy demands are compared in Figures 59 and 60, respectively. Below periods of 0.5, seconds the displacement demand of a structure with a yield force to weight ratio of 0.25 subject to the El Centro record is higher than the demand from any CSZ artificial record. Above 0.5 seconds, the El Centro displacement demand is between the demands for the CSZ four minute magnitude 9.5 and the three minute magnitude 8.5 records. The Olympia displacement demand is between the displacement demands for the four minute magnitude 9.5 and two minute magnitude 7.9 CSZ records.

Hysteretic energy demand for degrading stiffness models with yield force to weight ratios of 0.25 subject to El Centro is between the demands for the three minute magnitude 8.5 and the four minute magnitude 9.0 CSZ records. The Olympia hysteretic energy

Table 6 Ratios of energy dissipated for cycles at prescribed ductility demand levels to that energy stored at first yield

| Model | Ductility Level | | |
|---|---|---|---|
| | 2 | 3 | 4 |
| Bilinear | 7.6 | 15.2 | 22.8 |
| Degrading Stiffness | 3.9 | 8.4 | 13.1 |

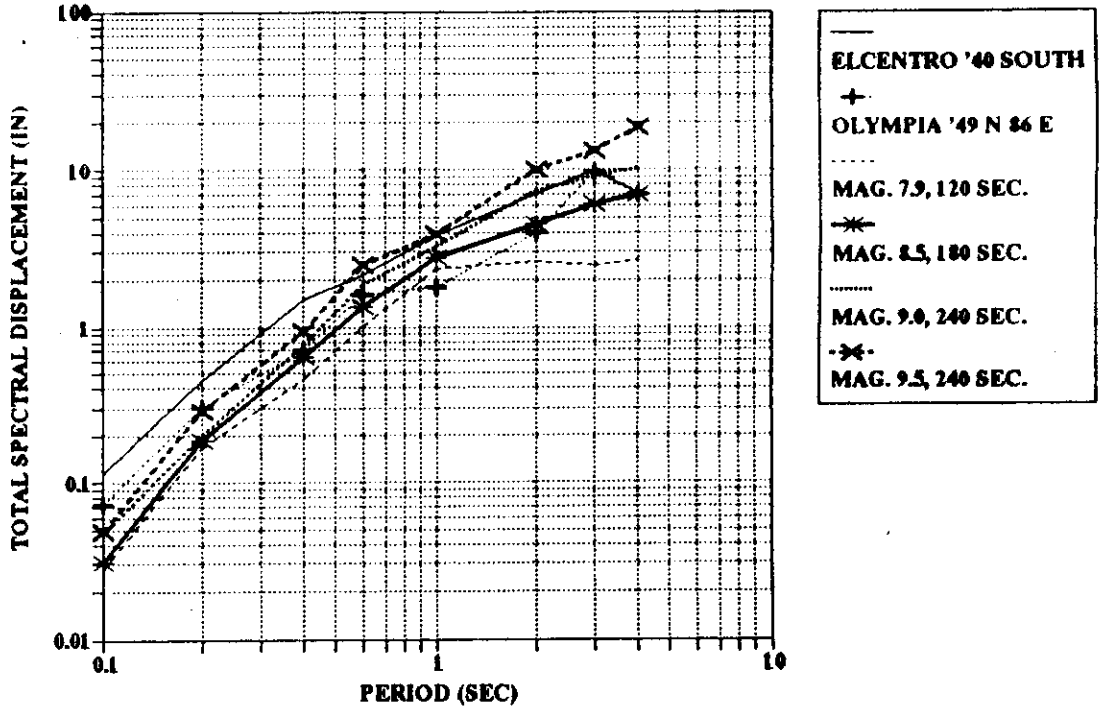


Figure 59 CSZ, El Centro, and Olympia displacement demands, degrading stiffness models (yf/wt = 0.25).

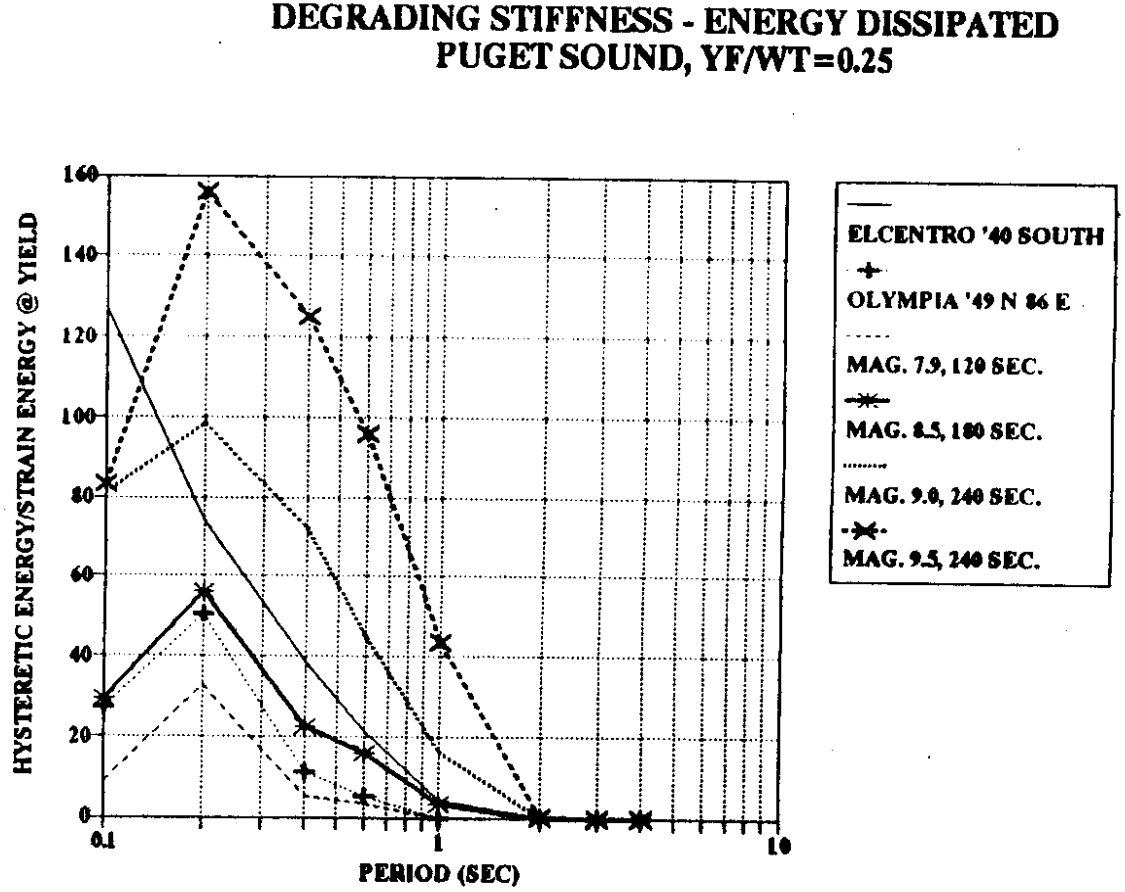


Figure 60 CSZ, El Centro, and Olympia hysteretic energy demands, degrading stiffness models (yf/wt = 0.25).

demand is between the demands of the two minute magnitude 7.9 record and the three minute magnitude 8.5 record. The equivalent number of inelastic cycles at a ductility demand, $\mu$, of 4 is 11.8 for a 0.2 second period model subject to the magnitude 9.5 record. This is the highest demand produced by any of the records, and it represents a high number of equivalent cycles that must be endured. In contrast, the magnitude 8.5 record produces fewer numbers of equivalent $\mu = 4$ cycles, for instance 4.2 at a period of 0.2 seconds. All the demands drop dramatically as the period is increased from 0.2 seconds.

The displacement demands for bi-linear models with a yield force to weight ratio of 0.125 are shown in Figure 61. For periods less than 0.3 seconds, displacement demands for El Centro are greater than the CSZ displacement demands. Above 0.3 seconds, the El Centro displacement demand is between the demands of the 4 minute magnitude 9.5 CSZ record and the 3 minute magnitude 8.5 record. Below a period of 0.5 seconds, the displacement demands for the Olympia record are nearly equal to the demands of the magnitude 9.0 and 9.5 CSZ records. Above 0.5 seconds, the Olympia displacement demands are as low as the demands of the magnitude 7.9 CSZ record near a 1 second period and as high as the magnitude 9.0 CSZ record near a 3 second period.

Hysteretic energy demands for a yield force to weight ratio of 0.125 are shown in Figure 62. For the El Centro record the demands are close to the demands for the 4 minute magnitude 9.0 CSZ record when the period is less than 0.1 seconds. Above 0.1 seconds, the demands for El Centro converge to the demands for the 3 minute magnitude 8.5 CSZ record. The Olympia hysteretic energy demands for the same model and structure strength are between the demands for the two minute magnitude 7.9 record and the three minute magnitude 8.5 CSZ record. The equivalent number of cycles to $\mu = 4$ for this structure strength is extreme, as high as 66, for the stiffest models. However for periods greater than 0.3 seconds and magnitudes less than or equal to 8.5, the number of cycles is less than 9 (200 divided by 22.8). This is a high value, although most numbers of

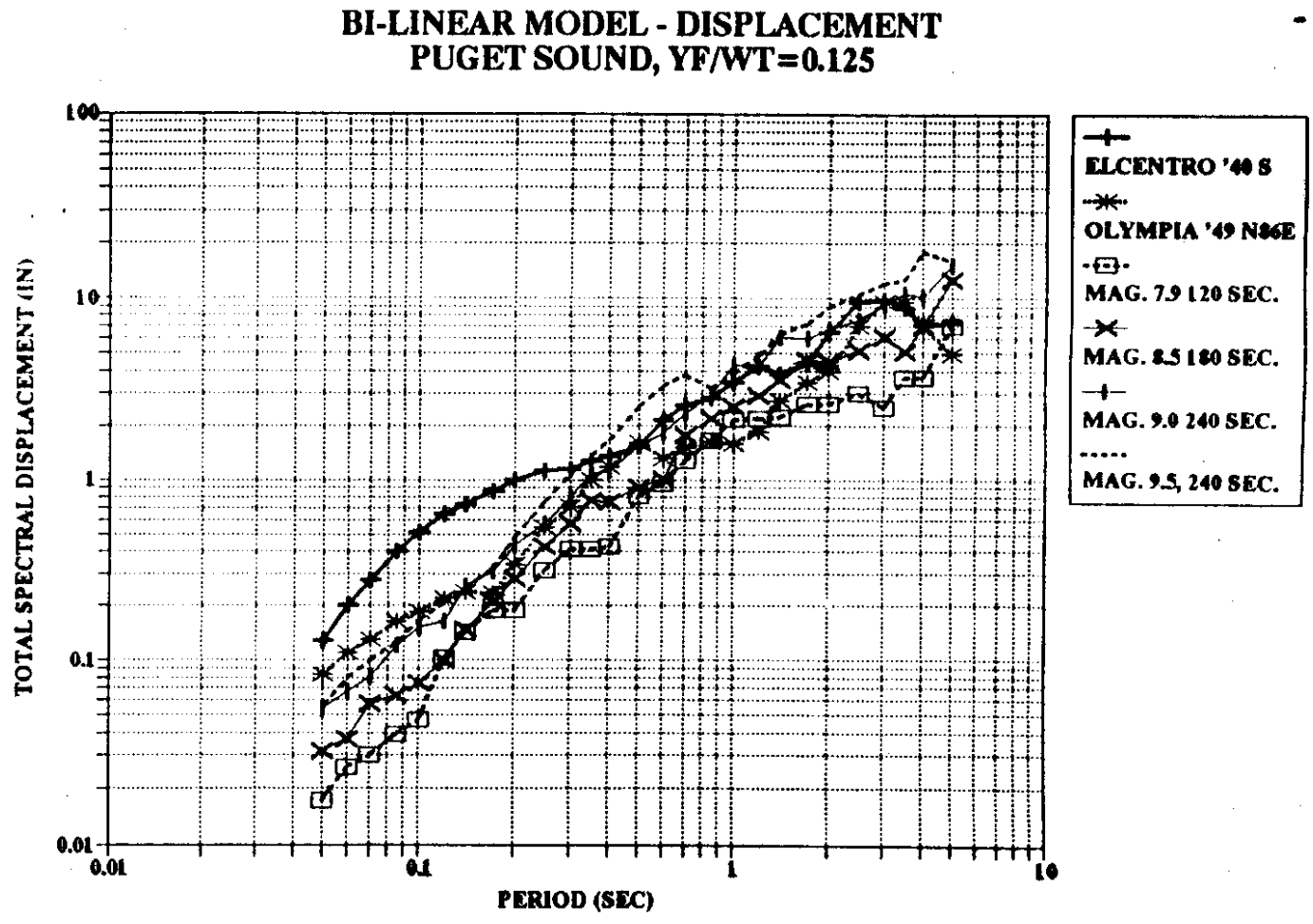


Figure 61 CSZ, El Centro, and Olympia displacement demands, bi-linear models, (yf/wt = 0.125).

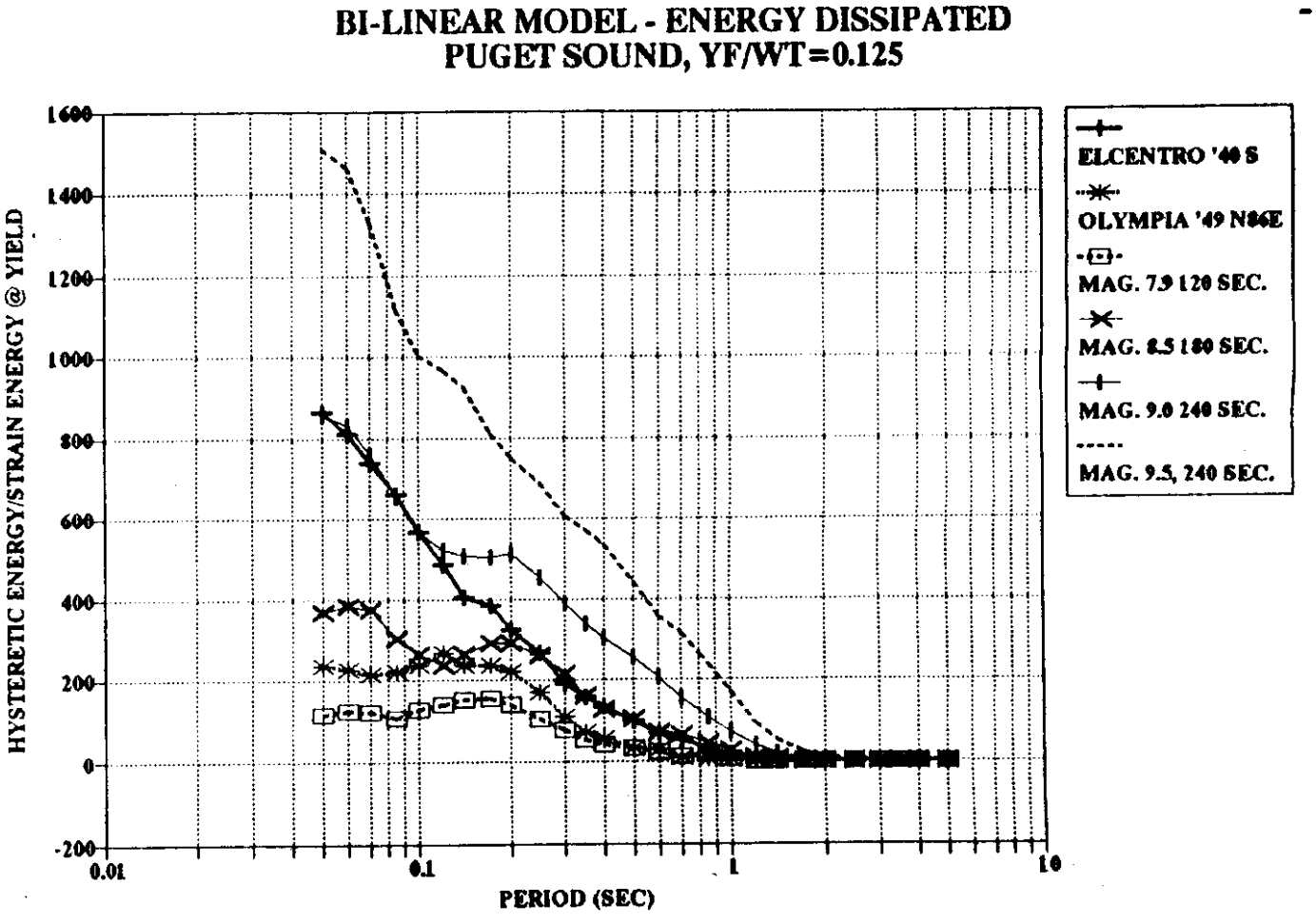


Figure 62 CSZ, El Centro, and Olympia hysteretic energy demands, bi-linear models (yf/wt = 0.125).

equivalent cycles in this period range are less than 5, a tolerable value for well constructed structures.

For a degrading stiffness model with a yield force to weight ratio of 0.125, the displacement demands for El Centro are greater than to the 4 minute magnitude 9.5 CSZ record when the period is less than 0.3 seconds. See Figure 63. For larger periods, the displacement demands for El Centro are nearly equal to the demands for the 4 minute magnitude 9.0 CSZ record. The demands for the Olympia record are between those for the 4 minute magnitude 9.5 and the 2 minute magnitude 7.9 CSZ records.

The hysteretic energy demand is shown in Figure 64. For El Centro the demands are between those for the 3 minute magnitude 8.5 and the two minute magnitude 7.9 CSZ records. The hysteretic energy demands for Olympia are between the demands for the 2 minute magnitude 7.9 CSZ record and the 3 minute magnitude 8.5 CSZ record. When the energy demands for the 0.125 yield force to weight model are converted to equivalent numbers of $\mu = 4$ cycles, it is evident that the demands are quite high for the stiffer structures. Since the proportionality constant between the energy stored at first yield and that dissipated for each $\mu = 4$ cycle is 13.1, a level of energy demand of 131 on the ordinate of Figure 64 corresponds to 10 equivalent cycles. Only structures with periods greater than 0.5 seconds subject to magnitude 8.5 records or smaller experience such demands. The implication of this is that structures with such low yield force to weight ratios, 0.125, should be avoided if the period of vibration is shorter than about 0.5 seconds.

Example inelastic half cycle counts for bi-linear and degrading stiffness models with yield force to weight ratios of 0.25 are shown in Figures 65 and 66, respectively. The counts for El Centro and Olympia are lower than those of CSZ artificial records up to ductility ranges of 2.5 to 3, for structures with yield force to weight ratios of 0.25. This same trend holds for periods above 0.2 seconds, and it also holds for structures with yield

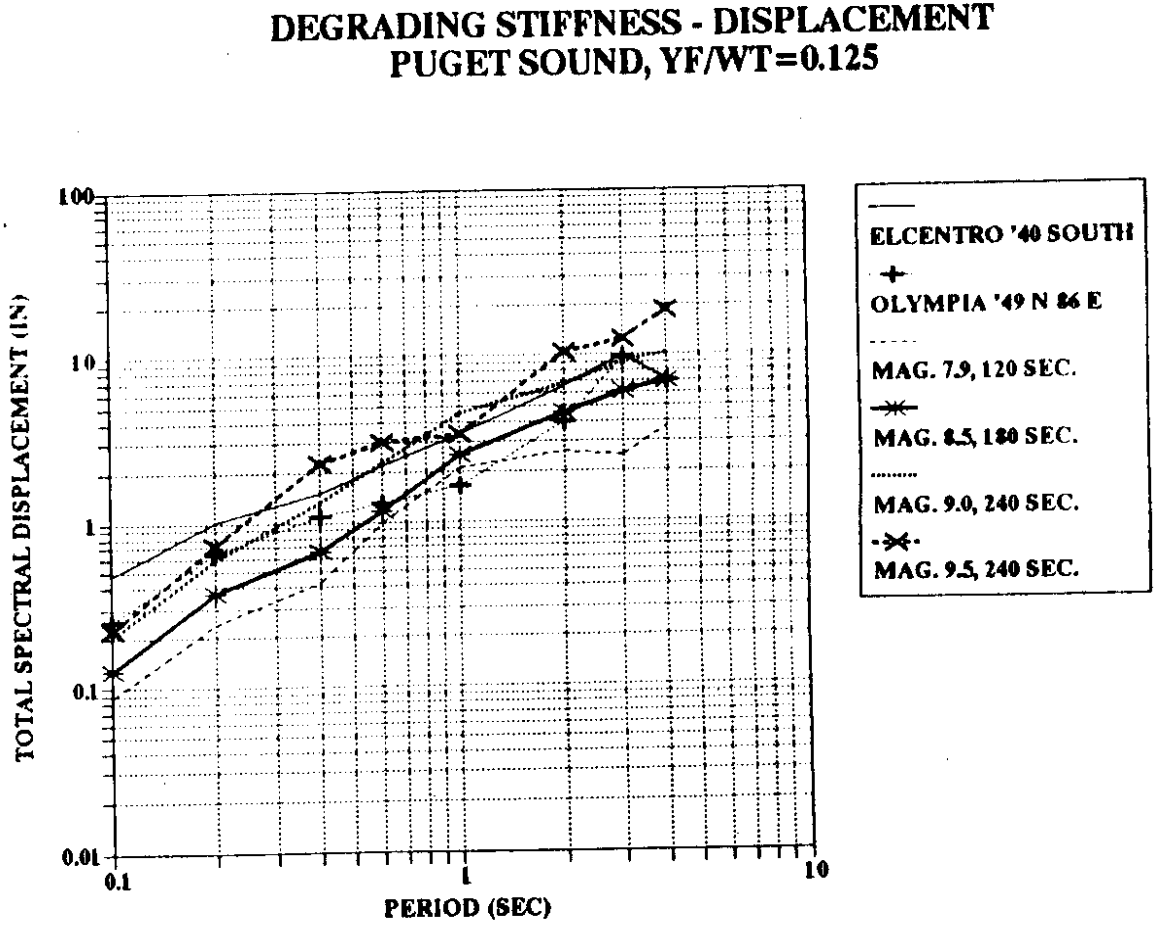


Figure 63 CSZ, El Centro, and Olympia displacement demands, degrading stiffness models, (yf/wt = 0.125).

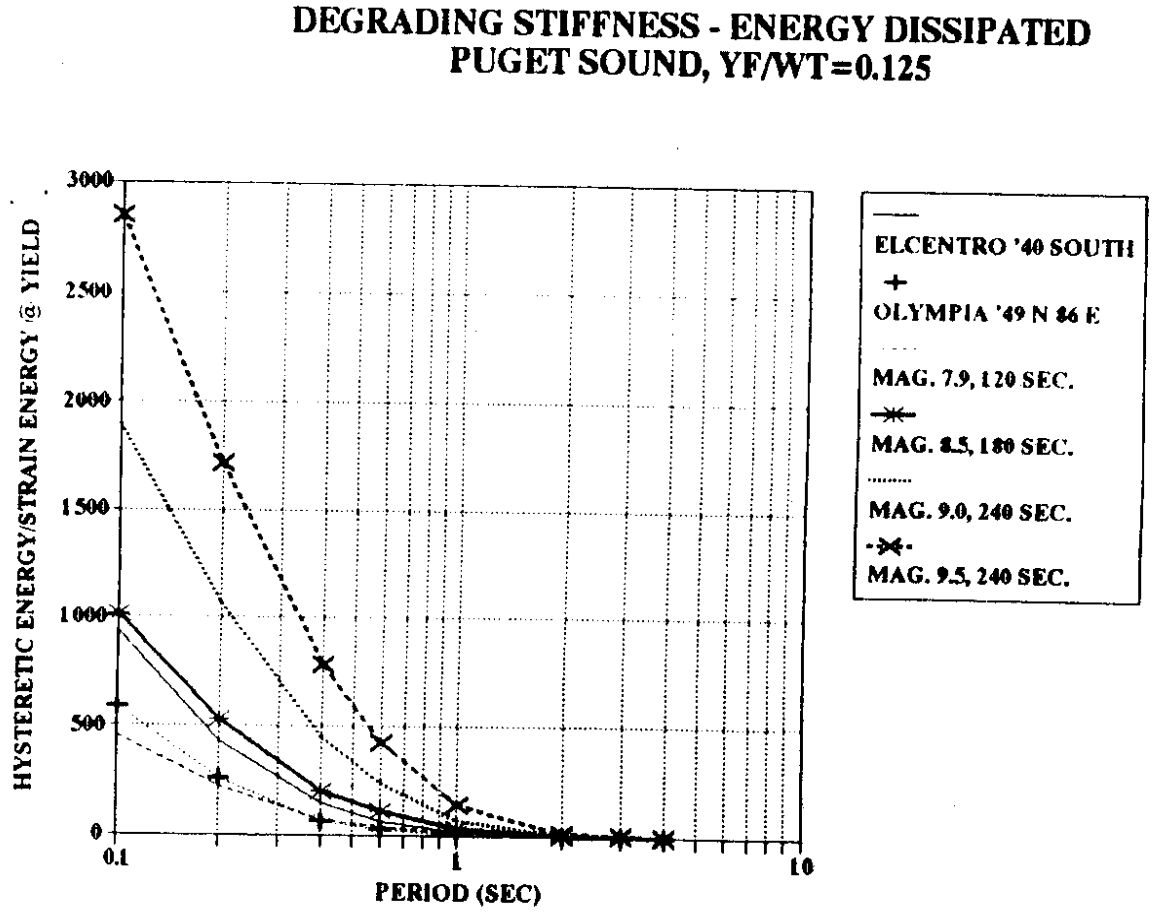


Figure 64 CSZ, El Centro, and Olympia hysteretic energy demands, degrading stiffness models (yf/wt = 0.125).

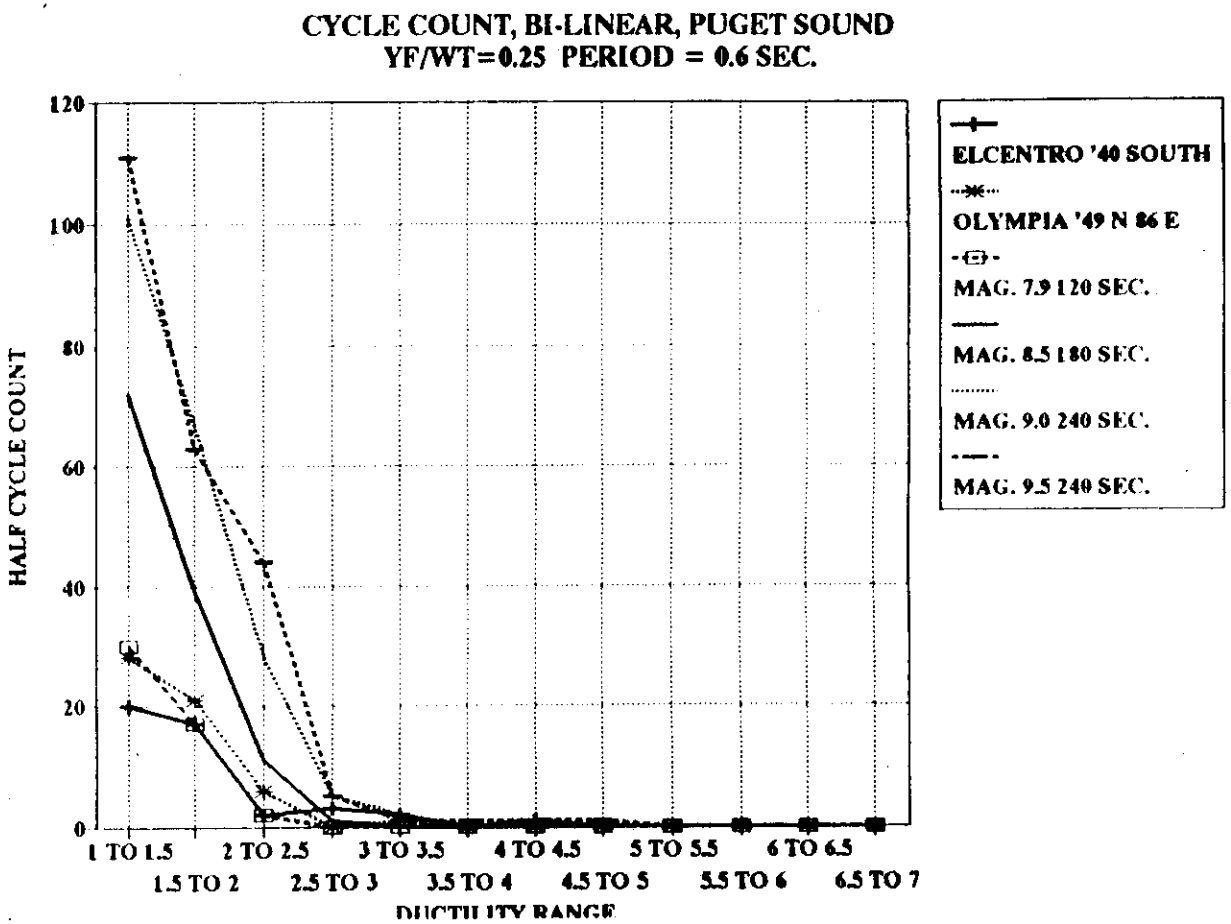


Figure 65 CSZ, El Centro, and Olympia inelastic cycle counts, bi-linear models, yf/wt = 0.25.

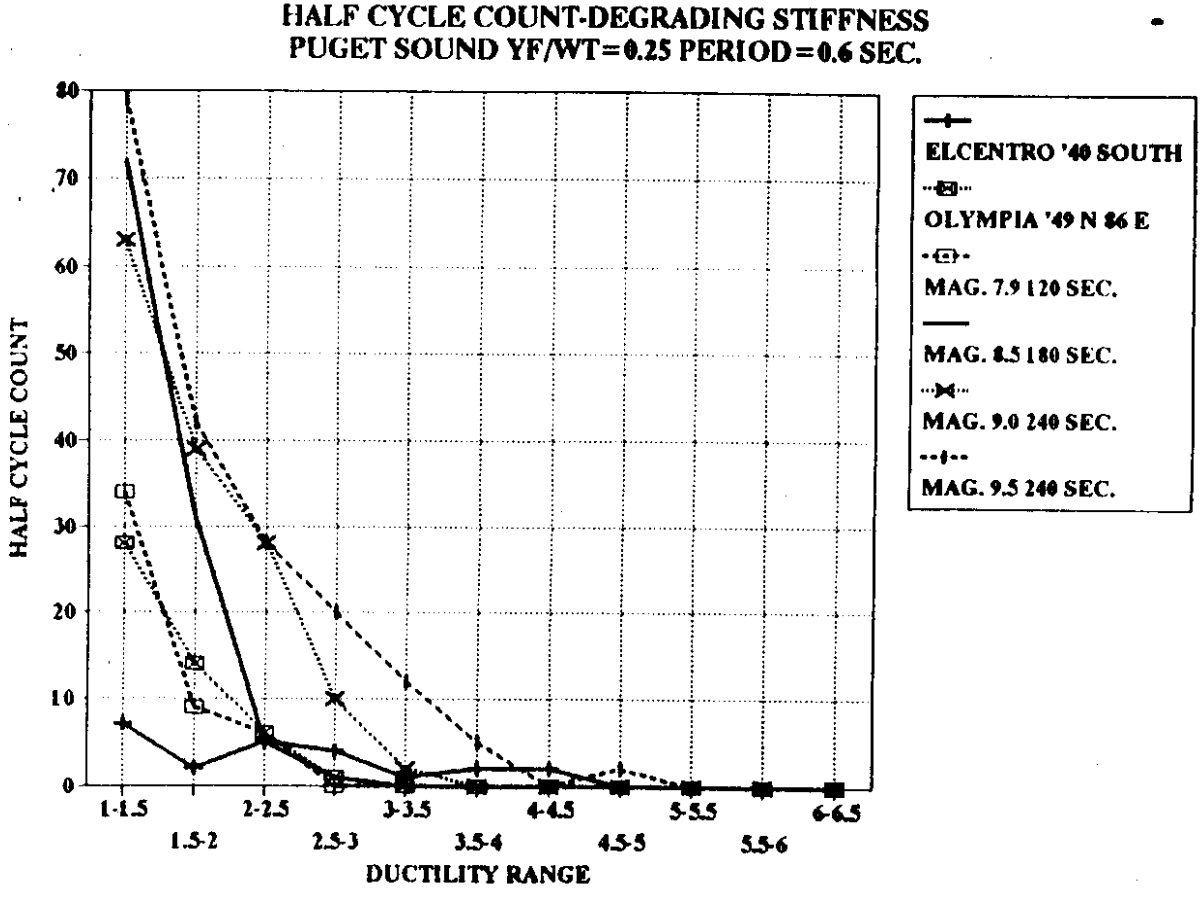


Figure 66 CSZ, El Centro, and Olympia inelastic cycle counts, degrading stiffness models, yf/wt = 0.25.

force to weight ratios of 0.125, as shown in Figures 67 and 68. It is important to note that for the both strength structures there are many displacement cycles in the ductility demand ranges less than 4. Thus although high numbers of equivalent cycles to $\mu = 4$ were cited above, some of the inelastic energy is being dissipated during smaller ductility cycles. However, the cycle counts for a yield force to weight ratio of 0.125 and a degrading stiffness model are still quite high. In Figure 68, for instance, several of the larger events produce more than 10 half-cycles in the $\mu = 4$ to 5 range.

## 4.2 Comparisons with Response to Code Compatible Acceleration Records.

As was discussed in the research approach section, AASHTO spectrum compatible artificial records were generated. These records reflect the seismic shaking levels implied by the AASHTO code. Therefore, by comparing the response produced by the CSZ artificial records with the response from AASHTO code compatible records, a measure of the severity of the CSZ response relative to code prescribed response is obtained.
For firm soil sites, a code compatible acceleration record based on an AASHTO site value of 1.0 was used. In Figure 69 inelastic displacement demands for bi-linear models with yield force to weight ratios of 0.25 are shown for the longest duration Puget Sound artificial acceleration records and for a code compatible artificial record. For structures with periods less than 0.1 seconds, the displacement demands for the code compatible record are higher than all the Puget Sound artificial records. For longer periods the demands between CSZ and the AASHTO records vary. Near 1 second, the displacement demands for the code compatible record drops as low as the demands caused by the 2 minute magnitude 7.9 record. In fact at a period of 0.7 seconds, the displacement demand for the four minute magnitude 9.5 CSZ artificial record is 2.7 times the demand

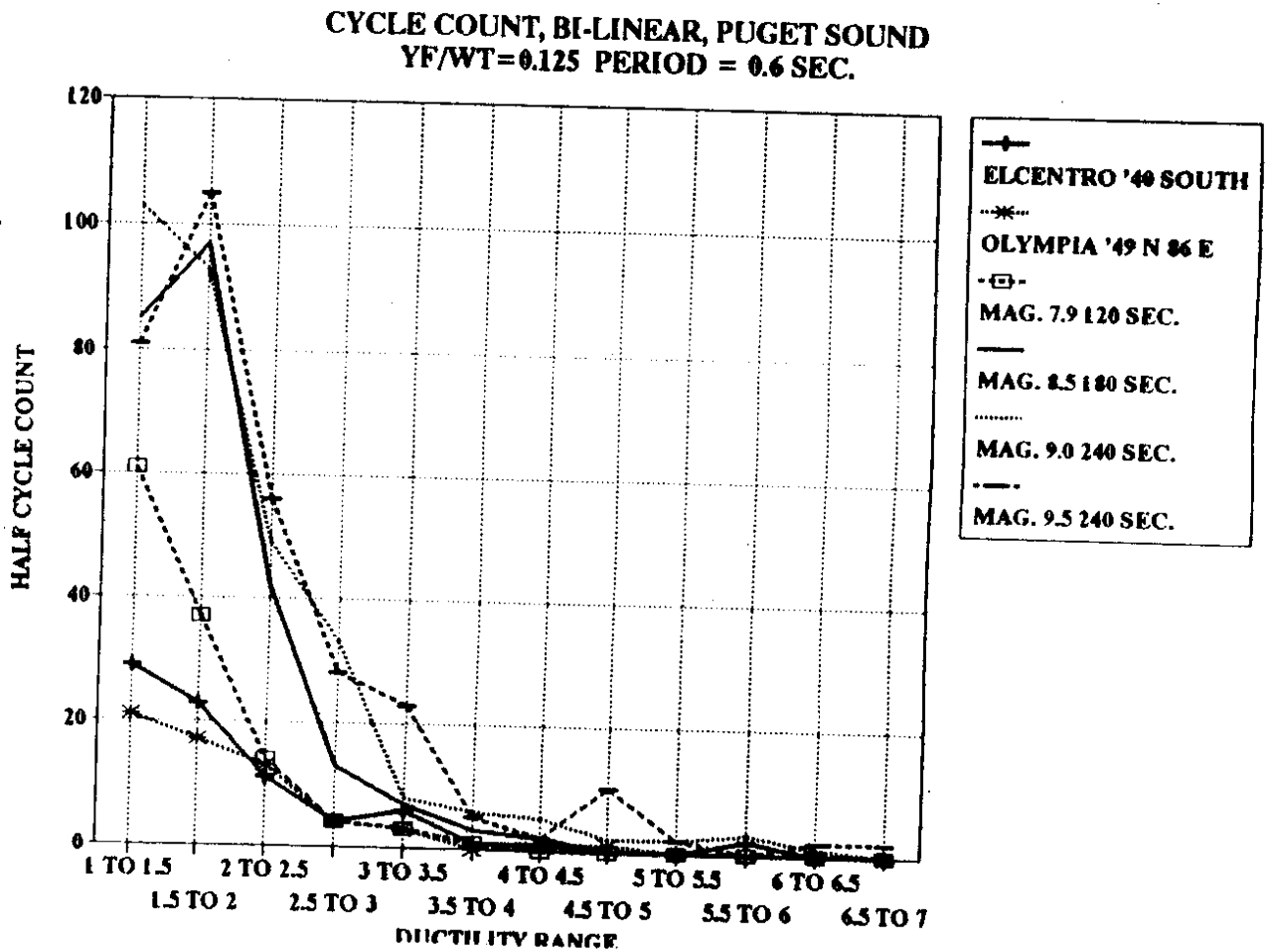


Figure 67 CSZ, El Centro, and Olympia inelastic cycle counts, bi-linear models, yf/wt = 0.125

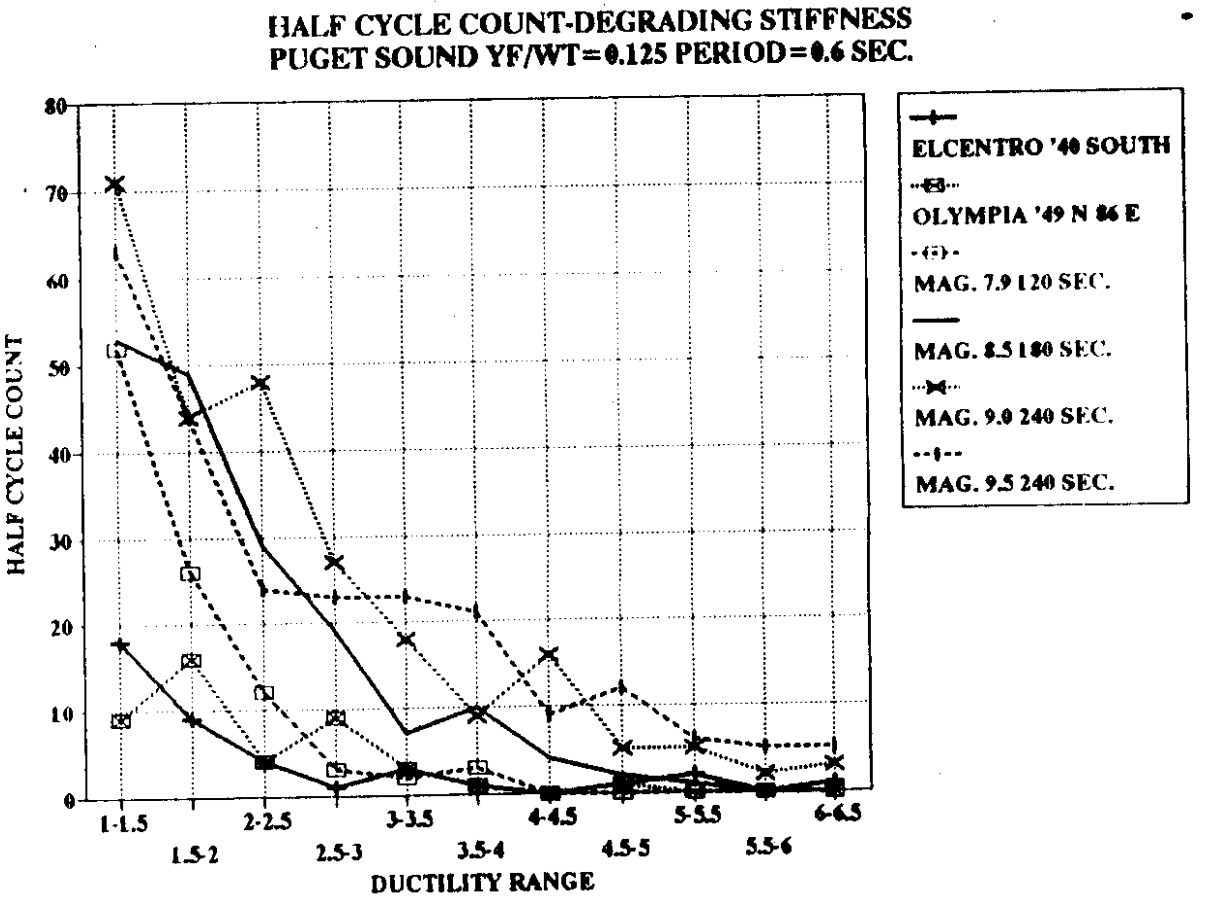


Figure 68 CSZ, El Centro, and Olympia inelastic cycle counts, degrading stiffness models, yf/wt = 0.125.

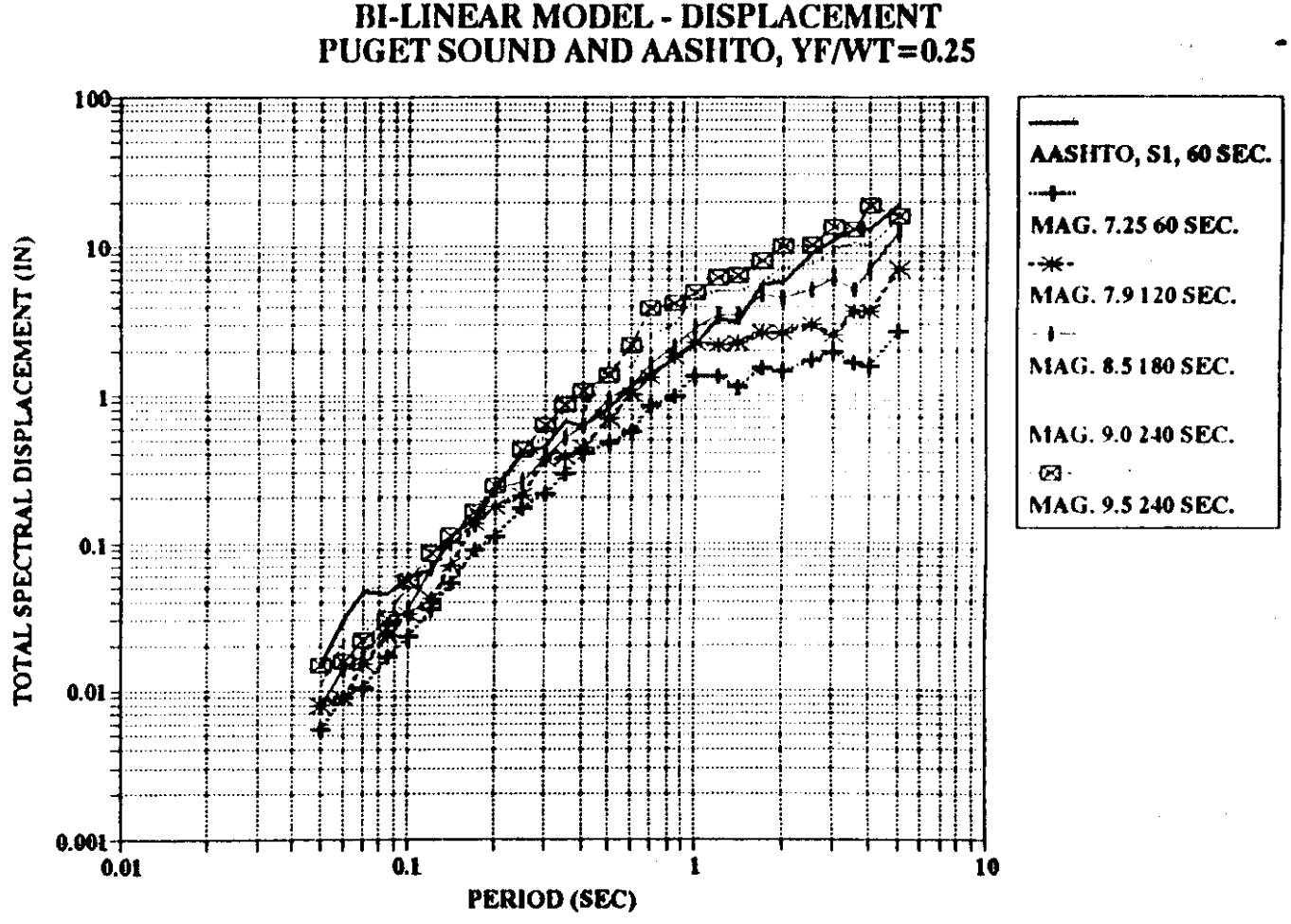


Figure 69 CSZ and AASHTO Code compatible displacement demand, bilinear models, yf/wt = 0.25.

for the AASHTO compatible record. In contrast, near 4 seconds the AASHTO demands are as high as the four minute magnitude 9.5 record.

Figure 70 shows the relation between hysteretic energy demand for the code compatible acceleration record and the CSZ acceleration records attenuated to Puget Sound for a bi-linear model with a yield force to weight ratio of 0.25. Below a period of about 0.15 seconds, the hysteretic energy demand for the code compatible record is higher than that of all the CSZ record demands. Above this period, the code compatible energy demand quickly drops to a value between the demand for a three minute magnitude 8.5 and a two minute magnitude 7.9 Puget Sound record. The value of normalized hysteretic energy on this plot that corresponds to a single complete cycle of displacement at $\mu = 4$ is 22.8. It can be seen that all the records produce demands less than three cycles, and the AASHTO and magnitude 8.5 or lower records produce one or less cycles for periods over 0.15 seconds.

For a degrading stiffness model with a yield force to weight ratio of 0.25, the displacement demand is shown in Figure 71. The demands for the code compatible record are between the demands for the two minute magnitude 7.9 and the 4 minute magnitude 9.5 Puget Sound records.

For degrading stiffness models with a yield force to weight ratio of 0.25, the hysteretic energy demand is shown in Figure 72. The demands for the code compatible artificial record lie between the demands for the four minute magnitude 9.0 and the three minute magnitude 8.5 Puget Sound records in the period range below 0.15 seconds. Above 0.15 seconds, the hysteretic energy demands for the code compatible record are approximately equal to the demands for the two minute magnitude 7.9 Puget Sound record.

The inelastic half cycle counts for a bi-linear model with a yield force to weight ratio of 0.25 and a period of 0.6 seconds are shown in Figure 73. The counts for the code

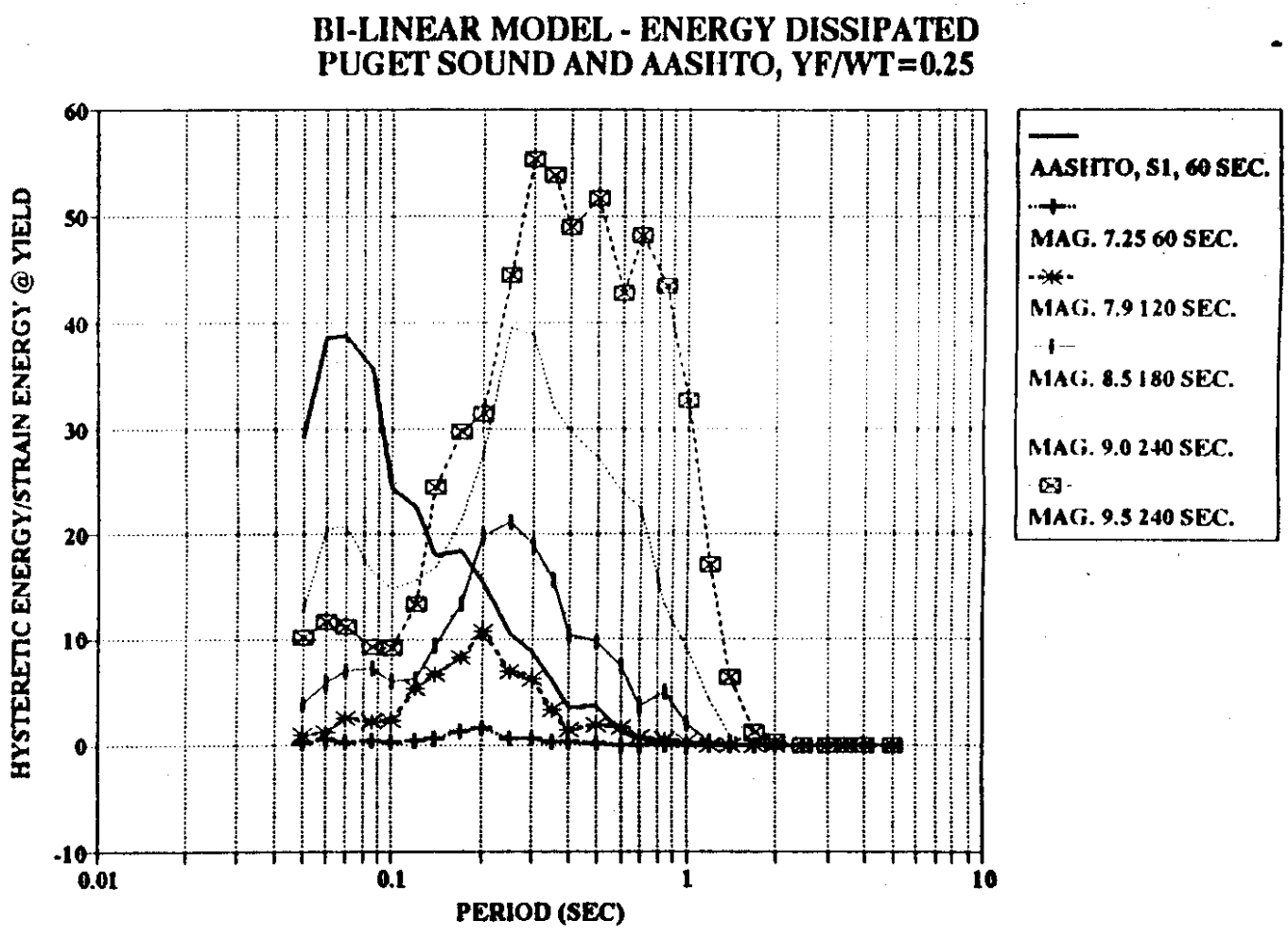


Figure 70 CSZ and AASHTO Code compatible hysteretic energy demand, bilinear models, yf/wt = 0.25.

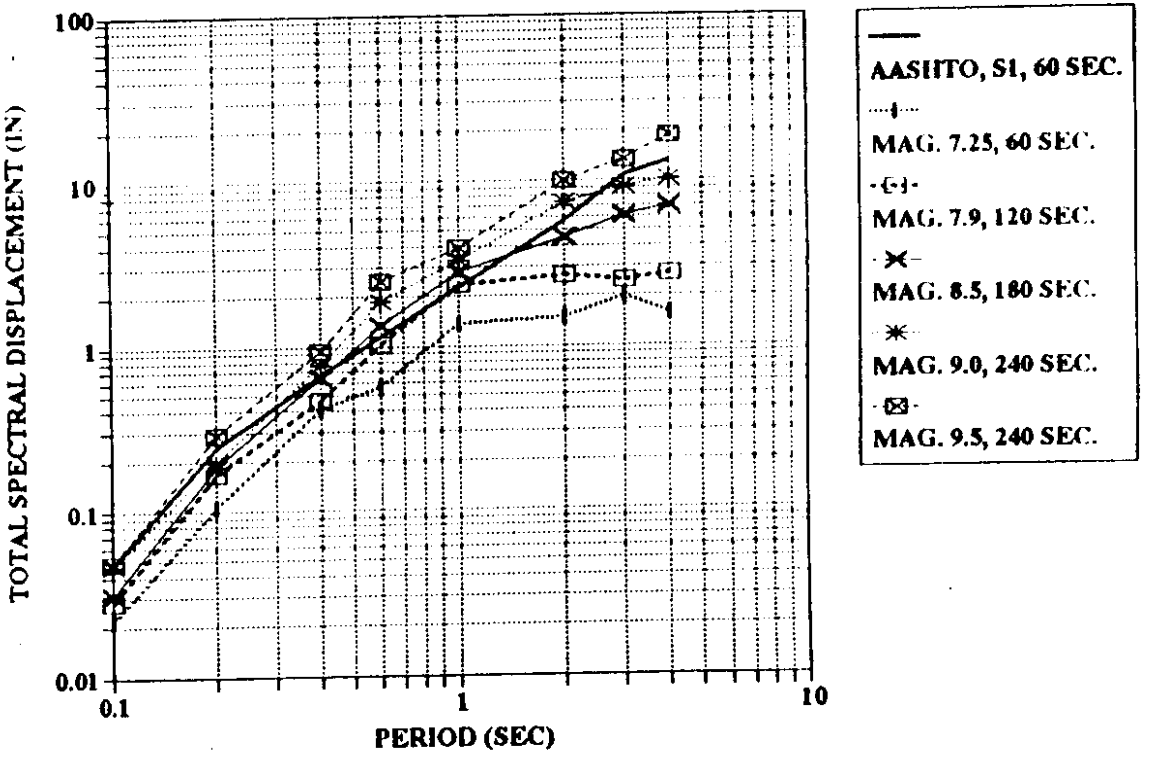


Figure 71 CSZ and AASHTO Code compatible displacement demand, degrading stiffness models, yf/wt = 0.25.

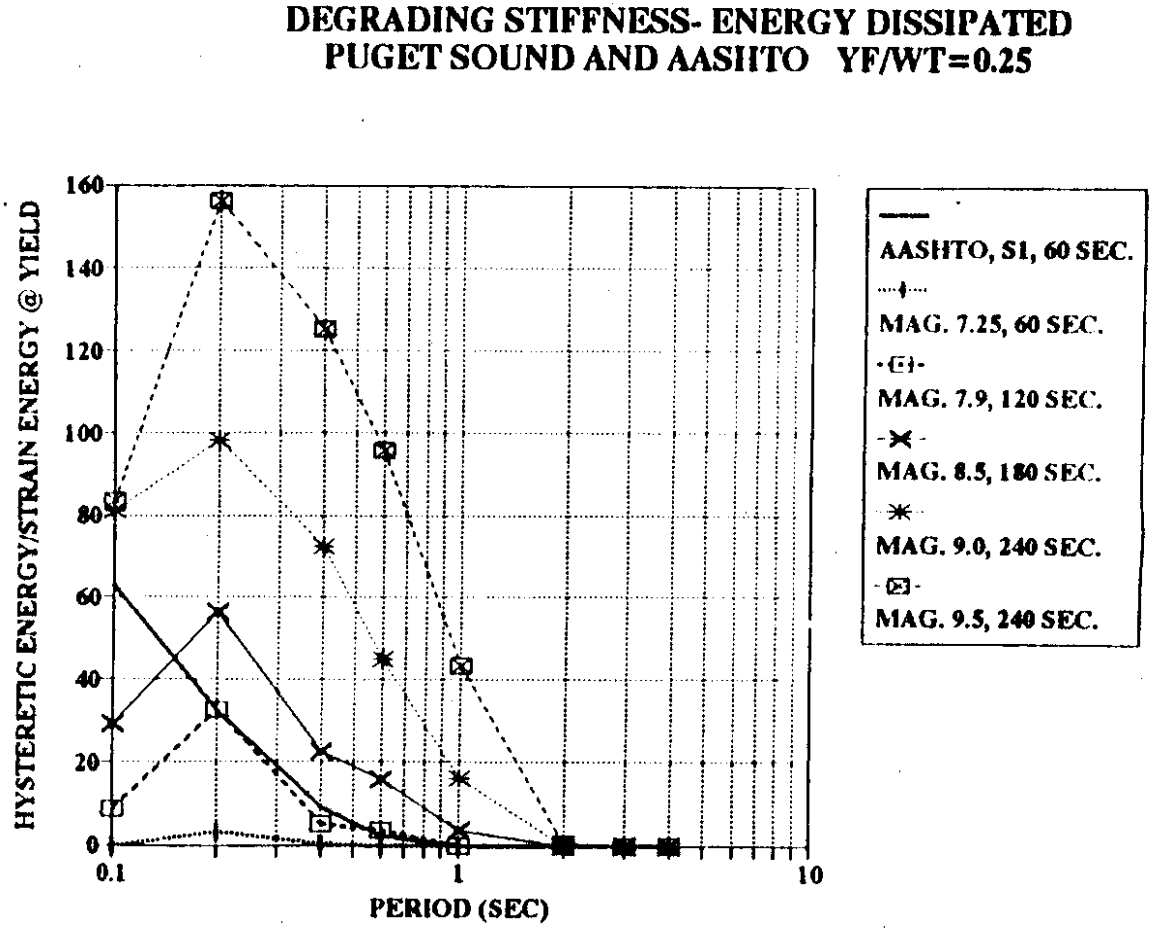


Figure 72 CSZ and AASHTO Code compatible displacement demand, degrading stiffness models, yf/wt = 0.25

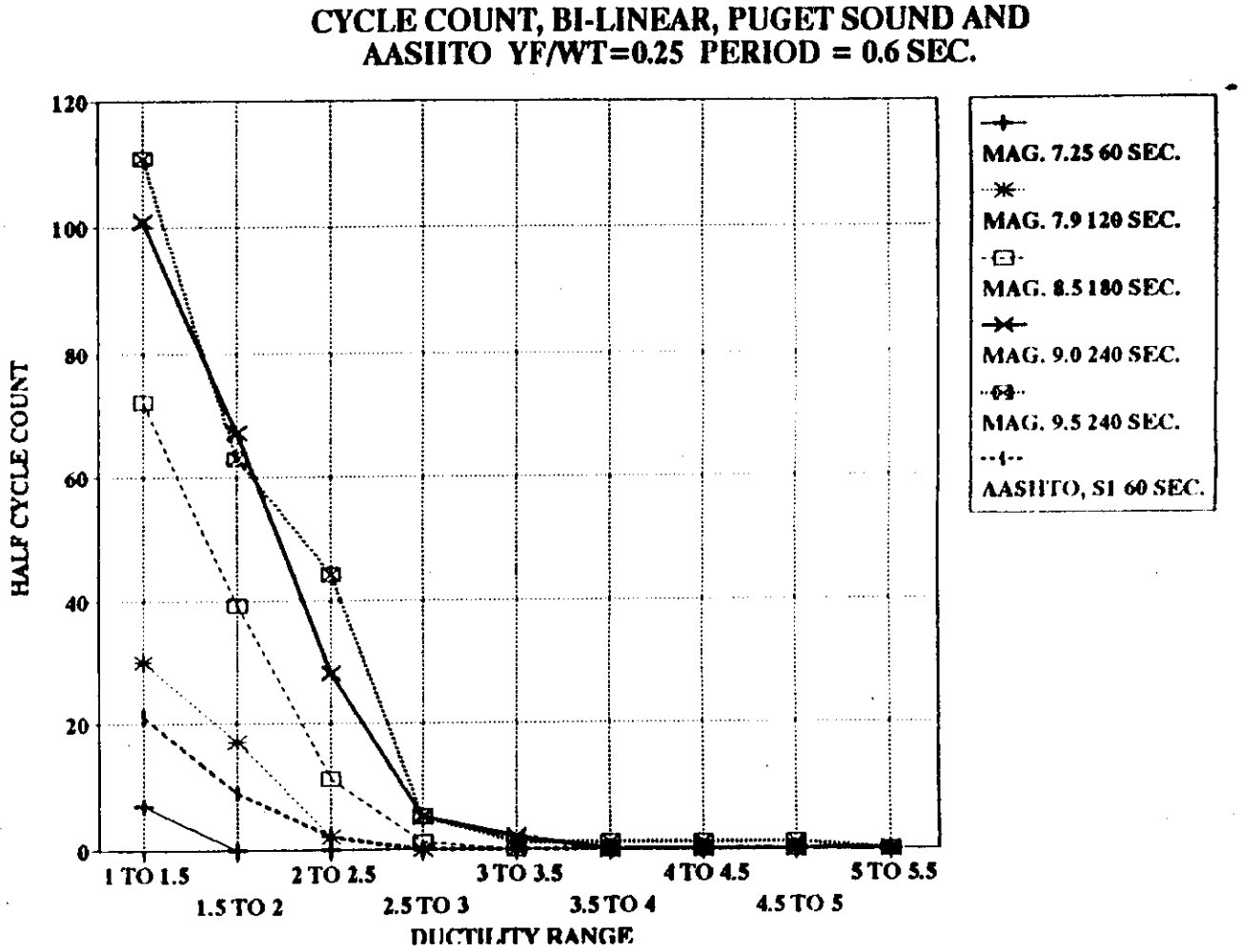


Figure 73 CSZ and AASHTO Code compatible inelastic half cycle counts, bi-linear models, yf/wt = 0.25.

compatible record are approximately equal to those of the two minute magnitude 7.9 CSZ record over the entire ductility range. Figure 74 provides the same information for a degrading stiffness model with the same strength and period. The inelastic half cycle counts for the code compatible record are less than two minute magnitude 7.9 CSZ record, for ductility ranges below 2.5 to 3. Above that range the code compatible inelastic half cycle count is nearly zero. Similar trends were observed for structures with yield force to weight ratios of 0.125. See Figures 75 and 76. Also note that the numbers of half cycles are larger for the weaker structures and that for the two largest earthquakes relatively many large ductility demand cycles are present.

## 4.3 Comparisons to Laboratory Testing Results

In the previous sections the hysteretic energy demands have been related to the number of equivalent cycles at a ductility level of four. This conversion was made by dividing the hysteretic energy demands expressed as multiples of the energy stored at first yield by the constants given in Table 6. This same conversion has been made for the bilinear structural model for ductilities equal to two and four as shown in Figures 77 and 78. These two figures provide the equivalent number for cycles for all periods, and they provide a basis for comparison with laboratory testing results. A ductility demand of four is often used as a minimum that a tested subassembly should be able to survive without significant loss of strength or stiffness. As can be seen in Figure 78 and has been described in the previous section, the ductility demands for records with magnitude 8.5 and less the demands are not extreme, since only several cycles at $\mu = 4$ are produced. However, similar demands for degrading stiffness models were higher, as shown above.

A more rigorous measure of CSZ damage demand is determined by comparing the number of half cycles experienced in response to CSZ artificial records to the number of

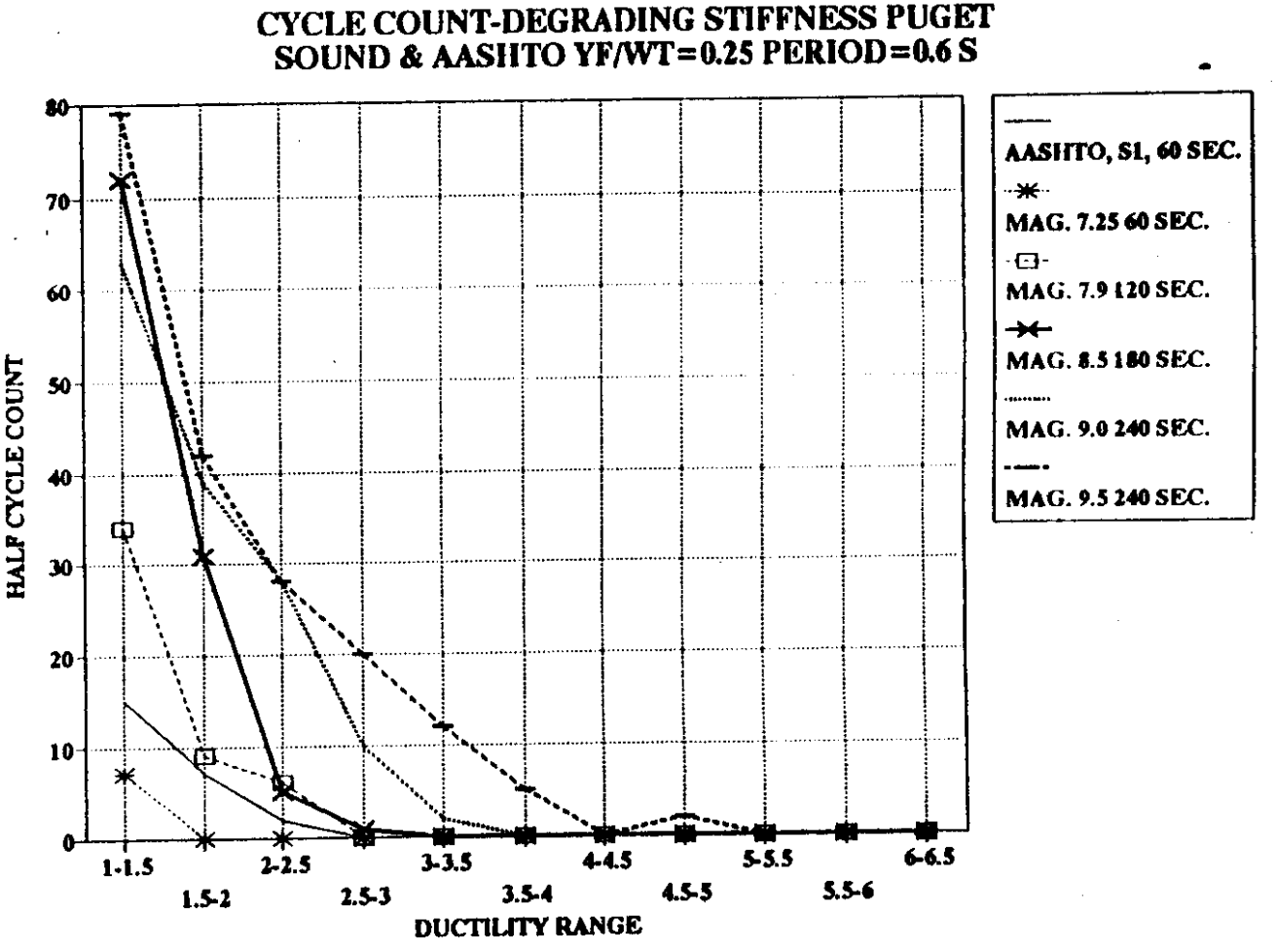


Figure 74 CSZ and AASHTO Code compatible inelastic half cycle counts, degrading stiffness model, yf/wt = 0.25.

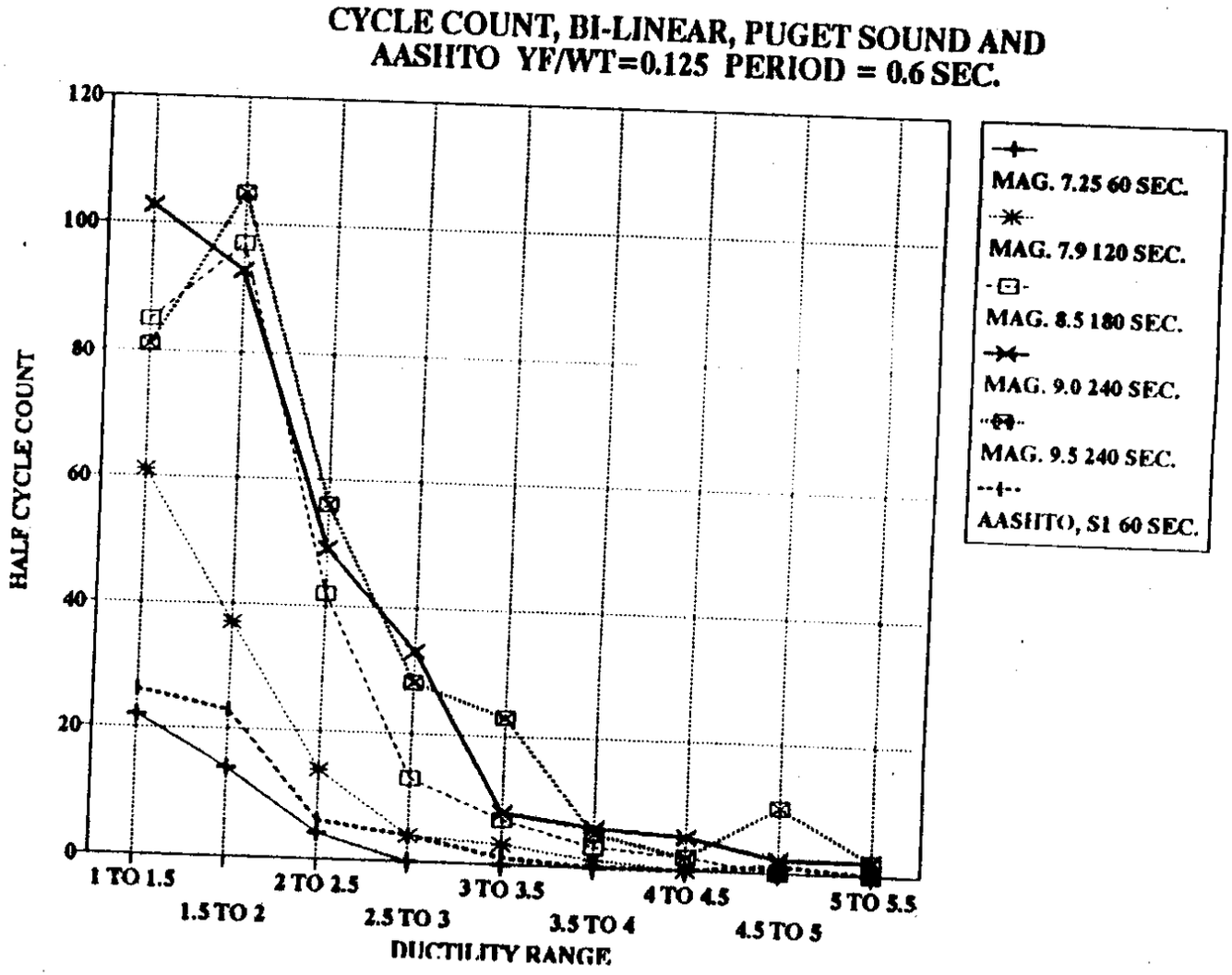


Figure 75 CSZ and AASHTO Code compatible inelastic half cycle counts, bi-linear model, yf/wt = 0.125.

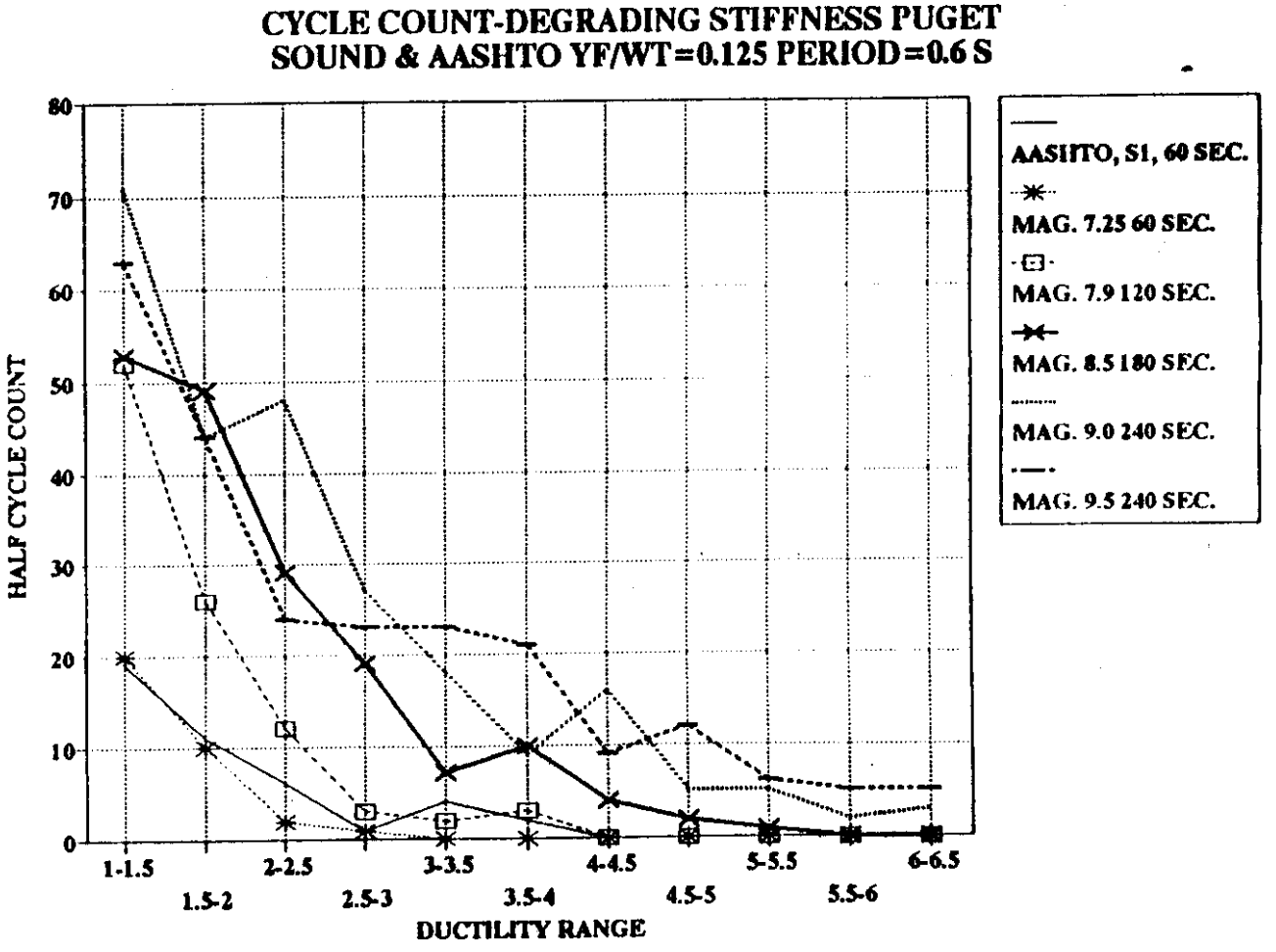


Figure 76 CSZ and AASHTO Code compatible inelastic half cycle counts, degrading stiffness model, yf/wt = 0.125.

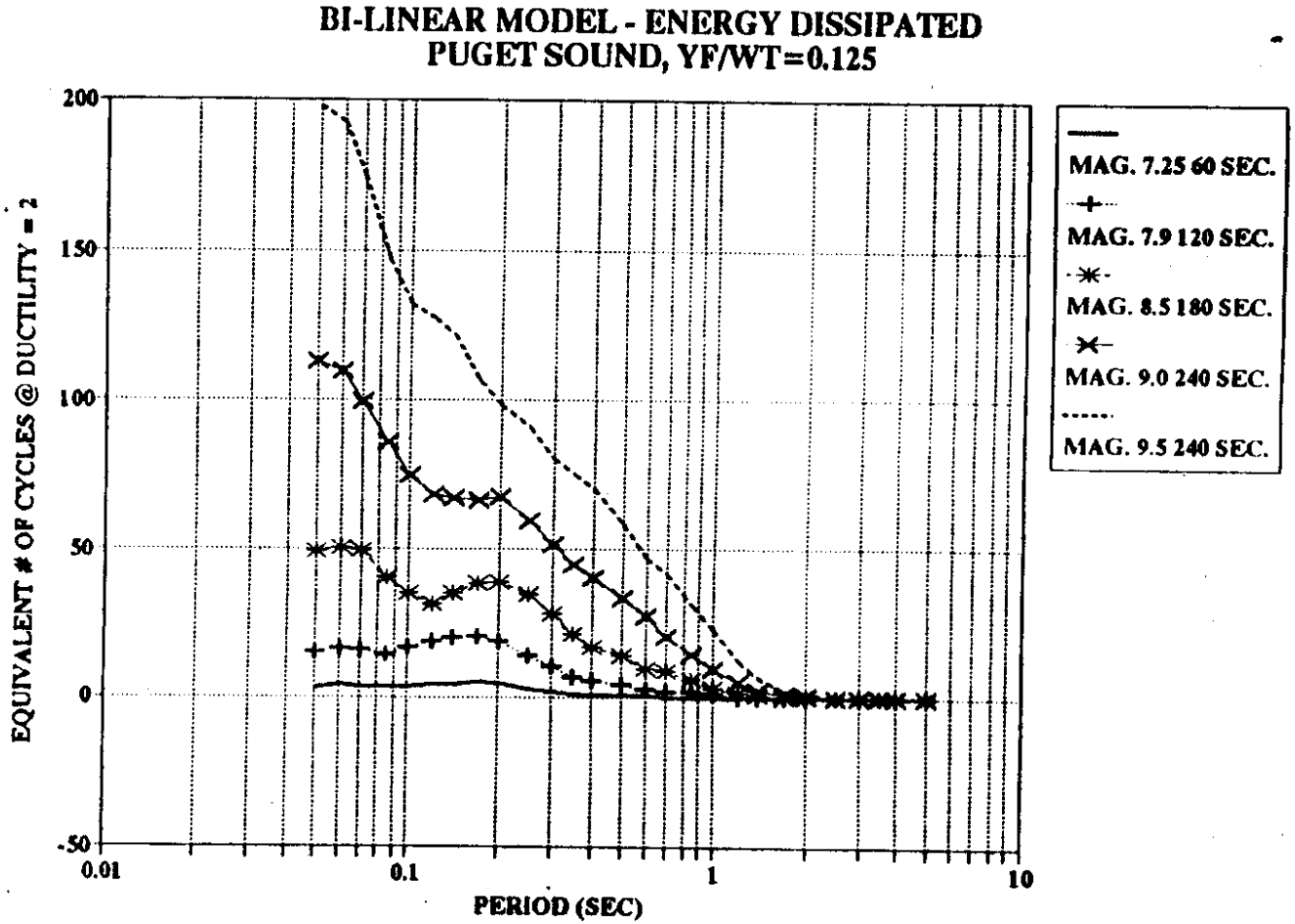


Figure 77 CSZ hysteretic energy demand expressed as equivalent number of cycles at ductility 2.

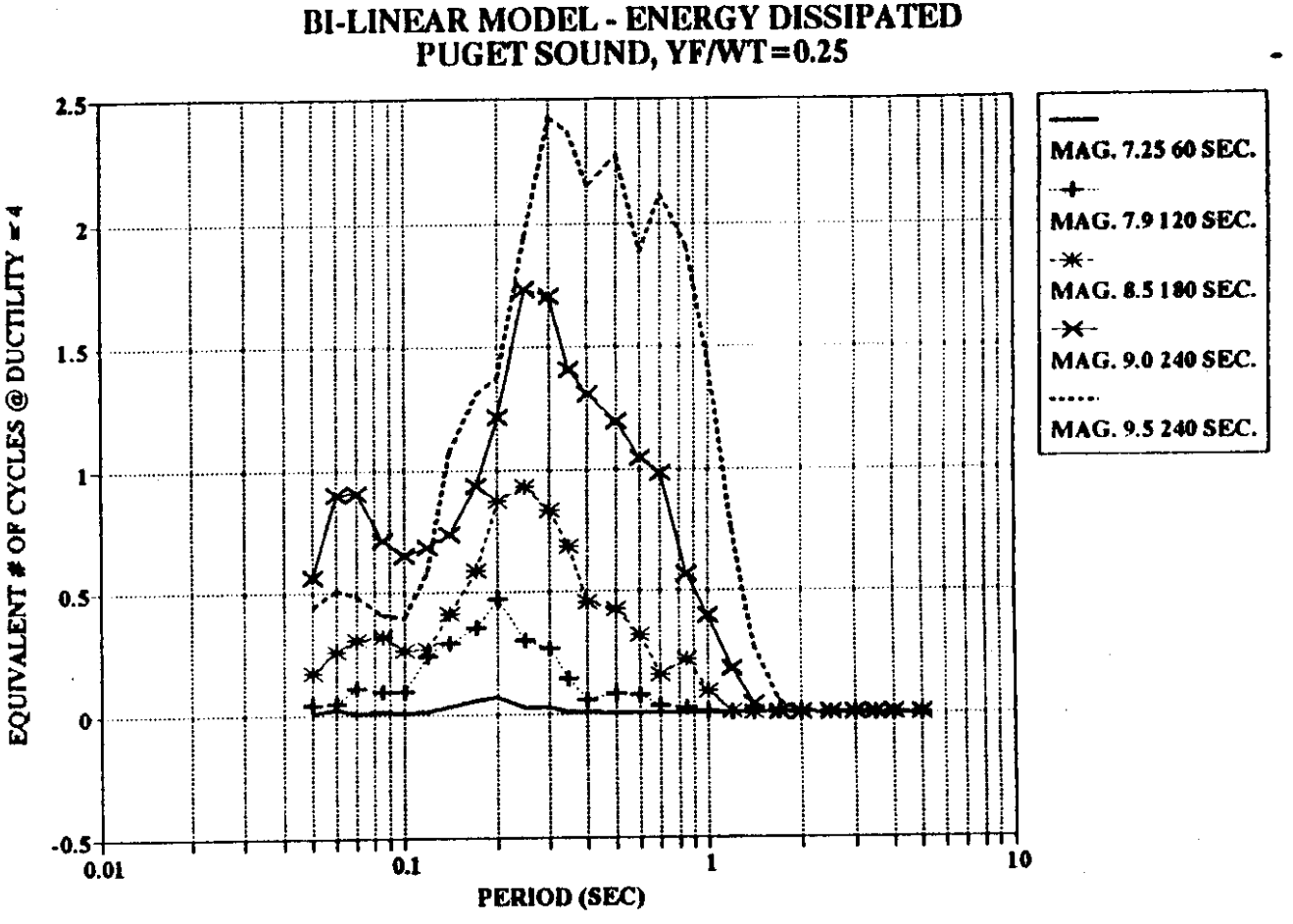


Figure 78 CSZ hysteretic energy demand expressed as equivalent number of cycles at ductility 4.

half cycles used in typical laboratory testing. Since the detailing practices that are specified for seismic load resisting systems are based upon adequate performance of structural models tested to failure in the laboratory, it is reasonable to compare the displacements obtained from the analyses with those imposed during typical tests. A typical testing ductility demand sequence is that used by Chai (40), which was described in the background section.

Figures 79 and 80 compare the number of half cycles demanded of a bi-linear model during a CSZ artificial record with the number of half cycles used by Chai. Figures 81 and 82 compare the same half cycle demands for a degrading stiffness model. Note that the CSZ artificial records produce many more half cycles with ductilities less than three than are imposed on typical test specimens. However, the laboratory testing sequence is more severe in the higher ductility ranges than are the CSZ demands. The implication of this is that if specimens did not fail until the higher ductility demands were reached, then they would probably survive such large demands in an earthquake. However, there is no indication that the specimens would be able to endure the great number of low level ductility demands without loss of strength, since testing typically does not focus on this aspect of performance.

## 4.4 Application: Assessing the Demands of a CSZ Earthquake on an Existing Structure

Results from this research may be used to estimate the CSZ earthquake demands that may be placed upon a structure. This section describes how to estimate demands for a given structure, provided that it can be generalized as a single-degree-of-freedom structure with either a bilinear or a degrading stiffness load-displacement relationship.

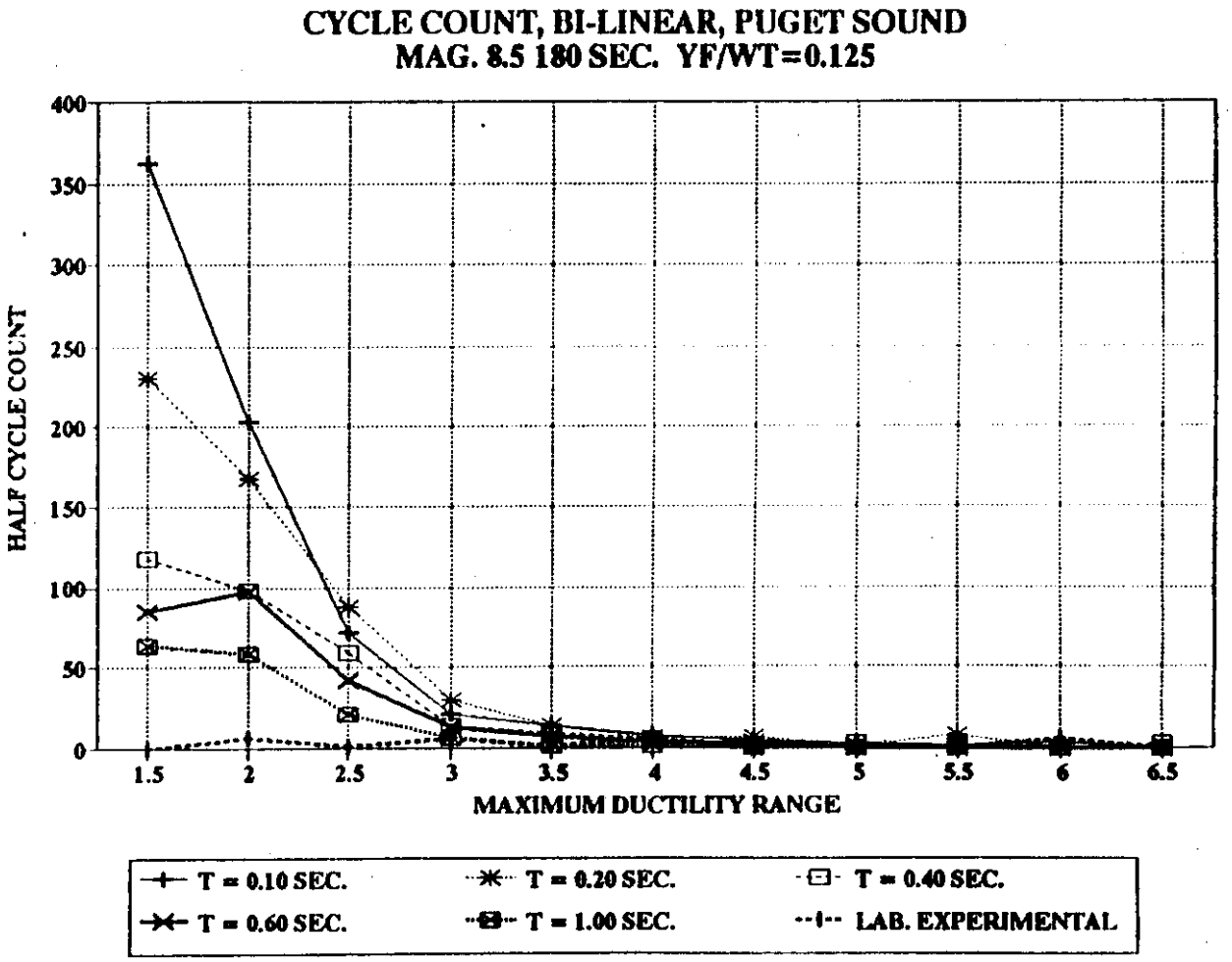


Figure 79 CSZ and Chai's laboratory inelastic half-cycle count, bi-linear model, yf/wt = 0.125

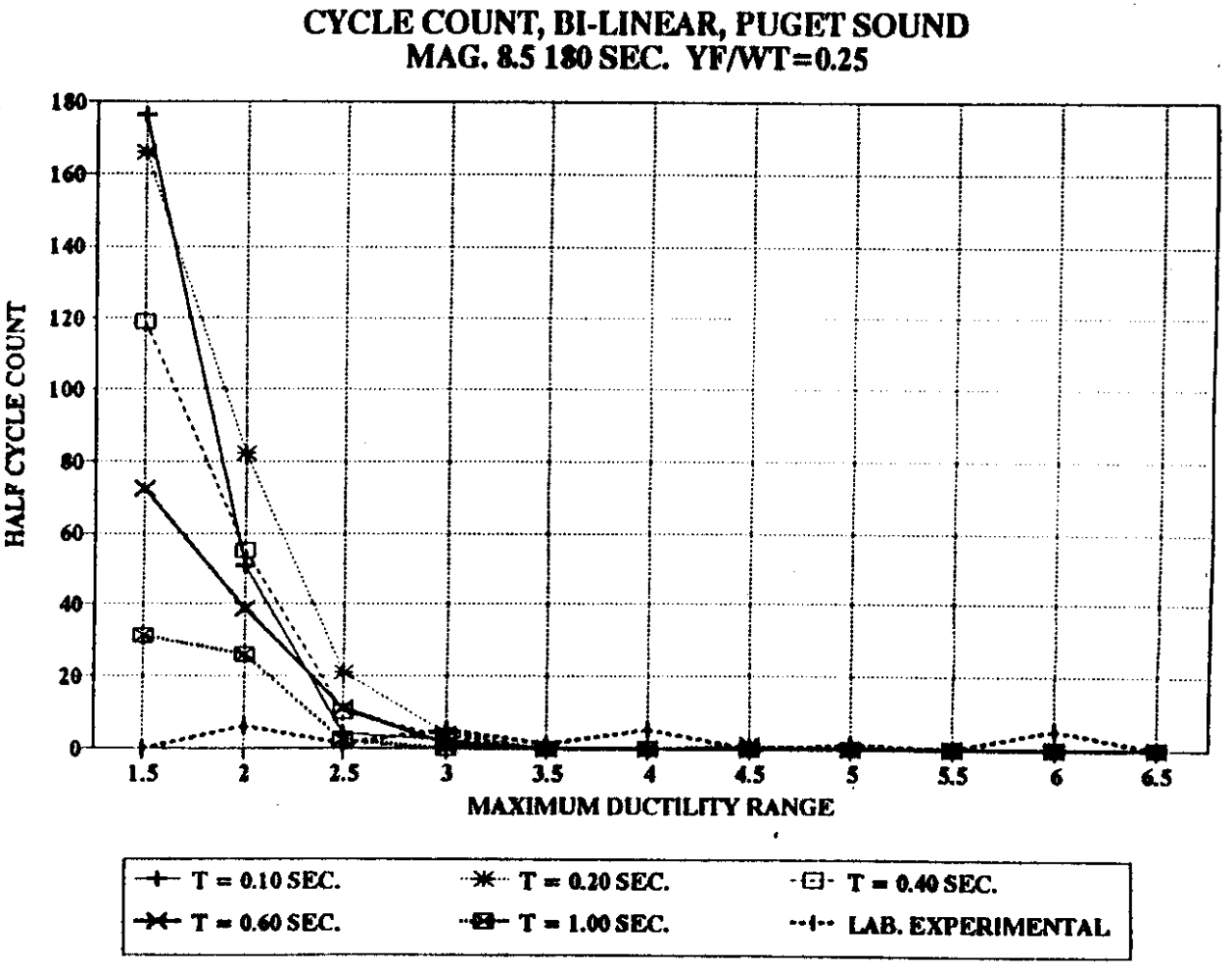


Figure 80 CSZ and Chai's laboratory inelastic half-cycle count, bi-linear model, yf/wt = 0.25

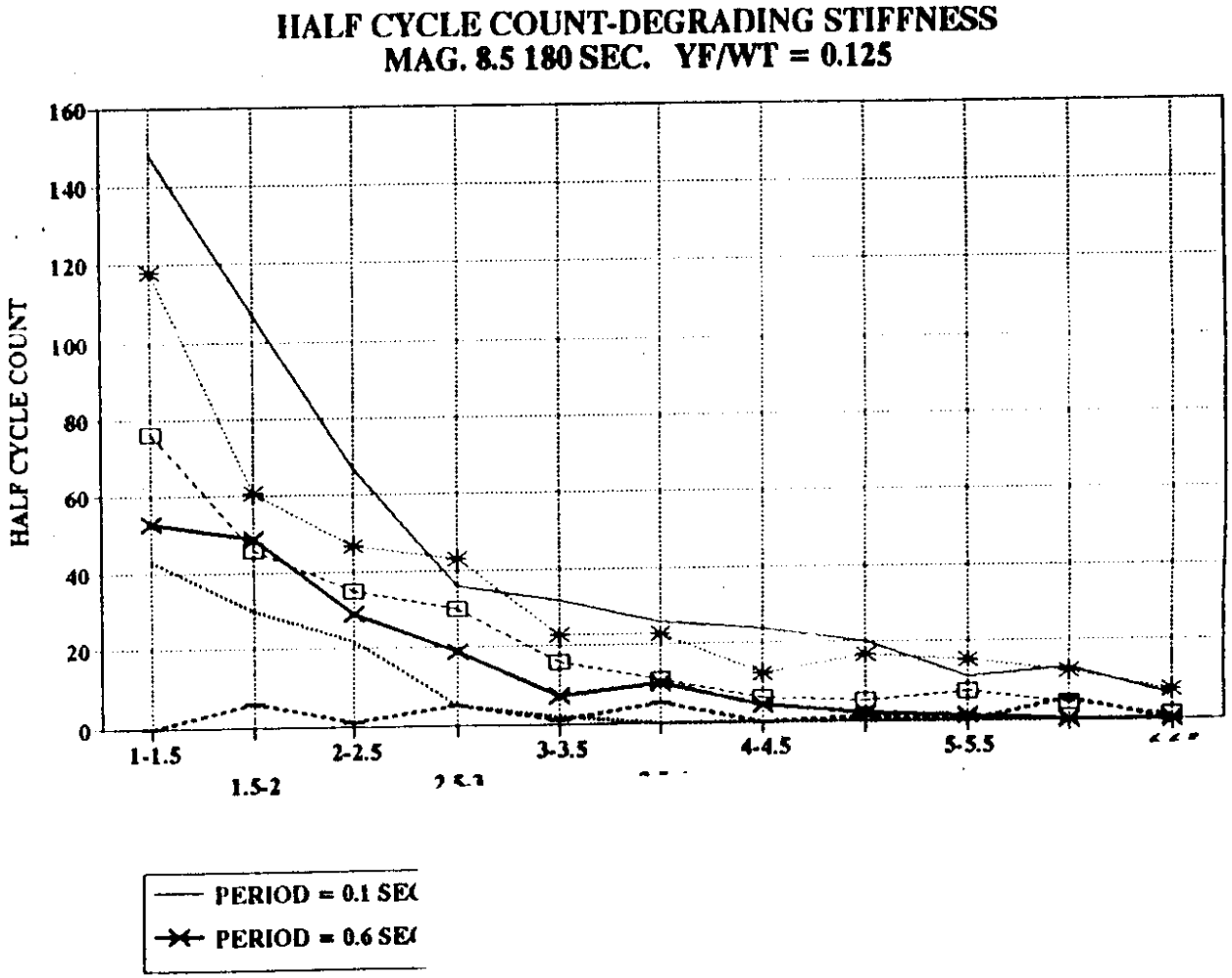


Figure 81 CSZ and Chai's laboratory inelastic half-cycle count, degrading stiffness model, yf/wt = 0.125

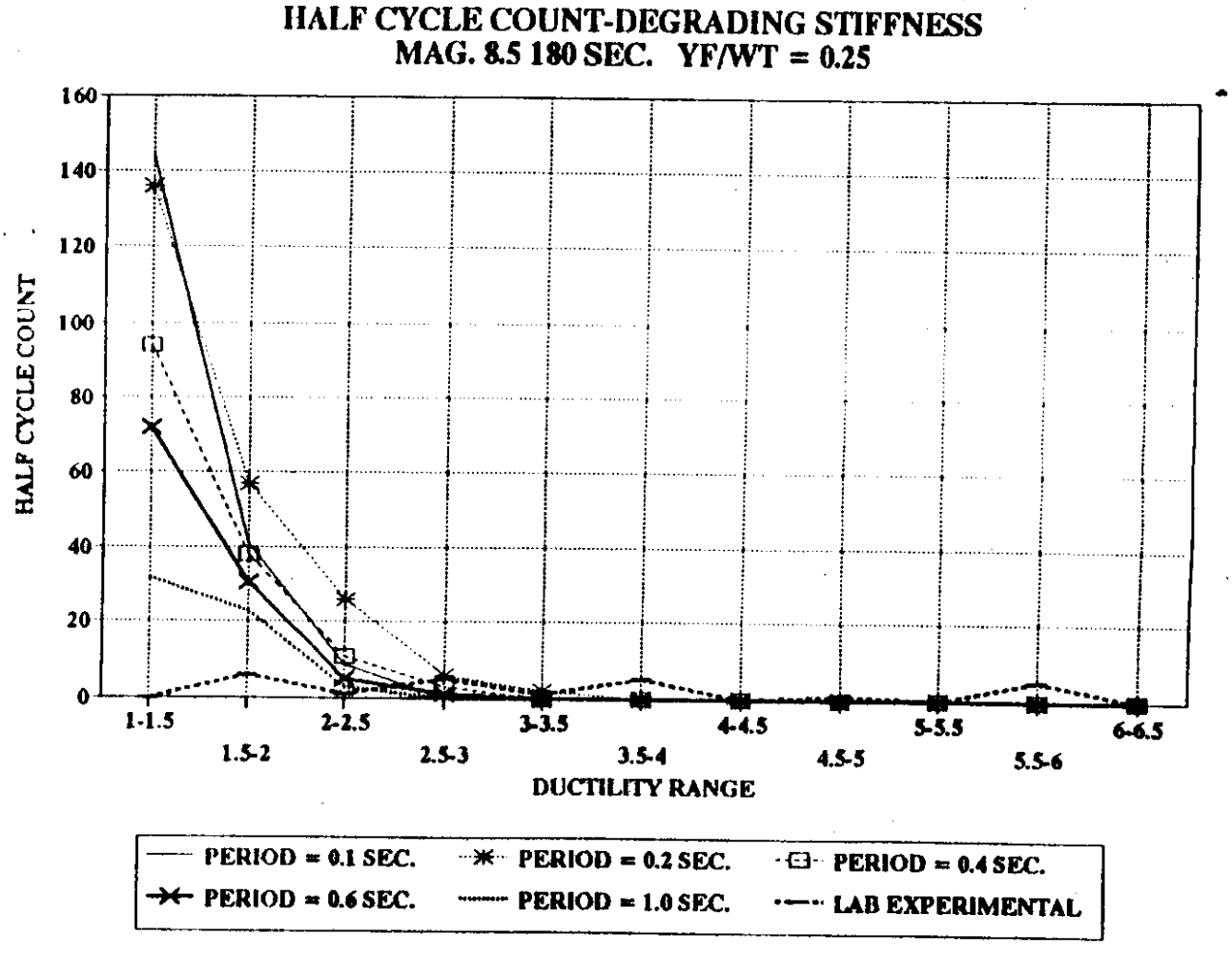


Figure 82 CSZ and Chai's laboratory inelastic half-cycle count, degrading stiffness model, yf/wt = 0.25

To estimate the CSZ demands on a single-degree-of-freedom structure, the following quantities must be known: 1) the structural weight that will participate as reactive mass under lateral shaking, 2) the natural period of vibration of the structure, and 3) the structure's yield force to weight ratio.

The structure's yield force to weight ratio should be determined from a plastic collapse or "push-over" analysis. Such an analysis will produce a load-displacement curve similar to that shown in Figures 24 and 25. The structure's yield force to weight ratio is defined by the intersection of tangent to the initial load displacement path and the tangent to the final load displacement path, as shown in the figures. The load at this intersection is the structure's yield force, which may be divided by the structural weight to obtain the yield force to weight ratio. In general, the load displacement relation will not be bilinear as is shown in the figures. Therefore an approximate bilinear relationship will have to be generated before using the data presented in this report. Several approximations may be used in order to bracket the expected demands.

With the figures given in this chapter and those given in Appendices A and B, the displacement and damage demands for various magnitude and duration CSZ events may be estimated. The graphs for degrading stiffness models should be used for reinforced concrete structures, and the graphs for bi-linear models should be used for steel structures.

The following is as an example of how to calculate the demands for a reinforced concrete structure located in the Puget Sound basin. The structure has a weight of 100 kips, a period of 0.6 seconds, and a yield force to weight ratio of 0.25. The displacement demands can be estimated using Figure A.5. If subject to a three minute duration, magnitude 8.5 CSZ earthquake, such a structure is estimated to have a maximum displacement of approximately 1.5 inches. From Figure B.5 the estimated hysteretic energy demand for such a structure, is 1.8 in-kips per kip of structure weight. Therefore, the hysteretic energy demand is estimated to be 180 in kips for the structure. The yield

displacement is calculated using the yield force and the stiffness as 0.88 inches. The maximum ductility demand can then be estimated by dividing the maximum displacement, 1.5 inches, by the yield displacement. This gives a ductility demand of 1.7, which is not a particularly high value. Additionally, the number of equivalent displacement cycles at a specified ductility demand can be calculated using the constants in Table 6. In this case the maximum demand was 1.7. Therefore the number of equivalent cycles is calculated for a ductility value of two, rather than four. The amount of strain energy stored at yield must first be found using the yield force and the elastic stiffness. This energy is 22.0 kip-in. The hysteretic energy dissipated normalized by the energy at yield is: 180 divided by 22.0, or 8.17. Thus the number of equivalent cycles at $\mu = 2$ is: 8.17 divided by 3.9, or 2.1. Again, this is not a particularly high demand. The inference from these results is that this bridge would probably not suffer a great deal of damage if it were subjected to ground shaking similar to that of the magnitude 8.5 CSZ record.

## 4.5 Application: Limiting the Demands of a CSZ Earthquake on a New Structure

Results from this research may be used to limit the inelastic demands that would be placed on a structure by a given CSZ earthquake. This approach can be used in the design process to ensure that a structure possesses sufficient strength to limit the potential inelastic response. The limitation that a structure be represented by a generalized single-degree-of-freedom system required in the previous section also applies in this section. To limit the demands on a structure by a CSZ earthquake, the following quantities must be known: 1) the earthquake magnitude, duration, and epicentral distance, 2) the natural period of vibration of the structure, and 3) the number of equivalent cycles at a specified ductility level to which the response is to be limited.

The strategy of the approach is to determine a target, minimum yield force to weight ratio for the structure. The inference is: if the structure as a greater strength than that specified, then the inelastic demands will be less than the limiting amount from item 3) above. If the relationship between the actual yield force to weight ratio and the design base shear given by Equations 11 and 12 in Chapter 2 were known, then the response modification factor, R, that would produce the minimum strength at the desired period could be calculated. However, this relationship is often not precisely known, and as a result, the process of obtaining the correct strength for the design would be iterative.

The following is an example of how to determine the limiting strength for a structure. The earthquake for which the damage is to be limited is the magnitude 9.0, 240 second CSZ event. The structure is made of reinforced concrete, is located in the Puget Sound basin, and has a period 0.6 seconds. The structure is to be limited to eight equivalent cycles at a ductility demand of 4. The specified quantities are arbitrary and are for example only.

The degrading stiffness results shown in Figures 60 and 64 are used to determine the inelastic energy demands for this type of structure. From Figure 60, the demand expressed as a multiple of the energy stored at yield would be approximately 45 for a 0.25 yield force to weight ratio. From Figure 64, the demand would be roughly 250 for a 0.125 yield force to weight ratio. Using a constant of proportionality equal to 13.1 from Table 6, the equivalent number of cycles at $\mu$ =4 at each of the two strength ratios is 3.4 and 19.1, respectively. To limit the damage to that corresponding to eight equivalent cycles, the yield force to weight ratio is determined by linear interpolation. The value determined is 0.21. This is the target yield force to weight ratio to be used to design the structure.

To determine the response modification factor, R, that would produce a yield force to weight ratio of 0.21, Equations 11 and 12 can be used. However, the relation between the actual yield and design base shear levels must be known. If for the example structure,

the actual lateral yield strength of the structure equals the design base shear, then the required R would be 1.6; that assumes A = 0.2 g and S = 1.0 in Equations 11 and 12. If the actual strength were 1.25 times the design base shear, as the result of material overstrength for example, then the required R would be 2.0. However, the values of R that are actually selected should not exceed those currently specified.

## 4.6 Appraisal of Results: Uncertainties and Assumptions Made in This Research

The results evaluated above have been reached by making several assumptions and by using information that contains some uncertainties. In this section, these assumptions and uncertainties are reviewed and discussed.

The response to postulated CSZ earthquake ground motion has been estimated using the current predictions of seismologists, geotechnical engineers, and geophysicists. There has been discussion whether giant CSZ earthquakes are even possible. Geologic evidence suggests that they have occurred in the past and that they will occur again, but recurrence intervals and magnitudes are still uncertain.

Ground motion predictions have been made by Crouse (1991) and Heaton and Hartzell (1986a). Both of these predictions are based on data from other subduction zones in the world and contain much uncertainty. Heaton and Hartzell's (1986a) predictions for a maximum event and for average events use empirical Green's functions from Japan and teleseismic record matching. No records exactly fit the existing teleseismic records, with some being closer approximations than others. Crouse's (1991) response spectra for median events are statistical with a calculated uncertainty. Crouse's (1991) data base contains no earthquakes with moment magnitudes greater than 8.2, yet he predicts ground motion for moment magnitude 9.5 earthquakes. There is uncertainty in such an extrapolation.

The maximum credible CSZ earthquake is also uncertain and subject to discussion. Crouse (1991) and Heaton and Kanamori (1984) suggest a maximum credible event near Mw = 8.5. Heaton and Hartzell (1986a) suggest a magnitude 9.5 earthquake as a maximum event.

The duration of postulated earthquakes is also uncertain. Estimates have been made using both historical accounts of unrecorded, large magnitude, subduction earthquakes and upper bounds from recorded earthquakes. The maximum magnitude earthquake in the upper bound data base was around magnitude 8. Extrapolating as high as magnitude 9.5 contains uncertainties.

Another uncertainty is the process of generating artificial acceleration records. The method used to generate records utilizes a random number generator to determine acceleration wave phase angles. The program attempts to match an input response spectrum, but does not exactly do so. The non-stationary behavior of the accelerogram is then based on an input envelope. The acceleration envelope used in this study was estimated from Heaton and Hartzell's (1986a) artificial accelogram. An actual CSZ acceleration history envelope might be different.

Finally, there is uncertainty in the response implied by the structural models of actual structures. Hysteretic models only approximate actual behavior and may not capture all of the relevant phenomena. For instance, unlike the models used in this research, actual structures may degrade in strength after repeated inelastic cycling.

Due to these uncertainties final conclusions as to the damage ability of great Cascadia subduction zone earthquakes can not be reached from this research . However, the research is believed to be based upon reasonable estimates of the postulated ground motions and structural response. Definite trends were observed in the results, and these trends may have implications in establishing design criteria and laboratory testing for CSZ earthquakes.

# CHAPTER 5

# CONCLUSIONS, RECOMMENDATIONS AND IMPLEMENTATION

In Chapter 4, an evaluation of the response-history results showed that the damage produced by the largest magnitude, long-duration CSZ earthquakes would be higher than the damage predicted using current design code compatible acceleration records or previously recorded Western U.S. strong ground motions. However, there were many uncertainties and assumptions made in modeling both the postulated ground motion and the response behavior, as noted in Section 4.4. If the assumptions are reasonable and depending on the size of the maximum credible earthquake, then some changes in current design code criteria and in laboratory testing procedures may be warranted. This chapter summarizes the significant findings of this research, comments on possible changes in seismic design criteria for the Pacific Northwest, and suggests additional research.

## 5.1 Significant Characteristics in Response and Their Implications to Current Seismic Design Criteria

The implications of this research rely on the characteristics and trends noted in the response to the artificial CSZ records, actual records, and code compatible records. These characteristics were described in the sections on findings and interpretation. Several characteristics pertain to all of the results. An example is the observed decrease in response that occurs with an increase in structural strength. Other characteristics pertain to the comparison of CSZ response with that from actual records, with that from code compatible records, and with laboratory testing. These characteristics are summarized in this section of the report, and their implications are also discussed.

Total displacement demands produced by CSZ records were not excessive, except for stiff structures with low strength. When subjected to the four minute magnitude 9.5 CSZ record, structures with periods less than 0.2 seconds and yield force to weight ratios of 0.125 had displacement ductility demands as high as 20. However, such structures are uncommon, since current design procedures typically prevent the design of short period structures with such low strength. More common structures, those with longer periods or with higher yield force to weight ratios, have displacement ductility demands less than 8 when subjected to the same record. Additionally, the acceleration records for the lower magnitude earthquakes produce smaller ductility demands. The lack of excessive displacement demands is important, since existing structures may not be subject to displacement demands greater than those currently expected.

Damage, based upon total dissipated hysteretic or inelastic energy, has a directly proportional relationship to the duration of the record. However, total displacement does not, since it is nearly independent of the duration. Structures subjected to long-duration CSZ records undergo considerable inelastic action, much of which occurs in displacement cycles of low ductility demand. Thus, damage accumulates as the result of the repeated cycles, although the displacement demands may not be excessive.

The estimated response is elastic for long period structures. Depending upon the acceleration record intensity, duration, and the structure strength, the lower bound of the elastic response period range lies between 0.50 and 3.0 seconds. Elastic response in this period range is significant because ground motion predictions are most uncertain in this region. This trend.was evident for both structural models used in this research.

Increasing a structure's yield strength relative to its weight decreases the amount of inelastic response. Structures with higher yield force to weight ratios had displacement demands of lower ductility and dissipated less hysteretic energy than structures with lower yield force to weight ratios. As the yield force to weight ratio approaches 0.50 the

structure response becomes nearly elastic, regardless of the period range or the acceleration record used. Thus displacement and damage demands can be reduced by increasing a given structure's strength.

Typically, acceleration records become more intense for sites closer to the earthquake epicenter. This leads to larger displacement and hysteretic energy demands for such sites. Therefore coast range sites are expected to experience more damage and higher displacement demands than will Puget Sound sites for subduction earthquakes. These higher demands due to location need to be considered when establishing regional design criteria. Since this increase in demand is due to the increase in ground motion, it should be reflected in the effective peak acceleration, EPA, of the site, which is expressed in the AASHTO code by the acceleration coefficient, A. By increasing A, the design yield force to weight ratio is increased, which in turn reduces the inelastic response. The design EPA ultimately depends upon a region's seismicity, and it can be based deterministically upon a maximum credible event or probabilistically upon a probability of exceedence, neither of which are established for a CSZ event.

The various estimated ground motions produce different predictions of displacement and damage demand. Acceleration records based upon Heaton and Hartzell's maximum credible event are much more intense than are the records based upon Crouse's median spectra. Therefore Heaton and Hartzell's maximum event produces the highest displacements and highest damage demands. It is evident that if design criteria are intended to limit the maximum displacements and damage demands for a maximum credible event then the spectrum selected to reflect such an event is of the highest importance. Currently the magnitude and thus the response spectrum of this event is not well established.

Site soil conditions amplify ground motion and the corresponding structural response. The amplification occurs in period ranges that depend upon the soil's unique

properties. Inelastic displacement demands and dissipated hysteretic energy demands are amplified but, generally, not in proportion to the amplification of elastic spectra. The increase in inelastic displacements may not be a great concern since ductility demands are generally within tolerable limits. The increase in damage, as defined as the amount of dissipated hysteretic energy, is due to the combined effects of long duration and increased displacements. The increases over the predictions of damage made without soil amplification are dependent upon the soil type, structure yield force, and structure period. No generally applicable trends were observed for the different soils. Therefore, extrapolation to other soil types would not be appropriate. However, the two soil types that were used in the study produced the largest amplification of elastic spectra of all the Washington soil types except for soft, liquefiable soils. Thus, additional studies to estimate inelastic demands using the soil groups not used in this study may be warranted.

Comparing demands produced from CSZ records based upon Crouse's median spectra with demands produced from previously recorded or code compatible records reveals the relative severity of CSZ records. Existing records, such as El Centro and Olympia, have been important in the development of current design criteria. Displacement and inelastic energy demands produced by El Centro and code compatible records are greater than the demands produced by a magnitude 8.5 Puget Sound record with a three minute duration. This implies that if the 8.5 event were to be considered the maximum credible event and the design criteria were based upon this event, then no changes to the current criteria would be warranted. However, if the maximum credible event is larger, then changes in criteria probably are needed.

Half-cycle counts, in the displacement ductility range below 3, produced by CSZ records are greater than half cycle counts produced by laboratory tests, El Centro, or code compatible records. For structures with yield force to weight ratios of 0.125, the half-cycle counts produced by CSZ records may warrant additional laboratory testing.

Currently used testing sequences produce more cycles in the higher ductility ranges and fewer cycles in the lower ductility ranges than do the CSZ records. Therefore, the adequacy of structural elements and sub-assemblages subjected to such large numbers of inelastic cycles in the lower ductility demand ranges may need to be assessed experimentally.

The intent of current code criteria is not to prevent damage from occurring, but to prevent structural collapse in large earthquakes and limit damage in moderate earthquakes. The damage demands, as expressed as total hysteretic energy dissipated, produced by a three minute magnitude 8.5 CSZ record attenuated to Puget Sound sites are less than the demands produced by El Centro and code compatible records. Displacement demands of code compatible and El Centro records are as great as the demands produced by a four minute magnitude 9.5 Puget Sound record for some periods. Only CSZ inelastic half-cycle counts at low ductility levels are greater than inelastic half-cycle counts for El Centro and code compatible records.

By not changing the code criteria, inferred damage from CSZ earthquakes will probably not exceed the damage inferred by current code criteria if the maximum credible event is less than a three minute magnitude 8.5 earthquake compatible with Crouse's median spectra and if structural elements can withstand additional cycles at low ductilities without loss of strength. For greater magnitude and longer duration maximum credible events, the code specified structural strength could be increased to keep structural response at a level that is currently inferred by code criteria. To account for increases in regional ground shaking intensity, the effective peak acceleration, EPA, could be increased. To account for increases in damage due to duration, the response modification factor, R, could be decreased. The amount of reduction in R depends upon the magnitude and duration of the maximum credible event, the period of the structure, and the level of desired damage demand.

## 5.2 Recommendations and Implementation

As a result of this research the following actions are recommended:

1) Learn more about the maximum design earthquake. This should include: the recurrence interval of such an event, the moment magnitude, the ground motion attenuation behavior, the maximum ground motions, and the elastic response spectra resulting from such an event. This research is based upon current estimations of postulated CSZ earthquakes There are considerable uncertainties in such estimations, and some effort should be made to reduce these uncertainties.

2) Retain the current seismic code design and detailing provisions. Current design and detailing provisions have produced structures that have shown ductile behavior and not collapsed in recent California earthquakes. Crouse (30) believes the maximum credible CSZ earthquake has a moment magnitude of 8.5. Puget Sound ground motions from a magnitude 8.5 earthquake produced displacement and damage demands less than or nearly equal to the demands of code compatible records and previously recorded records, which were important in the development of the current design provisions. Current detailing provisions should be adequate for preventing collapse in a magnitude 8.5 CSZ earthquake for sites in Puget Sound. This statement is based upon the comparisons of energy demands that were related as equivalent cycles at a ductility demand of four.

3) Use the data produced by this research to determine the displacement and damage demands from postulated CSZ earthquakes. In cases where an estimate of the

demands that a CSZ earthquake might impose upon a specific structure is desired, the methods outlined in Chapter 4 may be used. This may be done either for existing or new structures.

4) Perform additional research in the following areas:

a) Investigate the ability of structural elements and sub-assemblages to endure large numbers of inelastic cycles at low ductility demand levels (extreme displacement of one to three times the yield displacement). This research showed that postulated CSZ earthquakes may produce structural damage demands with a large number of low demand cycles, and current laboratory testing schemes typically do not subject specimens to such loading.

b) Determine, for both new construction and for older structures, the relationship between the design base shear and the actual yield force. Such an undertaking would provide insight into the amounts, if any, of overstrength that exist and that would be beneficial in reducing damage potential. "Push-over" or plastic collapse analyses would provide the information with which to compare the design lateral forces. This information would allow a better assessment of damage potential to be made.

c) Perform similar research to that included in this project using more yield force to weight ratio values. Results of this research showed a considerable drop in damage demand with an increase in the structure's yield force to weight ratio. Only three yield force to weight ratios were used: 0.125,

0.25, and 0.50. Additional research using values, from 0.05 to 0.25, should be performed to better determine the relationship between yield force to weight ratio to damage demands.

d) Perform similar research to that included in this project using different structural hysteretic models, including degrading strength models. This research only investigated response according to two hysteretic models. These models do not degrade in strength. Such performance is realistic only for a limited number of hysteretic cycles, depending on the quality of the structural detailing.

e) Determine whether the results from this research can be applied to more complicated structures. This research investigated response to single-degree-of-freedom structures with only one yielding region. Actual structures with more than one potential plastic hinge location will behave differently. Results from this research should not be extrapolated to more complex structures if such structures can not be generalized as single-degree-of-freedom systems with clearly defined structural yield points.

## ACKNOWLEDGMENTS

This research report herein was conducted under Agreement T9234 by Washington State University. Dr. M. Lee Marsh, Assistant Professor, Civil and Environmental Engineering, and Mr. Christopher M. Gianotti, Research Assistant, were the principal investigators for this study.

The contributions of the following Washington State Department of Transportation personnel to this research project are also gratefully acknowledged: Mr. Keith Anderson, Research Specialist; Mr. Ed Henley, Bridge Technology Development Engineer; Mr. Al Kilian, Chief Geotechnical Engineer; Mr. Yesh Mhatre, Bridge Design Engineer; Mrs. Barbara Russo, Librarian; Mr. Dick Stoddard, Structure Computer System Engineer; Mr. Mark Wallace, Bridge Design Engineer; and Dr. Hongzhi Zhang, Bridge Design Engineer.

## REFERENCES


1. Mohraz, Bijan, and Elghadamsi, Fawzi, E. (1989) "Earthquake Ground Motion and Response Spectra." *The Seismic Design Handbook,* Naeim, Farzad, Ed., Van Nostrand Reinhold, New York, N.Y., 32-80.
2. Heaton, Thomas H. and Hartzell, Stephen H. (1986a) "Estimation of Strong Ground Motions from Hypothetical Earthquakes on the Cascadia Subduction Zone, Pacific Northwest." U.S. Geological Survey Open File Report 86-328.
3. Tsiatas, George; Fragaszy, Richard; Ho, Carlton; and Kornher, Karen (1989) *Design Response Spectra for Washington State Bridges,* Technical Report, Washington State Department of Transportation.
4. "Uniform Building Code" (1991) International Conference of Building Officials.
5. "Guide Specifications for the Seismic Design of Highway Bridges" (1983) American Association of State Highway Transportation Officials.
6. Noson, L.L.; Qamar, A.; and Thorsen, G.W. (1988) *Washington State Earthquake Hazards,* Washington Division of Geology and Earth Resources, Info. Circular 85.
7. McCrumb, Dennis R.; Galister, Richard W.; West, Donald O.; Crosson, Robert S.; Ludwin, Ruth S.; Hancock, William E.; and Mann, Lawrence V. (1989) "Tectonics, Seismicity, and Engineering Seismology in Washington." *Engineering Geology in Washington,* Vol. I, Washington Division of Geology and Earth Resources Bulletin 78, p 97-120.
8. Atwater, Brian (1987) "Evidence for Great Holocene Earthquakes Along the Outer Coast of Washington State." *Science,* 236, 22 May 1987, 942-944.
9. Savage, J.C. and Lisowski, M. (1991) "Strain Measurements and the Potential for a Great Subduction Earthquake off the Coast of Washington." *Science,* 252, 5 April 1991, 101-103.

10. Heaton, Thomas H. and Kanamori, Hiroo (1984) "Seismic Potential Associated with the Subduction in the Northwestern United States." *Bulletin of the Seismological Society of America*, 74(3), 933-941.

11. Heaton, Thomas H. and Hartzell, Stephen H. (1986b) "Source Characteristics of Hypothetical Subduction Earthquakes in the Northwestern United States." *Bulletin of the Seismological Society of America*, 76(3), 675-708.

12. Heaton, Thomas H. and Hartzell, Stephen H. (1987) "Earthquake Hazards on the Cascadia Subduction Zone." *Science*, 236, April 10, 1987, 162-168.

13. Taber, John J., and Smith, Stewart W. (1985) "Seismicity and Focal Mechanisms Associated with the Subduction of the Juan de Fuca Plate beneath the Olympic Peninsula, Washington." *Bulletin of the Seismological Society of America*, 75(1), 237-249.

14. Weaver, C.S. and Smith, S.W. (1983) "Regional Tectonic and Earthquake Hazard Implications of a Crustal Fault Zone in Southwestern Washington." *Journal of Geophysical Research*, 88, 10371-10383.

15. Abe, Katsuyuki (1977) "Tectonic Implications of the Large Shioya-Oki Earthquakes of 1938" *Tectonophysics* (41) 269-289.

16. Heaton, Thomas H. and Snavely, Parke D. (1985) "Possible Tsunami along the Northwestern Coast of the United States Inferred from the Indian Traditions." *Bulletin of the Seismological Society of America*, 75(5), 1455-1460.

17. Ando, Masataka and Balazs, Emery I. (1979) "Geodetic Evidence for Aseismic Subduction of the Juan de Fuca Plate" *Journal of Geophysical Research* (84) B6, 3023-3028.

18. Steinbrugge, Karl V. and Flores, Rodrigo A. (1963) "The Chilean Earthquake of May, 1960: A Structural Engineering Viewpoint." *Bulletin of the Seismological Society of America*, 53(2), 225-307.

19. Plafker, George (1965) "Tectonic Deformation Associated with the 1964 Alaska Earthquake" *Science*, (148) 3678, 1675-1687.

20. Swan, J.G. (1868) "The Indians of Cape Flattery, at the Entrance to the Strait of Juan de Fuca, Washington" *Smithsonian Contributions to Knowledge, 220.*

21. Housner, George W. and Jennings, Paul C. (1973) "Reconstituted Earthquake Ground Motion at Anchorage." *The Great Alaska Earthquake of 1964*, National Academy of Sciences, 43-48.

22. Anderson, J.G.; Bodin, P.; Brune, J.N.; Prince, J.; Singh, S.K.; Quass, R.; and Onate,M. (1986) "Strong Ground Motion from the Michoacan, Mexico, Earthquake." *Science*, 233, 5 September, 1043-1049.

23. Popov, E.P. (1987) "Observations on the Mexico Earthquake of 19 September 1985." *Engineering Structures*, 9, April, 74-83.

24. Reiter, Leon. (1990) *Earthquake Hazard Analysis* Columbia University Press, New York, N.Y.

25. "NEHRP Recommended Provisions for the Development of Seismic Regulations for New Buildings " (1991). Federal Emergency Management Agency, 223.

26. Bolt, Bruce A. (1989) "The Nature of Earthquake Ground Motion." *The Seismic Design Handbook*, Naeim, Farzad, Ed., Van Nostrand Reinhold, New York, N.Y., 1-31.

27. Trifunac, M.D., and Brady, A.G. (1975) "A Study on the duration of Strong Earthquake Ground Motion." *Bulletin of the Seismological Society of America,* 65(3), 581-626

28. Saint Amand, Pierre (1961) *Los Terremotos de Mayo Chile 1960* NOTS TP 2701, Naval Ordinance Test Station, China Lake California.

29. Housner, George W. (1963) "An Engineering Report on the Chilean Earthquake of May 1960." *Bulletin of the Seismological Society of America*, 53(2), 219-223.

30. Crouse, C.B. (1991) "Ground-Motion Attenuation Equations for Earthquakes on the Cascadia Subduction Zone." *Earthquake Spectra*, EERI, 7(2), 201-236.

31. WPPSS (Washington Public Power Supply System) (1988) "Cascadia Subduction zone: An Evaluation of Earthquake Potential and Implications to WNP-3." Report submitted to U.S. Nuclear Regulatory Commission, June.

32. Chang, F. K. and Krinitzsky, E.L. (1977) "Duration, Spectral Content and Predominant Period of Strong Motion Earthquake records in the Western United States," *U.S. Army Engineers Waterways Experimental Station, Miscellaneous Paper S-73-1*, Vicksburg, MS.

33. Krinitzsky, E.L.; Chang, F. K.; and Nuttli, Otto W. (1987b) "Parameters for Specifying Magnitude-Related Earthquake Ground Motions." *State-of-the-Art For Assessing Earthquake Hazards in the United States. Report 26*, Miscellaneous Paper S-73-1, U.S. Army Corps of Engineers, Waterways Experimental Station, Vicksburg, MS.

34. Donovan, N.C. (1973) "Earthquake Hazards for Buildings" *Building Practices for Disaster Mitigation, Building Research Services Number 46*, National Bureau of Standards, U.S. Department of Commerce, 82-111.

35. Powell, Graham H. and Allahabadi, Rakesh (1988) "Seismic Damage Prediction by Deterministic Concepts and Procedures," *Earthquake Engineering and Structural Dynamics*, 16, 719-734,

36. Zahrah, Tony F. and Hall, William J. (1984) "Earthquake Energy Absorption in SDOF Structures," *Journal of Structural Engineering, ASCE*, 110(8), 1757-1772.

37. Uang, Chia-Mia, and Bertero, Vitelmo V. (1990). "Evaluation of Seismic Energy in Structures," *Earthquake Engineering and Structural Dynamics*, (19), 77-90.

38. Jeong, Garrett D. and Iwan, Wilfred D. (1988) "The Effect of Earthquake Duration on the Damage of Structures," *Earthquake Engineering and Structural Dynamics*, 16, 1201-1211.

39. Dowling, N.E. (1972) "Fatigue Failure Predictions for Complicated Stress-Strain Histories," *Journal of Materials, JMLSA* 7(1), 71-87.

40. Chai, Yuk Hon (1991) *Steel Jacketing of Circular Reinforced Concrete Bridge Columns for Enhanced Flexural Performance*, Doctoral Dissertation, University of California, San Diego.

41. Popov, Egor P. and Pinkney, R. Bruce (1969) "Cyclic Yield Reversal in Steel Connections," *Journal of the Structural Division, ASCE*, ST3, 327-353.

42. Krinitzsky, E.L. and Chang, F. K. (1987) "Parameters for Specifying Intensity-Related Earthquake Ground Motions," *State-of-the-Art For Assessing Earthquake Hazards in the United States. Report 25*, Miscellaneous Paper S-73-1, U.S. Army Corps of Engineers, Waterways Experimental Station, Vicksburg MS.

43. Housner, G. W. and Jennings, P.C. (1964) "Generation of Artificial Earthquakes," *Journal of the Mechanics Division, ASCE*, EM1, 113-149.

44. Gasparini, D.A. and Vanmarcke, E.H. (1976) "Simulated Earthquake Motions Compatible with Prescribed Response Spectra," Massachusetts Institute of Technology, Department of Civil Engineering Research Report R76-4.

45. SIMQKE, A Program for Artificial Motion Generation. User's Manual and Documentation (1976) Massachusetts Institute of Technology, Department of Civil Engineering.

46. Stanton, John F. (1992) SPECTRUM, A Program for Determining the Inelastic Response History of SDOF Structures, University of Washington, Seattle, WA.

47. Menegotto, M. and Pinto, P. (1973) "Method of Analysis for a Cyclically Loaded Reinforced Concrete Plane Frames including Changes in Geometry and Nonelastic Behavior of Elements under Combined Normal Force and Bending," *IABSE Symposium on Resistance and Ultimate Deformability of Structures Acted on by Well-Defined Repeated Loads*, Lisbon.

48. Kannan, Amin E. and Powell, Graham H. (1975) *DRAIN2D, A General Purpose Computer Program for the Dynamic Analysis of Inelastic Plane Structures with User's Guide.* Reports 73-6 and 73-22. University of California, Berkeley, National Information Service for Earthquake Engineering.

# APPENDIX A

CSZ Displacement Demand

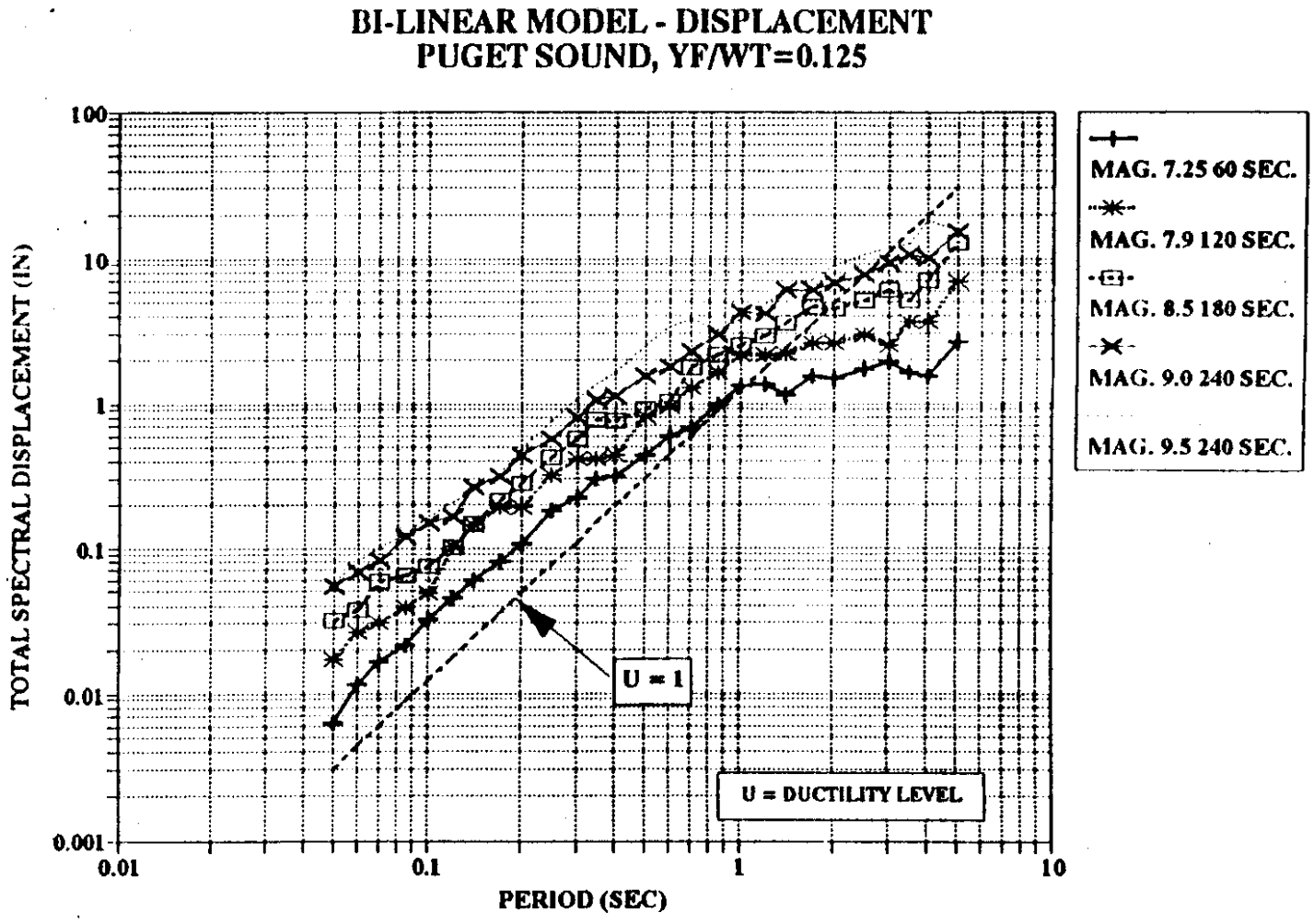


Figure A 1 Puget Sound displacement demand, bi-linear model, yf/wt = 0.125

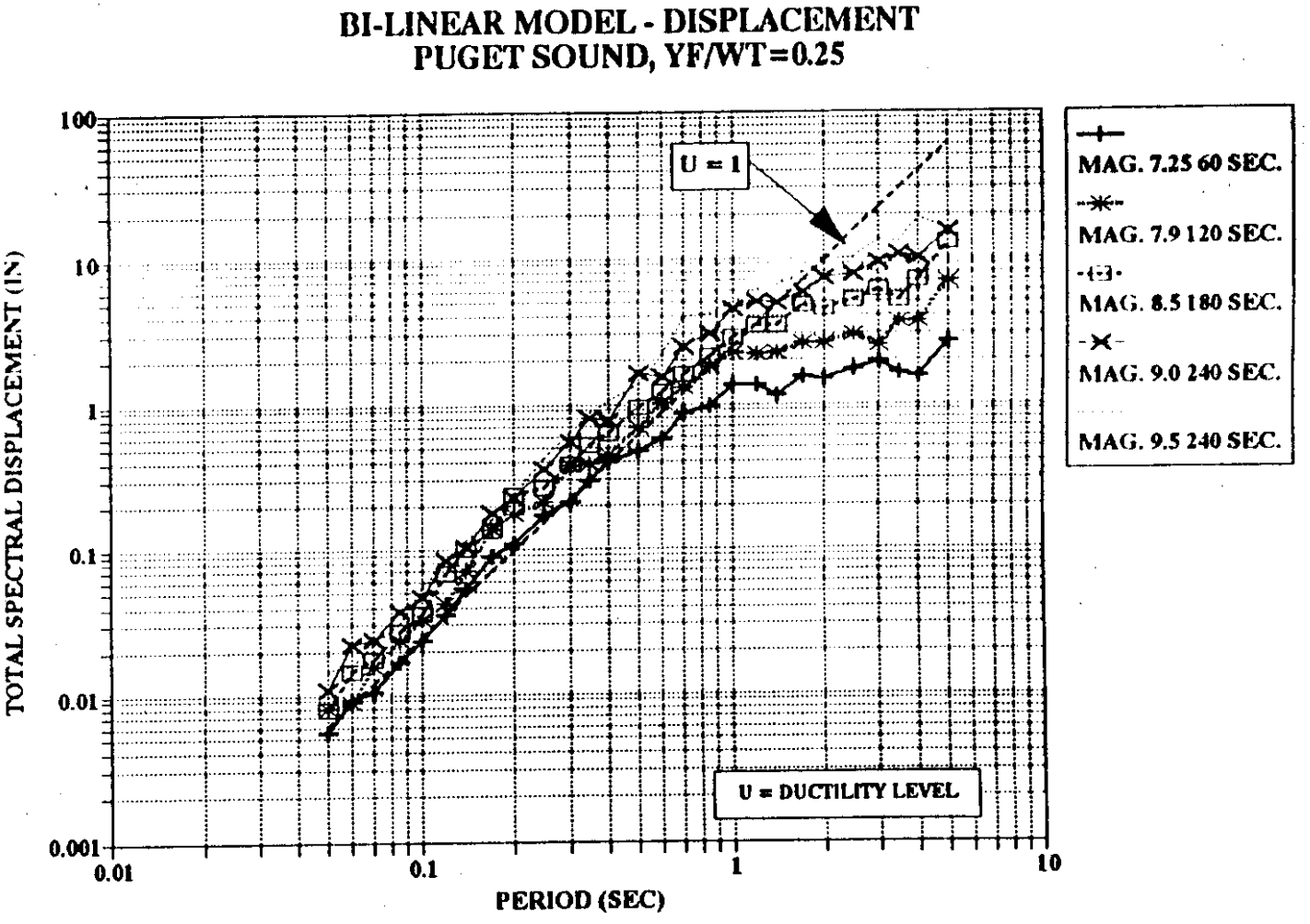


Figure A 2 Puget Sound displacement demand, bi-linear model, yf/wt = 0.25

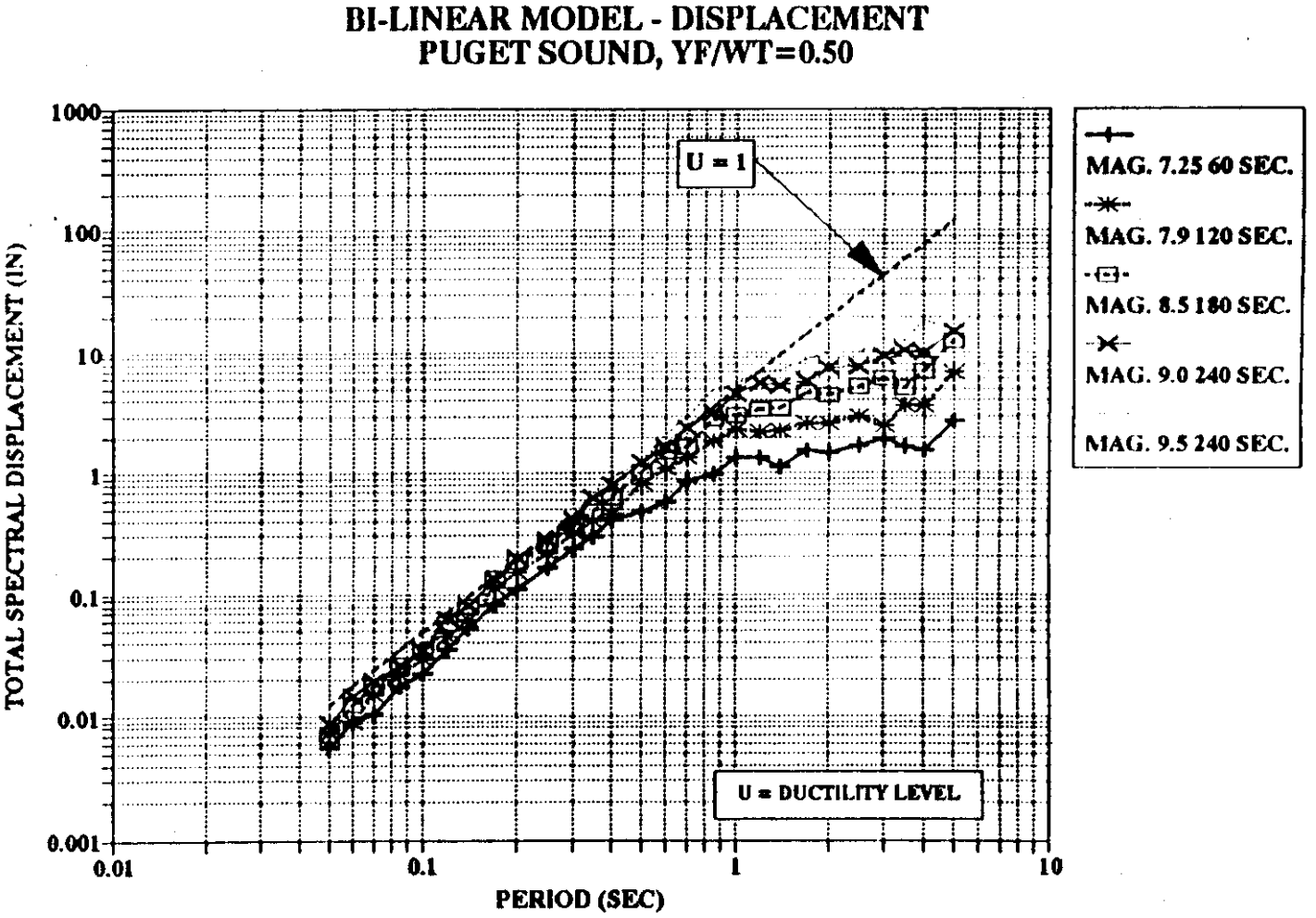


Figure A 3 Puget Sound displacement demand, bi-linear model, yf/wt = 0.50

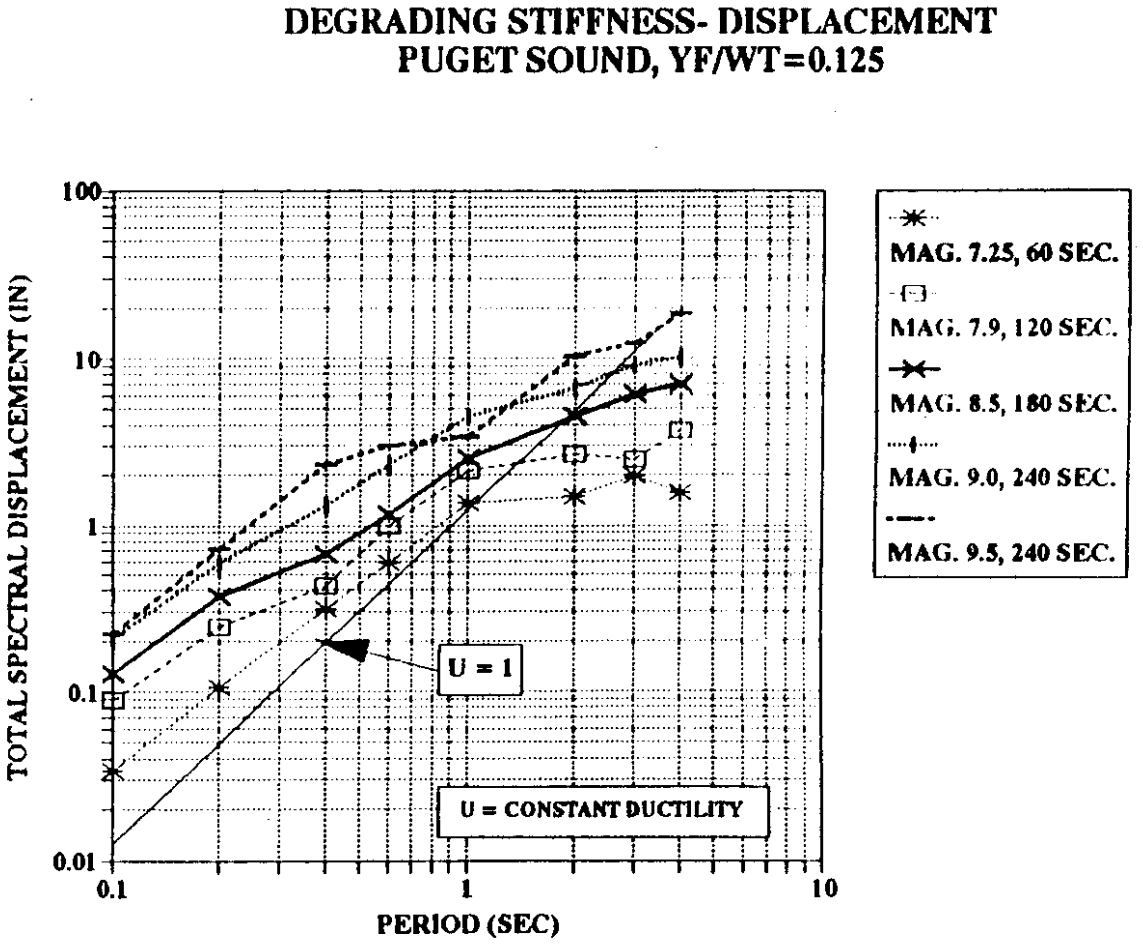


Figure A 4 Puget Sound displacement demand, degrading stiffness model, yf/wt = 0.125

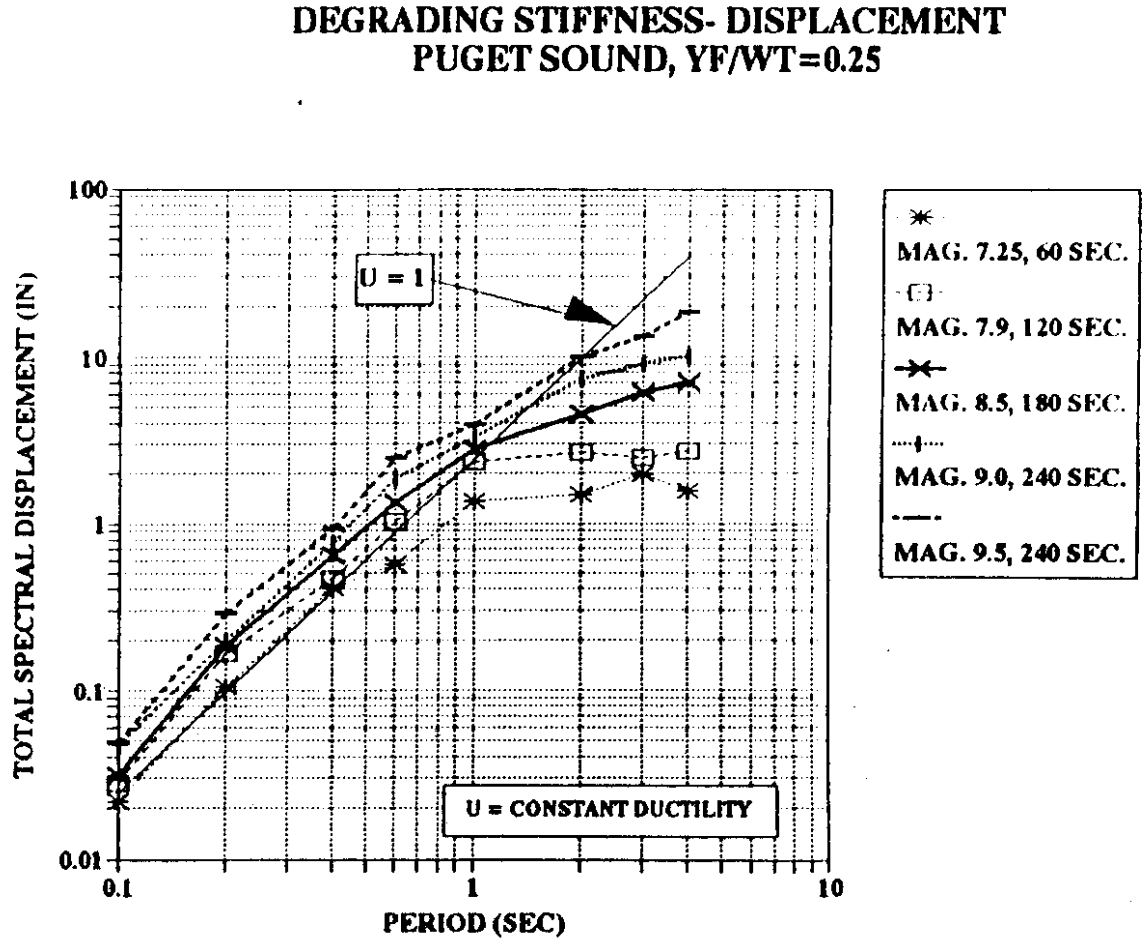


Figure A 5 Puget Sound displacement demand, degrading stiffness model, yf/wt = 0.25

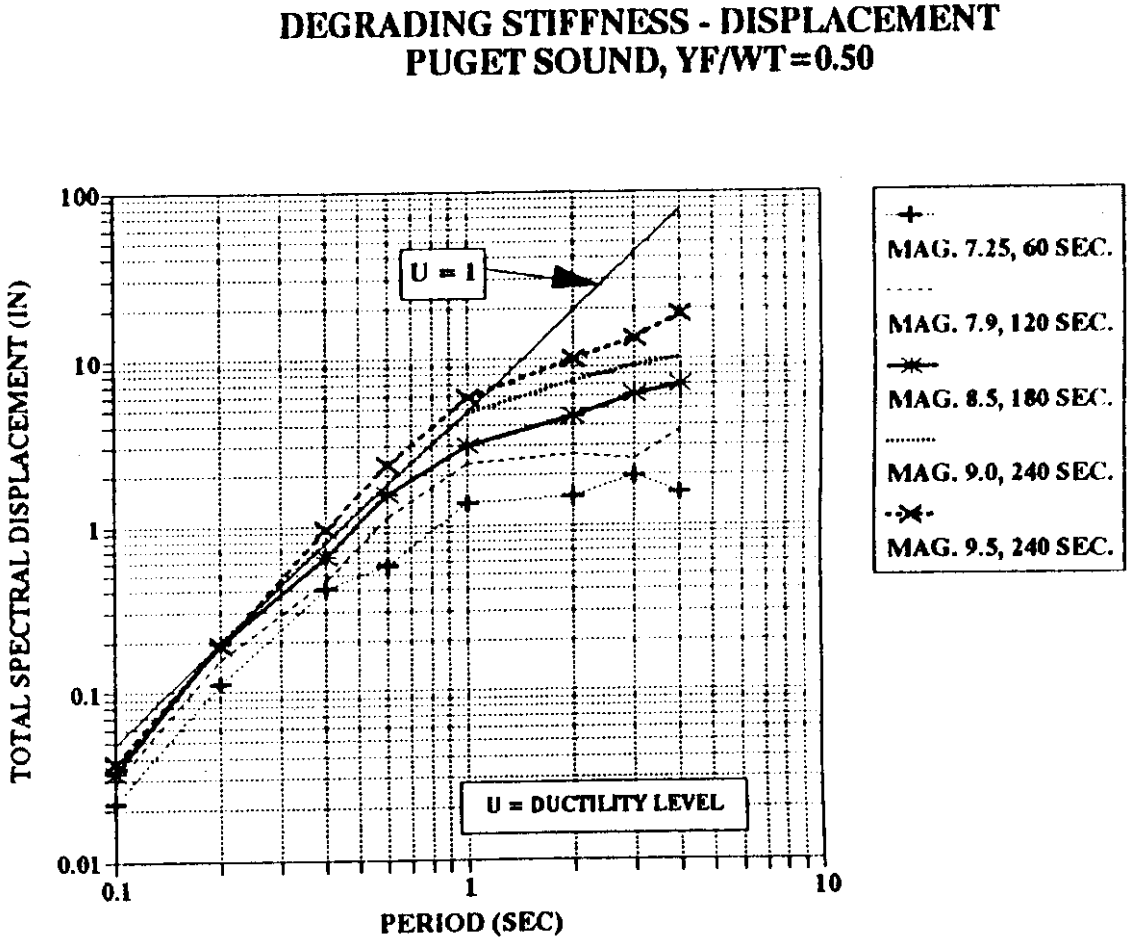


Figure A 6 Puget Sound displacement demand, degrading stiffness model, yf/wt = 0.50

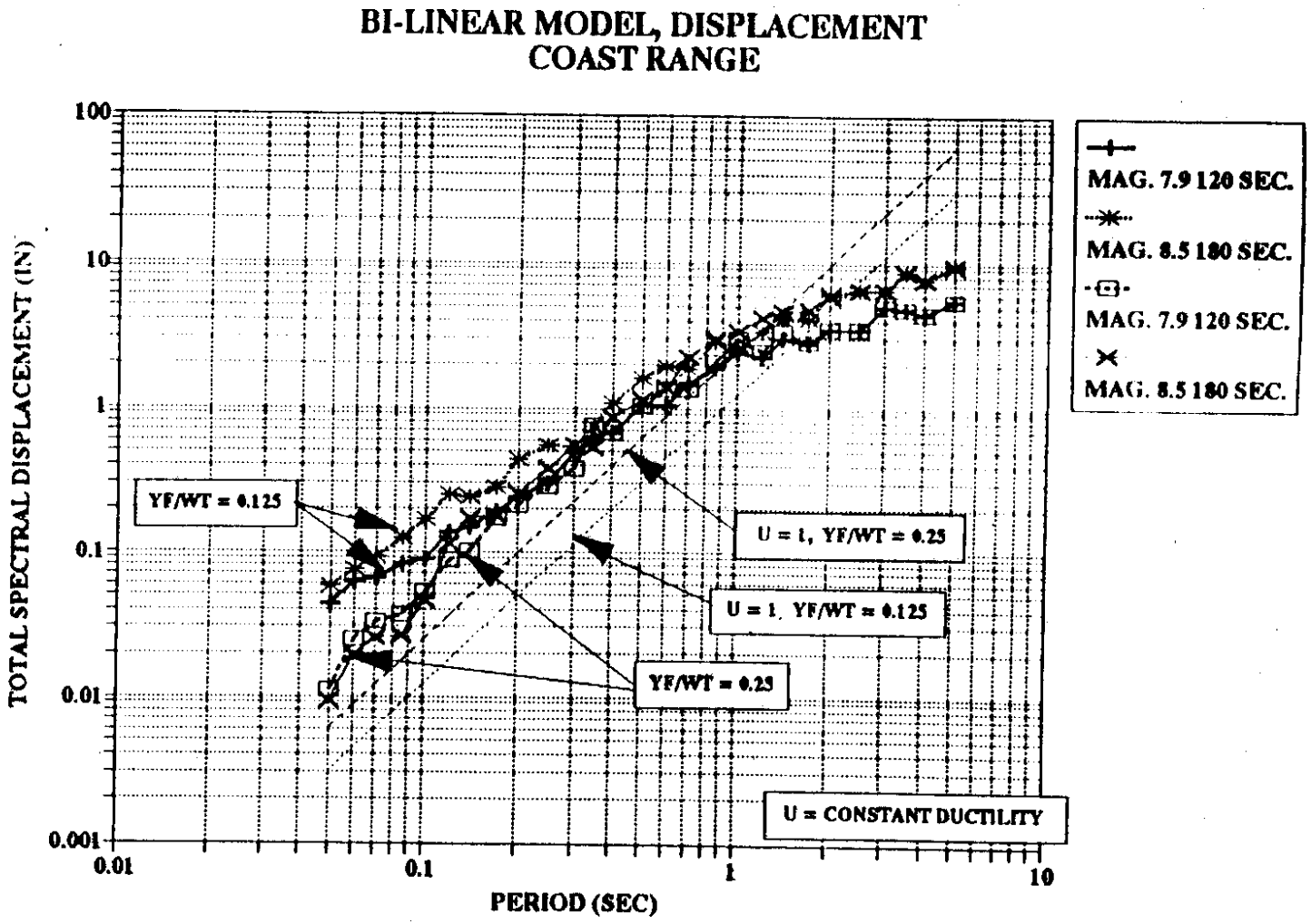


Figure A.7 Coast range displacement demand, bi-linear model

# APPENDIX B

CSZ Hysteretic Energy Demand

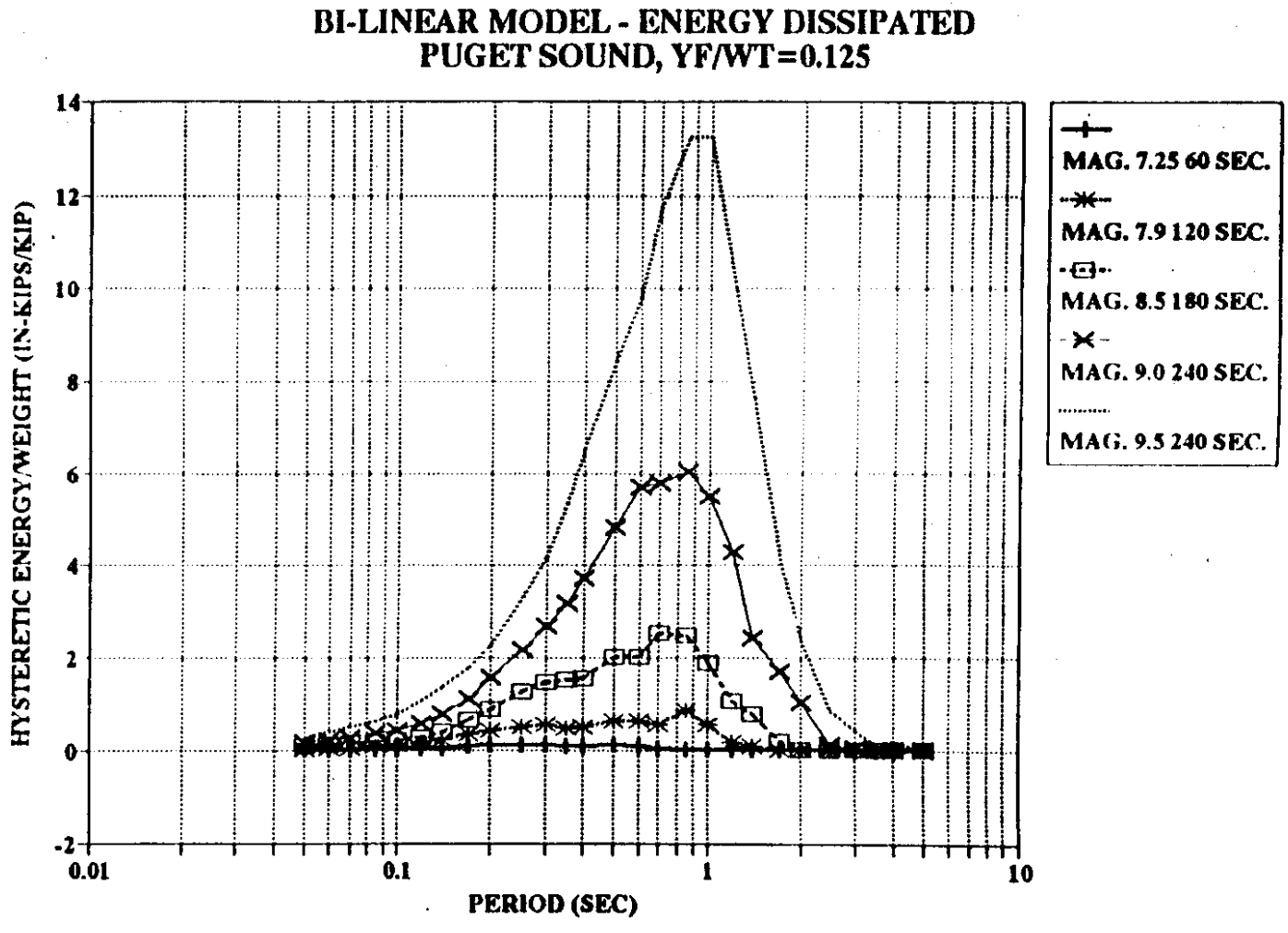


Figure B.1 Puget Sound hysteretic energy demand, bi-linear model, yf/wt= 0.125

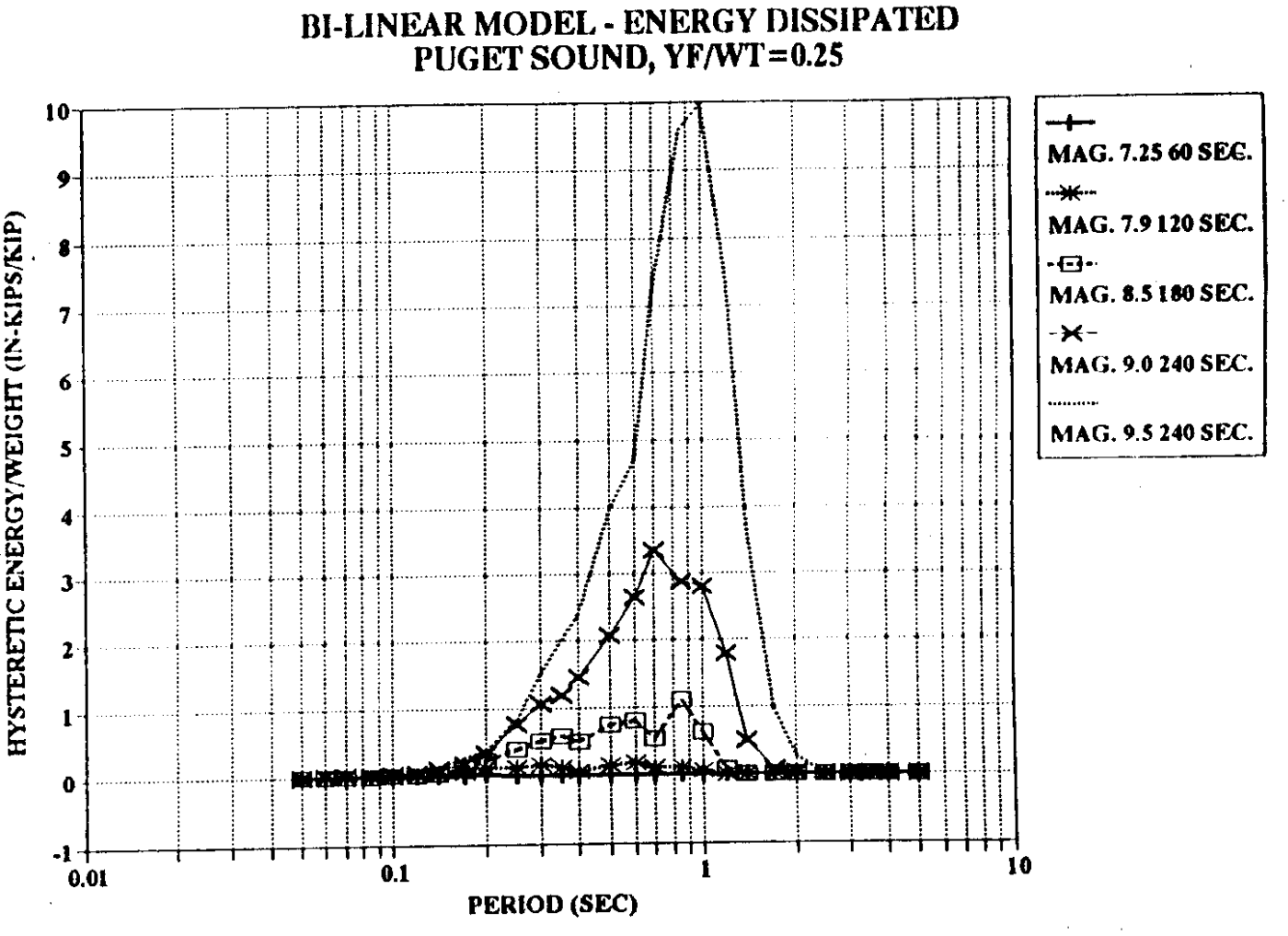


Figure B 2 Puget Sound hysteretic energy demand, bi-linear model, yf/wt= 0.25

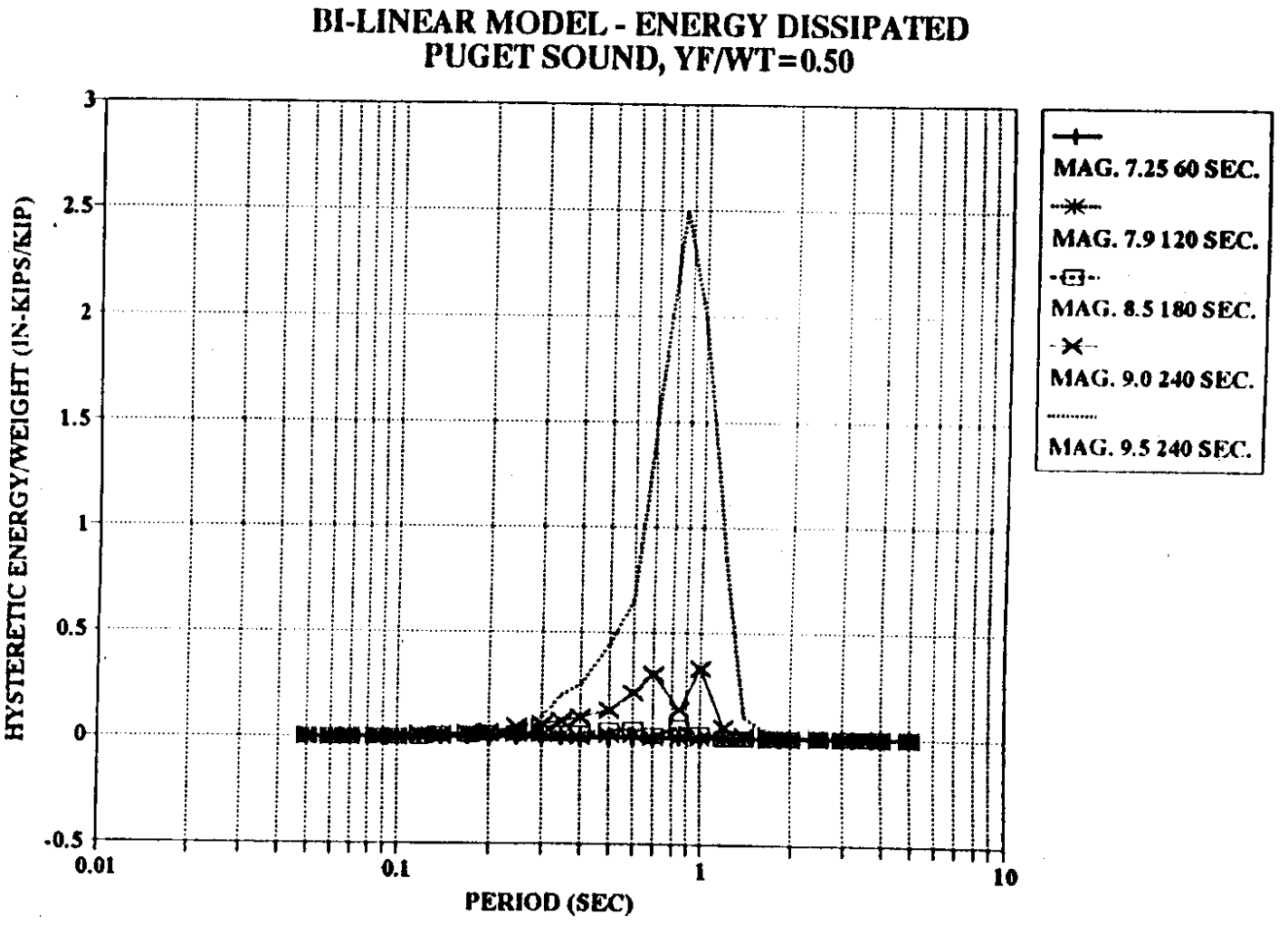


Figure B 3 Puget Sound hysteretic energy demand, bi-linear model, yf/wt= 0.50

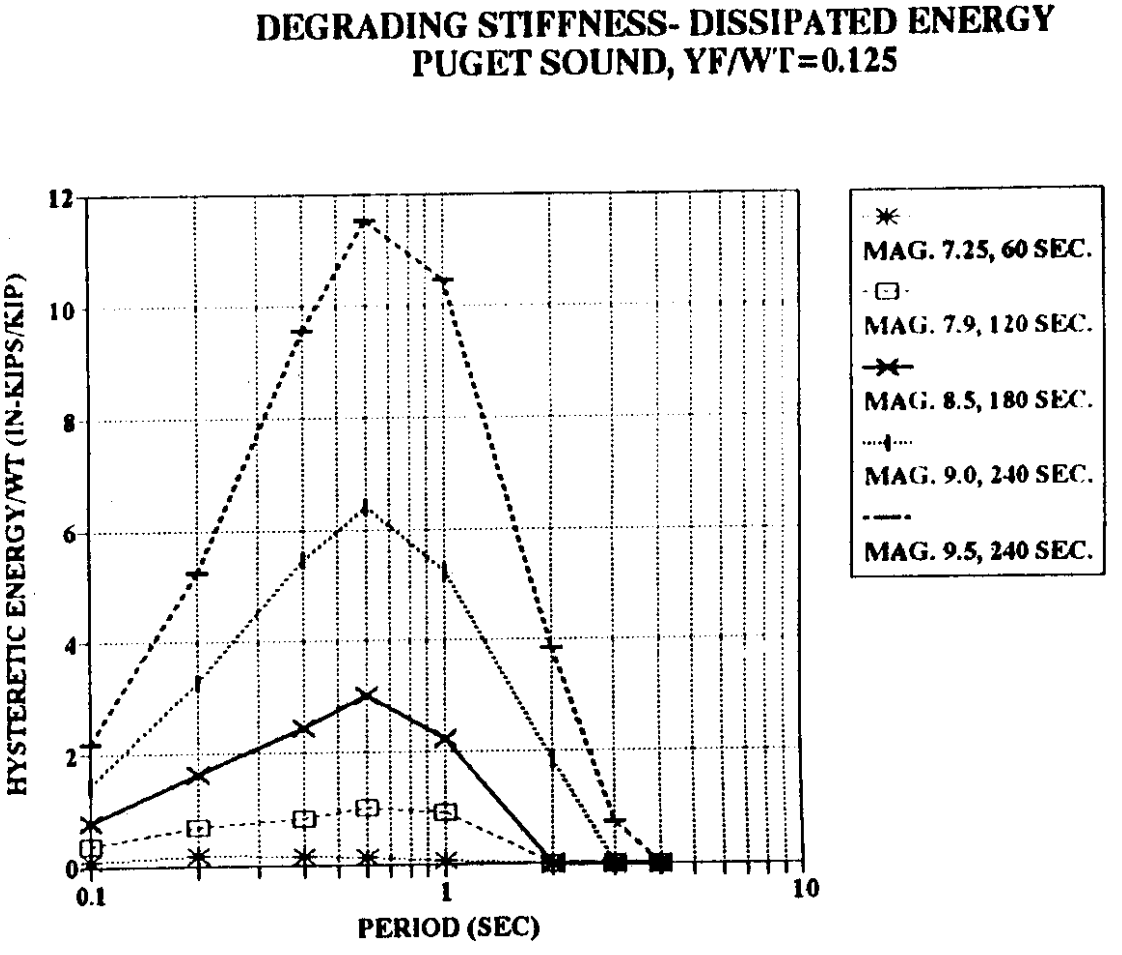


Figure B.4 Puget Sound hysteretic energy demand, degrading stiffness model, vf/wt = 0.125

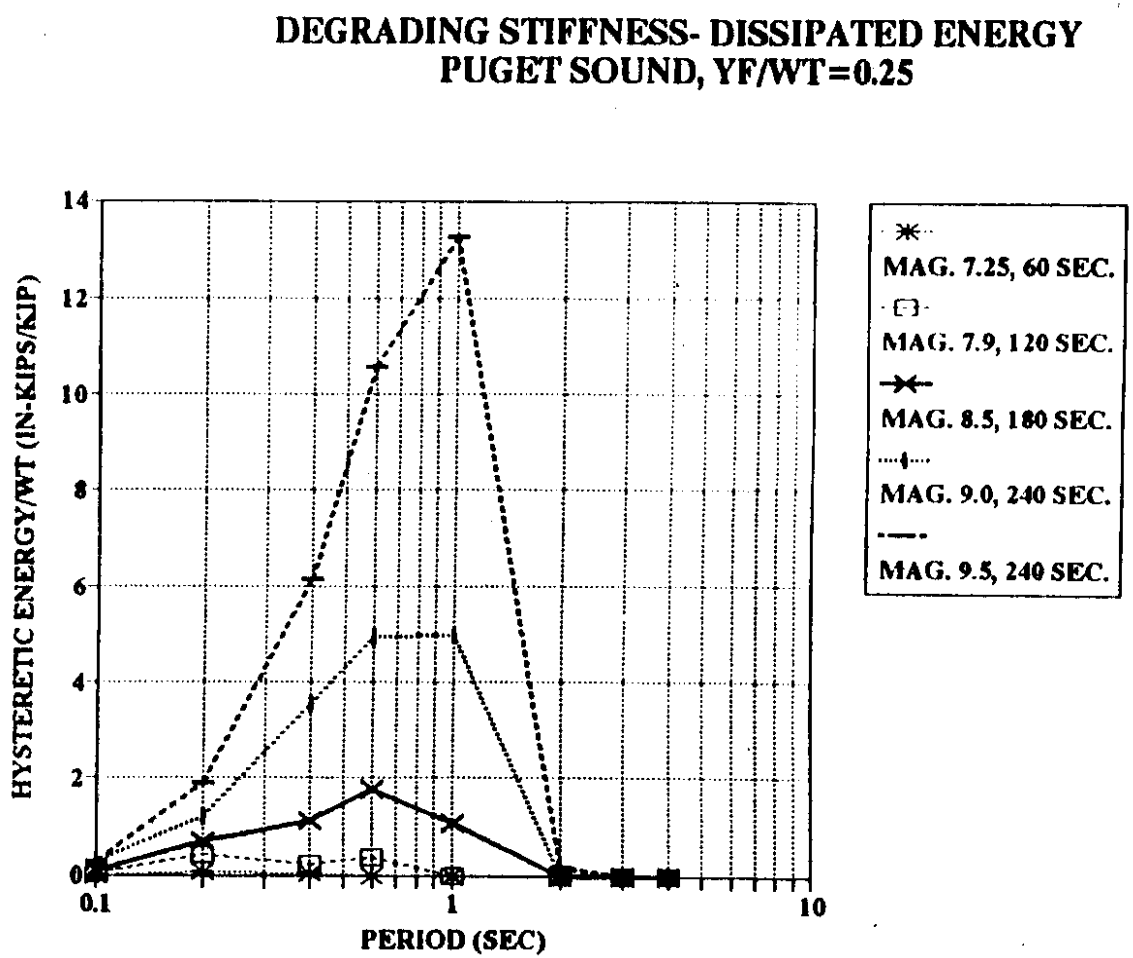


Figure B.5 Puget Sound hysteretic energy demand, degrading stiffness model, yf/wt = 0.25

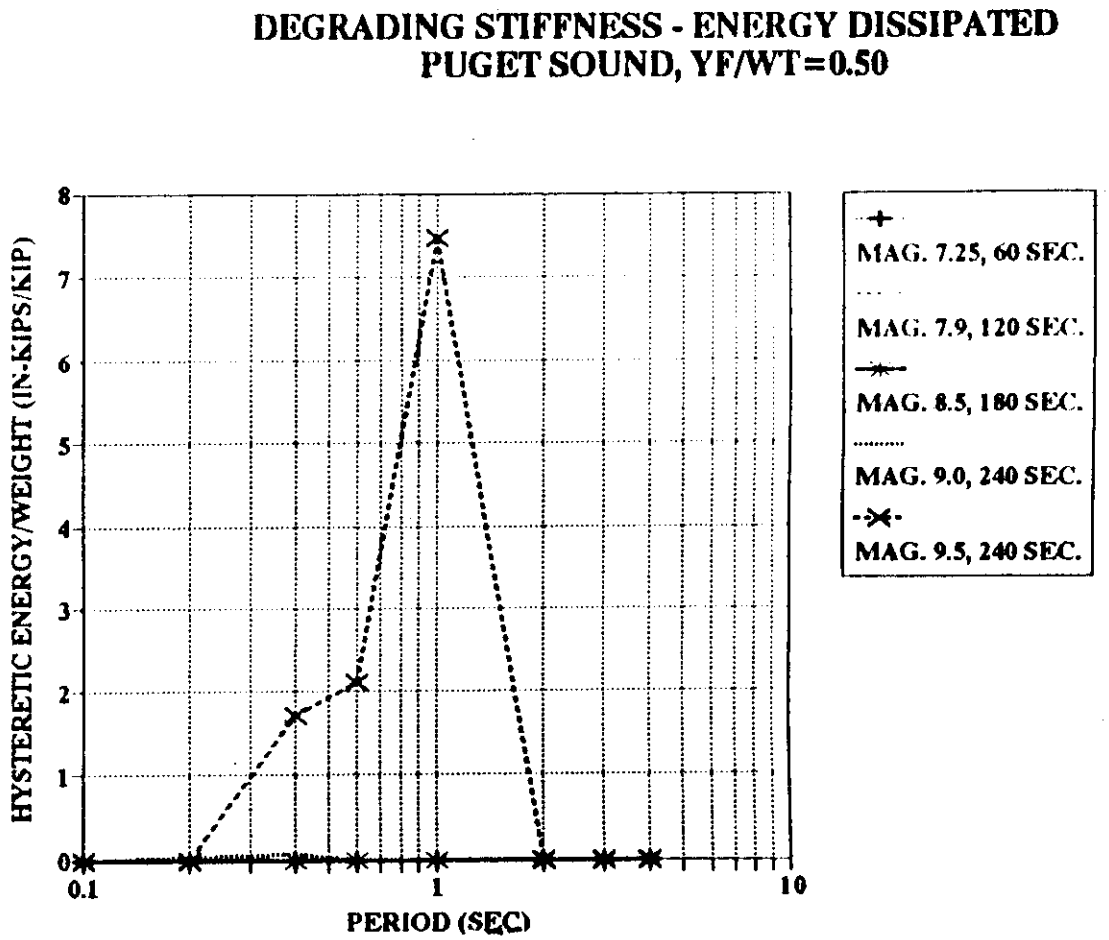


Figure B.6 Puget Sound hysteretic energy demand, degrading stiffness model, yf/wt = 0.50

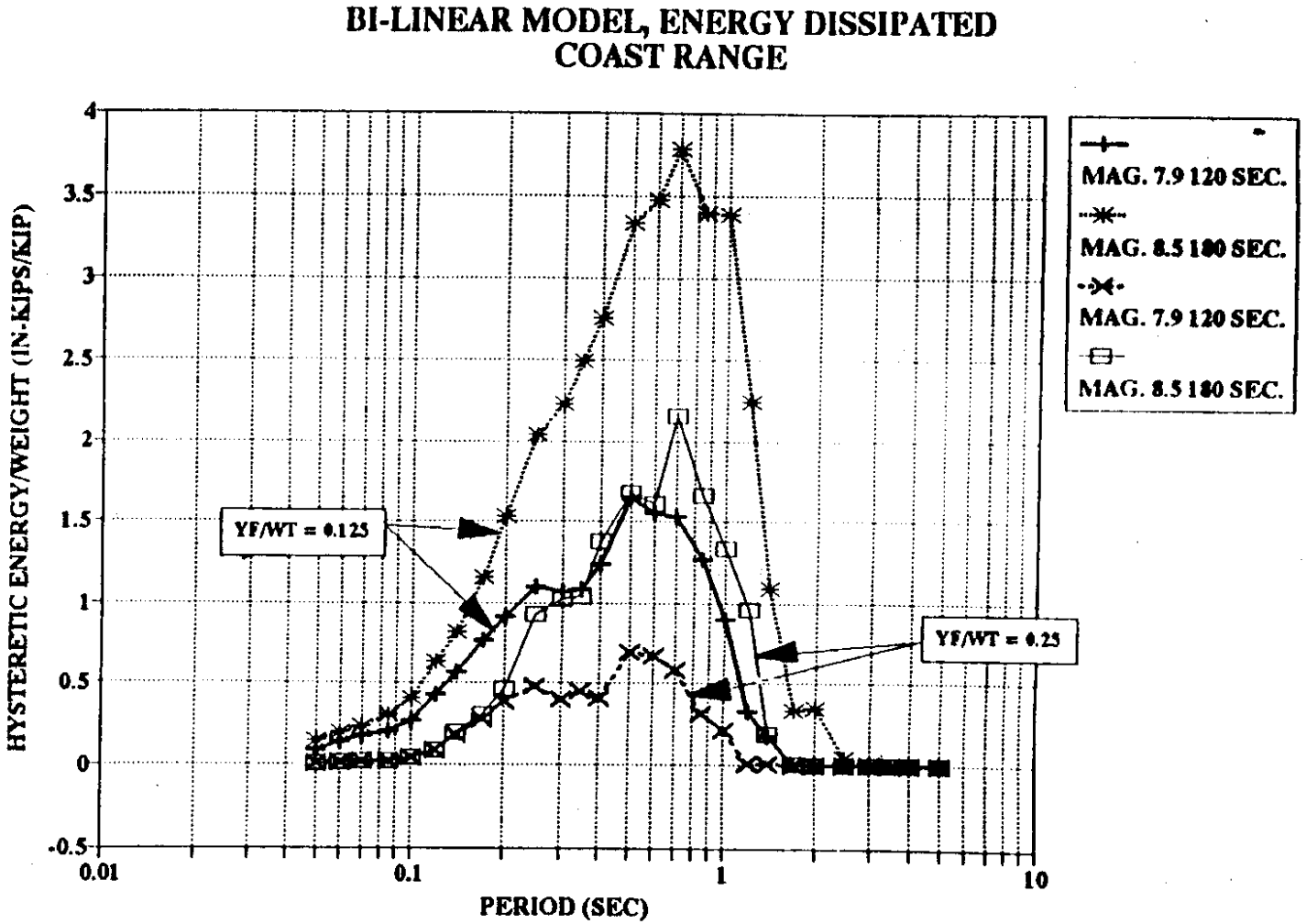


Figure B.7 Coast range hysteretic energy demand, bi-linear model